Underwater Adhesion between Biopolymer Model Surfaces and Hydrogels

Zuxiang Xu

PSL UNIVERSITÉ PARIS

THÈSE DE DOCTORAT
DE L'UNIVERSITÉ PSL

Préparée à l'Ecole Supérieure de Physique et de Chimie Industrielles de la ville de Paris (ESPCI Paris)

Underwater Adhesion between Biopolymer Model Surfaces and Hydrogels

Adhésion en Milieu Aqueux entre Adhésifs et Surfaces Modèles à Base d'Hydrogels Biopolymères

Soutenue par

Zuxiang XU

Le 26 Septembre 2022

Ecole doctorale n° 397

Physique et Chimie des Matériaux

Spécialité

Chimie des Matériaux

Composition du jury :

Laurent, CORTE Professeur, Mines ParisTech	*Président*
Fouzia, BOULMEDAIS Directeur de recherche, CNRS	*Rapporteur*
Florence, AGNELY Professeur, Université Paris-Saclay	*Rapporteur*
Guillaume, SUDRE Maître de conférences, Université Claude Bernard Lyon	*Examinateur*
Yvette, TRAN Maître de conférences, ESPCI Paris	*Directeur de thèse*
Dominique, HOURDET Professeur, Sorbonne Université	*Co-directeur de thèse*
Costantino, CRETON Directeur de recherche, CNRS	*Co-encadrant*

ESPCI PARIS | PSL

Acknowledgements

I wish to express my gratitude to all those who have offered me invaluable help during the four years of my PhD in ESPCI Paris and PSL University.

First, I would like to express my appreciation to my supervisors: Dr. Yvette TRAN, Prof. Dominique HOURDET and Prof. Costantino CRETON. Dr. Yvette TRAN is my director of thesis, who supervised me during all my PhD and especially the part about hydrogel thin coatings. I have learnt surface chemistry and got a lot of opportunities to communicate and work with French students in varied stages. Prof. Dominique HOURDET is my co-supervisor who has kindly taught me a lot of things about biopolymers, networks and hydrogels. He is always a person to have fantastic discussion. Prof. Costantino CRETON is also one of my supervisors, who has brought me many significant inspirations of underwater adhesion study. Although I was not very good at working on polymer theories, he still kindly explains and discusses with me. His very detailed corrections about how to show and present data let me learn how to think scientifically. Definitely, doing a PhD under their supervisions is always a big treasure for myself.

I am very grateful for the financial support from China Scholarship Council (CSC) through CSC-ParisTech Doctoral Program.

Then I thank Dr. Francisco J. CEDANO-SERRANO for his early exploration of gelatins and his careful training for underwater probe tack test.

I appreciate the chances and experiences of working and supervising interns during my four years in SIMM lab. The work about gelatin coatings from Alexandre TAOUM (year 2019), Esther LEITAO (year 2020) and Léa MILENKOVIC (year 2021) and the work about patterns and tough hydrogels from Junhao MA (year 2022) have helped the completion of this thesis a lot.

The thesis also relies on the great support from Dr. Ekkachai MARTWONG who helped me with polymer chemistry and hydrogel thin films, Dr. Guylaine DUCOURET with rheology, Mohamed HANAFI with TGA and DSC, Dr. Bruno BRESSON with AFM (especially underwater test).

At this moment, I also want to express my thanks to the SIMM lab and a lot of people in our lab, who bring me a significant and unforgettable experience in Paris. I would like to thank Dr. Yinjun CHEN for the initial guidance in the lab, Dr. Gabriel E. SANOJA for the discussion about double-network, Julie LE BRUN for the comparison of gelatin with her collagen, Dr. Anusree AUGUSTINE for working in hydrogel thin film together and processing our photomasks, Dr. Hao LUO for the discussion of abbreviations and equations. Moreover, during my four years, I really appreciate sharing the office H.310 with all my office-mates: Dr. Ludovic FEIGE, Dr. Gaétan GRIMALDI D'ESDRA, Dr. Guillaume VOTTE, Dr. Gaëlle MELLOT, Maxime BES, Ombeline TAISNE and Svetlana GLUKHOVA, who have helped me with French and created a peaceful, friendly and perfect working environment.

In addition to working in ESPCI, I am also deeply grateful for the happy time with several friends in Paris: Dr. Daming ZHENG, Chenghao XIN and Zeyuan XU. We have been enjoying our lives together not only in Paris and France, but also Europe, from which I learn more about different people, scenery, history, arts, traditions and customs.

Last but not least, I would like to express my gratitude to my beloved parents and grandparents who have always been helping me out of difficulties and supporting me to go through this path of scientific research. In a sense, the choice of studying in a distant place and doing a PhD for four years is a challenge to some Chinese old traditions, but I still get enlightened and firm encouragements and supports from my family, which let me persevere under difficult circumstances.

The road you have traveled, the books you have read, and the people you have loved are all hidden in your current temperament.

movie <*Casablanca*>

Table of Contents

Chapter 3. Molecular Mechanisms of Underwater Adhesion of Gelatins

Chapter 4. Reversible Underwater Adhesion between Tough Biopolymer Hydrogel and Surface Grafted with Hydrogel Microstructures

List of Abbreviations and Symbols

AAc	Acrylic acid
AAm	Acrylamide
AIBN	2,2'-azobis(2-methylpropionitrile)
AMA	Allyl methacrylate
EDC	*N*-(3-dimethylaminopropyl)-*N'*-ethylcarbodiimide hydrochloride
DMAEMA	2-(Dimethylamino)ethyl methacrylate
DMF	Dimethylformamide
DSP	Dexamethasone sodium phosphate
ene-functionalized PDMAEMA	Poly(2-(dimethylamino)ethyl methacrylate-*co*-allyl methacrylate)
GA	Gelatin type A
GB	Gelatin type B
MBAA	*N,N'*-methylenebisacrylamide
NHS	*N*-hydroxysuccinimide
PAAc	Poly(acrylic acid)
PAAm	Polyacrylamide
PBS	Phosphate buffered saline
PDMA	Poly(*N,N*-dimethylacrylamide)
PDMAEMA	Poly(2-(dimethylamino)ethyl methacrylate)
PDMS	Polydimethylsiloxane
PNIPAM	Poly(*N*-isopropylacrylamide)
VA044	2,2'-Azobis[2-(2-imidazolin-2-yl)propane] dihydrochloride

α	One of Mark-Houwink parameters
α_d	The degree of dissociation of functional groups at certain pH
Γ	Fracture energy
Γ_0	Fracture energy from contributions of interfacial binding
Γ_D	Fracture energy from contributions of bulk cohesion
ε	Strain
ε_0	Vacuum permittivity constant
$\varepsilon_{fracture}$	Fracture strain
ε_r	The dielectric constant of the measuring fluid
ε-amino	Free amino groups
ζ	Zeta potential
ζ_{plateau}	Plateau value of zeta potential
η	Viscosity of the streaming potential measuring fluid
λ	Activation length of a bond
σ	Stress
σ_a	Areal charge density existing at the solid/liquid interface at a specific pH
$\sigma_{fracture}$	Fracture stress
Σ_i	Areal density of electrostatic interactions at interface
$\Sigma_{i\text{-}film}$	Areal charge density of polymer film
$\Sigma_{i\text{-}gel}$	Areal charge density surface of hydrogel
Σ_{gel}	Volume charge density of bulk of hydrogel
$\tau_{\text{-}}$	The characteristic time of bond dissociation
ϕ_0	Polymer fraction in as-prepared state

ϕ_p	Polymer fraction in equilibrated state
ω	The speed of spin for spin-coating
b	The C-N bond length in a peptide bond
c	Polymer concentration in kg m^{-3}
c_+	Positive charge concentration of polymer
C_p	Polymer concentration for spin-coating
C^∞	The ion concentration of the streaming solution
d	Edge distance between hexagons on hydrogel thin films
e_0	The charge of an electron
E	Young's modulus
E_{cross}	Efficiency of chemical crosslinking
f	The functionality of junctions in a polymer network
f_{ch}	The functionality of chemical crosslinks in a polymer network
f_{ph}	The functionality of physical crosslinks in a polymer network
E	Young's modulus
F	Faraday constant
G, G_0	Shear modulus
G'	Storage modulus measured by rheology
G''	Loss modulus measured by rheology
G_{ch}	Chemical crosslinking contributions on shear modulus
G_{eq}	Shear modulus in equilibrated state
G_{ph}	Physical crosslinking contributions on shear modulus
k	Specific conductivity of the measuring fluid for streaming potential
k_1, k_2	Coefficients in mathematical manipulation of Chaudhury's model

k_B	Boltzmann's constant
$k_{s\text{-}enthalpic}$	The spring constant of a polymer chain in its enthalpic limit
k_s	Linear spring constant of a polymer chain
l	Side length of hexagonal patterns on polymer hydrogel thin films
L	End-to-end distance between crosslinks in equilibrated state
L_0	End-to-end distance between crosslinks in as-prepared state
m	Weight of polymer
m_{dry}	Weight of macroscopic hydrogel in dry state
m_{wet}	Weight of macroscopic hydrogel in equilibrium wet state
M	The molecular weight of polymer
M_{amino}	The molecular weight of amino acid in gelatin
M_{ch}	Average molecular weight between chemical networks
M_{ph}	Average molecular weight between physical networks
M_n	Number-average molecular weight
$M_{monomer}$	Molecular weight of a monomer
M_w	Weight-average molecular weight
M_x	Molecular weight between crosslinks
N_a	Areal density of total groups capable of dissociating per unit area
N_{av}	Avogadro's constant
N_c	Number of monomers between crosslinks
$N_{monomer}$	Number of monomers on a polymer chain
n	Number of bonds in the polymer chain that can dissociate
$n_{100\%\text{-}cross}$	Number of crosslinks when all the EDC/NHS participate in crosslinking
$n_{\varepsilon\text{-}amino}$	Mole number of free amino groups

n_{cross}	Number of crosslinks in the network
n_{chain}	Number of polymer chains
n_{EDC}	The mole number of EDC
n_i	Refractive index
p	The pressure inside fluid channel of streaming potential test
pI	Isoelectric point
R	Gas constant
SR	Swelling ratio
T	Absolute temperature
T_0	Thickness of macroscopic hydrogels
Th_{dry}	Dry thickness of films in air
Th_{wet}	Wet thickness of films in water
U	Streaming potential at zero net current conditions
U_c	The bond energy of covalent bond
V	Pulling velocity on the bond
V_{deb}	Debonding rate
W_a	Work of adhesion
w_{amino}	The weight fraction of amino acid in gelatin

AFM	Atomic force microscopy
CLAG	CrossLinking and grating
DN	Double-network
DSC	Differential scanning calorimetry
ESEM	Environmental scanning electron microscope

FTIR	Fourier transform infrared
LbL	Layer-by-layer assemblies
SEM	Scanning electron microscope
SN	Single-network

General Introduction

Underwater adhesion working on surfaces submerged in aqueous media or in wet conditions are playing an important role in underwater sensors, marine industry, biomedical applications, *etc*. The main challenge is from the existence of water that significantly decreases adhesion performance, resulting in weaker adhesion in water than in air. In order to solve this problem, bioadhesion provides significant inspirations for the development of underwater adhesives. The main strategy to fabricate underwater adhesives usually focuses on the interface/surface binding and bulk cohesion of adhesives. A good interfacial binding ensures the clinging of adhesive, while strong cohesion holds the adhesion and prevent the separation from bulk. However, those two effects addictively and simultaneously contribute to adhesion in general, limiting the understand of their individual contributions.

Recently, our group has developed a model system for studying bioadhesion, which allows to separate the contribution of surface and bulk properties to adhesion by using two independent materials. One material is a thin film of polymer hydrogel (hundreds of nanometers) with controlled chemistry and topography, which is chemically attached onto a solid substrate. The other material is a macroscopic hydrogel (~ mm) with controlled molecular structure and viscoelasticity. Both materials have to be strong and tough to bear underwater tests. Since both materials are crosslinked hydrogel, but with difference in microscopic or macroscopic scale, they have only difference in surface and bulk properties. The model system provides a separate study of surface and bulk contributions on adhesion.

Significant researches about the model system on synthetic systems have been done by previous PhD students in the group: Guillaume SUDRE (Université Pierre et Marie Curie (UPMC) Paris VI, 2011), Jennifer MACRON (Université Pierre et Marie Curie (UPMC) Paris VI, 2014) and Francisco J. CEDANO-SERRANO (Sorbonne Université, 2019). G. Sudre et al. designed a probe tack device for underwater situations, which was able to control pH, ionic strength and temperature (*Soft Matter* 2012, 8, 8184-8193). The measuring conditions, such as contact time and debonding velocity, have significant influences on adhesion. J. Macron et al. studied the effect of hydrogel equilibration on adhesion (*Macromolecules* 2018, 51, 7556–7566). The adhesion energy systematically decreased as the gel swelled from as-prepared state to equilibrium, while increased linearly with the elastic modulus of the gel. F. J. Cedano-

Serrano et al. used the model system to study the relationship between molecular structure and work of adhesion (*Macromolecules* 2019, 52, 3852−3862). The work of adhesion increased with the decrease in elastic modulus and can be modeled semi-quantitatively. Those researches were about synthetic materials, of which the chemical structure and physical chemistry properties are easy to be controlled. In order to understand underwater bioadhesion process, biosourced polymer model systems are developed here, in which the hydrogel thin film mimics biosurfaces while the bulk hydrogel mimics biotissues and bioadhesives.

In this manuscript, model systems are used for the study of separated contribution of interface interaction and bulk cohesion to adhesion properties. The first model system uses gelatins to mimic the chemical structure of biosystems, as gelatin is a representative biopolymer containing amino acids. Gelatin type A and type B with different isoelectric points are chosen to synthesize macroscopic hydrogels and thin films, respectively. The gelatin films are synthesized by Cross-Linking and Grafting (CLAG) strategy to have both thermal and interfacial stabilities. The network structure of macroscopic hydrogels is controlled by physical and chemical crosslinks. Underwater adhesion between the film and bulk hydrogel is measured using the home-made probe tack setup. The mechanisms of macroscopic bioadhesion are put in perspective with the microscopic structure and physico-chemistry of biomaterials. Related work is in Chapter 2 and 3, of which **Chapter 2** generally discusses about the architecture and physical chemistry of gelatin films/coatings. The Chapter 2 also includes a work in collaboration with Oticon Medical company for the development of new materials for surgical implants. I had the opportunity to supervise the M2 master interns, Alexandre TAOUM (year 2019), Esther LEITAO (year 2020) and Léa MILENKOVIC (year 2021). On the other hand, **Chapter 3** studies the relationship of underwater adhesion and microscopic structure of gelatin hydrogels. This work was partially carried out in collaboration with Francisco J. CEDANO-SERRANO, in particular for the study of the properties of both gelatin A and B (including molecular weight, concentration of carboxylic acids and amino groups by titration), synthesis of gelatin B films and gelatin A macroscopic hydrogels and the streaming potential measurements of thin films.

The other model system is for the focus on surface topography effect on adhesion. The topography is controlled by lithography, with hexagon patterns of size of 20-200 μm. The underwater adhesion is studied with a strong and tough biopolymer hydrogel with kappa-carrageenan. Related work is in **Chapter 4**. Ene-functionalized PDMAEMA is synthesized with the help of Dr. Ekkachai MARTWONG who is currently an assistant professor in

Rajamangala University of Technology Suvarnabhumi (Thailand). A part of this work was made by co-supervising the M2 internship of Junhao MA (year 2022).

This manuscript contains four chapters. The **Chapter 1** is an overview of bioadhesion and underwater adhesives from the view of interface interactions and bulk cohesion. The **Chapter 2** reports the fabrication of surface-attached gelatin coatings on various substrates. The **Chapter 3** is about the study of underwater adhesion between gelatins. The **Chapter 4** reports underwater adhesion between a strong biopolymer hydrogel and a substrate grafted with periodical microscopic patterns. The **Chapter 2** and **Chapter 3** are written in formats of "articles". **Chapter 4** is in a template of "communications". The last three chapters contain related supporting information after each of them.

In **Chapter 1**, there is an overview from bioadhesion in nature to bioinspired underwater adhesives developed artificially. The objective of this first chapter is to provide a general overview of adhesion in aqueous environments by presenting the essential aspects related to bioadhesion, underwater adhesives, and the different measures of underwater adhesion. There is a general introduction to bioadhesion and underwater adhesives, noting the main challenges related to the presence of water and giving some examples of bioinspired artificial adhesives developed to overcome this problem. Since interfacial bonding plays an important role in adhesive bonding, while bulk properties determine how well an adhesive can resist to deformation, the different strategies used to design adhesives in aqueous media will be discussed separately, focusing on interface and bulk properties. Similarly, several widely used methods for adhesion measurements in aqueous media are introduced and compared. Since both surface adhesion and volume cohesion contribute to adhesion performance, some model systems are studied by separating surface and volume properties independently. In order to have a better understanding of the bioadhesion process, the objective of this thesis was to develop biopolymer-based model systems, with well-controlled structure and physicochemical properties, to study adhesion properties in aqueous media under controlled environments: temperature, pH, ionic strength.

Chapter 2 describes a simple and easy approach to building grafted biopolymer coatings on various substrates that could have potential applications in the fields of biotechnology and biomedicine. Biopolymer coatings are thin layers of chemical networks of gelatin hydrogels attached on substrates, with good chemical and thermal stability. Gelatin hydrogel coatings are synthesized using the CLAG (Cross-Linking and Grafting) strategy, which consists of

simultaneous crosslinking and surface grafting of gelatin chains via peptide bonds. The CLAG strategy is performed on different substrates such as flat silicon surfaces and silicon microfibers. The thickness of the coatings can vary over a wide range from a few nanometers to several micrometers, by changing the coating parameters or by using a multilayer strategy. The physicochemical properties are finely characterized, such as the swelling of the hydrogel coating which is controlled by the concentration of the chemical crosslinking reagent and the aqueous conditions. The biodegradation properties of the coatings are also studied. Finally, gelatin coatings have been shown to be a very efficient platform for the delivery of drugs such as dexamethasone.

In **Chapter 3**, since studying the relationship between molecular structure, viscoelasticity and adhesion properties of biosystems is important for building bioinspired underwater adhesives. In this work, gelatins have been used to fabricate a model system that allows the separation of surface and bulk contributions to adhesion. The underwater adhesion of macroscopic gelatin type A hydrogels against surface-attached microscopic gelatin type B thin films has been studied. The molecular structure and viscoelasticity of macroscopic hydrogels are controlled by an additional chemical network on physical gelatin network of triple-helices, to study their contributions on underwater adhesion. The results show that at low temperature, the work of adhesion increases with the level of physical crosslinks (increase of the polymer volume fraction and shear modulus), while it decreases with the increasing contribution of chemical crosslinks studied at high temperature. The chemical contribution on adhesion energy is predicted by Chaudhury's model with the key parameters such as the interface interaction surface density and the number of monomers between crosslinks. We also find that the additional chemical crosslinks reduce the physical crosslinking density without disturbing the underwater adhesion energy. This work provides the relationship between microscopic structure of gelatin hydrogels and macroscopic underwater adhesion performance, giving inspirations for designing bioadhesives.

In **Chapter 4**, we report reversible underwater adhesion between a biopolymer-based hydrogel double-network and a surface grafted with hydrogel microstructures. This study with two model systems designed from biosourced and biocompatible polymers allows to understand the mechanisms of underwater bioadhesion by separating the contributions of volume and surface to the adhesion, in particular by determining the effect of the surface topography on the adhesion properties. The molecular interactions are finely controlled by electrostatic complexations between the negatively charged adhesive and the positively charged surface. The

adhesive is a tough double-network structure containing a physical network based on kappa-carrageenan and agarose biopolymers and a chemical network of poly(dimethylacrylamide). The surface is grafted with microscopic hexagonal poly(2-(dimethylamino)ethyl methacrylate) (PDMAEMA) hydrogel structures patterned by photolithography. The adhesive properties between the double-network and the surface are measured in water by a home-made experimental probe-tack device. The effects of topography (hexagonal structure size) and aqueous environment (pH and ionic strength) on the adhesion are investigated. This work could give inspirations for designing bioadhesives.

Chapter 1

From Bioadhesion to Underwater Adhesives

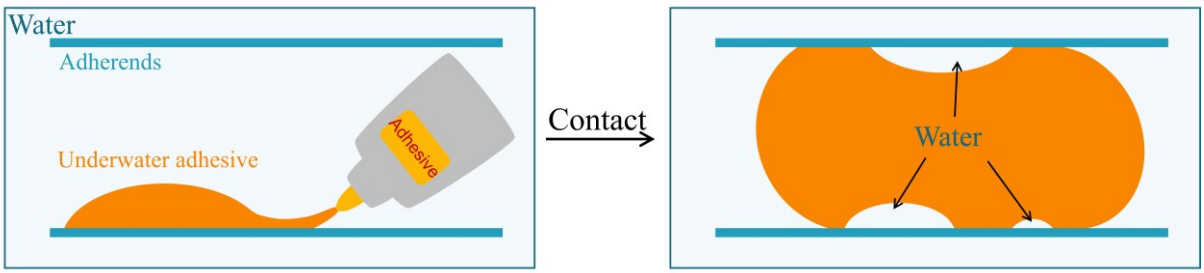

Gluing underwater adhesive

Adhesive-substrate interface

Abstract

Underwater adhesives play an important role in our daily lives, but the presence of water severely limits their development and applications. Taking inspirations from nature, i.e. understanding and mimicking bioadhesion processes, is fundamental for the design and development of tough adhesives in aqueous media. The objective of this first chapter is to provide a general overview of adhesion in aqueous environments by presenting the essential aspects related to bioadhesion, underwater adhesives, and the different measures of underwater adhesion. **Section 1** is a general introduction to bioadhesion and underwater adhesives, noting the main challenges related to the presence of water and giving some examples of bioinspired artificial adhesives developed to overcome this problem. Since interfacial bonding plays an important role in adhesive bonding, while bulk properties determine how well an adhesive can resist to deformation, the different strategies used to design adhesives in aqueous media will be discussed separately, focusing on interface (**Section 2**) and bulk properties (**Section 3**). Similarly, several widely used methods for adhesion measurements in aqueous media are introduced and compared (**Section 4**). Since both surface adhesion and volume cohesion contribute to adhesion performance, some model systems are studied by separating surface and volume properties independently (**Section 5**). In order to have a better understanding of the bioadhesion process, the objective of this thesis was to develop biopolymer-based model systems, with well-controlled structure and physicochemical properties, to study adhesion properties in aqueous media under controlled environments: temperature, pH, ionic strength (**Section 6**).

Résumé

Les adhésifs en milieu aqueux jouent un rôle important dans notre vie quotidienne, mais la présence d'eau limite sérieusement leur développement et leurs applications. S'inspirer de la nature, c'est à dire comprendre et imiter les processus de bioadhésion est fondamental pour la conception et le développement d'adhésifs robustes en milieu aqueux. L'objectif de ce premier chapitre est de donner un aperçu général de l'adhésion dans les environnements aqueux en présentant les aspects essentiels liés à la bioadhésion, les adhésifs en milieu aqueux et les différentes mesures d'adhérence en environnement aqueux. La **Section 1** est une introduction générale sur la bioadhésion et les adhésifs en milieu aqueux, faisant état des principaux défis liés à la présence de l'eau et donnant quelques exemples d'adhésifs artificiels bioinspirés développés pour surmonter ce problème. Étant donné que la liaison interfaciale joue un rôle important dans l'accrochage des adhésifs, tandis que les propriétés en volume déterminent la façon dont un adhésif peut résister à la déformation, les différentes stratégies utilisées pour concevoir des adhésifs en milieux aqueux seront discutées séparément, en se concentrant sur l'interface (**Section 2**) et les propriétés en volume (**Section 3**). De même, plusieurs méthodes largement utilisées pour les mesures d'adhérence en milieu aqueux sont introduites et comparées (**Section 4**). Étant donné que l'adhérence de surface et la cohésion en volume contribuent toutes deux aux performances d'adhésion, certains systèmes modèles sont étudiés en séparant indépendamment les propriétés de surface de celles du volume (**Section 5**). Afin d'avoir une meilleure compréhension du processus de bioadhésion, l'objectif de cette thèse a été de développer des systèmes modèles à base de biopolymères, avec une structure et des propriétés physico-chimiques bien contrôlées, pour étudier les propriétés d'adhésion en milieu aqueux dans des environnements contrôlés : température, pH, force ionique (**Section 6**).

Table of Contents

Chapter 1. From Bioadhesion to Underwater Adhesives

1 Adhesion, Underwater Adhesion and Bioadhesion in Nature

1.1 Adhesion and Underwater Adhesion

Adhesives are playing an important role in our daily lives, because of the wide applications in modern industry and biomedicine. A material holding surfaces of two separate items that binds them together and resists their separation is called an adhesive. Adhesion refers to the tendency of an adhesive to cling to the adherends.

Although working on dry solid surfaces and in the dry state is the most commonly case, adhesives working on surfaces submerged in aqueous media or in wet conditions are more attractive in underwater sensors,[1-5] marine industry,[6-8] biomedical applications,[9-14] *etc*.[15] However, the existence of water significantly decreases adhesion performance, resulting in weaker adhesion in water than in air. One of the negative water effects comes from the interface, where a hydration layer forms on the surface of materials inside aqueous environments. At the molecular scale, the formation of a hydration layer prevents the bridging and bonding between adhesive and adherends and can compete with the interfacial interactions. At the macroscopic level, the presence of a hydration layer also disturbs the actual contact area between the surfaces. Moreover, the other reason comes from the bulk of an adhesive, in which water molecules permeate into the adhesive, causing plasticization, swelling, erosion, degradation or hydrolysis of adhesives, which results in the deterioration of the mechanical properties and bulk cohesion of the adhesive.[16-19] Therefore, facing the challenge of the presence of water, the development of strong underwater adhesives working effectively in aqueous media has been attracting a lot of interests.

1.2 Bioadhesion in Nature

The most common and efficient way to develop underwater adhesives is to take the insights and inspirations from nature. Creatures, especially marine creatures have tremendous strategies to realize underwater adhesion, which is called bioadhesion. They are able to secrete bioadhesives with specific chemical structures or utilize specific microstructures to realize strong and controllable adhesion in variable conditions.

Sea mussels and sandcastle worms are the most investigated creatures for underwater adhesion, bringing a lot of inspirations to create synthetic analogs underwater adhesives. Not

only because they secrete bioadhesives to adhere onto different types of surfaces, but also because their bioadhesives can realize adhesion in sea water, which has a high salinity, a slightly basic pH and changeable temperature.

Sea mussels are well-known to have robust adhesion to wet, salt-encrusted, corroded and slimy surfaces. The adhesion mechanisms of mussels have been well-studied very recently. The mussel foot produces and injects mussel foot proteins (mfps) to form byssal threads, which are thin (~ 0.3 mm) and flexible (**Figure 1a, b**).[20-23] The threads attach to various surfaces, including stone, wood, concrete, shell and iron, by their ends which are called byssal plaques. The byssal plaque generates from the solidification of mfps by metal chelation, of which the metal ions (iron and vanadium ions) come from sea water and are stored in intracellular metal storage particles. The mfps are rich in 3,4-dihydroxypolyalanine (DOPA), which gives a strong bond to almost any type of material surface by forming either non-covalent interactions or covalent interaction to different substrates.[24-27] Not only chemistry, but also the architecture of the plaques is important for underwater adhesion performance. The byssal plaque is observed to be a fiber-reinforced porous solid expected to toughen structural adhesives by stopping cracks, enabling reversible deformation and increasing energy dissipation (**Figure 1c**).[28]

On the other side, *phragmatopoma californica*, commly known as sandcastle worm, constructs protective shells as its "home" by gluing mineral particles together with proteinaceous glue (**Figure 1d-f**). The adhesive works very fast (~ 30 s) and is stable in sea water, which brings a lot of inspirations to build underwater adhesives. Sandcastle worm glue mainly contains different types of adhesive proteins with opposite charges. The proteins have at least 10% aromatic amino acids residues, which contain tyrosine and tyrosine hydroxylase (known as DOPA). DOPA originates from the post-translational modification of tyrosine by tyrosinase. Those components in sandcastle worm glue are secreted and stored separately in different types of secretory granules inside the adhesive glands. The bioadhesive is initially fluid but rapidly solidifies after the mixture of oppositely charged components is exposed in sea water, generating complex coacervates, which is self-supported in turbulent environments.[29] Firstly, the solidification comes from the change in pH from acidic gland to slightly basic sea water, causing the complexation between polysulfates and magnesium ions (Mg^{2+}) initially from the preorganized adhesive modules.[30-31] Secondly, the increase in pH changes the metal ion content, by forming stronger complexation with multivalent ions from sea water (including calcium, ferric, manganese and zinc ions).[25, 32] Those metal ions are able to form ionic bonds or to coordinate with DOPA. Lastly, catechol oxidase remains active after the glue is fully cured.

Over a longer time range from several hours to several days, the enzyme catechol oxidase oxidizes DOPA into DOPA-quinone, subsequently leading to the formation of covalent bonds that contribute to the cohesion of the adhesive.[33-34] The sandcastle worm glue after curing has a foam-like structure, providing its ultimate cohesive strength (**Figure 1f**).[35-36]

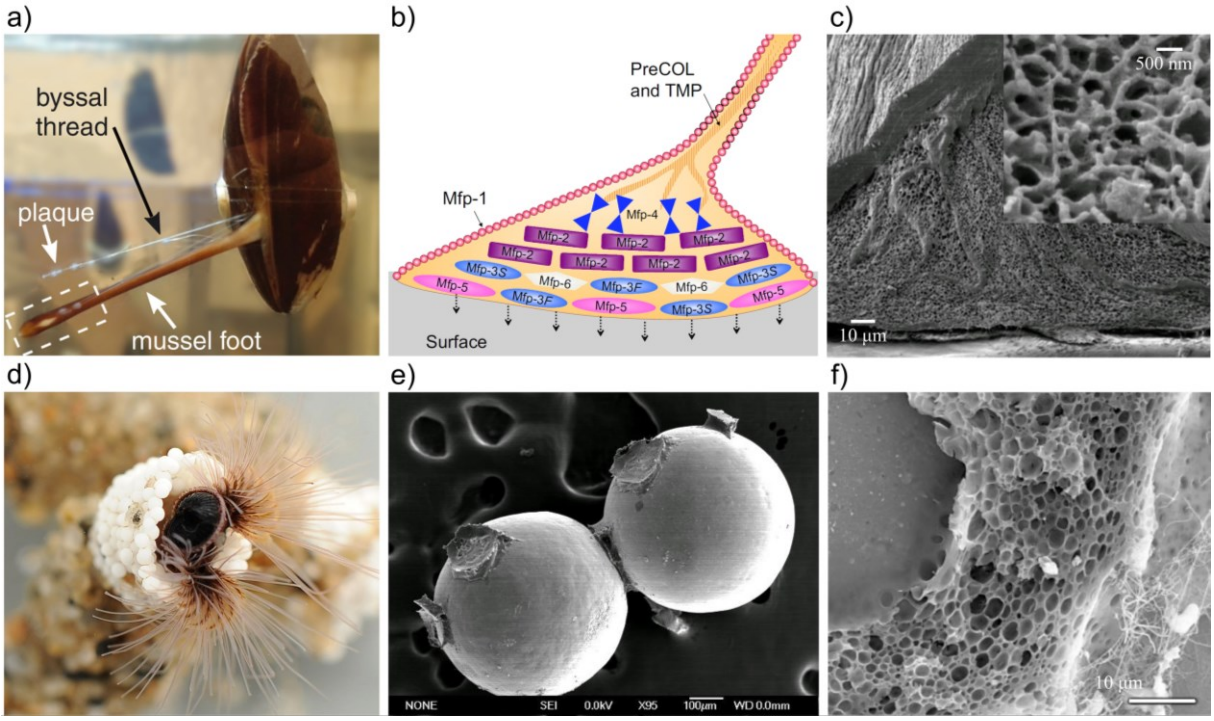

Figure 1. Bioadhesion of sea mussels and sandcastle worms. a) Photography of a sea mussel as well as its foot, byssal thread and plaque. Photo from Priemel et al.[37] b) Schematic representation of the distribution of known proteins in the byssal thread and plaque. Figure from Waite et al.[28] c) SEM image of cross-section of byssal plaque. Figure reproduced from Waite et al.[28] d) Photography of a sandcastle worm making a tube out of sand (yellow) and beads of zirconium oxide (white). e) SEM image of intact sandcastle worm glue on beads removed from a reconstructed tube. f) Cross-section of sandcastle worm glue made by lyophilization. Figures from Stewart et al.[35]

Although the adhesives of sea mussels and sandcastle worms have different characteristics, they have very similar strategies based on DOPA, which is considered to play a dominant role in both surface binding and adhesive cohesion. DOPA can interact covalently or non-covalently with both the surface and other moieties inside the adhesive, mainly through H-bonding, electrostatic interaction, π–π interaction, cation–π interaction, metal coordination and disulfide bond (**Figure 2**).[17] This wide range of interactions increases the versatility of their adhesives

against different substrates and under different conditions, enabling those creatures to adhere to multiple surfaces.

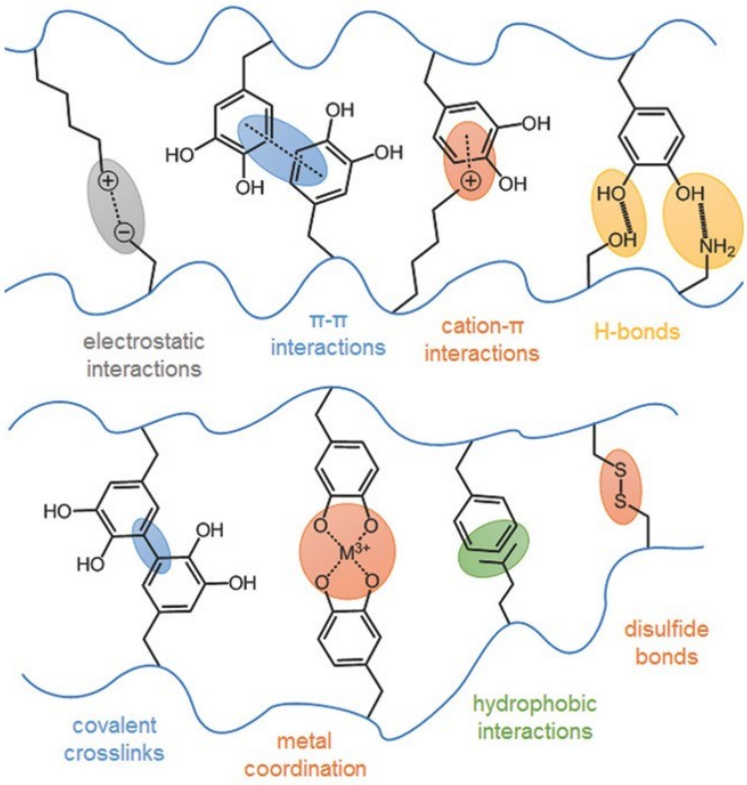

Figure 2. An overview of some DOPA-based molecular interactions found or hypothesized for wet adhesion (surface or cohesion) by sea mussels and sandcastle worms. Figure from Hofman et al.[17]

Another types of aquatic creatures use specialized micro/nanostructures to realize temporary underwater adhesion. Remora, which is also called suckerfish, attaches itself to a bigger fish for transportation, protection and food reasons. The attachment is by using a suction disk located on the top of its head (**Figure 3a**), which is capable of attaching to surfaces of varying roughness and stiffness even under high shear conditions.[38] By physical suction, it is able to adhere to various surfaces, to avoid the drawbacks of molecular interactions. The suction disk could be divided into three large parts: lip, lamellae and spinule (**Figure 3b**). The lamella is deformed actively to generate pressure difference between the inside and outside of the suction disk. The lip maintains the sealing. The spinule with hairs of diameter ~ 300 μm enhances the frictional force, minimizing the sliding motion in the contact area between the suction disk and the host from the horizontal drag force of water.[39-40]

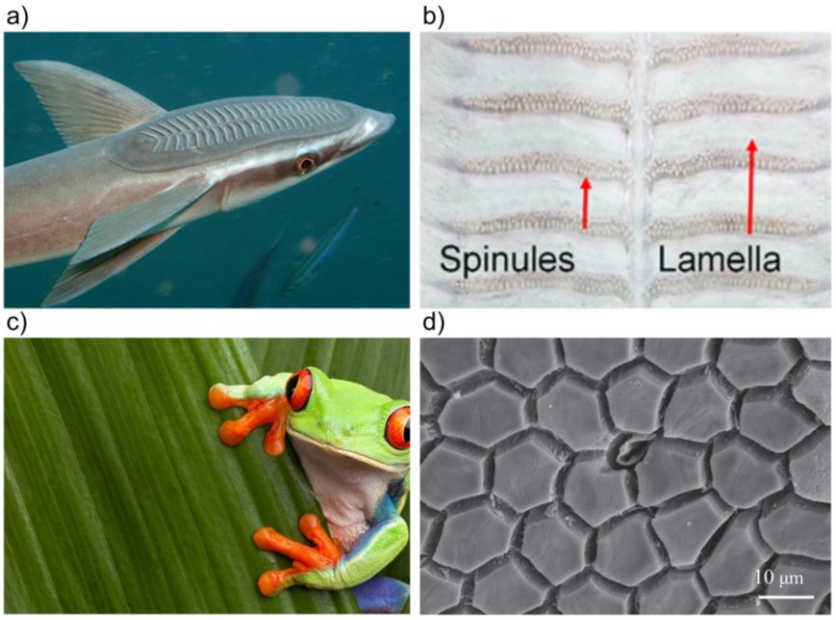

Figure 3. Microstructure of remora and tree frog. a) Photography of a remora. b) Structure of remora's suction disk. Figure from Lee et al.[39] c) Photography of a tree frog on a leaf. d) SEM image of polygonal epithelial cells of staurois parvus. Figure reproduced from Drotlef et al.[41]

The tree frog climbs flexibly on wet plant blades and jumps freely between leaves in wet environments (**Figure 3c**). The main adhesion mechanism is expected to be capillarity and Stefan adhesion,[16] which could come from the toe pads with protuberant polygonal epithelial cells (**Figure 3d**). The channels between the cells and nanopillars accelerate the drainage of excess water and reduce hydrodynamic repulsion.[41-45] So when a tree frog attempts to attach onto the wet surfaces, those microstructures promote the formation of contact. Moreover, the mucus on the surfaces of toe pads secreted by the mucous glands also plays an important role during adhesion. As a wetting agent, the mucus is spread in the channels on the pad surfaces to help the removal of water at the contact area.[43, 46] The secreted mucus also has self-cleaning ability to shed surface contaminants, to have recoverable adhesion.[47]

Creatures have very complex and elegant strategies to realize underwater adhesion. They basically focus on two main effects: surface or interface between adhesive and adherend, and the cohesion in the bulk of the adhesive. It is important to mimic those strategies inspired by biosystems, to build artificial underwater adhesives. Both interfacial adhesion and bulk cohesion is important for strong adhesion. When an adhesive is detached from the substrate, the scission of the interfacial binding gives a work of adhesion Γ_0. Meanwhile, the detaching inevitably generates deformations of bulk adhesive to dissipate mechanical energy, giving a further contribution of Γ_D, which can depend or be proportional to Γ_0.[48-51] Assuming that the

mechanical dissipation of adherends and friction on the interface are neglected, the total adhesion energy (Γ) is

$$\Gamma = \Gamma_0(1 + \Gamma_D) \quad (1)$$

As an intrinsically collective contribution to adhesion energy, the two effects are coupled and not independent. Further and systematical study about the independent effect of surface and bulk is relevant for understanding and development of underwater adhesives. Most underwater adhesives scientifically realize adhesion by synergistic contribution of interface interaction and bulk cohesion, but in this overview we will consider the most important contributions. In the **Section 3** and **Section 4**, a systematic overview of bioinspired underwater adhesives from the perspective of surface and bulk is provided, respectively.

2 Bioinspired Underwater Adhesives Focusing on Interfaces

Since the fundamental purpose of an adhesive is to bind two separate items together, surfaces or interfaces between adhesive and adherend is a key parameter in the design and construction of underwater adhesives. As described in **Equation 1**, Γ_0 and Γ_D both and together contribute on adhesion energy. Some underwater adhesives target surface properties to improve underwater adhesion, by changing interfacial molecular interactions, using physical suctions for attraction and to dehydrate the interface.

2.1 Types of interfacial molecular interactions

A simple way to enhance adhesion to increase the real density or the strength of molecular interactions between adhesives and adherends. In the case of bioadhesion, especially if we consider adhesives working for various substrates and conditions, multiple non-covalent interactions collectively contribute to interfacial binding. In real, it is difficult to generate enough adhesion by only single non-covalent bond, because they are vulnerable upon environmental change (e.g. ionic strength, pH change, temperature). It is also difficult to separately discuss the interfacial and cohesive role of bonds in adhesives, as a given type of bond usually exists in both interface and bulk. In this **Section 2.1**, representative molecular interactions including non-covalent and covalent bonds for the construction of adhesives are described as interfacial interactions. Their contributions on cohesive properties are discussed in **Section 3**.

Although all molecular interactions are fundamentally electrostatic in nature and can be described by some variation of Coulomb's laws, in this manuscript, the "electrostatic interaction" here refers to the interaction between formally charged species. Interactions between partial charges are referred to by other names. Covalent bond refers to the interatomic linkage that results from the sharing of an electron pair between two atoms. Those molecular interactions, such as hydrogen bond, electrostatic interaction, hydrophobic association and covalent bond, display different bond energies and specific advantages that have been used to design underwater adhesive interfaces.

2.1.1 Non-covalent bonds

Hydrogen bond is a short ranged and directional interaction between a hydrogen atom which is covalently bound to a more electronegative atom or group, and another electronegative atom bearing a lone pair of electrons which is the hydrogen bond acceptor. Because of the reversibility of the hydrogen bond, it has been used to design synthetic adhesives. A simple hydrogen bond is weak (10-40 kJ mol^{-1})[52] and intermolecular hydrogen bonds can be strongly weakened by the existence of water molecules, indicating that simple hydrogen bonds do not fit the condition for underwater adhesion. Even in mussels and sandcastle worms, hydrogen bonds only partially contribute to the strong surface bonding via DOPA. The catechol group on DOPA also undergoes other interactions such as metal coordination and covalent bonding. Therefore, using only hydrogen bonding to design underwater adhesives presents an inherent difficulty, especially when it comes to establishing strong interactions at interfaces.

Electrostatic interactions take place among charged species and can be either attractive or repulsive, depending on the signs of the charges. In adhesion science, electrostatic interactions are usually attractive, and also play an important role in the adhesive processing and performance of mussels and sandcastle worms. The strength of electrostatic interactions can be controlled by ionic strength or by the pH of the aqueous solution, thus, the adhesion realized by electrostatic interactions in water is tunable. However, electrostatic interactions are diminished in highly concentrated salt solutions,[52] such as in sea water and also under physiological conditions relative to pure water.

Hydrophobic associations are important in marine adhesives. For example, the sandcastle worm glues are expected to promote the formation of coacervates by hydrophobic association. The hydrophobic groups in mussel proteins protect DOPA against oxidation and reinforce the

plaque by hydrophobic association and hydrogen bond (**Section 1.2**). An interesting strategy involving hydrophobic associations to build underwater adhesive is supramolecular host-guest chemistry (also called host-guest recognition). The "host" is a macrocycle with a hydrophilic external shell and a hydrophobic internal pocket. The external hydrophilicity enables its solubility in polar solvents, while the hydrophobicity of the pocket promotes the accommodation of nonpolar guest molecules. The hydrophobic association is one of the most important driving forces for interaction between host and guest molecules.[53] Harada and co-workers introduced cyclodextrins (CDs) into polymer materials.[54-56] Covalently crosslinked polyacrylamide hydrogels were separately functionalized by β-CD host and adamantane (Ad) guest side groups. Good adhesion strength (~ 5.1 MPa) was reached by dropping a thin water layer between host and guest gels (**Figure 4a**).[57] Ahn et al. used host molecules cucurbit[7]uril (CB[7]) and guest molecules aminomethylferrocene (Fc) to functionalize two separate silicon surfaces, obtaining a "loop" and "hook" surface, respectively (**Figure 4b**).[58] The CB[7] loop surface and Fc hook surface formed a velcro-like structure, showing strong but reversible adhesion in water. The lap shear adhesion strength reached 1.12 MPa. Moreover, the chemically switchable adhesion could be achieved by changing the valence state of the Fc guests. The oxidation of Fc into Fc^+ decreased the binding affinity to CB[7], weakening the adhesion. There is a good reversibility and selectivity of host-guest adhesives, but they cannot be used as a universal glue, because the adhesion strongly depends on surfaces with specific functional groups.

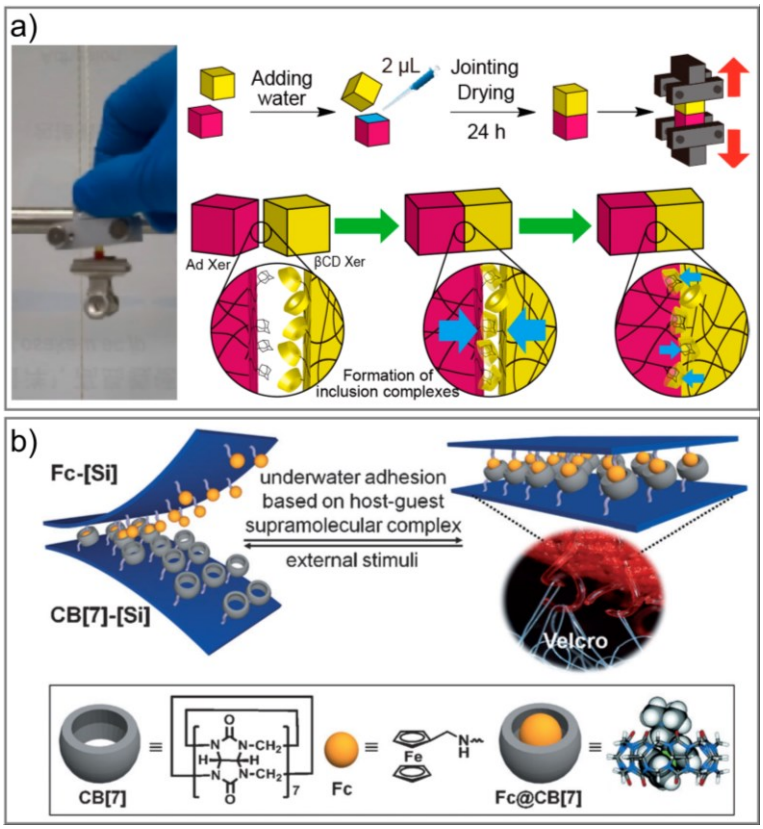

Figure 4. Underwater adhesives based on supramolecular host-guest chemistry. a) Adhesion between β-CD host and adamantane (Ad) guest hydrogels. Figure reproduced from Kakuta et al.[57] b) "Velcro" with two surfaces modified by CB[7] and Fc. The adhesion is mechanically and chemically reversible. Figure from Ahn et al.[58]

Those non-covalent bonds have complex contributions to the interfacial interactions of adhesives to various surfaces, but the contribution of each of them is still not well-quantified. Meanwhile, as reversible and dynamic bonds, they are also widely used in the bulk of adhesives to increase the strength and reversibility of bulk cohesion, which is discussed in **Section 3**.

2.1.2 Covalent bond

When two or more atoms come together to form a molecule, the forces that tightly bind the atoms together within the molecule are called covalent forces, and the interatomic bonds formed are called covalent or chemical bonds.[52] Covalent bonds are commonly strong (C-C bond strength is ~ 360 kJ mol^{-1}) and irreversible, so even in nature, both sea mussels and sandcastle worms partially use covalent bonds to realize adhesion. Therefore, it is possible to realize extremely strong adhesion with covalent bonds. Yuk et al. developed tough bonding of hydrogels onto diverse surfaces, by incorporating covalent bonds at interfaces.[49] The tough

hydrogels were double network, with polyacrylamide (PAAm) or polyethylene glycol diacrylate (PEGDA) as the second network. The substrates were glass, silicon wafer, titanium, aluminium and mica ceramic, modified by 3-(trimethoxysilyl) propyl methacrylate (TMSPMA) (**Figure 5a**). The second network was covalently crosslinked to the silanes on the surfaces, to form covalent bonds at the interface. Moreover, for underwater cases, the equilibration of the hydrogel anchored on various substrates in pure water didn't change the adhesion obviously. The strong interfacial interaction as well as the toughness of double network hydrogel collectively contributed to the adhesion energy (**Figure 5b**).

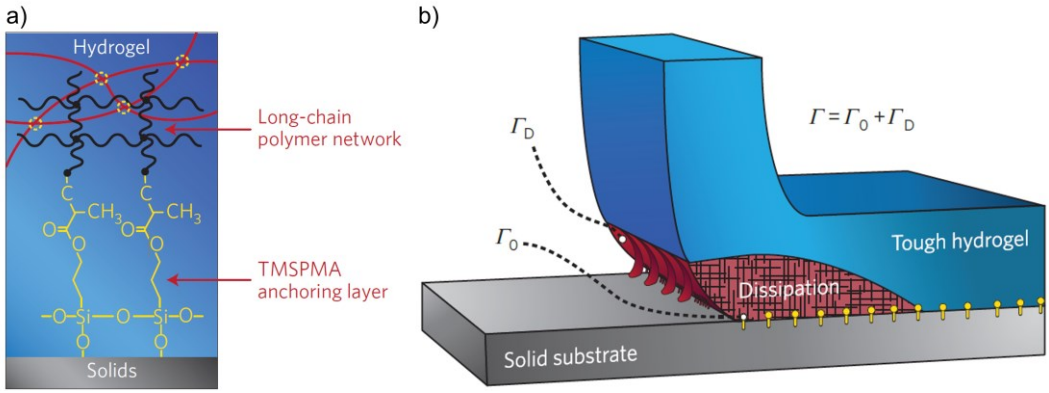

Figure 5. Adhesion of hydrogels to surfaces by covalent bonds. a) Chemistry at the interface between hydrogel and substrate. b) The chemical anchoring gives a relatively high intrinsic work of adhesion Γ_0, while the energy dissipation capability of hydrogels further contributes to the total interfacial toughness by Γ_D. Figures from Yuk et al.[49]

Typical covalent bonds are strong but fail irreversibly, limiting the balance between strength and reversibility of adhesives. This could be improved by dynamic covalent bonds, such as disulfide bridges, imines and Diels-Alder chemistry. The bonding or debonding of dynamic covalent bonds could be triggered by external stimulus, similarly to non-covalent bonds.[59] Deng et al. designed an interfacial adhesion between two gels by acylhydrazone bonds.[60] The two original gels were a hydrogel and an organogel with the same integrated structure, which were both poly (ethylene glycol) (PEG) with acylhydrazone bond as crosslinking point in the networks (**Figure 6a**). When the two gels were brought into contact, an adhesion between two gels was obtained in 10 min, with a tensile strength of ~ 60 kPa. At the interface, an emulsion layer that rapidly formed after the contact of water and oil phases was a key point for adhesion, because the layer accelerated the growth of a dynamic polymer networks across the interface through dynamic acylhydrazone bonding (**Figure 6b**). Although most dynamic covalent bonds

are not suitable for reversible underwater cases, they still give an important inspiration for strong and reversible adhesion.

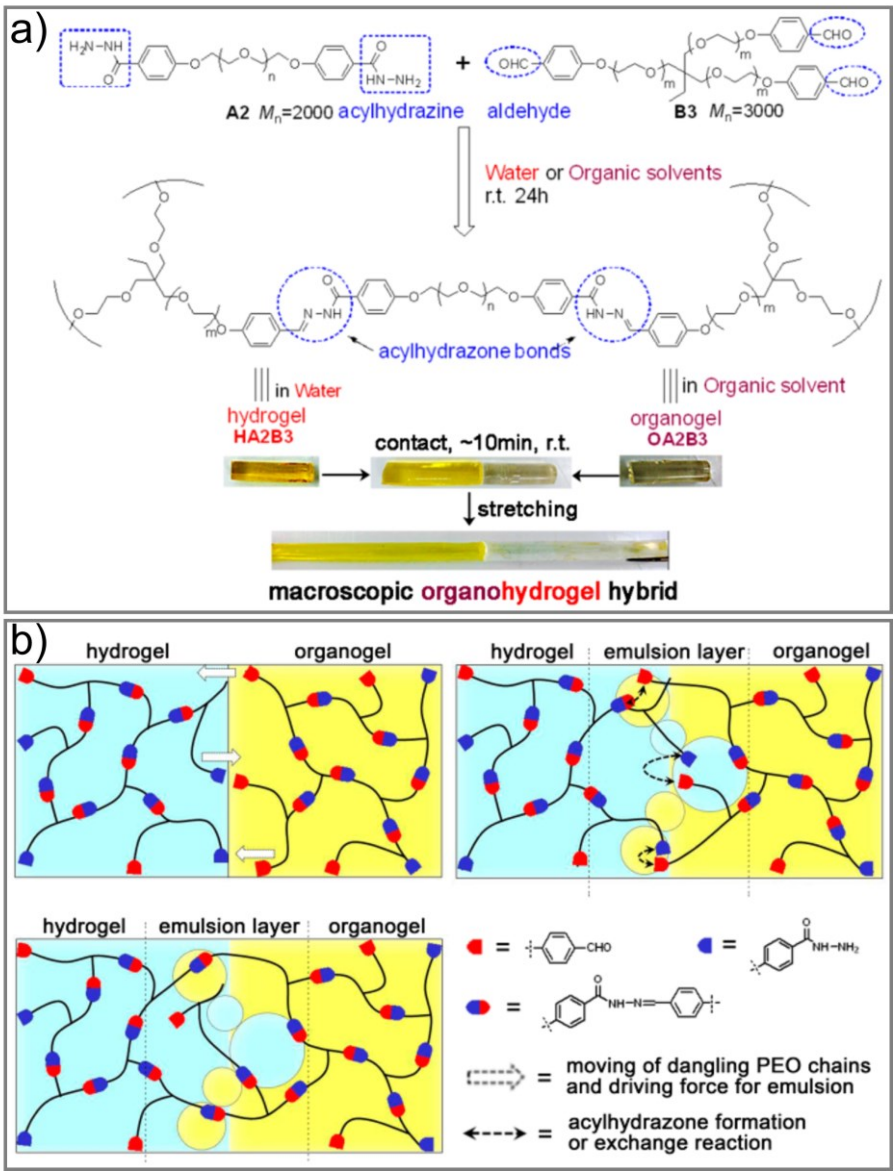

Figure 6. Adhesion between a hydrogel and an organogel by dynamic covalent acylhydrazone bonds. a) Preparation of hydrogel and organogel with the same polymer network crosslinked by acylhydrazone bonds. The organic solvent of the organogel was anisole. b) The presence of an emulsion layer was found as a crucial factor for strong adhesion. Figures reproduced from Deng et al.[60]

2.1.3 Catechol chemistry

Recently, there have been significant improvements in the study of mussel adhesion as well as mussel-inspired catechol chemistry to design underwater adhesives. Since the catechol group

can form strong bonds with various substrates in water, catechol chemistry is equally important for both surface adhesion and bulk cohesion. In **Section 1.2**, the DOPA-based molecular interactions were shown in **Figure 2**. Further studies show that catecholic amino acid widely exists in mfps and the molecular interactions stem from dopamine and other analogues (**Figure 7**). Generally, the catechol groups form a strong surface adhesion and cohesion by a combination of various covalent and non-covalent interactions. The covalent interactions are based on the DOPA-quinone crosslinking, which results from the oxidation of catechol groups to reactive *o*-quinones.[24, 61-63] The non-covalent interactions include metal coordination, hydrophobic interactions, cation–π interactions, and hydrogen bonds.[64-76] The catechol chemistry simultaneously contributes to interfacial strength and cohesion. As there are a lot of adhesives based on catechol chemistry, which are incorporated in different kinds of materials, they will be discussed in relative sections with specific materials. In the following paragraphs, some examples of building underwater adhesives focusing on the interface are introduced.

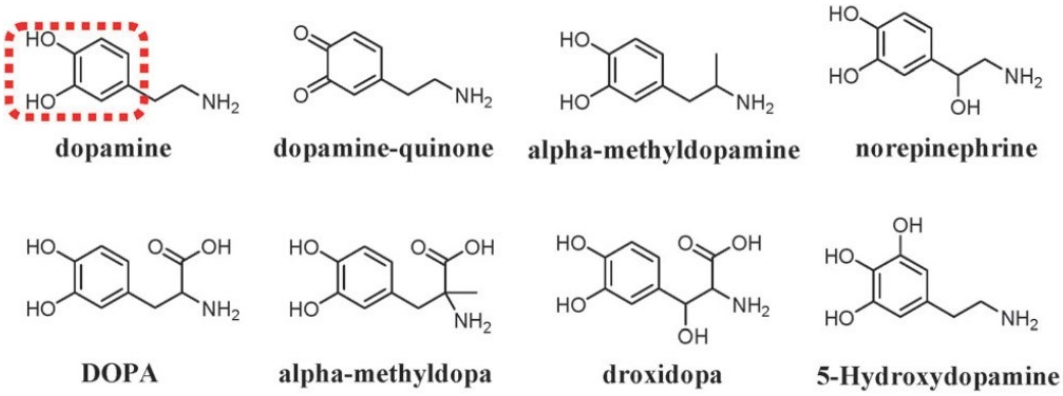

Figure 7. Chemical structure of dopamine and its analogues. Figure from Ye et al.[77]

Based on catechol chemistry, some polyphenolic polymers with catechol or gallol groups have been synthesized as underwater adhesives (**Figure 8**). The polymer structure influences the adhesion strength. Firstly, an optimized molecular weight is important for increasing adhesion strength.[78] Because low molecular weight promotes effective wetting of the adherends, while higher molecular weight is usually positive for enhancing the cohesion through chain entanglement, there is an optimum molecular weight for DOPA-based polymer adhesives. Secondly, the type of phenolic compounds including phenol, catechol and gallol also influences adhesion properties.[79-80] Gallol-based polymers have much higher adhesion than catechol-based polymers because the tridentate-related interactions are stronger and more stable than bidentate- and monodentate-related interactions. Moreover, the chemical structures also influence the adhesion performance of DOPA-based polymers. For example, the ionic groups (cationic or

anionic) on side chains can improve adhesion through ionic, coordinate or hydrogen bond.[81-82] In addition, the underwater adhesion strength increases with the increase in polarity of polymer backbones.[83]

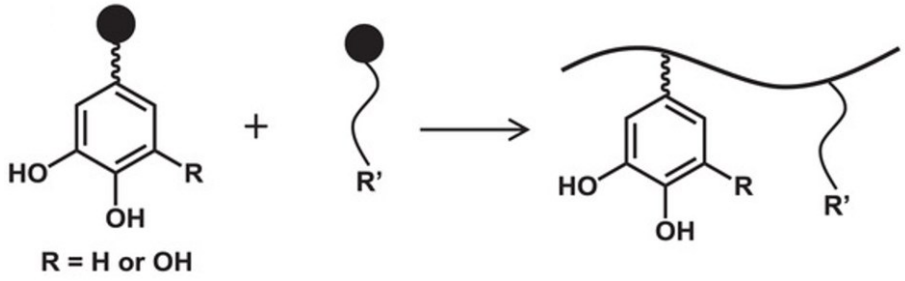

Figure 8. Catechol-based polymer adhesives by incorporation of catechol (R = H) or gallol (R = OH) group onto polymer chains. Figure from Fan et al.[18]

Some DOPA-based adhesives have been developed to have strong underwater surface adhesion. Ahn et al. functionalized low-molecular-weight zwitterionic surfactants with two short aliphatic carbon tails, with a catechol unit at the end of one tail (**Figure 9**).[84] In this molecule, the increase in hydrophobicity by carbon tail leads to a decrease in solubility and promotes resistance to catechol oxidation.[85] Adhesion could be further improved via covalent crosslinking of the catechol groups through oxidation. Adhesion was measured by the surface force apparatus (SFA, introduced in **Section 4**) and atomic force microscope (AFM, introduced in **Section 4**) with a silicon dioxide particle probe. The oxidized molecule has an increased underwater adhesion energy with increasing oxidation time, which is over 40 mJ m^{-2}. As shown in **Figure 9**, a double bilayer mechanism is expected for adhesion, in which one bilayer is formed by the attachment of the molecule to the surface by catechol groups through hydrogen bonding, while the other end with aliphatic carbon tails forms hydrophobic associations with the second layer. During contact, the outer catechol groups on the bilayer can form hydrogen bond with the other surface, resulting in a double bilayer.

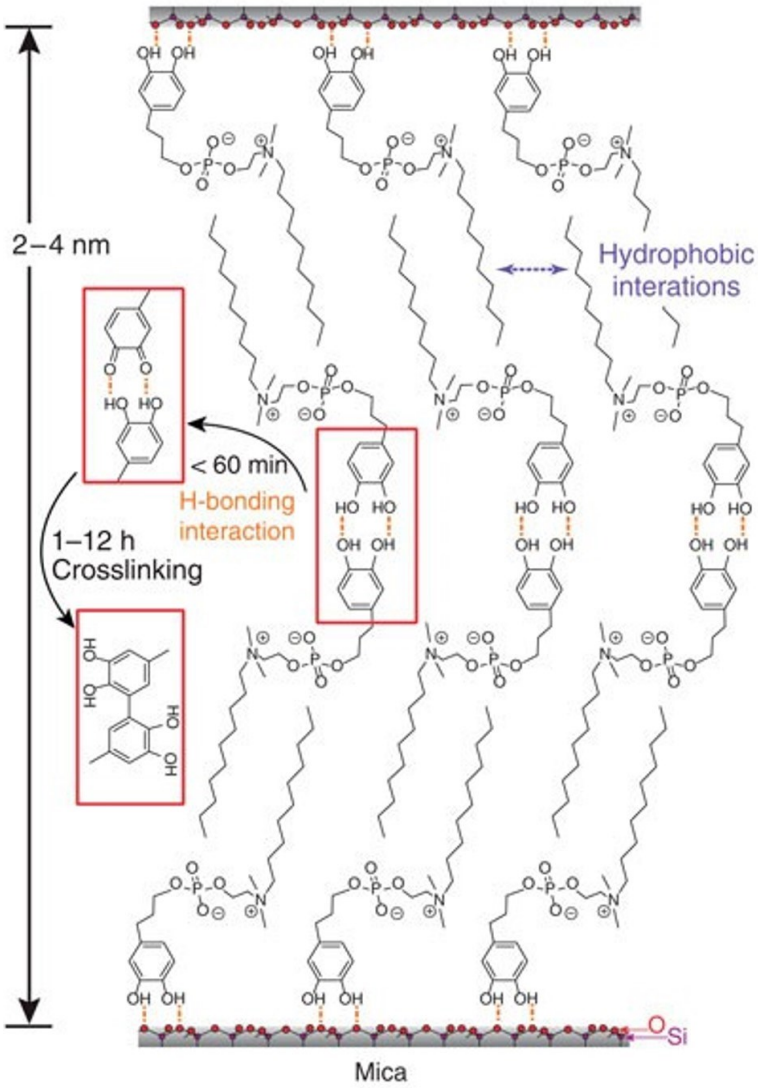

Figure 9. A surfactant of amphiphilic zwitterions as adhesive. Scheme of the double bilayer mechanism, realized by hydrogen bond and hydrophobic association. The adhesion was further improved by covalent crosslinking through DOPA oxidation. Figure from Ahn et al.[84]

2.2 Surface modification for physical suction

The presence of water at interfaces generally reduces the actual contact force and area between the adhesive and adherend. Taking inspiration of marine creatures, such as the octopus and the remora, the development of microstructured surfaces to control adhesion appears as an efficient response to this problem.

Pang and coworkers developed an underwater adhesive by mimicking the suction cups of octopus.[86] Some dome-like protuberances of radius from 15 μm to 500 μm were fabricated (**Figure 10a**). By an applied preload, the interfacial water was trapped in the upper chamber, which made the lower part serve as vacuum chamber by minimizing the volume of trapped air

in it.[86-87] Since the stresses create at the interface did not rely on any molecular interactions, this adhesive showed a strong adhesion to various substrates and under different conditions, such as dry, moist, underwater and even oil environments. For example, the adhesion strength underwater increased from ~ 10 kPa (no patterns) to ~ 40 kPa (dome-like protuberances of radius = 50 μm). The adhesion was also repeatable to be used for more than 10 000 times. To enhance the performance in peeling test, the microstructure was further improved by developing meniscus-controlled 3D microtips.[88] The adhesion for various substrates, conditions and under surface deformations could be improved by combining suction and water drainage channels,[89-91] which is discussed in **Section 2.3.3**. Another inspiration is fabricating the structure of remora, Lee at al. designed a polydimethylsiloxane (PDMS) adhesive with lamellar structure, on which there were ordered spinules a size of micrometers (**Figure 10b**).[39] The underwater adhesion strength was ~ 200 kPa.

In this biomimicry strategy, there are also other artificial microstructures to achieve suction. Hensel and coworkers developed an adhesive with deformable cupped microstructures (**Figure 10c**). There was an increase in adhesion by creating cavities in the microtip.[92-93] The adhesive exhibited a retraction velocity-dependent adhesion: there was a low adhesion region of strength less than 0.2 MPa when the velocity was slower than 10 μm s^{-1}, and high adhesion region of strength over ~ 1 MPa when the velocity was faster than 20 μm s^{-1}.[94] This was because faster and stronger pulling improved the sealing ability, resulting in an enhancement of adhesion.

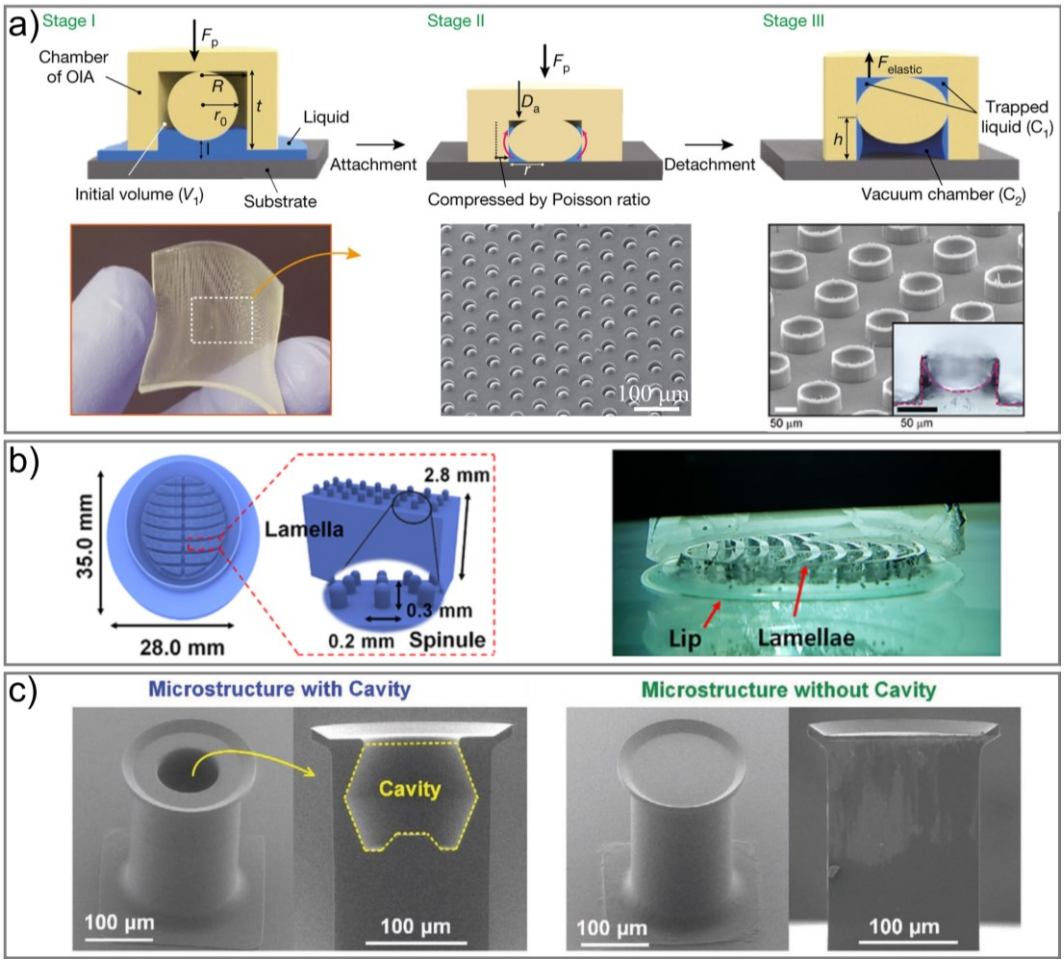

Figure 10. Adhesives based on suction by designing microscopic surface structure. a) Octopus-inspired adhesive: suction mechanism, photo, SEM image of microstructure and meniscus-controlled 3D microtips. Figure reproduced from Pang and co-workers[86, 88] and Wilker.[87] b) Remora-inspired PDMS underwater adhesive. The design of the lamella with ordered spinules on it. Figure from Lee et al.[39] c) Cupped microstructure with and without cavity inside. Figure from Wang et al.[92]

2.3 Dehydration of interfaces

As discussed in **Section 1.1**, water has a negative effect for underwater adhesion. In addition to strengthen the interfacial interactions, another straightforward way to solve this problem is to break down the hydration layer appearing at the interface to limit the water effect. This could be accomplished by increasing hydrophobicity, absorbing water into the adhesive and repulsing water by a microscopic design of surfaces.[95-96] Some of those strategies are realized by a modification of the bulk or involve an enhancement in the level of cohesion to realize strong underwater adhesion, but it is the dehydration of interfaces that is more remarkable and the real

solution to treat the water effect in underwater conditions. Therefore, these strategies are all discussed in this section about interfaces.

2.3.1 Increasing hydrophobicity

First, the increase in hydrophobicity of underwater adhesives could increase the adhesion performance, especially when targeting hydrophobic substrates. For both hydrophobic and hydrophilic adhesives, increasing hydrophobicity is an effective approach to destroy the interfacial hydrated layer and to increase underwater adhesion.

Increasing hydrophobicity can break the hydration layer at interfaces, because hydrophobic functionalities prevent the water penetration at the interface during the contact of adhesion process. For hydrophobic materials, this method is easier, for instance, by simply adding a hydrophobic solvent to the surface of hydrophobic adhesives.[95] Dolez et al. compared the hydrophobicity effect on underwater adhesion of two epoxy resins.[97] Against hydrophobic plastic substrates, they found that the relatively more hydrophobic vinyl-based ester resin had much more underwater adhesion strength (2.5-3.2 MPa) than that of less hydrophobic resin (1.2-1.8 MPa). Moreover, the more hydrophobic resin kept its underwater adhesion without loss for over one month, while the less hydrophobic one lost half its adhesion strength after 20 days, indicating a water-aging behavior of the less hydrophobic resin. In addition, the hydrophobicity of the epoxy resin could also be tuned by the curing agent, to enhance underwater adhesion.[98] Joy et al. developed a polyester glue, with sebacic acid on the side chains to reduce T_g and to increase hydrophobicity of the polymer, catechol groups to provide strong interfacial interactions, and coumarin units to enable UV-initiated crosslinking (**Figure 11a**).[96, 99] The lap shear strength of this adhesive reached 650 kPa, which was not much weaker than that in air (~ 800 kPa). Liu et al. added silicone fluids into a reactive polydimethylsiloxane (PDMS) precursor to design a water-immiscible hydrophobic fluid adhesive that can repel surface water through hydrophobic exclusion.[100] As shown in **Figure 11b**, a small amount of silane and macromolecular silicone fluid were added into the PDMS precursor to construct the injectable underwater adhesive. After the injection, because of the low surface energy of silicone, the water at the boundary layer was displaced and the adhesive spread on the surface. Then the adhesive solidified through the crosslinking of the PDMS network. The covalent bonds from the silane groups also contributed to the interfacial adhesion. The adhesive showed a good performance for various substrates including glass, PDMS and biotissues. For instance, the lap shear adhesion strength reached over 160 kPa on glass in 15 min.

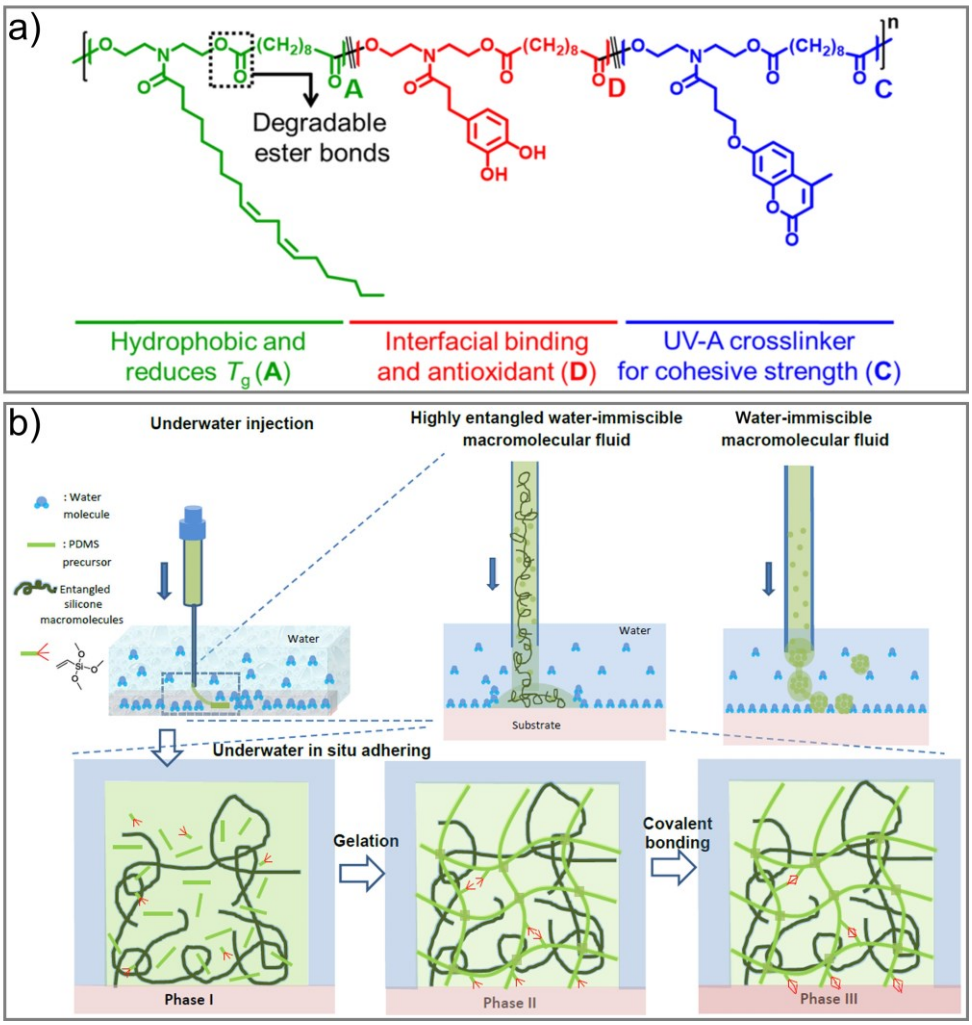

Figure 11. Increase underwater adhesion by increasing hydrophobicity of polymers. a) A polyester melt as a glue, with sebacic acid, catechol groups and coumarin units on the side chains. Figure from Narayanan et al.[99] b) A PDMS adhesive with silicone fluids to repel surface water through hydrophobic exclusion. Figure from Liu et al.[100]

Comparing with hydrophobic systems, it is more difficult to achieve strong underwater adhesion with hydrophilic adhesives such as hydrogels made from hydrophilic polymers and becoming highly swollen networks. Common hydrogel adhesives usually have poor underwater adhesion strength less than 20 kPa.[18] There are many strategies aiming to trigger hydrophobicity into hydrogels to tackle this problem. Liu et al. utilized water-dimethyl sulfoxide (DMSO) solvent exchange to tune hydrophobic aggregation from organogel to hydrogel to reach strong underwater adhesion.[101] The organogel was obtained by random copolymerization of acrylic acid (AAc), butyl acrylate (BA) and acrylated adenine (Aa) in DMSO. After being applied to adhere on substrates underwater, the organogel was transformed into a hydrogel by replacing DMSO with water (**Figure 12a**). The swelling in water induced the aggregation of hydrophobic

segments of BA, which not only destroyed the hydrated layer and improved the cohesion of gels but also endowed gels with nonswelling behavior. The lap shear adhesion strength could reach 70 kPa after immersion for 24 h. Han et al. synthesized a hydrogel with hydrophobic surface, to repel water molecules away from the interface. Firstly, a hydrophilic hydrogel was synthesized with acrylamide (AAm) as hydrophilic monomer and stearyl methacrylate (C_{18}) as hydrophobic monomer, sodium dodecyl sulfate (SDS), in which the hydrophobic alkyl chains of the C_{18} units aggregated inside SDS micelles to form dynamic hydrophobic associations.[102] After an immersion process in a Fe^{3+} solution, a larger micelle structure was formed, because SDS micelles reassemble into large structures when exposed to high ionic strength solutions. After being washed by water, the surfactant molecules on top layer was removed, generating exposed alkyl chains of C_{18}, which made the surface of hydrogel more hydrophobic (**Figure 12b**). As a result, the hydrophobic tails of C_{18} on the hydrogel surface can displace the water molecules at the interface. The Fe^{3+} immersion increased the underwater adhesion strength of hydrogel from none to ~ 40 kPa.

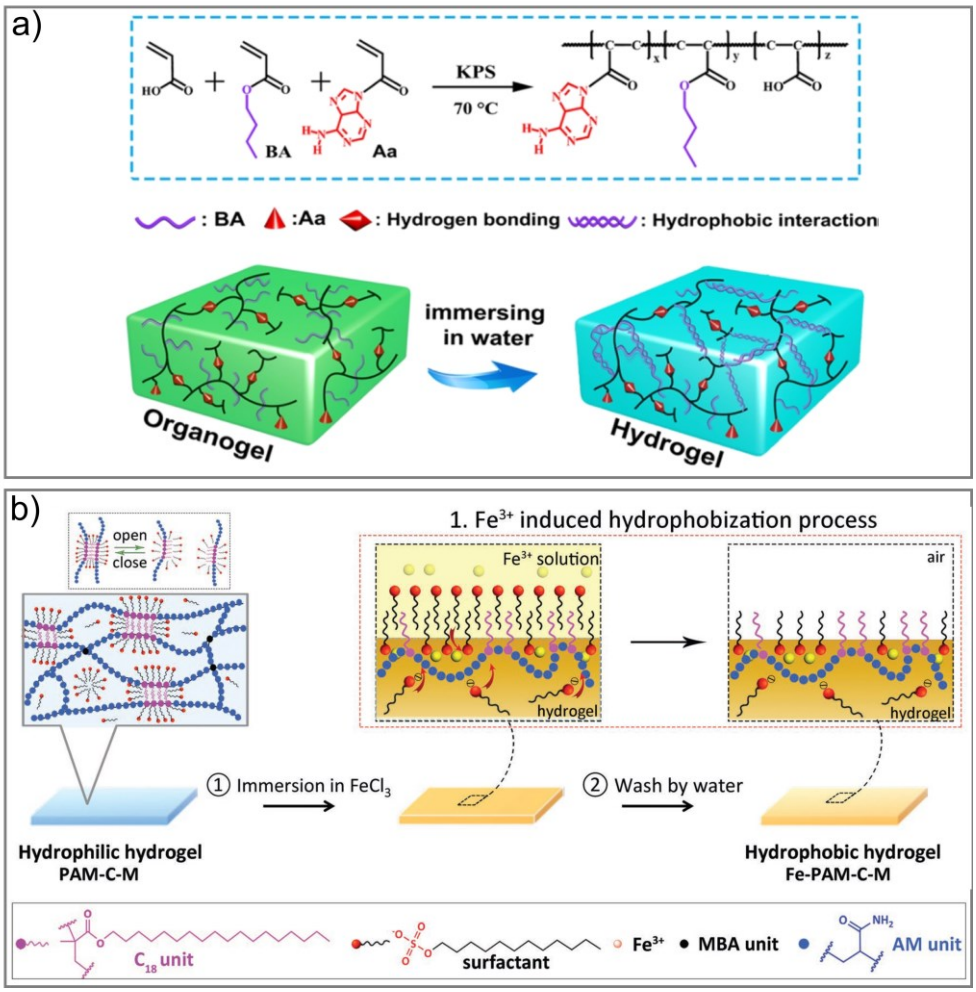

Figure 12. Increasing hydrophobicity of hydrogel adhesives. a) Organic gel as strong underwater adhesives through solvent-exchange-induced hydrophobic associations. Figure from Liu et al.[101] b) Fe^{3+}-induced hydrophobization at the hydrogel surface to enhance underwater adhesion. Figure reproduced from Han et al.[102]

2.3.2 Water-absorbing compositions

As hydrophilic underwater adhesives have a greater challenge in the removal of the hydration layer, using water-absorbing compositions is a smart way to remove interfacial water, including using hygroscopic polymers and water-absorbing fillers.

Yuk et al. developed a tissue adhesive called dry double-sided tape (DST), which was able to absorb interfacial water and form covalent bonds with biological tissues.[103] The DST was made by mixing a biopolymer (gelatin or chitosan) and crosslinked poly(acrylic acid) (PAAc) grafted with *N*-hydrosuccinimide ester (NHS ester). Since the DST was used in the dry state, it was able to absorb water. Subsequently, the NHS ester groups grafted on the PAAc coupled

covalently with primary amine groups on various tissues quickly (**Figure 13a**). The gluing of two porcine skins reached ~ 700 J m^{-2} (measured by a peeling test). Other hygroscopic polymers such as poly(vinylpyrrolidone) (PVP)[104] and polyethylenimine (PEI)[105] were also reported to be able to absorb water at adhesive interface and strengthen underwater adhesion.

Another way is to introduce water-absorbing fillers in adhesives. Pan et al. mixed inorganic filler called ye'elimite ($Ca_4(AlO_2)_6SO_3$) into the precursor of poly(acrylamide) (PAAm) hydrogel with crosslinker and initiator.[106] Once the precursor was injected onto the wet substrate surface, ye'elimite absorbed the interfacial water by hydration to generate ettringite and $Al(OH)_3$ nanocrystals (**Figure 13b**). The hydration process of ye'elimite also formed crosslinks to accelerate the gelation of the hydrogel and to strengthen the gel. Finally, the hydrogels achieved an adhesion strength of ~ 3 MPa by lap shearing on aluminum substrates.

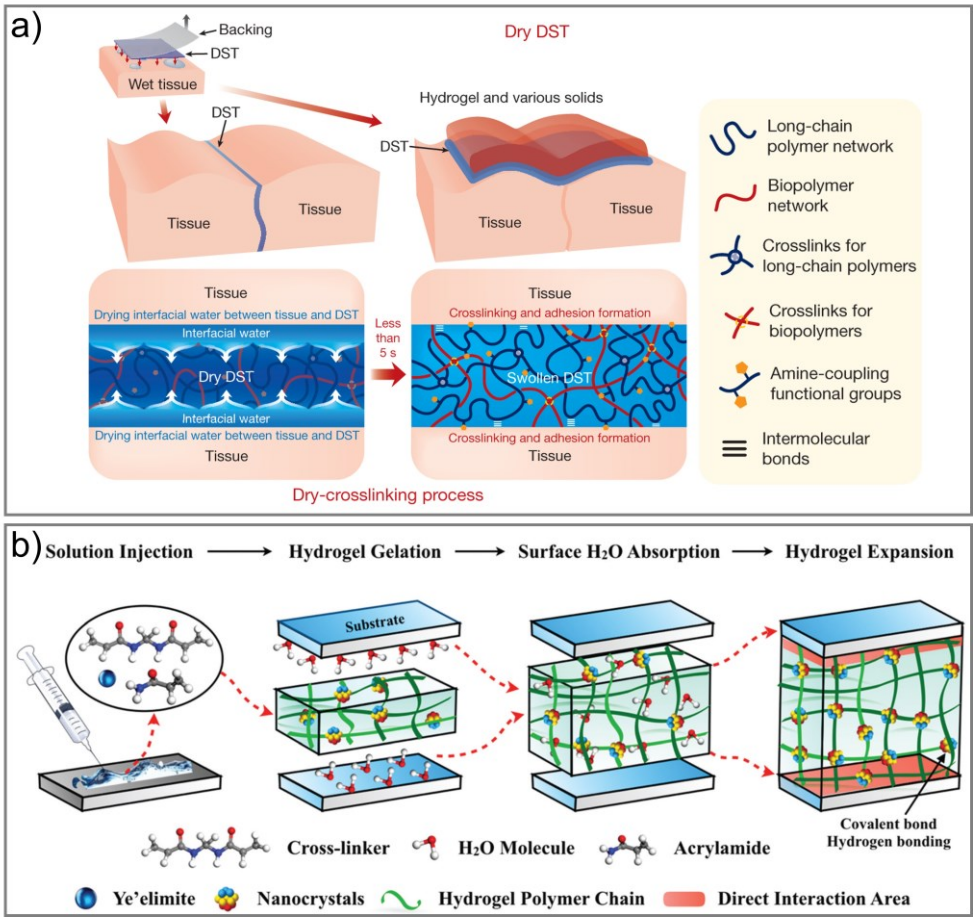

Figure 13. Underwater adhesives based on water-absorbing compositions. a) DST as tissue adhesive for various adherends. The dry-crosslinking mechanism of absorbing interfacial water and forming covalent bonds between the DST and tissues. Figure reproduced from Yuk et al.[103] b) Design of ye'elimite composite PAAm hydrogel as underwater adhesive. The ye'elimite

promoted water absorbance and the gelation of the hydrogel. Figure reproduced from Pan et al.[106]

2.3.3 Microstructure to build water drainage tunnels

Another way to dehydrate the surface is designing microscopic channels on the surface, into which water can be expelled. The inspiration is mainly from amphibian adhesion systems via hexagonal architectures, for instance, the toe pads of tree frog introduced in **Section 1.2**.

Inspired by the structure of clingfish adhesion disc, Gong and coworkers designed a patterned hydrogel with hexagonal facets and grooves on the surface (**Figure 14a**).[107] The grooves can rapidly drain water during the contact and delay crack propagation during the detachment. The underwater adhesion strength reached ~ 20 kPa with an increase of 5 times comparing with flat gels without any patterns, but the debonding energy (~ 10 J m^{-2}) had an increase of over 30 times. This phenomenon was related to the much better deformability of pillar-like pattern, endowing longer displacement during debonding.

Pang and coworkers designed a series of adhesives for electronic skin. The adhesives contained hierarchical architectures with a soft sublayer (PDMS or hydrogel) and a patterned convex layer with suction cups on top of it. The convex layer was patterned with lines,[89] hexagons[90] and microwrinkles.[91] Those patterns formed connective channels, which were able to act as tunnels for water drainage. For instance, **Figure 14b** shows a hierarchical hydrogel adhesive with ravines formed between line patterns.[89] The suction cup on the line formed interaction with substrates while the ravines played the role of water channel. The adhesion strength was around 15-60 kPa depending on the type of substrates. As used for electronic skin glues, the channels didn't only drain water during the contact to wet surfaces, but also drained sweat secreted from the skin, to keep the attachment and monitoring of biosignals.

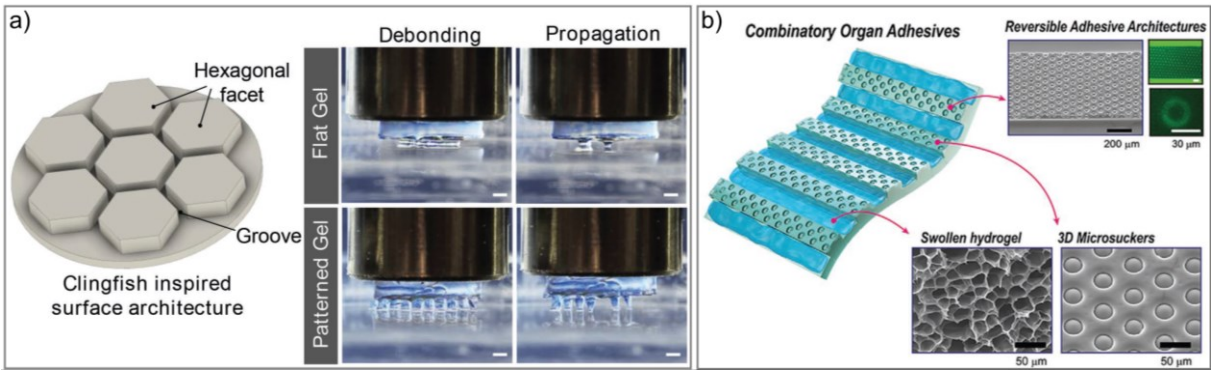

Figure 14. Adhesives based on the design of surface microstructure to build channels for water drainage. a) A hydrogel surface with hexagonal facets separated by grooves. The photography of the debonding process. Figure reproduced from Rao et al.[107] b) A hierarchical hydrogel adhesive, with SEM images showing microchannels embedded in hydrogel and structure of 3D microsuckers. Figure from Kim et al.[89]

3 Bioinspired Underwater Adhesives Focusing on Bulk Properties

For an adhesive, the binding at the interface is one important issue for its adhesion performance, as discussed above (**Section 2**). However, if the mechanical properties of the adhesive are very weak, no matter how strong the interface adhesion is, the attachment must fail in the bulk (so-called cohesive failure). The strength of the adhesive bulk, which is often called cohesion in the adhesion science community, is also essential for a high adhesion energy (**Equation 1**). Therefore, there have been some underwater adhesives focusing on optimizing bulk properties to improve adhesion. The main purpose is to strengthen the adhesive bulk by the incorporation of energy dissipation mechanisms.

3.1 Complex coacervates

A complex coacervate is a liquid consisting of a polymer-rich liquid phase in thermodynamic equilibrium with a dilute phase (**Figure 15**). A coacervate originates from the liquid-liquid phase separation of a solution, commonly driven by covalent or non-covalent interactions. Complex coacervates are particularly suitable for underwater adhesion, because of their fluidic but water immiscible properties[108-109] and wettability.[110] However, there are mainly two challenges for complex coacervates to be used as underwater adhesives: setting speed and strength. On one hand, the mixing strategy is easy to implement, but generally the droplet coalescence is too slow for the usage as underwater adhesive. Thus, there remains a challenge

to develop coacervates with fast complexation capability. On the other hand, a strong underwater adhesive requires that coacervates have a sufficient fracture energy to maintain the cohesion. The complex coacervate liquid transforms into a solid-like material by the introduction of covalent or non-covalent but strong interactions activated by an external trigger such as higher pH in seawater, metal ion coordination and temperature change. The speed and strength of the transition could be improved by accelerating the formation process and enhancing the strength of interactions.

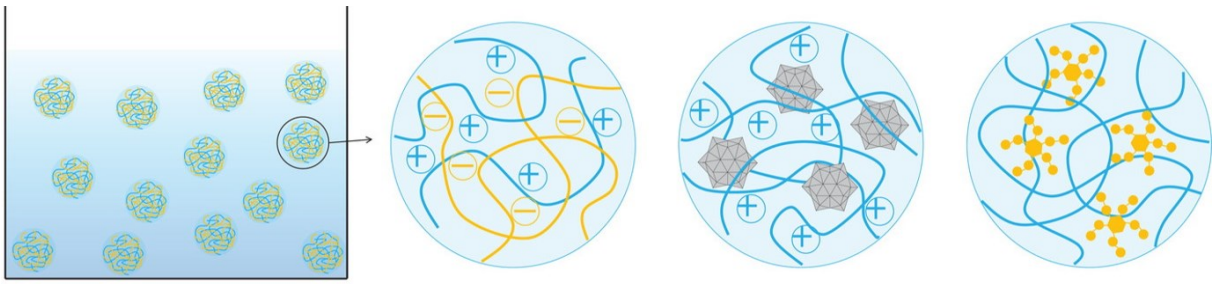

Figure 15. Schematic of complex coacervates based on oppositely charged polyelectrolytes, polycations and anionic polyoxometalates, hydrogen bond. Figure from Fan et al.[18]

Some DOPA-based coacervates based on electrostatic interactions mimicking sandcastle worm glue (introduced in **Section 1.2**) were designed as underwater adhesives. Stewart and co-workers synthesized an anionic polymer containing phosphate and catechol groups, and a cationic polymer with amine groups (**Figure 16a**).[111] Mixing the oppositely charged polymers generated a dense coacervate, which was injectable to adhere to a surface underwater. Covalent crosslinking formed through catechol moieties solidified the adhesive, resulting in strong underwater adhesion after curing. In addition, a second polymer network within the crosslinked network could increase the shear adhesion strength from ~ 0.6 MPa to ~ 1 MPa.[112] Waite and co-workers designed a synthetic coacervate as underwater adhesive with fast complexation by solvent exchange.[113] The adhesive consisted of two oppositely charged polymers: a polyanion as a copolymer of partially catechol-functionalized poly(acrylic acid), and a polycation of quaternized chitosan with bis(trifluoromethane-sulphonyl)imide (Tf_2N^-) as counter ion (**Figure 16b**). The adhesive was the mixture of oppositely charged polymers in DMSO. Electrostatic complexation of the polymers was suppressed in DMSO, but could be triggered by solvent exchange between DMSO and water, because of the deprotonation of carboxyl groups in water gives rise to the complex formation between polyacrylate and chitosan. After being injected to a substrate immersed in water, a robust underwater contact adhesion ~ 2 J m^{-2} formed rapidly after around 25 s.

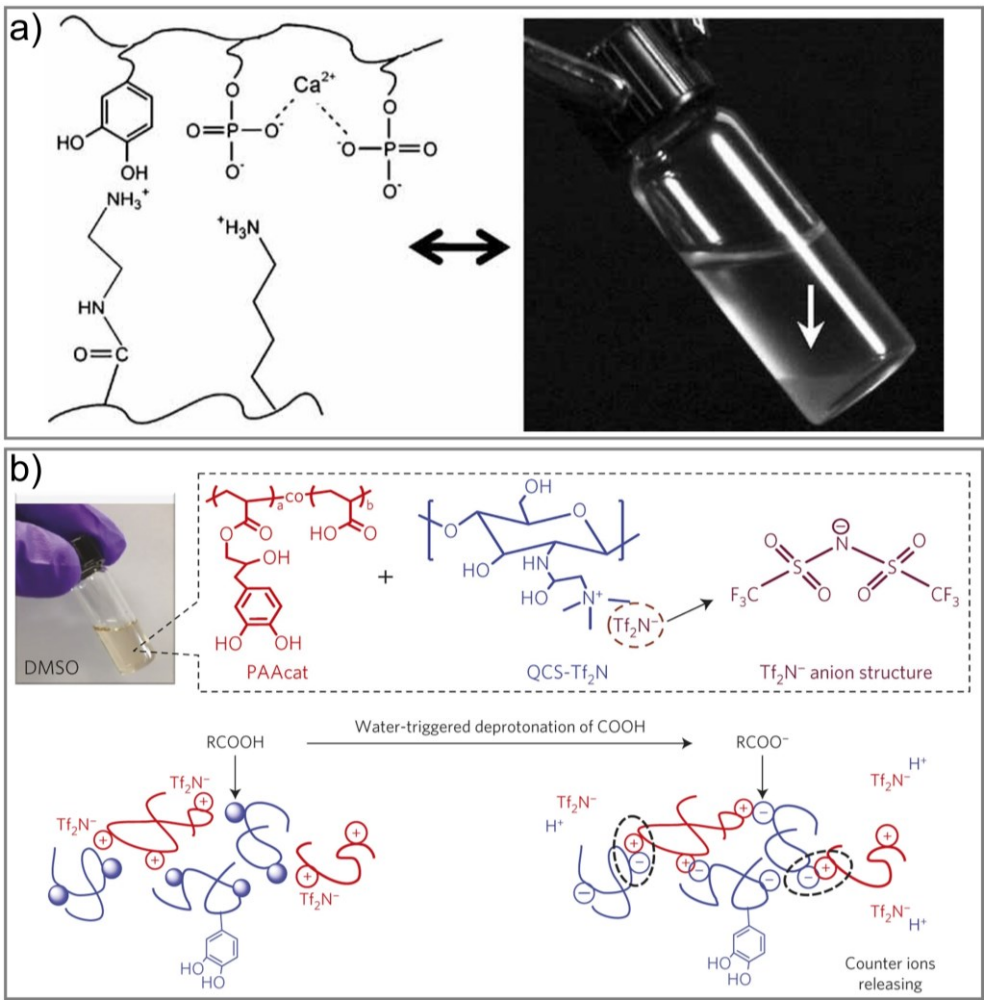

Figure 16. DOPA-based complex coacervates. a) Adhesive comprises DOPA-containing polyphosphate, polyaminated gelatin and divalent cations. Figure from Shao et al.[111] b) An adhesive forms coacervation by solvent exchange: a polyanion of catechol-functionalized poly(acrylic acid), and a polycation of quaternized chitosan with Tf_2N^- as counter ion. Figure reproduced from Zhao et al.[113]

In addition to typical polyelectrolyte complex coacervates based on electrostatic interactions, hydrogen bond and hydrophobic associations could also be used to fabricate coacervates. Lee and co-workers used tannic acid to crosslink nonionic linear polymers including polyvinyl acetate (PVA) and polyethylene glycol (PEG), to construct coacervates.[114-115] As shown in **Figure 17**, tannic acid is rich in pyrogallol and catechol groups, to form strong hydrogen bonds with PVA and PEG, resulting in coacervates. The adhesion strength of the coacervates was around 0.1-0.2 MPa. Moreover, the adhesion performance lasted for over 24 h and had a good reversibility to maintain most adhesion after 10 adhesion-detachment cycles. Similarly, Peng et al. used silicotungstic acid and PEG to form a coacervate in water.[116] The adhesion strength of

the coacervate on wet surfaces of biological tissue is much higher than that on dried surfaces because the presence of water increased the mobility of the PEG chains, indicating a good underwater adhesion property.

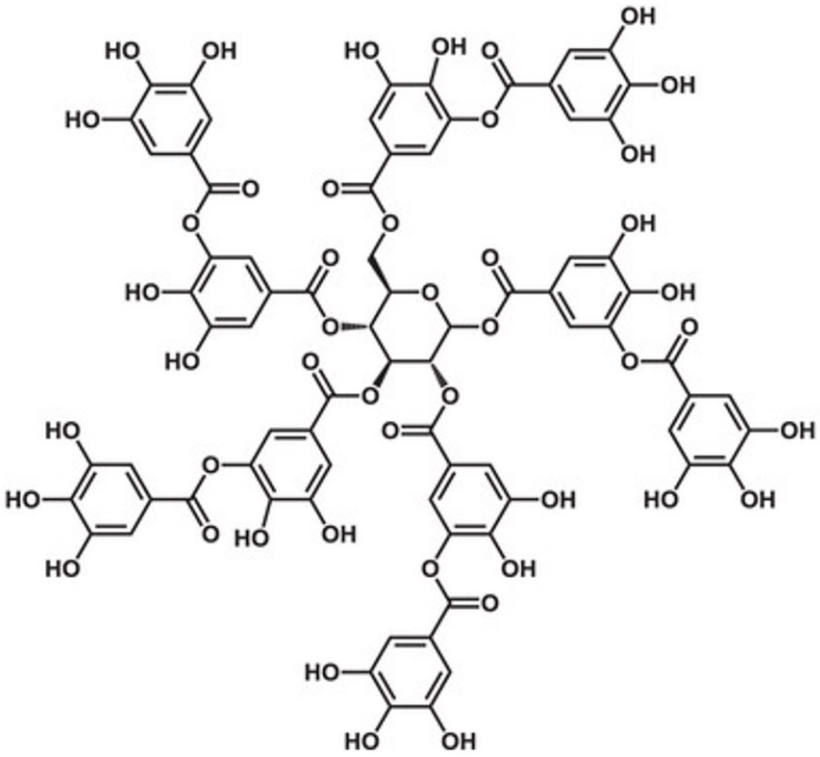

Figure 17. Chemical structure of tannic acid. Figure from Fan et al.[18]

To increase the strength of adhesion, combination of multiple non-covalent interactions rather than a single interaction to fabricate coacervates is a good way. Cui et al. synthesized a hyperbranched polymer with a hydrophobic backbone and hydrophilic catechol side branches (**Figure 18a**).[117] Once the polymer contacts with water, the self-aggregation of the hydrophobic backbone formed coacervates while reducing the interfacial hydration layer. This step made it possible to have a closer contact of catechol branches to the surface and resulted in rapid and strong underwater adhesion (~ 250 kPa) in various aqueous conditions and surfaces. Recently, Peng et al. reported an adhesive by the coacervation of tannic acid and polymer micelles (poly(ethylene glycol)$_{77}$-*b*-poly(propylene glycol)$_{29}$-*b*-poly(ethylene glycol)$_{77}$, F68), driven by hydrogen bond and hydrophobic associations.[118] As shown in **Figure 18b**, the micelle has a hydrophobic poly(propylene glycol) (PPG) core and a hydrophilic poly(ethylene glycol) (PEG) shell. The coacervation was mainly driven by the hydrogen bond between TA and the PEG shells and the hydrophobic PPG cores. The complex coacervate exhibited a robust, instant and

repeatable underwater adhesion, with a tensile adhesion strength up to 1.1 MPa on porcine skin, which could be maintained for at least 1000 cycles.

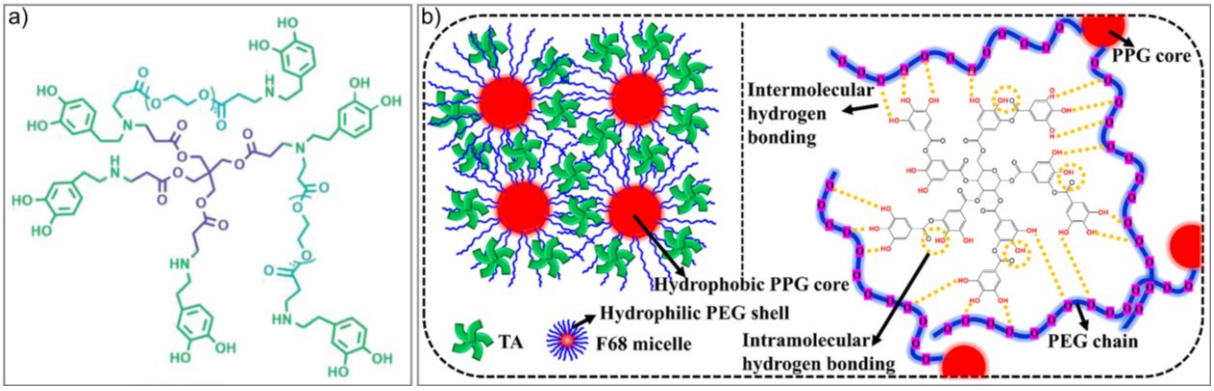

Figure 18. Complex coacervates combining multiple non-covalent interactions. a) A hyperbranched polymer with a hydrophobic backbone and hydrophilic catechol side branches. Figure from Cui et al.[117] b) A coacervate contains tannic acid (TA) and poly(ethylene glycol)$_{77}$-*b*-poly(propylene glycol)$_{29}$-*b*-poly(ethylene glycol)$_{77}$ (F68) micelle. Figure from Peng et al.[118]

In order to realize better injectability and fast gluing, responsive coacervates were also synthesized. Kamperman and co-workers grafted poly(*N*-isopropyl acrylamide) (PNIPAM) segment onto a series polyelectrolytes (grafting both polyanion and polycation) to form complex coacervates, as multi-responsive underwater adhesives (**Figure 19a**).[119-123] The adhesive was originally a fluid coacervate at room temperature and had a high ionic strength inside. Benefitting from the thermo-responsiveness of PNIPAM segments, increasing temperature triggered the self-association of PNIPAM by hydrophobic association, generating the transformation of a fluid "glue" into a viscoelastic hydrogel, as an underwater adhesive (**Figure 19b**). The adhesion strength measured by a probe tack test increased by 2 orders of magnitude after heating (0.1 to 10 kPa).[119] The coacervation was additionally improved by collectively or separately being initiated by temperature and ionic strength. Because stronger electrostatic interactions between oppositely charged polyelectrolyte chains formed during the diffusion of salt ions into the external medium. As a result, collective temperature and salt triggered adhesion was 7.2 J m^{-2}, while the independent adhesion was 1.6 and 6.5 J m^{-2}, respectively.[120]

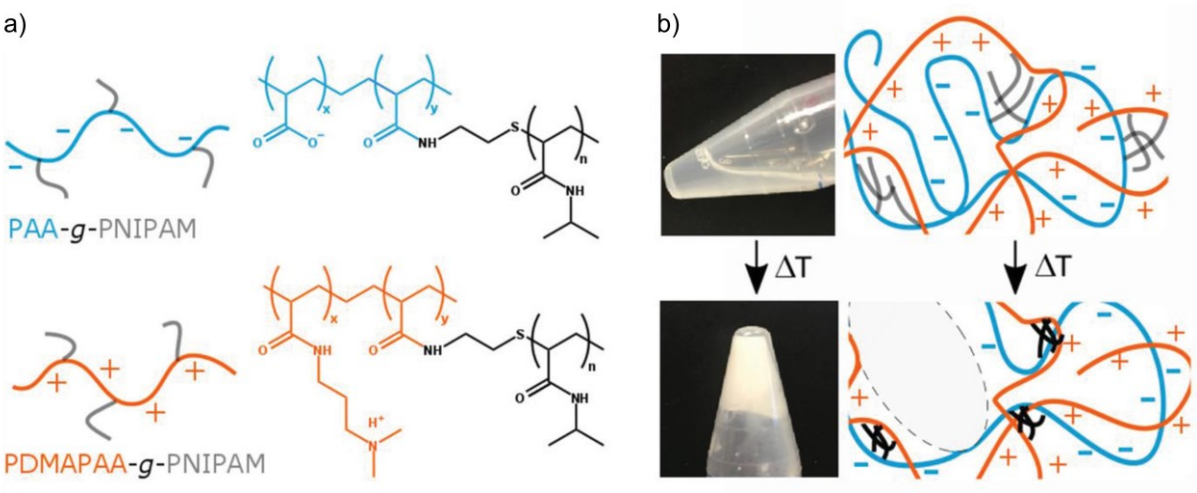

Figure 19. A coacervate by mixing oppositely charged polymer both grafted by poly(*N*-isopropyl acrylamide) (PNIPAM) segments. a) Chemical structure of polymers. b) Temperature triggered gelation as an underwater adhesive. Figures from Dompé et al.[119]

3.2 Well-crosslinked hydrogels

To realize a strong cohesion of the bulk adhesive, strong and tough hydrogels with good energy dissipation mechanisms have been used as underwater adhesives. Typically, chemically crosslinked single network hydrogels are weak and fragile, due to the inhomogeneous distribution of crosslinks, causing stress concentration. One of the main strategies to build strong and tough hydrogels is to incorporate efficient energy dissipation mechanisms.

Suo and co-workers reported a highly stretchable and tough double network (DN) hydrogel, with Ca^{2+}-crosslinked alginate as the first network and polyacrylamide as the second network,[124] which was further improved as a strong underwater adhesive. The tough DN hydrogel was used as a dissipative matrix, on the top of which there was a layer of bridging polymer such as chitosan or poly(acrylic acid) as adhesive surface (**Figure 20**).[125] The adhesive surface adheres to the substrate by electrostatic interactions, covalent bonds, and physical interpenetration, while the dissipative matrix amplifies energy dissipation through hysteresis. Both of the layers synergistically lead to high adhesion energies (~ 1000 J m^{-2}) on wet surfaces containing blood such as porcine skin.

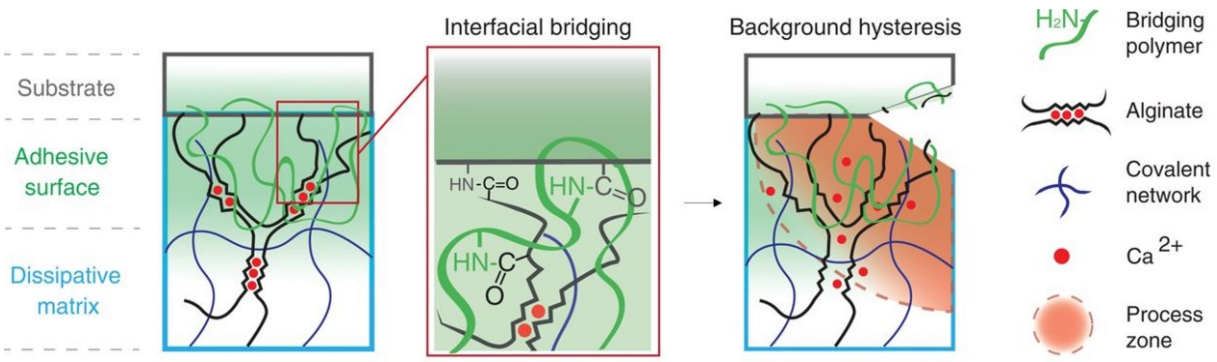

Figure 20. Design of tough adhesives with a dissipative matrix and an adhesive surface. The energy dissipation from dissipative matrix and interfacial bridging from the adhesive surface are both important for strong underwater adhesion. Figure from Li et al.[125]

Gong and coworkers reported another important tough polyampholyte hydrogel, which was a physical hydrogel obtained by copolymerization of oppositely charged ionic monomers around the charge balance point at high concentration.[126] This type of polyampholyte gel was used as adhesive after being covalently crosslinked to have sufficient strength.[127] Since both cationic and anionic charges are present in the gel, the polyampholyte gel was able to adhere both to anionic and cationic gels (both serve as substrates) (**Figure 21a**). For instance, against anionic substrates, a maximum adhesion energy of ~ 30 J m^{-2} measured in lap shear and a tensile strength of 236 kPa were reached. On the contrary, adhesion to neutral hydrogels was much weaker with only ~ 0.4 J m^{-2} of adhesion energy by lap shear and 42 kPa of tensile strength. The polyampholyte hydrogel also adhere to various substrates with charges, regardless of the nature of the surface charge (**Figure 21b**).

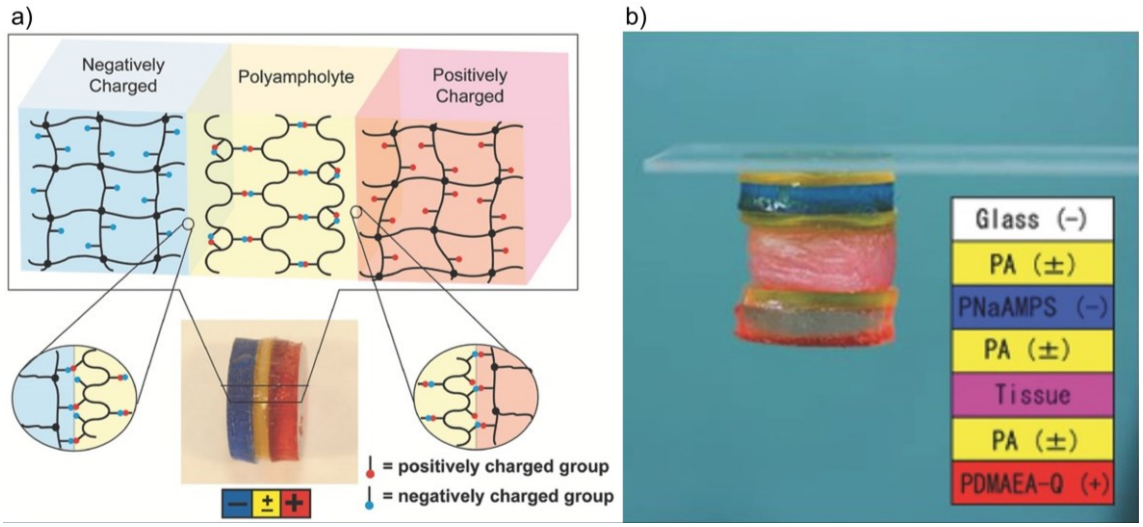

Figure 21. Polyampholyte gels with equal amounts of positive and negative charges as an adhesive. a) The polyampholyte gels adhered to both anionic and cationic hydrogels. The blue

and red dots in the network represent anionic and cationic charges, respectively. b) The polyampholyte gel also adhered to glass and pork tissue that are both moderately charged. PA refers to polyampholyte. Figures from Roy et al.[127]

Electrostatic interactions are commonly used to design underwater adhesives, but their effectiveness normally diminishes in concentrated salt solutions, such as physiological conditions and seawater, due to the Debye screening effect.[52] In biosystems, amino acids with cationic–aromatic sequences, provide an inspiration of cation-π interactions for designing marine adhesives.[128] In aqueous solutions, cation-π interaction is found to be stronger than hydrogen bond and probably even stronger than charge-charge interaction,[67, 129-130] which is introduced into underwater adhesives to increase bulk cohesion. Fan et al. synthesized copolymer hydrogels with adjacent cation-aromatic sequences, which maintain cohesion in seawater by cation-π interaction (**Figure 22**).[131] The gels show good mechanical properties (with Young's modulus ~ 0.28 MPa) because the cation-π interaction in the network provides an energy dissipation mechanism. Based on this strong bulk cohesion, the hydrogels show fast, strong and reversible adhesion against negatively charged surfaces in 0.7 M NaCl solution, with adhesion strength ~ 60 kPa and work of adhesion ~ 25 J m^{-2} measured by probe tack test. The cation-π interaction is effective to reach strong underwater adhesion, not only because of its high strength in salt solutions, but also due to the repelling of water by aromatic groups. In order to limit the swelling of this hydrogel in water to further improve the underwater performance, the authors increased the fraction of aromatic monomers used for copolymerization.[132]

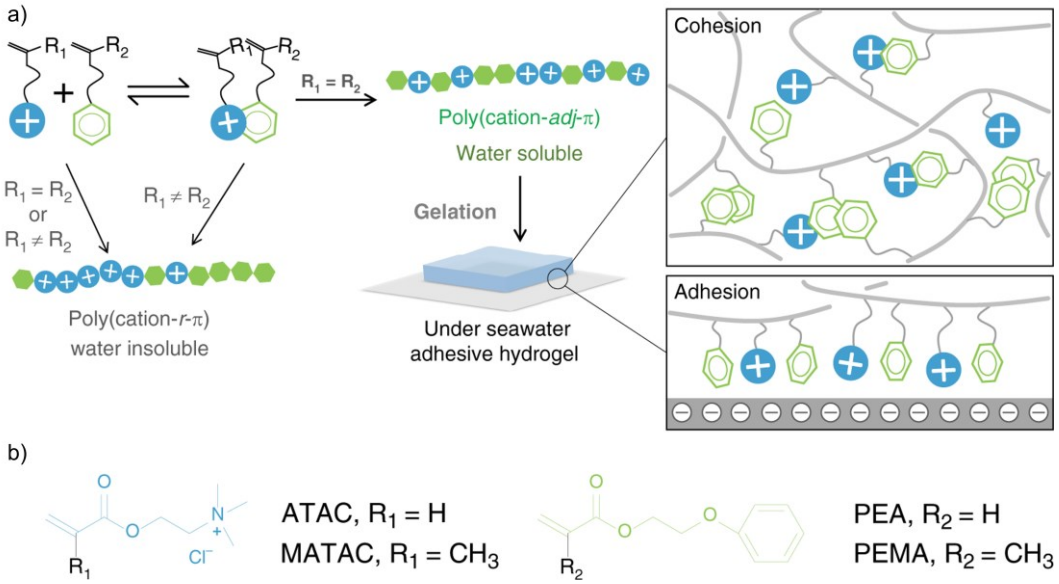

Figure 22. Hydrogels based on cation-π interaction. a) Synthesis of hydrogels with adjacent cationic-aromatic sequences synthesized by free-radical polymerization. The gel maintains good cohesion in seawater. b) Monomers used for synthesis. Figures from Fan et al.[131]

Inspired by DOPA-based molecular interactions, some synthetic hydrogels have been also developed by directly incorporating DOPA or catechol functionalities into their network.[133] Shan et al. synthesized a PEG based hydrogel based on phenylborate esters, of which the adhesion was tunable by a pH change.[134] The hydrogel was formed by mixing four-armed PEG-dopamine and four-armed PEG-boronic acid under alkaline conditions (**Figure 23a**). The Lap shear strength on glass slides and on porcine skins was 4.1 and 5.2 kPa, respectively. Moreover, the dynamic character of the phenylborate-catechol bonds enabled a reversible adhesion by tuning the pH. Another example is reported by Cholewinski et al., who developed a composite glue with separate dopamine layers and an alginate polymer layer.[135-136] Both adherends were coated with an aqueous solution by mixing dopamine, ferric ions and tris(hydroxymethyl) aminomethane (D-Fe-Tris), between which an alginate solution was then injected. A sandwich-like structure was formed between substrates after pressing (**Figure 23b**). The auto-oxidation of dopamine into polydopamine (in Tris-HCl solution, pH 8.5) let the D-Fe-Tris solution be coated onto substrates.[137] The catechol group on the dopamine and carboxylate group on the alginate were coupled by ferric ion coordination. Both the formation of polydopamine and metal coordination gave a strong cohesion to the adhesive. An underwater adhesion strength of ~ 400 kPa was achieved by tensile test.

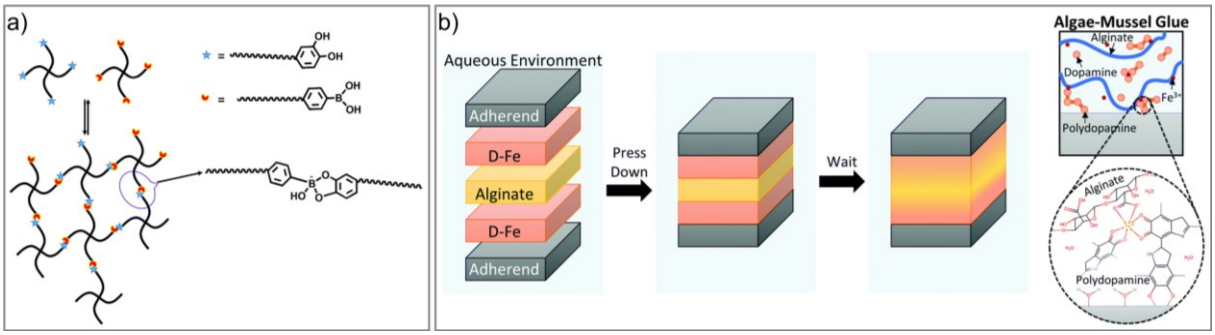

Figure 23. Hydrogels based on catechol chemistry as underwater adhesives. a) PEG hydrogel based on phenylborate esters, formed by mixing four-armed PEG-dopamine and four-armed PEG-boronic acid under alkaline conditions. Figure from Shan et al.[134] b) A composite glue with separated dopamine layers and an alginate polymer layer. Figure reproduced from Cholewinski et al.[135]

4 Measurements of Underwater Adhesion

4.1 Typical Underwater Adhesion Measurements

Measuring adhesion is a challenge because adhesion is not a simple physical chemistry property. Adhesion strongly depends on the experimental method, such as debonding rate, pulling direction and even substrate shape. Moreover, adhesion is not only a property of the interface but also of the global bonding system. So it also depends on the experimental conditions such as temperature, solvent medium, contact time between substrate and adhesive, mechanical properties of both substrate and adhesive, *etc*. Therefore, the specific measurement method of the adhesion should be selected and adapted to the specific requirements of potential use of the adhesive. Furthermore, testing underwater adhesion is much more difficult because it requires a sophisticated design of the setup to add an aqueous solution. The most commonly used measuring methods for underwater adhesion are shown in **Figure 24**.

The surface force apparatus (SFA) is a widely used measurement for directly testing intermolecular forces,[138-140] which is also adapted for underwater adhesion tests.[141-143] As shown in **Figure 24a**, the SFA contains two curved molecularly smooth surfaces of mica between which the interaction forces are measured. When the two curved cylinders have the same radius of curvature (typically radius = 1 cm), this so-called “crossed cylinder geometry” is mathematically equivalent to the interaction between a flat surface and a sphere. SFA is a

precise technique for the characterization of interfacial adhesion between molecular monolayers or multilayers.[23, 52, 144]

Similar to SFA, atomic force microscope (AFM) is another way to directly measure the surface forces (**Figure 24b**).[145] It measures the force between a surface and a fine tip or a colloidal probe (AFM-CP).[146-147] AFM can work with either hard or soft materials and under various aqueous environment.[148] Therefore, it has a great potential to measure adhesion energy derived from specific molecular interactions. However, SFA and AFM method give no information about the bulk mechanical properties of either adhesives or about the macroscopic adherence.

The lap shear test is used in most studies about adhesion for wet or submerged substrates.[31, 58, 96, 99-101, 106, 127, 134, 149-151] As shown in **Figure 24c**, an adhesive is placed between two parallel adherends with a given contact area. This process usually demands a slight compressive force to form good contact. By pulling apart the adherends in shear, a force-displacement information can be obtained. The adhesion strength is defined as the maximum tensile force per unit area required for joint failure. The lap shear test is a straightforward way to measure adhesion, but it does not provide details useful to separate interfacial bonding and bulk dissipation and failure can be complex. It is nevertheless very well adapted to structural adhesives that form strong bonds. The tensile test of a so-called butt joint is a similar test as lap shear by separating the adherends through a tensile geometry (**Figure 24d**).

The peel test is also a way to measure adhesion, by which studies the tape-type adhesion of for wet substrates. 90° peeling (**Figure 24e**) is more common for underwater cases. The adhesive and substrate are joined together underwater, after which the adhesive is peeled from the substrate with an angle of 90°. The adhesion strength of the 90° peel test is defined as the average steady-state force per width of the peeled strip (a single number). Some of other conventional peel tests including 180°, T and cylinder peel and are also shown in **Figure 24f**. However, a detailed knowledge of the structure, deformation, stress filed and failure of the debonding region during detachment during the detachment is complex to be considered especially for different materials.[152-154] The result also strongly depends on the thickness of the layer and on the peel angle.[51] The peel test does not provide an easy way to control the contact time and pressure. It is more suitable for specific systems with certain modulus and viscoelasticity.

Probe tack test, schematically shown in **Figure 24g**, provides very different and complementary information on the adhesion of soft materials. There are two main cases for probe tack test. One is that a flat probe with a solid adhesive moves to form contact with the substrate, the other one is a naked probe contacts with fluid adhesive on the substrate. The test involves pressing the adhesive at a given compressive stress and contact time. Then the probe and the substrate are separated by removing the probe at a constant rate, which is the so-called debonding or detachment process. During the detachment, the loading force is measured as a function of time or distance. Comparing with other macroscopic adhesion tests, lap shear and peel test, the advantage of the probe tack test is that it allows the application of well-defined strain history on soft adhesives before detachment.

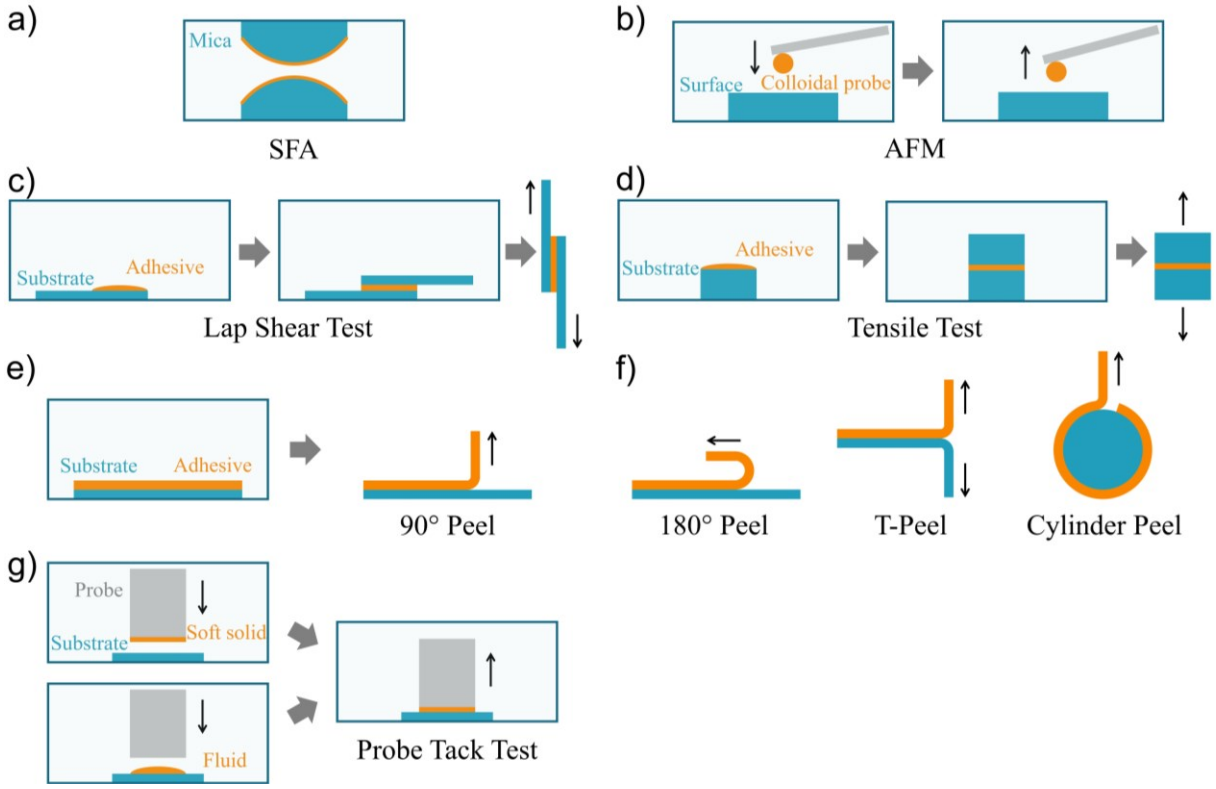

Figure 24. Illustration of commonly used underwater adhesion measurement methods. a) SFA test. b) AFM test. c) Lap shear test. d) Tensile test. e) 90° peel test. f) Other peel tests. g) Probe tack test.

4.2 Underwater Probe Tack Test

A significant progress in underwater probe tack test was reported by Sudre et al., who designed a home-made device for probe tack underwater adhesion tests, allowing the visualization of the contact and *in situ* control of aqueous conditions during the measurement.[155]

As shown in **Figure 25**, the adhesion is carried out in the sample chamber, which could be in water or in air. The probe is a solid surface attached at the end of a cylinder connected to the mobile part of an Instron machine (model 5333, Instron®, France), while the other material is either and adhesive layer or a substrate, attached to the fixed part of the machine. The sample chamber is surrounded by another heating chamber, which is connected to a thermostated liquid to control the temperature in the sample chamber. The samples including the substrate and the soft adhesive are held by a sample holder to ensure a fixed position of the samples during the measurement as originally described by Macron et al.[156] The contact between probe surface and adhesive or substrate can be checked through a mirror below the samples (vertical direction) and a window on the side of the sample chamber. Several screws are used to adjust the alignment between probe and substrate and ensure a good (full area) contact at the interface. The probe tack test can be carried out in the device, with the movement of probe controlled and force-displacement recorded by an Instron machine.

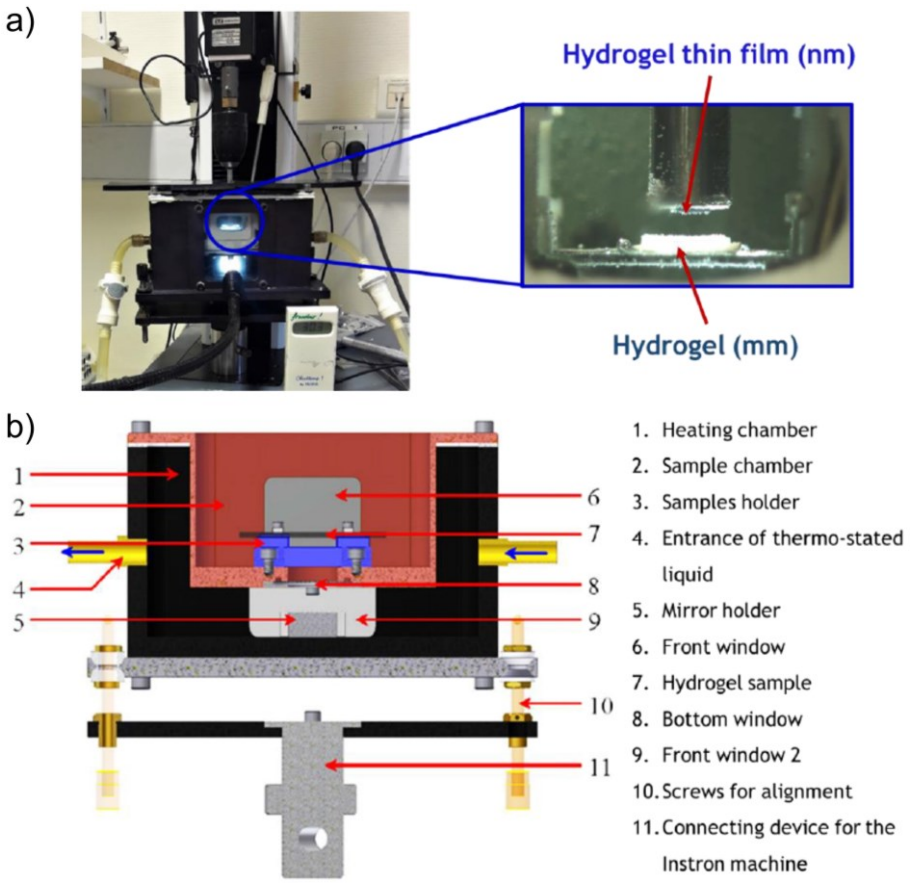

Figure 25. A home-made setup for underwater probe tack test designed by Sudre et al. a) Photographs of the device during the measurement. Underwater, it is able to measure adhesion between a solid surface and a soft material. Photo from Cedano-Serrano.[157] b) Details and components of the device. Figure reproduced from Sudre et al.[155]

The probe tack test is very sensitive to experimental conditions, such as contact time, contact pressure and debonding rate, which should be well-controlled in the measurement.[155-156] Cedano-Serrano et al. and Macron et al. found that more variables should be taken into account to improve the reproducibility of the results.[156-157] First, the alignment is done in air while the adhesion takes place in water. Since the adhesion in air is much stronger than in water, the surface could be broken during the tuning of alignment, causing a wrong measurement of underwater adhesion. One way to solve this problem is using an additional, inert and thin film (e.g. Parafilm®) to cover the surface during alignment. The film doesn't influence the alignment but protects the surface well (**Figure 26a**). Secondly, the homogeneity of the composition of the contact surface is important. For the case where the surface is modified by spin-coating a thin film, this could be realized by coating the film on a bigger surface of silicon wafer and then cutting the wafer into smaller size, to avoid the inhomogeneity of coatings at the edges (**Figure 26b**). Third, the macroscopic adhesive has to be firmly attached and fixed at the bottom of the setup, to obtain the real information of adhesion. One option is to use strong glue to fix the adhesive on the surface of a glass slide (e.g. cyanoacrylate adhesive), which is fast but only suitable for a quick test because the cyanoacrylate adhesive could diffuse into the adhesive. Another option is to clamp the bulk adhesive to fix the position, which is used for longer tests but the samples should be bigger than the other option (**Figure 26c**). Last but not least, the surface area for measurement should be smaller than the probe area, in order to avoid hydrodynamic and bending effects during the detachment (**Figure 26d**).

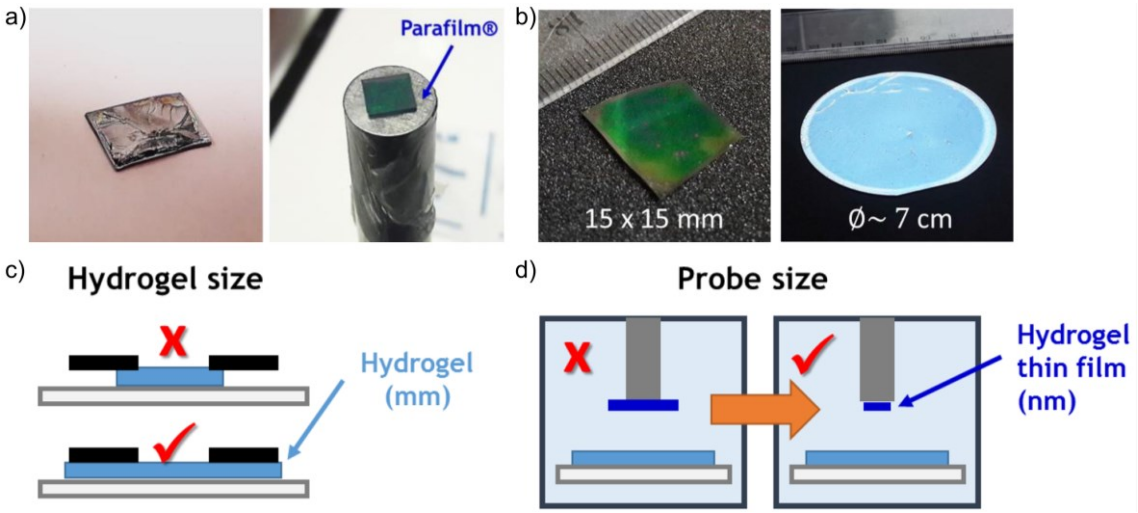

Figure 26. Some effects in the probe tack test to improve the reproducibility of the results. a) Alignment in air sometimes causes surface failure. Using Parafilm® to cover the solid surface when control the alignment of the surface can solve this problem. b) Spin-coating on a larger surface and cutting it into smaller size provides a better homogeneity than directly coating on

small surfaces. c) Fixing macroscopic adhesive firmly. d) The surface area of for testing should be smaller than that of the probe. Figures reproduced from Cedano-Serrano.[157]

In addition, the probe tack test is also suitable for measuring fluid adhesives, as shown in **Figure 24g**.[158-159] The device in **Figure 25** was also used for measuring underwater adhesion of complex coacervates. Based on a parallel contact and underwater detachment, the underwater adhesion of several types of coacervates has been measured. A proper amount of coacervate is deposited between a homogeneous layer and a glass surface, as a replacement of the macroscopic hydrogel in **Figure 25a**. Vahdati et al. synthesized complex coacervates which was able to experience salt-induced sol-gel transition.[160] The coacervates were from poly(2-acrylamido-2-methylpropane sulfonic acid) (PAMPS) and poly(*N,N*-[(dimethylamino) propyl]methacrylamide) (PMADAP) with degrees of polymerization (DP) about 100. The underwater probe tack test is shown in **Figure 27**. After an immersion in 0.1 M NaCl solution for 1 h, the fluid-like coacervate transform into gel-like adhesive, of which the adhesion energy is measured by recording the stress and strain during debonding. Similarly, the coacervates reported by Kamperman and co-workers, which are able to undergo gelation by temperature or ionic strength triggers (discussed in **Section 3.1**), were also measured by this device.[119-123] After the deposition of coavervates to reach a good contact with both two sides of substrate, hot water or NaCl solution with optimized temperature or ionic strength (collectively or separately) is poured to treat the gelation of coacervates. Finally, the underwater adhesion measurement takes place by debonding. The probe tack test ensures the parallel contact and detachment of both soft solid and fluid adhesives with well-controlled stress and strain history on adhesives before detachment.

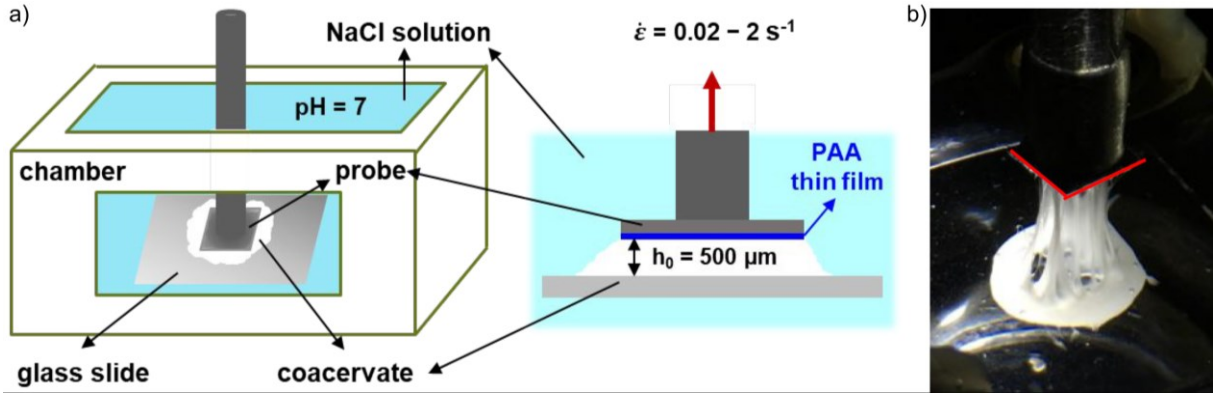

Figure 27. Probe tack measuring of complex coavervates *via* salt-induced sol-gel transition. a) A proper amount of coacervate is placed between a glass slide and a PAAc film inside chamber

filling with NaCl solution. b) The photography of the coacervates during debonding, after the transition from fluid-like solution to gel-like adhesive. Figures from Vahdati et al.[160]

5 Model Systems for Studying Underwater Adhesion

As discussed in **Section 2** and **Section 3**, the effect of the interface (mainly strength of molecular interactions and contact) and bulk properties (cohesion) of adhesives both contribute significantly to the underwater adhesion performance. However, those two effects usually exist together during adhesion, limiting the understanding of their individual contributions. Recently, the SIMM lab has developed an original methodology to study the separate contributions of interface and bulk for underwater adhesion, by a model system containing a thin film (submicron) of polymer (brush or hydrogel) and macroscopic hydrogel (**Figure 28**). The thin film can be used to tune the interfacial interactions, while the macroscopic hydrogel can mimic bioadhesives and biotissues in its bulk properties. The thin films are synthesized by a CrossLinking and Grafting (CLAG) strategy, in which a layer of polymer network (thickness ~ hundred nm) is grafted onto a silicon wafer.[161-163] The thin films on solid substrate only have properties of a surface, in chemistry and topography. The other material, macroscopic hydrogels, work as soft adhesives (thickness ~ mm) with controlled viscoelasticity. When both of the materials are crosslinked hydrogels, their only difference is microscopic or macroscopic, which is surface or bulk respectively. The model system divides the two important effects controlling adhesion: interfacial interactions and bulk properties into independent materials, to study their individual effects. The measurement method was probe tack test underwater, as introduced in **Section 4.2**.

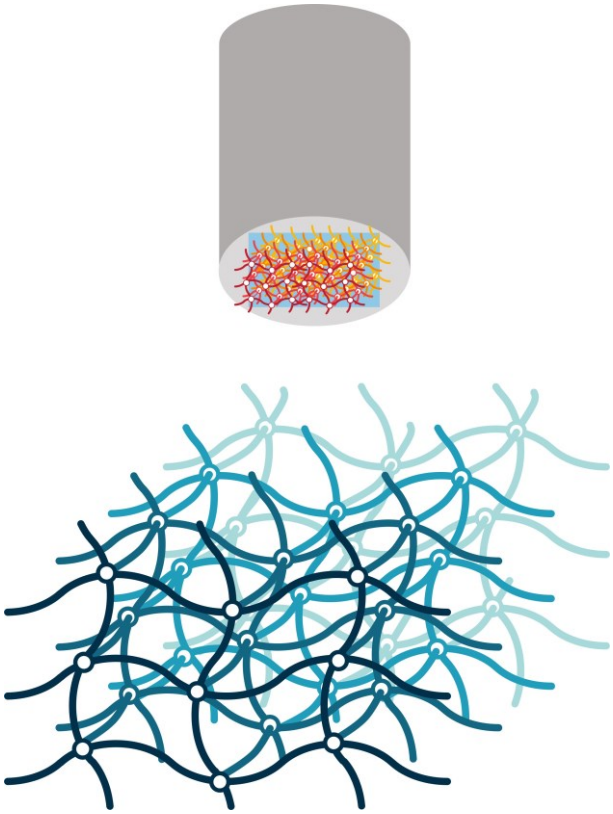

Figure 28. Illustration of the model system. The cyan network at the bottom represents macroscopic hydrogel. The red and orange network refers to the microscopic hydrogel thin film, which is attached to a solid substrate (blue) on the top of a probe.

Sudre et al. investigated the underwater adhesion between poly(*N*,*N*-dimethylacrylamide) (PDMA) hydrogels and a surface of poly(acrylic acid) (PAAc) brushes.[155] The underwater adhesion was controlled by tuning the pH because the hydrogen bonding between PDMA and PAAc is pH-sensitive. The adhesion was also strongly dependent on the debonding rate and contact time. Macron et al. studied the influence of the swelling equilibrium of hydrogels on the underwater adhesion between the same PDMA/PAAc couple.[156] The equilibration led to changes in mechanical properties such as the elastic modulus. The study showed that underwater adhesion always decreases as the hydrogels swell to equilibrium, regardless of the initial polymer concentration and degree of crosslinking. In order to study the underwater adhesion between oppositely charged polyelectrolytes, Cedano-Serrano et al. developed a model system of PAAc hydrogel thin film and poly(2-(methacryloyloxy)-ethyltrimethylammonium chloride-co-acrylamide) macroscopic hydrogel.[164] With this system, it was shown that the macroscopic adhesion depended linearly on the density of binding sites at the interface and that the work of adhesion increased with the shear modulus of the hydrogels, as could be modelled semi-quantitatively.

6 Objectives of the Thesis

6.1 General objectives

While the adhesion between synthetic materials has been well-studied experimentally and theoretically, there is still a lack of knowledge on bioadhesion, which could be tackled by using a biopolymer system.[51] However, this idea is limited by the difficulty in designing a model structure and controlling physical chemistry properties of the biopolymer and biopolymer made materials. With the model system described in **Section 5**, fabricating a biopolymer system with a well-controlled structure and physical chemistry can help us to understand bioadhesion. Therefore, the general objective of this thesis is to synthesize model microscopic hydrogel thin films and macroscopic hydrogels, to study the influence of their microscopic structure on macroscopic underwater adhesion performance. The objective includes the synthesis of these new materials, the characterization of their structure and surface and bulk properties and finally their underwater adhesion properties.

First, in order to mimic the biosurfaces, we aim to synthesize polymer hydrogel thin films with a well-controlled structure and physical chemistry. The objective is divided into two tasks: a) mimicking the chemistry of the biosurfaces by constructing biopolymer hydrogel thin films. b) mimicking the microstructure of patterned biosurfaces (e.g. similar to the polygonal epithelial cells of tree frogs).

Second, the macroscopic hydrogel as the other material in the model system, is also important. Similar to the hydrogel thin films, we aim to synthesize biopolymer hydrogels with well controlled network mesh sizes and viscoelastic properties to mimic biological tissues and bioadhesives. This objective is also divided into two tasks: a) mimicking the chemical structure of biological tissues by constructing hydrogels with a biopolymer containing amino acids. b) mimicking the mechanical properties of biological tissues by fabricating strong and tough biopolymer hydrogels.

Finally, in order to understand this bioadhesion process, we will study the underwater adhesion of the model systems. With a well-controlled structure and physical chemistry of both thin films and bulk hydrogels, we aim to study the relationship between the microscopic structure and macroscopic adhesion performance of the materials.

In order to achieve the three basic objectives above, there are three related chapters in this manuscript (**Chapter 2**, **Chapter 3** and **Chapter 4**), of which the detailed objectives are introduced in the next paragraphs.

6.2 Surface-attached biopolymer coatings

In **Chapter 2**, we aim to mimic the chemistry of biosurfaces by constructing biopolymer hydrogel thin films. The stability of the chemical attachment of the film on the surface is important to obtain the real adhesion between surface and adhesives. Moreover, to control the physical chemistry of the films, their thickness, equilibrium swelling in water and biodegradation are studied in various conditions. Finally, as this method is simple and versatile, another objective is to apply the synthesis to different substrates and explore the applications.

6.3 Model system based on gelatins to study bioadhesion

In **Chapter 3**, we aim to mimic the chemical structure of biological tissues by constructing hydrogels made from biopolymers containing amino acids. From the well-controlled network structure to the viscoelasticity of hydrogels, we aim to study the relationship between the structure and mechanical properties of the bulk hydrogels and the work of adhesion against the thin films.

6.4 Model system based on tough biopolymer hydrogel and surface grafted with hydrogel microstructures

In **Chapter 4**, we aim to mimic biosystems and study the surface topography effect on adhesion. For the surface, in addition to the homogeneous polymer films, patterned films with microscopic hexagonal arrays were prepared in order to control the surface roughness and mimic biosufaces such as epithelial cells of tree frogs. For the macroscopic hydrogels, it is also important to mimic the mechanical properties of biosystems because biotissues such as muscle and cartilage are strong and tough.[165-168] In this chapter, we aim to study the underwater adhesion between the hydrogel thin films with arranged hexagon patterns and strong biopolymer hydrogels, to understand the individual effect of surface pattern on adhesion.

In summary, the objective of this thesis is to understand bioadhesion by biopolymer model system that separate surface binding and bulk cohesion. The individual effect of surface chemistry, topography and bulk viscoelasticity on adhesion is the objective.

References

1. Yu, Z.; Wu, P., Underwater Communication and Optical Camouflage Ionogels. *Advanced Materials* **2021,** *33* (24), 2008479.

2. Sun, C.; Luo, J.; Jia, T.; Hou, C.; Li, Y.; Zhang, Q.; Wang, H., Water-resistant and underwater adhesive ion-conducting gel for motion-robust bioelectric monitoring. *Chemical Engineering Journal* **2022,** *431*, 134012.

3. Zhang, C.; Zhou, Y.; Han, H.; Zheng, H.; Xu, W.; Wang, Z., Dopamine-Triggered Hydrogels with High Transparency, Self-Adhesion, and Thermoresponse as Skinlike Sensors. *ACS Nano* **2021,** *15* (1), 1785-1794.

4. Drotlef, D.-M.; Amjadi, M.; Yunusa, M.; Sitti, M., Bioinspired Composite Microfibers for Skin Adhesion and Signal Amplification of Wearable Sensors. *Advanced Materials* **2017,** *29* (28), 1701353.

5. Wei, J.; Zheng, Y.; Chen, T., A fully hydrophobic ionogel enables highly efficient wearable underwater sensors and communicators. *Materials Horizons* **2021,** *8* (10), 2761-2770.

6. Corigliano, P.; Crupi, V.; Bertagna, S.; Marinò, A., Bio-Based Adhesives for Wooden Boatbuilding. *Journal of Marine Science and Engineering* **2021,** *9* (1), 28.

7. Li, X.; Deng, Y.; Lai, J.; Zhao, G.; Dong, S., Tough, Long-Term, Water-Resistant, and Underwater Adhesion of Low-Molecular-Weight Supramolecular Adhesives. *Journal of the American Chemical Society* **2020,** *142* (11), 5371-5379.

8. Yang, N.; Yuan, R.; You, D.; Zhang, Q.; Wang, J.; Xuan, H.; Ge, L., Gallol-based constant underwater coating adhesives for severe aqueous conditions. *Colloids and Surfaces A: Physicochemical and Engineering Aspects* **2022,** *634*, 127948.

9. Nam, S.; Mooney, D., Polymeric Tissue Adhesives. *Chemical Reviews* **2021,** *121* (18), 11336-11384.

10. Zhou, J.; Wu, Y.; Zhang, X.; Lai, J.; Li, Y.; Xing, J.; Teng, L.; Chen, J., Enzyme Catalyzed Hydrogel as Versatile Bioadhesive for Tissue Wound Hemostasis, Bonding, and Continuous Repair. *Biomacromolecules* **2021,** *22* (4), 1346-1356.

11. Chen, X.; Yuk, H.; Wu, J.; Nabzdyk, C. S.; Zhao, X., Instant tough bioadhesive with triggerable benign detachment. *Proceedings of the National Academy of Sciences* **2020,** *117* (27), 15497-15503.

12. Islam, M. S.; Reineke, J.; Kaushik, R.; Woyengo, T.; Baride, A.; Alqahtani, M. S.; Perumal, O., Bioadhesive Food Protein Nanoparticles as Pediatric Oral Drug Delivery System. *ACS Applied Materials & Interfaces* **2019,** *11* (20), 18062-18073.

13. Sani, E. S.; Kheirkhah, A.; Rana, D.; Sun, Z.; Foulsham, W.; Sheikhi, A.; Khademhosseini, A.; Dana, R.; Annabi, N., Sutureless repair of corneal injuries using naturally derived bioadhesive hydrogels. *Science Advances* **2019,** *5* (3), eaav1281.

14. Wu, S. J.; Yuk, H.; Wu, J.; Nabzdyk, C. S.; Zhao, X., A Multifunctional Origami Patch for Minimally Invasive Tissue Sealing. *Advanced Materials* **2021,** *33* (11), 2007667.

15. Tian, Y.; Huang, X.; Cheng, Y.; Niu, Y.; Ma, J.; Zhao, Y.; Kou, X.; Ke, Q., Applications of adhesives in textiles: A review. *European Polymer Journal* **2022,** *167*, 111089.

16. Chen, Y.; Meng, J.; Gu, Z.; Wan, X.; Jiang, L.; Wang, S., Bioinspired Multiscale Wet Adhesive Surfaces: Structures and Controlled Adhesion. *Advanced Functional Materials* **2020,** *30* (5), 1905287.

17. Hofman, A. H.; van Hees, I. A.; Yang, J.; Kamperman, M., Bioinspired Underwater Adhesives by Using the Supramolecular Toolbox. *Advanced Materials* **2018,** *30* (19), 1704640.

18. Fan, H.; Gong, J. P., Bioinspired Underwater Adhesives. *Advanced Materials* **2021,** *33* (44), 2102983.

19. Cui, C.; Liu, W., Recent advances in wet adhesives: Adhesion mechanism, design principle and applications. *Progress in Polymer Science* **2021,** *116*, 101388.

20. Qureshi, D. A.; Goffredo, S.; Kim, Y.; Han, Y.; Guo, M.; Ryu, S.; Qin, Z., Why mussel byssal plaques are tiny yet strong in attachment. *Matter* **2022,** *5* (2), 710-724.

21. Waite, J. H., Adhesion à la Moule1. *Integrative and Comparative Biology* **2002,** *42* (6), 1172-1180.

22. Wei, W.; Tan, Y.; Martinez Rodriguez, N. R.; Yu, J.; Israelachvili, J. N.; Waite, J. H., A mussel-derived one component adhesive coacervate. *Acta Biomaterialia* **2014,** *10* (4), 1663-1670.

23. Lee, B. P.; Messersmith, P. B.; Israelachvili, J. N.; Waite, J. H., Mussel-Inspired Adhesives and Coatings. *Annual Review of Materials Research* **2011,** *41* (1), 99-132.

24. Yu, M.; Hwang, J.; Deming, T. J., Role of l-3,4-Dihydroxyphenylalanine in Mussel Adhesive Proteins. *Journal of the American Chemical Society* **1999,** *121* (24), 5825-5826.

25. Stewart, R. J.; Ransom, T. C.; Hlady, V., Natural underwater adhesives. *Journal of Polymer Science Part B: Polymer Physics* **2011,** *49* (11), 757-771.

26. Kord Forooshani, P.; Lee, B. P., Recent approaches in designing bioadhesive materials inspired by mussel adhesive protein. *Journal of Polymer Science Part A: Polymer Chemistry* **2017,** *55* (1), 9-33.

27. DeMartini, D. G.; Errico, J. M.; Sjoestroem, S.; Fenster, A.; Waite, J. H., A cohort of new adhesive proteins identified from transcriptomic analysis of mussel foot glands. *Journal of The Royal Society Interface* **2017,** *14* (131), 20170151.

28. Waite, J. H., Mussel adhesion – essential footwork. *Journal of Experimental Biology* **2017,** *220* (4), 517-530.

29. Wang, C. S.; Stewart, R. J., Localization of the bioadhesive precursors of the sandcastle worm, Phragmatopoma californica (Fewkes). *Journal of Experimental Biology* **2012,** *215* (2), 351-361.

30. Zhao, H.; Sun, C.; Stewart, R. J.; Waite, J. H., Cement Proteins of the Tube-building Polychaete Phragmatopoma californica*. *Journal of Biological Chemistry* **2005,** *280* (52), 42938-42944.

31. Stewart, R. J.; Wang, C. S.; Shao, H., Complex coacervates as a foundation for synthetic underwater adhesives. *Advances in Colloid and Interface Science* **2011,** *167* (1), 85-93.

32. Stewart, R. J.; Wang, C. S.; Song, I. T.; Jones, J. P., The role of coacervation and phase transitions in the sandcastle worm adhesive system. *Advances in Colloid and Interface Science* **2017,** *239*, 88-96.

33. Yang, J.; Cohen Stuart, M. A.; Kamperman, M., Jack of all trades: versatile catechol crosslinking mechanisms. *Chemical Society Reviews* **2014,** *43* (24), 8271-8298.

34. Wang, C. S.; Stewart, R. J., Multipart Copolyelectrolyte Adhesive of the Sandcastle Worm, Phragmatopoma californica (Fewkes): Catechol Oxidase Catalyzed Curing through Peptidyl-DOPA. *Biomacromolecules* **2013,** *14* (5), 1607-1617.

35. Stewart, R. J.; Weaver, J. C.; Morse, D. E.; Waite, J. H., The tube cement of Phragmatopoma californica: a solid foam. *Journal of Experimental Biology* **2004,** *207* (26), 4727-4734.

36. Stevens, M. J.; Steren, R. E.; Hlady, V.; Stewart, R. J., Multiscale Structure of the Underwater Adhesive of Phragmatopoma Californica: a Nanostructured Latex with a Steep Microporosity Gradient. *Langmuir* **2007,** *23* (9), 5045-5049.

37. Priemel, T.; Palia, G.; Förste, F.; Jehle, F.; Sviben, S.; Mantouvalou, I.; Zaslansky, P.; Bertinetti, L.; Harrington, M. J., Microfluidic-like fabrication of metal ion–cured bioadhesives by mussels. *Science* **2021,** *374* (6564), 206-211.

38. Beckert, M.; Flammang, B. E.; Anderson, E. J.; Nadler, J. H., Theoretical and computational fluid dynamics of an attached remora (Echeneis naucrates). *Zoology* **2016,** *119* (5), 430-438.

39. Lee, S. H.; Song, H. W.; Kang, B. S.; Kwak, M. K., Remora-Inspired Reversible Adhesive for Underwater Applications. *ACS Applied Materials & Interfaces* **2019,** *11* (50), 47571-47576.

40. Gamel, K. M.; Garner, A. M.; Flammang, B. E., Bioinspired remora adhesive disc offers insight into evolution. *Bioinspiration & Biomimetics* **2019,** *14* (5), 056014.

41. Drotlef, D. M.; Appel, E.; Peisker, H.; Dening, K.; del Campo, A.; Gorb, S. N.; Barnes, W. J. P., Morphological studies of the toe pads of the rock frog, Staurois parvus (family: Ranidae) and their relevance to the development of new biomimetically inspired reversible adhesives. *Interface Focus* **2015,** *5* (1), 20140036.

42. Langowski, J. K. A.; Dodou, D.; Kamperman, M.; van Leeuwen, J. L., Tree frog attachment: mechanisms, challenges, and perspectives. *Frontiers in Zoology* **2018,** *15* (1), 32.

43. Scholz, I.; Barnes, W. J. P.; Smith, J. M.; Baumgartner, W., Ultrastructure and physical properties of an adhesive surface, the toe pad epithelium of the tree frog, Litoria caerulea White. *Journal of Experimental Biology* **2009,** *212* (2), 155-162.

44. Iturri, J.; Xue, L.; Kappl, M.; García-Fernández, L.; Barnes, W. J. P.; Butt, H.-J.; del Campo, A., Torrent Frog-Inspired Adhesives: Attachment to Flooded Surfaces. *Advanced Functional Materials* **2015,** *25* (10), 1499-1505.

45. Wang, X.; Tan, D.; Zhang, X.; Lei, Y.; Xue, L., Effective Elastic Modulus of Structured Adhesives: From Biology to Biomimetics. *Biomimetics* **2017,** *2* (3), 10.

46. Meng, F.; Liu, Q.; Wang, X.; Tan, D.; Xue, L.; Barnes, W. J. P., Tree frog adhesion biomimetics: opportunities for the development of new, smart adhesives that adhere under wet

conditions. *Philosophical Transactions of the Royal Society A: Mathematical, Physical and Engineering Sciences* **2019,** *377* (2150), 20190131.

47. Crawford, N.; Endlein, T.; Barnes, W. J. P., Self-cleaning in tree frog toe pads; a mechanism for recovering from contamination without the need for grooming. *Journal of Experimental Biology* **2012,** *215* (22), 3965-3972.

48. Lake, G. J.; Thomas, A. G.; Tabor, D., The strength of highly elastic materials. *Proceedings of the Royal Society of London. Series A. Mathematical and Physical Sciences* **1967,** *300* (1460), 108-119.

49. Yuk, H.; Zhang, T.; Lin, S.; Parada, G. A.; Zhao, X., Tough bonding of hydrogels to diverse non-porous surfaces. *Nature Materials* **2016,** *15* (2), 190-196.

50. Gent, A. N., Adhesion and Strength of Viscoelastic Solids. Is There a Relationship between Adhesion and Bulk Properties? *Langmuir* **1996,** *12* (19), 4492-4496.

51. Creton, C.; Ciccotti, M., Fracture and adhesion of soft materials: a review. *Reports on Progress in Physics* **2016,** *79* (4), 046601.

52. Israelachvili, J. N., *Intermolecular and Surface Forces*. Academic Press: 2011.

53. Barrow, S. J.; Kasera, S.; Rowland, M. J.; del Barrio, J.; Scherman, O. A., Cucurbituril-Based Molecular Recognition. *Chemical Reviews* **2015,** *115* (22), 12320-12406.

54. Tomatsu, I.; Hashidzume, A.; Harada, A., Contrast Viscosity Changes upon Photoirradiation for Mixtures of Poly(acrylic acid)-Based α-Cyclodextrin and Azobenzene Polymers. *Journal of the American Chemical Society* **2006,** *128* (7), 2226-2227.

55. Takashima, Y.; Hatanaka, S.; Otsubo, M.; Nakahata, M.; Kakuta, T.; Hashidzume, A.; Yamaguchi, H.; Harada, A., Expansion–contraction of photoresponsive artificial muscle regulated by host–guest interactions. *Nature Communications* **2012,** *3* (1), 1270.

56. Harada, A.; Kobayashi, R.; Takashima, Y.; Hashidzume, A.; Yamaguchi, H., Macroscopic self-assembly through molecular recognition. *Nature Chemistry* **2011,** *3* (1), 34-37.

57. Kakuta, T.; Takashima, Y.; Sano, T.; Nakamura, T.; Kobayashi, Y.; Yamaguchi, H.; Harada, A., Adhesion between Semihard Polymer Materials Containing Cyclodextrin and Adamantane Based on Host–Guest Interactions. *Macromolecules* **2015,** *48* (3), 732-738.

58. Ahn, Y.; Jang, Y.; Selvapalam, N.; Yun, G.; Kim, K., Supramolecular Velcro for Reversible Underwater Adhesion. *Angewandte Chemie International Edition* **2013,** *52* (11), 3140-3144.

59. García, F.; Smulders, M. M. J., Dynamic covalent polymers. *Journal of Polymer Science Part A: Polymer Chemistry* **2016,** *54* (22), 3551-3577.

60. Deng, G.; Ma, Q.; Yu, H.; Zhang, Y.; Yan, Z.; Liu, F.; Liu, C.; Jiang, H.; Chen, Y., Macroscopic Organohydrogel Hybrid from Rapid Adhesion between Dynamic Covalent Hydrogel and Organogel. *ACS Macro Letters* **2015,** *4* (4), 467-471.

61. Liu, B.; Burdine, L.; Kodadek, T., Chemistry of Periodate-Mediated Cross-Linking of 3,4-Dihydroxylphenylalanine-Containing Molecules to Proteins. *Journal of the American Chemical Society* **2006,** *128* (47), 15228-15235.

62. Matos-Pérez, C. R.; White, J. D.; Wilker, J. J., Polymer Composition and Substrate Influences on the Adhesive Bonding of a Biomimetic, Cross-Linking Polymer. *Journal of the American Chemical Society* **2012,** *134* (22), 9498-9505.

63. Yang, J.; Keijsers, J.; van Heek, M.; Stuiver, A.; Cohen Stuart, M. A.; Kamperman, M., The effect of molecular composition and crosslinking on adhesion of a bio-inspired adhesive. *Polymer Chemistry* **2015,** *6* (16), 3121-3130.

64. Krogsgaard, M.; Nue, V.; Birkedal, H., Mussel-Inspired Materials: Self-Healing through Coordination Chemistry. *Chemistry – A European Journal* **2016,** *22* (3), 844-857.

65. Lu, Q.; Danner, E.; Waite, J. H.; Israelachvili, J. N.; Zeng, H.; Hwang, D. S., Adhesion of mussel foot proteins to different substrate surfaces. *Journal of The Royal Society Interface* **2013,** *10* (79), 20120759.

66. Yu, J.; Kan, Y.; Rapp, M.; Danner, E.; Wei, W.; Das, S.; Miller, D. R.; Chen, Y.; Waite, J. H.; Israelachvili, J. N., Adaptive hydrophobic and hydrophilic interactions of mussel foot proteins with organic thin films. *Proceedings of the National Academy of Sciences* **2013,** *110* (39), 15680-15685.

67. Gallivan, J. P.; Dougherty, D. A., A Computational Study of Cation−π Interactions vs Salt Bridges in Aqueous Media: Implications for Protein Engineering. *Journal of the American Chemical Society* **2000,** *122* (5), 870-874.

68. Anderson, T. H.; Yu, J.; Estrada, A.; Hammer, M. U.; Waite, J. H.; Israelachvili, J. N., The Contribution of DOPA to Substrate–Peptide Adhesion and Internal Cohesion of Mussel-Inspired Synthetic Peptide Films. *Advanced Functional Materials* **2010,** *20* (23), 4196-4205.

69. Donaldson, S. H.; Das, S.; Gebbie, M. A.; Rapp, M.; Jones, L. C.; Roiter, Y.; Koenig, P. H.; Gizaw, Y.; Israelachvili, J. N., Asymmetric Electrostatic and Hydrophobic–Hydrophilic Interaction Forces between Mica Surfaces and Silicone Polymer Thin Films. *ACS Nano* **2013,** *7* (11), 10094-10104.

70. Das, S.; Miller, D. R.; Kaufman, Y.; Martinez Rodriguez, N. R.; Pallaoro, A.; Harrington, M. J.; Gylys, M.; Israelachvili, J. N.; Waite, J. H., Tough Coating Proteins: Subtle Sequence Variation Modulates Cohesion. *Biomacromolecules* **2015,** *16* (3), 1002-1008.

71. Harrington, M. J.; Masic, A.; Holten-Andersen, N.; Waite, J. H.; Fratzl, P., Iron-Clad Fibers: A Metal-Based Biological Strategy for Hard Flexible Coatings. *Science* **2010,** *328* (5975), 216-220.

72. Ahn, B. K.; Lee, D. W.; Israelachvili, J. N.; Waite, J. H., Surface-initiated self-healing of polymers in aqueous media. *Nature Materials* **2014,** *13* (9), 867-872.

73. Li, S.-C.; Wang, J.-g.; Jacobson, P.; Gong, X. Q.; Selloni, A.; Diebold, U., Iron-Clad Fibers: A Metal-Based Biological Strategy for Hard Flexible CoatingsCorrelation between Bonding Geometry and Band Gap States at Organic−Inorganic Interfaces: Catechol on Rutile TiO2(110). *Journal of the American Chemical Society* **2009,** *131* (3), 980-984.

74. Lin, Q.; Gourdon, D.; Sun, C.; Holten-Andersen, N.; Anderson, T. H.; Waite, J. H.; Israelachvili, J. N., Adhesion mechanisms of the mussel foot proteins mfp-1 and mfp-3. *Proceedings of the National Academy of Sciences* **2007,** *104* (10), 3782-3786.

75. Zeng, H.; Hwang, D. S.; Israelachvili, J. N.; Waite, J. H., Strong reversible Fe³⁺-mediated bridging between dopa-containing protein films in water. *Proceedings of the National Academy of Sciences* **2010,** *107* (29), 12850-12853.

76. Holten-Andersen, N.; Harrington, M. J.; Birkedal, H.; Lee, B. P.; Messersmith, P. B.; Lee, K. Y. C.; Waite, J. H., pH-induced metal-ligand cross-links inspired by mussel yield self-healing polymer networks with near-covalent elastic moduli. *Proceedings of the National Academy of Sciences* **2011,** *108* (7), 2651-2655.

77. Ye, Q.; Zhou, F.; Liu, W., Bioinspired catecholic chemistry for surface modification. *Chemical Society Reviews* **2011,** *40* (7), 4244-4258.

78. North, M. A.; Del Grosso, C. A.; Wilker, J. J., High Strength Underwater Bonding with Polymer Mimics of Mussel Adhesive Proteins. *ACS Applied Materials & Interfaces* **2017,** *9* (8), 7866-7872.

79. Zhan, K.; Kim, C.; Sung, K.; Ejima, H.; Yoshie, N., Tunicate-Inspired Gallol Polymers for Underwater Adhesive: A Comparative Study of Catechol and Gallol. *Biomacromolecules* **2017,** *18* (9), 2959-2966.

80. Yu, J.; Cheng, B.; Ejima, H., Effect of molecular weight and polymer composition on gallol-functionalized underwater adhesive. *Journal of Materials Chemistry B* **2020,** *8* (31), 6798-6801.

81. White, J. D.; Wilker, J. J., Underwater Bonding with Charged Polymer Mimics of Marine Mussel Adhesive Proteins. *Macromolecules* **2011,** *44* (13), 5085-5088.

82. Jones, T. A.; Wilker, J. J., Influences of Phosphates on the Adhesion of a Catechol-Containing Polymer. *ACS Applied Polymer Materials* **2020,** *2* (11), 4632-4639.

83. Mu, Y.; Wu, X.; Pei, D.; Wu, Z.; Zhang, C.; Zhou, D.; Wan, X., Contribution of the Polarity of Mussel-Inspired Adhesives in the Realization of Strong Underwater Bonding. *ACS Biomaterials Science & Engineering* **2017,** *3* (12), 3133-3140.

84. Ahn, B. K.; Das, S.; Linstadt, R.; Kaufman, Y.; Martinez-Rodriguez, N. R.; Mirshafian, R.; Kesselman, E.; Talmon, Y.; Lipshutz, B. H.; Israelachvili, J. N.; Waite, J. H., High-performance mussel-inspired adhesives of reduced complexity. *Nature Communications* **2015,** *6* (1), 8663.

85. Seo, S.; Das, S.; Zalicki, P. J.; Mirshafian, R.; Eisenbach, C. D.; Israelachvili, J. N.; Waite, J. H.; Ahn, B. K., Microphase Behavior and Enhanced Wet-Cohesion of Synthetic Copolyampholytes Inspired by a Mussel Foot Protein. *Journal of the American Chemical Society* **2015,** *137* (29), 9214-9217.

86. Baik, S.; Kim, D. W.; Park, Y.; Lee, T.-J.; Ho Bhang, S.; Pang, C., A wet-tolerant adhesive patch inspired by protuberances in suction cups of octopi. *Nature* **2017,** *546* (7658), 396-400.

87. Wilker, J. J., How to suck like an octopus. *Nature* **2017,** *546* (7658), 358-359.

88. Baik, S.; Kim, J.; Lee, H. J.; Lee, T. H.; Pang, C., Highly Adaptable and Biocompatible Octopus-Like Adhesive Patches with Meniscus-Controlled Unfoldable 3D Microtips for Underwater Surface and Hairy Skin. *Advanced Science* **2018,** *5* (8), 1800100.

89. Kim, D. W.; Song, K.-I.; Seong, D.; Lee, Y. S.; Baik, S.; Song, J. H.; Lee, H. J.; Son, D.; Pang, C., Electrostatic–Mechanical Synergistic In Situ Multiscale Tissue Adhesion for Sustainable Residue-Free Bioelectronics Interfaces. *Advanced Materials* **2022,** *34* (5), 2105338.

90. Kim, D. W.; Baik, S.; Min, H.; Chun, S.; Lee, H. J.; Kim, K. H.; Lee, J. Y.; Pang, C., Highly Permeable Skin Patch with Conductive Hierarchical Architectures Inspired by Amphibians and Octopi for Omnidirectionally Enhanced Wet Adhesion. *Advanced Functional Materials* **2019,** *29* (13), 1807614.

91. Min, H.; Baik, S.; Kim, J.; Lee, J.; Bok, B.-G.; Song, J. H.; Kim, M.-S.; Pang, C., Tough Carbon Nanotube-Implanted Bioinspired Three-Dimensional Electrical Adhesive for Isotropically Stretchable Water-Repellent Bioelectronics. *Advanced Functional Materials* **2022,** *32* (8), 2107285.

92. Wang, Y.; Hensel, R., Bioinspired Underwater Adhesion to Rough Substrates by Cavity Collapse of Cupped Microstructures. *Advanced Functional Materials* **2021,** *31* (31), 2101787.

93. Wang, Y.; Kang, V.; Arzt, E.; Federle, W.; Hensel, R., Strong Wet and Dry Adhesion by Cupped Microstructures. *ACS Applied Materials & Interfaces* **2019,** *11* (29), 26483-26490.

94. Wang, Y.; Kang, V.; Federle, W.; Arzt, E.; Hensel, R., Switchable Underwater Adhesion by Deformable Cupped Microstructures. *Advanced Materials Interfaces* **2020,** *7* (23), 2001269.

95. Liu, J.; Wang, S.; Shen, Q.; Kong, L.; Huang, G.; Wu, J., Tough Underwater Super-tape Composed of Semi-interpenetrating Polymer Networks with a Water-Repelling Liquid Surface. *ACS Applied Materials & Interfaces* **2021,** *13* (1), 1535-1544.

96. Xu, Y.; Liu, Q.; Narayanan, A.; Jain, D.; Dhinojwala, A.; Joy, A., Mussel-Inspired Polyesters with Aliphatic Pendant Groups Demonstrate the Importance of Hydrophobicity in Underwater Adhesion. *Advanced Materials Interfaces* **2017,** *4* (22), 1700506.

97. Dolez, P.; Williams, C.; Goff, A.; Love, B., Properties of Photopolymerisable Acrylic Adhesives for Underwater Bonding. *Underwater Technology: The International Journal of The Society for Underwater* **2003,** *25*, 199-208.

98. Zhou, J.; Wan, Y.; Liu, N.; Yin, H.; Li, B.; Sun, D.; Ran, Q., Epoxy adhesive with high underwater adhesion and stability based on low viscosity modified Mannich bases. *Journal of Applied Polymer Science* **2018,** *135* (3), 45688.

99. Narayanan, A.; Kaur, S.; Peng, C.; Debnath, D.; Mishra, K.; Liu, Q.; Dhinojwala, A.; Joy, A., Viscosity Attunes the Adhesion of Bioinspired Low Modulus Polyester Adhesive Sealants to Wet Tissues. *Biomacromolecules* **2019,** *20* (7), 2577-2586.

100. Liu, Y.; Guan, G.; Li, Y.; Tan, J.; Cheng, P.; Yang, M.; Li, B.; Wang, Q.; Zhong, W.; Mequanint, K.; Zhu, C.; Xing, M., Gelation of highly entangled hydrophobic macromolecular fluid for ultrastrong underwater in situ fast tissue adhesion. *Science Advances* **2022,** *8* (20), eabm9744.

101. Liu, X.; Zhang, Q.; Duan, L.; Gao, G., Bioinspired Nucleobase-Driven Nonswellable Adhesive and Tough Gel with Excellent Underwater Adhesion. *ACS Applied Materials & Interfaces* **2019,** *11* (6), 6644-6651.

102. Han, L.; Wang, M.; Prieto-López, L. O.; Deng, X.; Cui, J., Self-Hydrophobization in a Dynamic Hydrogel for Creating Nonspecific Repeatable Underwater Adhesion. *Advanced Functional Materials* **2020,** *30* (7), 1907064.

103. Yuk, H.; Varela, C. E.; Nabzdyk, C. S.; Mao, X.; Padera, R. F.; Roche, E. T.; Zhao, X., Dry double-sided tape for adhesion of wet tissues and devices. *Nature* **2019,** *575* (7781), 169-174.

104. Zhou, Y.; Zhang, C.; Gao, S.; Zhang, B.; Sun, J.; Kai, J.-j.; Wang, B.; Wang, Z., Instant and Strong Underwater Adhesion by Coupling Hygroscopicity and In Situ Photocuring. *Chemistry of Materials* **2021,** *33* (22), 8822-8830.

105. Wang, Z.; Guo, L.; Xiao, H.; Cong, H.; Wang, S., A reversible underwater glue based on photo- and thermo-responsive dynamic covalent bonds. *Materials Horizons* **2020,** *7* (1), 282-288.

106. Pan, F.; Ye, S.; Wang, R.; She, W.; Liu, J.; Sun, Z.; Zhang, W., Hydrogel networks as underwater contact adhesives for different surfaces. *Materials Horizons* **2020,** *7* (8), 2063-2070.

107. Rao, P.; Sun, T. L.; Chen, L.; Takahashi, R.; Shinohara, G.; Guo, H.; King, D. R.; Kurokawa, T.; Gong, J. P., Tough Hydrogels with Fast, Strong, and Reversible Underwater Adhesion Based on a Multiscale Design. *Advanced Materials* **2018,** *30* (32), 1801884.

108. Gucht, J. v. d.; Spruijt, E.; Lemmers, M.; Cohen Stuart, M. A., Polyelectrolyte complexes: Bulk phases and colloidal systems. *Journal of Colloid and Interface Science* **2011,** *361* (2), 407-422.

109. Spruijt, E.; Westphal, A. H.; Borst, J. W.; Cohen Stuart, M. A.; van der Gucht, J., Binodal Compositions of Polyelectrolyte Complexes. *Macromolecules* **2010,** *43* (15), 6476-6484.

110. Spruijt, E.; Sprakel, J.; Lemmers, M.; Stuart, M. A. C.; van der Gucht, J., Relaxation Dynamics at Different Time Scales in Electrostatic Complexes: Time-Salt Superposition. *Physical Review Letters* **2010,** *105* (20), 208301.

111. Shao, H.; Stewart, R. J., Biomimetic Underwater Adhesives with Environmentally Triggered Setting Mechanisms. *Advanced Materials* **2010,** *22* (6), 729-733.

112. Kaur, S.; Weerasekare, G. M.; Stewart, R. J., Multiphase Adhesive Coacervates Inspired by the Sandcastle Worm. *ACS Applied Materials & Interfaces* **2011,** *3* (4), 941-944.

113. Zhao, Q.; Lee, D. W.; Ahn, B. K.; Seo, S.; Kaufman, Y.; Israelachvili, Jacob N.; Waite, J. H., Underwater contact adhesion and microarchitecture in polyelectrolyte complexes actuated by solvent exchange. *Nature Materials* **2016,** *15* (4), 407-412.

114. Kim, K.; Shin, M.; Koh, M.-Y.; Ryu, J. H.; Lee, M. S.; Hong, S.; Lee, H., TAPE: A Medical Adhesive Inspired by a Ubiquitous Compound in Plants. *Advanced Functional Materials* **2015,** *25* (16), 2402-2410.

115. Lee, D.; Hwang, H.; Kim, J.-S.; Park, J.; Youn, D.; Kim, D.; Hahn, J.; Seo, M.; Lee, H., VATA: A Poly(vinyl alcohol)- and Tannic Acid-Based Nontoxic Underwater Adhesive. *ACS Applied Materials & Interfaces* **2020,** *12* (18), 20933-20941.

116. Peng, Q.; Chen, J.; Zeng, Z.; Wang, T.; Xiang, L.; Peng, X.; Liu, J.; Zeng, H., Adhesive Coacervates Driven by Hydrogen-Bonding Interaction. *Small* **2020,** *16* (43), 2004132.

117. Cui, C.; Fan, C.; Wu, Y.; Xiao, M.; Wu, T.; Zhang, D.; Chen, X.; Liu, B.; Xu, Z.; Qu, B.; Liu, W., Water-Triggered Hyperbranched Polymer Universal Adhesives: From Strong Underwater Adhesion to Rapid Sealing Hemostasis. *Advanced Materials* **2019,** *31* (49), 1905761.

118. Peng, Q.; Wu, Q.; Chen, J.; Wang, T.; Wu, M.; Yang, D.; Peng, X.; Liu, J.; Zhang, H.; Zeng, H., Coacervate-Based Instant and Repeatable Underwater Adhesive with Anticancer and Antibacterial Properties. *ACS Applied Materials & Interfaces* **2021,** *13* (40), 48239-48251.

119. Dompé, M.; Cedano-Serrano, F. J.; Heckert, O.; van den Heuvel, N.; van der Gucht, J.; Tran, Y.; Hourdet, D.; Creton, C.; Kamperman, M., Thermoresponsive Complex Coacervate-Based Underwater Adhesive. *Advanced Materials* **2019,** *31* (21), 1808179.

120. Dompé, M.; Cedano-Serrano, F. J.; Vahdati, M.; van Westerveld, L.; Hourdet, D.; Creton, C.; van der Gucht, J.; Kodger, T.; Kamperman, M., Underwater Adhesion of Multiresponsive Complex Coacervates. *Advanced Materials Interfaces* **2020,** *7* (4), 1901785.

121. Dompé, M.; Cedano-Serrano, F. J.; Vahdati, M.; Sidoli, U.; Heckert, O.; Synytska, A.; Hourdet, D.; Creton, C.; van der Gucht, J.; Kodger, T.; Kamperman, M., Tuning the Interactions in Multiresponsive Complex Coacervate-Based Underwater Adhesives. *International Journal of Molecular Sciences* **2020,** *21* (1), 100.

122. van Hees, I. A.; Hofman, A. H.; Dompé, M.; van der Gucht, J.; Kamperman, M., Temperature-responsive polyelectrolyte complexes for bio-inspired underwater adhesives. *European Polymer Journal* **2020,** *141*, 110034.

123. Dompé, M.; Vahdati, M.; van Ligten, F.; Cedano-Serrano, F. J.; Hourdet, D.; Creton, C.; Zanetti, M.; Bracco, P.; van der Gucht, J.; Kodger, T.; Kamperman, M., Enhancement of the Adhesive Properties by Optimizing the Water Content in PNIPAM-Functionalized Complex Coacervates. *ACS Applied Polymer Materials* **2020,** *2* (4), 1722-1730.

124. Sun, J.-Y.; Zhao, X.; Illeperuma, W. R. K.; Chaudhuri, O.; Oh, K. H.; Mooney, D. J.; Vlassak, J. J.; Suo, Z., Highly stretchable and tough hydrogels. *Nature* **2012,** *489* (7414), 133-136.

125. Li, J.; Celiz, A. D.; Yang, J.; Yang, Q.; Wamala, I.; Whyte, W.; Seo, B. R.; Vasilyev, N. V.; Vlassak, J. J.; Suo, Z.; Mooney, D. J., Tough adhesives for diverse wet surfaces. *Science* **2017,** *357* (6349), 378-381.

126. Sun, T. L.; Kurokawa, T.; Kuroda, S.; Ihsan, A. B.; Akasaki, T.; Sato, K.; Haque, M. A.; Nakajima, T.; Gong, J. P., Physical hydrogels composed of polyampholytes demonstrate high toughness and viscoelasticity. *Nature Materials* **2013,** *12* (10), 932-937.

127. Roy, C. K.; Guo, H. L.; Sun, T. L.; Ihsan, A. B.; Kurokawa, T.; Takahata, M.; Nonoyama, T.; Nakajima, T.; Gong, J. P., Self-Adjustable Adhesion of Polyampholyte Hydrogels. *Advanced Materials* **2015,** *27* (45), 7344-7348.

128. Stuart McLaughlin; Jiyao Wang; Alok Gambhir; Murray, D., PIP2 and Proteins: Interactions, Organization, and Information Flow. *Annual Review of Biophysics and Biomolecular Structure* **2002,** *31* (1), 151-175.

129. Dougherty, D. A., The Cation−π Interaction. *Accounts of Chemical Research* **2013,** *46* (4), 885-893.

130. Mahadevi, A. S.; Sastry, G. N., Cation−π Interaction: Its Role and Relevance in Chemistry, Biology, and Material Science. *Chemical Reviews* **2013,** *113* (3), 2100-2138.

131. Fan, H.; Wang, J.; Tao, Z.; Huang, J.; Rao, P.; Kurokawa, T.; Gong, J. P., Adjacent cationic–aromatic sequences yield strong electrostatic adhesion of hydrogels in seawater. *Nature Communications* **2019,** *10* (1), 5127.

132. Fan, H.; Wang, J.; Gong, J. P., Barnacle Cement Proteins-Inspired Tough Hydrogels with Robust, Long-Lasting, and Repeatable Underwater Adhesion. *Advanced Functional Materials* **2021,** *31* (11), 2009334.

133. Moulay, S., Dopa/Catechol-Tethered Polymers: Bioadhesives and Biomimetic Adhesive Materials. *Polymer Reviews* **2014,** *54* (3), 436-513.

134. Shan, M.; Gong, C.; Li, B.; Wu, G., A pH, glucose, and dopamine triple-responsive, self-healable adhesive hydrogel formed by phenylborate–catechol complexation. *Polymer Chemistry* **2017,** *8* (19), 2997-3005.

135. Cholewinski, A.; Yang, F.; Zhao, B., Algae–mussel-inspired hydrogel composite glue for underwater bonding. *Materials Horizons* **2019,** *6* (2), 285-293.

136. Cholewinski, A.; Yang, F.; Zhao, B., Glycerol-Stabilized Algae–Mussel-Inspired Adhesives for Underwater Bonding. *Industrial & Engineering Chemistry Research* **2020,** *59* (34), 15255-15263.

137. Lee, H.; Dellatore, S. M.; Miller, W. M.; Messersmith, P. B., Mussel-Inspired Surface Chemistry for Multifunctional Coatings. *Science* **2007,** *318* (5849), 426-430.

138. Israelachvili, J. N.; Adams, G. E., Measurement of forces between two mica surfaces in aqueous electrolyte solutions in the range 0–100 nm. *Journal of the Chemical Society, Faraday Transactions 1: Physical Chemistry in Condensed Phases* **1978,** *74* (0), 975-1001.

139. Israelachvili, J. N.; Tabor, D., The measurement of van der Waals dispersion forces in the range 1.5 to 130 nm. *Proceedings of the Royal Society of London. A. Mathematical and Physical Sciences* **1972,** *331* (1584), 19-38.

140. Tabor, D.; Winterton, R. H. S., Surface Forces: Direct Measurement of Normal and Retarded van der Waals Forces. *Nature* **1968,** *219* (5159), 1120-1121.

141. Israelachvili, J. N.; Adams, G. E., Direct measurement of long range forces between two mica surfaces in aqueous KNO3 solutions. *Nature* **1976,** *262* (5571), 774-776.

142. Ruths, M.; Israelachvili, J., Surface Forces and Nanorheology of Molecularly Thin Films. In *Springer Handbook of Nanotechnology*, Bhushan, B., Ed. Springer Berlin Heidelberg: Berlin, Heidelberg, 2007; pp 859-924.

143. Restagno, F.; Crassous, J.; Charlaix, É.; Cottin-Bizonne, C.; Monchanin, M., A new surface forces apparatus for nanorheology. *Review of Scientific Instruments* **2002,** *73* (6), 2292-2297.

144. Valtiner, M.; Donaldson, S. H.; Gebbie, M. A.; Israelachvili, J. N., Hydrophobic Forces, Electrostatic Steering, and Acid–Base Bridging between Atomically Smooth Self-Assembled Monolayers and End-Functionalized PEGolated Lipid Bilayers. *Journal of the American Chemical Society* **2012,** *134* (3), 1746-1753.

145. Binnig, G.; Quate, C. F.; Gerber, C., Atomic Force Microscope. *Physical Review Letters* **1986,** *56* (9), 930-933.

146. Ducker, W. A.; Senden, T. J.; Pashley, R. M., Direct measurement of colloidal forces using an atomic force microscope. *Nature* **1991,** *353* (6341), 239-241.

147. Butt, H.-J., Measuring electrostatic, van der Waals, and hydration forces in electrolyte solutions with an atomic force microscope. *Biophysical Journal* **1991,** *60* (6), 1438-1444.

148. Butt, H.-J.; Cappella, B.; Kappl, M., Force measurements with the atomic force microscope: Technique, interpretation and applications. *Surface Science Reports* **2005,** *59* (1), 1-152.

149. Chung, H.; Grubbs, R. H., Rapidly Cross-Linkable DOPA Containing Terpolymer Adhesives and PEG-Based Cross-Linkers for Biomedical Applications. *Macromolecules* **2012,** *45* (24), 9666-9673.

150. Mussault, C.; Guo, H.; Sanson, N.; Hourdet, D.; Marcellan, A., Effect of responsive graft length on mechanical toughening and transparency in microphase-separated hydrogels. *Soft Matter* **2019,** *15* (43), 8653-8666.

151. Rose, S.; Prevoteau, A.; Elzière, P.; Hourdet, D.; Marcellan, A.; Leibler, L., Nanoparticle solutions as adhesives for gels and biological tissues. *Nature* **2014,** *505* (7483), 382-385.

152. Gardon, J. L., Peel adhesion. I. Some phenomenological aspects of the test. *Journal of Applied Polymer Science* **1963,** *7* (2), 625-641.

153. Villey, R.; Creton, C.; Cortet, P.-P.; Dalbe, M.-J.; Jet, T.; Saintyves, B.; Santucci, S.; Vanel, L.; Yarusso, D. J.; Ciccotti, M., Rate-dependent elastic hysteresis during the peeling of pressure sensitive adhesives. *Soft Matter* **2015,** *11* (17), 3480-3491.

154. Villey, R.; Cortet, P.-P.; Creton, C.; Ciccotti, M., In-situ measurement of the large strain response of the fibrillar debonding region during the steady peeling of pressure sensitive adhesives. *International Journal of Fracture* **2017,** *204* (2), 175-190.

155. Sudre, G.; Olanier, L.; Tran, Y.; Hourdet, D.; Creton, C., Reversible adhesion between a hydrogel and a polymer brush. *Soft Matter* **2012,** *8* (31), 8184-8193.

156. Macron, J.; Bresson, B.; Tran, Y.; Hourdet, D.; Creton, C., Equilibrium and Out-of-Equilibrium Adherence of Hydrogels against Polymer Brushes. *Macromolecules* **2018,** *51* (19), 7556-7566.

157. Cedano-Serrano, F. J. From molecular architecture and electrostatic interactions to underwater adherence of hydrogels. PhD Thesis, Sorbonne Université, 2019.

158. Vahdati, M.; Ducouret, G.; Creton, C.; Hourdet, D., Thermally Triggered Injectable Underwater Adhesives. *Macromolecular Rapid Communications* **2020,** *41* (7), 1900653.

159. Vahdati, M.; Ducouret, G.; Creton, C.; Hourdet, D., Topology-Specific Injectable Sticky Hydrogels. *Macromolecules* **2020,** *53* (22), 9779-9792.

160. Vahdati, M.; Cedano-Serrano, F. J.; Creton, C.; Hourdet, D., Coacervate-Based Underwater Adhesives in Physiological Conditions. *ACS Applied Polymer Materials* **2020,** *2* (8), 3397-3410.

161. Chollet, B.; Li, M.; Martwong, E.; Bresson, B.; Fretigny, C.; Tabeling, P.; Tran, Y., Multiscale Surface-Attached Hydrogel Thin Films with Tailored Architecture. *ACS Applied Materials & Interfaces* **2016,** *8* (18), 11729-11738.

162. Chollet, B.; D'Eramo, L.; Martwong, E.; Li, M.; Macron, J.; Mai, T. Q.; Tabeling, P.; Tran, Y., Tailoring Patterns of Surface-Attached Multiresponsive Polymer Networks. *ACS Applied Materials & Interfaces* **2016,** *8* (37), 24870-24879.

163. Li, M.; Bresson, B.; Cousin, F.; Fretigny, C.; Tran, Y., Submicrometric Films of Surface-Attached Polymer Network with Temperature-Responsive Properties. *Langmuir* **2015,** *31* (42), 11516-11524.

164. Cedano-Serrano, F. J.; Sidoli, U.; Synytska, A.; Tran, Y.; Hourdet, D.; Creton, C., From Molecular Electrostatic Interactions and Hydrogel Architecture to Macroscopic Underwater Adherence. *Macromolecules* **2019,** *52* (10), 3852-3862.

165. Xu, Z.; Li, J.; Gao, G.; Wang, Z.; Cong, Y.; Chen, J.; Yin, J.; Nie, L.; Fu, J., Tough and self-recoverable hydrogels crosslinked by triblock copolymer micelles and Fe3+ coordination. *Journal of Polymer Science Part B: Polymer Physics* **2018,** *56* (11), 865-876.

166. Simha, N. K.; Carlson, C. S.; Lewis, J. L., Evaluation of fracture toughness of cartilage by micropenetration. *Journal of Materials Science: Materials in Medicine* **2004,** *15* (5), 631-639.

167. Gong, J. P., Why are double network hydrogels so tough? *Soft Matter* **2010,** *6* (12), 2583-2590.

168. Gong, J. P., Materials both Tough and Soft. *Science* **2014,** *344* (6180), 161-162.

Chapter 2

Substrate-attached Hydrogel Thin Coatings with Gelatins

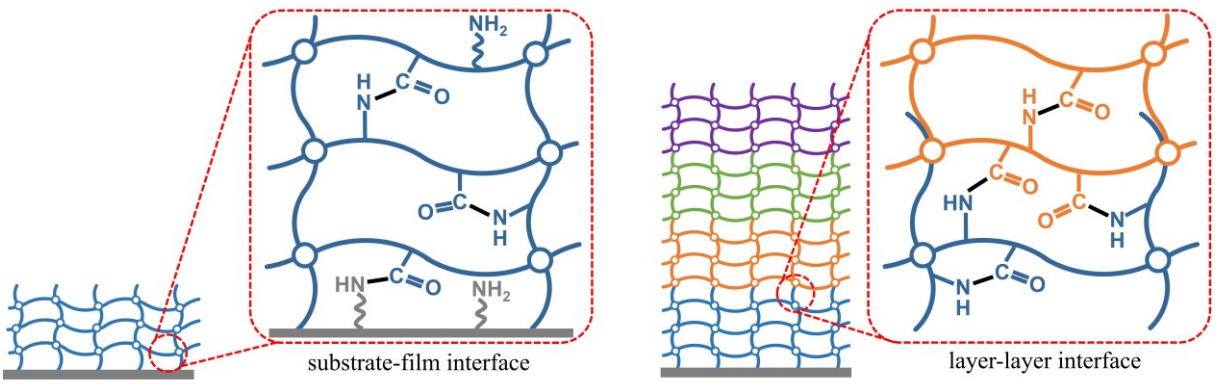

Hydrogel coatings and multilayers

Abstract

This chapter describes a simple and easy approach to building grafted biopolymer coatings on various substrates that could have potential applications in the fields of biotechnology and biomedicine. Biopolymer coatings are thin layers of chemical networks of gelatin hydrogels attached on substrates, with good chemical and thermal stability. Gelatin hydrogel coatings are synthesized using the CLAG (Cross-Linking and Grafting) strategy, which consists of simultaneous crosslinking and surface grafting of gelatin chains via peptide bonds. The CLAG strategy is performed on different substrates such as flat silicon surfaces and silicon microfibers. The thickness of the coatings can vary over a wide range from a few nanometers to several micrometers, by changing the coating parameters or by using a multilayer strategy. The physicochemical properties are finely characterized, such as the swelling of the hydrogel coating which is controlled by the concentration of the chemical crosslinking reagent and the aqueous conditions. The biodegradation properties of the coatings are also studied. Finally, gelatin coatings have been shown to be a very efficient platform for the delivery of drugs such as dexamethasone.

Résumé

Ce chapitre décrit une approche simple et facile pour construire des revêtements de biopolymères greffés sur divers substrats qui pourraient avoir des applications potentielles dans les domaines de la biotechnologie et de la biomédecine. Les revêtements de biopolymères sont des couches minces de réseaux chimiques d'hydrogels de gélatine attachés sur substrats, avec une bonne stabilité chimique et thermique. Les revêtements d'hydrogel de gélatine sont synthétisés à partir de la stratégie CLAG (pour Cross-Linking and Grafting) qui consiste à réticuler et à greffer en surface simultanément des chaînes de gélatine par des liaisons peptidiques. La stratégie CLAG est réalisée sur différents substrats tels que des surfaces planes de silicium et des microfibres de silicone. L'épaisseur des revêtements peut varier dans une large gamme de quelques nanomètres à plusieurs micromètres, en changeant les paramètres de dépôt ou en utilisant une stratégie multicouches. Les propriétés physico-chimiques sont finement caractérisées, comme le gonflement du revêtement d'hydrogel qui est contrôlé par la concentration du réactif de réticulation chimique et les conditions aqueuses. Les propriétés de biodégradation des revêtements sont également étudiées. Les revêtements de gélatine se sont enfin révélés être une plateforme très efficace pour la libération de médicaments tels que la dexaméthasone.

Table of Contents

Chapter 2. Substrate-attached Hydrogel Thin Coatings with Gelatins

1 Introduction

Biopolymer coatings have considerable potentials in food packaging,[1-2] chemical engineering[3-4] and biomedicine,[5] because biopolymers produced from natural sources exhibit good bioactivity, biocompatibility, bioresorbability and nontoxicity.[6] The most common approaches to construct polymer coatings are layer-by-layer assemblies[7] and polymer brushes.[8-9] Layer-by-layer assemblies are realized by assembling polymer layers by physical bonds, such as hydrogen bonding,[10-11] electrostatic interactions[12-13] and hydrophobic interactions,[14-15] which provide a facile fabrication of multicomponent films on solid substrates. Polymer brushes are polymer coatings where polymer chains are chemically grafted to the surfaces or supports.[16-19] However, both layer-by-layer assemblies and polymer brushes have some intrinsic inconveniences in making polymer coatings. The technology of layer-by-layer assemblies is characterized by a long preparation time and limited stability of the coatings.[20] Moreover, the thickness of polymer brushes is restricted at low submicrometer because of the limitations due to the length of polymer chains.[21-22]

Gelatin is a high molecular weight polypeptide derived from collagen.[23] As the primary protein component of animal connective tissues, gelatin is a representative biopolymer, which has promising applications in tissue engineering[24-25] and regeneration,[26] due to biocompatibility, thermo-sensitivity and tissue adhesiveness.[27] It is widely known that gelatin forms a physical network by intermolecular triple-helix when the solution is cooled, going through a sol-gel transition process. Yet, these physically crosslinked gels are neither thermally nor mechanically stable, which significantly limits the practical applications of gelatin hydrogels and coatings.[28] Therefore, it is important to explore a strategy to construct gelatin coatings with interfacial stability and thermal stability under temperature changes.

In the last decade, surface-attached hydrogel thin films, inspired by macroscopic hydrogels, have been an alternative to layer-by-layer assemblies and polymer brushes for making stable and durable polymer coatings.[29-30] A polymer network is much more stable at interfaces, because the polymer network is linked to the surface by multiple anchoring points, while in polymer brushes a polymer chain is grafted to the surface by only one functional group. A crosslinking and grafting (CLAG) strategy was developed by our group, to synthesize reliable and reproducible surface-attached hydrogel thin films. Generally, surface-attached hydrogel films were synthesized by simultaneously crosslinking and grafting polymers by thiol-ene click reaction, as described in details in previous papers.[20, 31-32] This is a simple and versatile approach

involving a wide variety of synthetic polymers/copolymers and providing a wide range of thickness from nanometers to micrometers. Exploring the CLAG strategy to biopolymer systems such as gelatins by constructing chemical crosslinking between polymer chains and chemical grafting, could improve both thermal and interfacial stability of the coatings, which is very promising for the potential applications of biopolymer coatings.

In this work, we report a simple, facile and versatile method inspired by CLAG, to fabricate surface-attached gelatin hydrogel thin coatings. In general, the gelatins are coated on amine-modified substrates and are then chemically crosslinked and grafted simultaneously by peptide reaction using *N*-(3-dimethylaminopropyl)-*N*'-ethylcarbodiimide hydrochloride (EDC) and *N*-hydroxysuccinimide (NHS) coupling agent. We show that the surface-attached gelatin hydrogel coatings are obtained with a wide range of thicknesses from nanometers to micrometers. Moreover, spin-coating is chosen for wafers and dip-coating for fibers, to meet the demand of different substrates and corresponding applications. The gelatins investigated are both type A and type B, which were produced from acid- and alkali-treated precursor respectively, with the main difference in isoelectric points. The physical chemistry including thickness, swelling and biodegradation are studied. The application in drug incorporation and release is also realized on fibers, as an example for surgical implants.

2 Experimental Section

2.1 Materials

Gelatin type A (from porcine skin, gel strength ~ 300 g bloom), gelatin type B (from bovine skin, gel strength ~ 225 g bloom), *N*-(3-dimethylaminopropyl)-*N'*-ethylcarbodiimide hydrochloride (EDC) and *N*-hydroxysuccinimide (NHS), dry toluene (anhydrous, 99.8%), phosphate buffered saline and dexamethasone sodium phosphate (DSP) were purchased from Sigma-Aldrich. (3-Aminopropyl)trimethoxysilane was obtained from abcr. Gute Chemie. Silicon wafers were purchased from Neyco. PDMS fibers were provided by Oticon Medical. Milli-Q water (Millipore) was used for all experiments. All chemicals were used without any further purification.

2.2 Amino-modification of substrates

Amino-modification of both silicon wafers and PDMS fibers was performed by silanization using (3-aminopropyl)trimethoxysilane. The silicon wafers were cleaned by O_2/O_3 inside UV ozone before being immersed in a solution of anhydrous toluene with 3 vol% of (3-aminopropyl)trimethoxysilane under nitrogen for 3 h. The same method was used on PDMS fibers, except the cleaning and activation by plasma treatment and the solvent used for silanization. The solvent selected has to be non-solvent for PDMS substrates to avoid from swelling and damaging the substrates. Toluene which was used for silicon substrate was replaced by absolute ethanol for silanization of PDMS fibers.

2.3 Synthesis of thin films on plane substrate

Both gelatin type A (GA) and gelatin type B (GB) thin films were synthesized by simultaneously crosslinking and grafting gelatin chains onto the amino-modified silicon wafers with peptide covalent bond as shown in **Figure 1a**. After being dissolved in Milli-Q water at 50 °C for 12 hours, gelatin solution was mixed with freshly prepared EDC/NHS aqueous solution. After a stirring of 30 s, the mixture was deposited on the amine-modified silicon wafer before spin-coating at 5000 rpm during 30 s. The spin-coating was also under ~50 °C to keep the gelatin in melting state rather than gel state. The gelatin film was left for 3 h under 50 °C to crosslink gelatin chains and graft the film onto the silicon wafer. Finally, after being washed in an ultrasonic bath with hot water (50 °C) to remove unreacted reagents (free polymers and EDC/NHS), the gelatin hydrogel thin film grafted onto silicon wafer was obtained. In all the gelatin solutions investigated, the concentration of EDC/NHS (1:1 in molar) to gelatin was kept at 2 mM for each weight percent of gelatin. For example, the EDC/NHS was 10 mM for 5 wt% gelatin solution.

2.4 Synthesis of coatings on microfibers

The coatings on fibers followed the same CLAG strategy of films on silicon wafers, but were obtained using dip-coating technique. Generally, as shown in **Figure 1b**, the amino-modified PDMS fibers were coated in a 10 wt% gelatin solution with 20 mM EDC/NHS. The dip-coating of gelatin on PDMS microfiber was under 55 °C and with immersion speed of 10 mm s^{-1}, immersion time of 10 s and withdrawal speed kept at 5 mm s^{-1}. Subsequently, the coated fiber

was left in an oven at 37 °C for 3 hours, before being washed in an ultrasonic bath in hot water (~50 °C) to remove unreacted reagents. Finally, the fiber was dried under a stream of nitrogen.

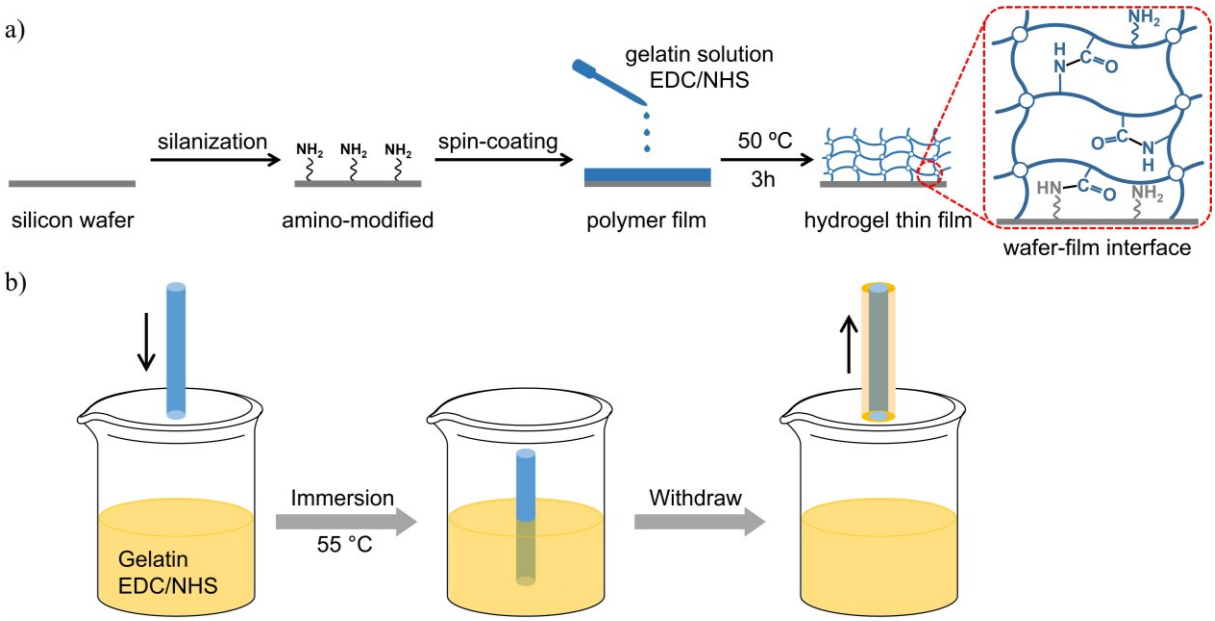

Figure 1. Synthesis process of surface-attached gelatin hydrogel films/coatings, by crosslinking and grafting gelatin chains onto the amino-modified silicon wafers and PDMS microfibers. a) Spin-coating on silicon wafers. b) Dip-coating on microfibers.

2.5 Synthesis of hydrogel multi-layers

The multi-layer gelatin coatings (on both silicon wafers and silicone fibers) were obtained by continuously coating another gelatin layer on top of the previous gelatin layer, rather than bare substrates. Before coating a new layer, the coating was washed in hot water (50 °C) to remove unreacted reagents.

2.6 Ellipsometry

The thickness of homogeneous hydrogel thin films on silicon wafers was measured with spectroscopic ellipsometer (UVISEL, Horiba). The angle of incidence was fixed at 60°, with a wavelength range from 400 nm to 800 nm. To determine the dry thickness (Th_{dry}) of gelatin film, the refractive index (n_i) of silicon substrate and gelatin was 3.87 and 1.50, respectively. In order to measure the wet thickness (Th_{wet}), *in situ* underwater measurements were performed using a liquid cell, with thin glass walls fixed perpendicularly to the light path. The gelatin film was modeled as a single layer, with a constant refractive index between that of water (n_i = 1.33) and of the polymer. Moreover, the swelling ratio of hydrogel films (SR) was calculated as

Th_{wet}/Th_{dry}, assuming that the polymer amount kept the same before and after being immersed underwater, since the hydrogel film was covalently attached to the substrate and the free polymer chains were considered to be removed by washing in hot water. The volume fraction of gelatins in swollen state was calculated by $\phi_p = 1/SR$. It is also able to control temperature, pH and ionic strength within the liquid cell, which also allows the measurements in different conditions.

2.7 Fourier transform infrared (FTIR) spectroscopy

Fourier transform infrared (FTIR) spectroscopy was performed on Bruker Tensor 27 in the attenuated total reflectance mode (ATR-IR), to confirm the presence of gelatin coatings on the PDMS fibers. Infrared spectra were recorded in the frequency range of 600−4000 cm^{-1}.

2.8 Scanning electron microscope (SEM)

SEM was used to determine the dry thickness of gelatin hydrogel coatings on fibers, and also to observe their swelling in humid environment. The samples were prepared by making a cross-section either in liquid nitrogen or with a sharp cutter. The measurement of dry thickness was operated under high vacuum so the sample was dehydrated. The swelling behavior of the gelatin coatings was measured using environmental SEM (ESEM) in humid atmosphere. With the help of a differential pumping system towards the bottom of the column, this ESEM could work at higher pressures (up to ~ 2000 Pa) around the sample, to suppress the phenomenon of evaporation of the water, while maintaining low pressure in the electron gun (10^{-6} to 10^{-7} torr). The temperature was fixed at 5 °C (over freezing point).

2.9 Incorporation/release of dexamethasone on gelatin coatings

Dexamethasone sodium phosphate (DSP) was incorporated and released by the gelatin coatings. The gelatin-coated fibers were immersed in a stock solution of DSP, with fixed concentration of 1 mg ml^{-1} and volume of 200 µl. The fiber loaded with DSP was then removed from the solution and transferred into water for release. The dry thickness of gelatin coatings on fibers for DSP release was kept at 5-6 µm.

2.10 Absorption UV-visible spectroscopy

The study of DSP release was carried out by UV-visible spectroscopy (UV-visible HP8453, France) by measuring the absorbance at 242 nm. The calibration of DSP absorbance was performed between 1 and 30 μg ml^{-1} (the range was limited by DSP absorbance). The concentration of DSP released from the coatings was determined by measuring the absorption of the rinsing aqueous solution after immersion of gelatin coated fibers.

3 Results and Discussion

3.1 Synthesis of gelatin thin films on plane substrates

Surface-attached hydrogel films are synthesized on the top of silicon wafers by simultaneously crosslinking and grafting gelatins via EDC/NHS coupling (**Figure 1a**). The intermolecular reaction of activated carboxylic acid residues with the free ε-amino groups residues of lysine on gelatin chains result in the creation of a peptide bond as crosslinking points.[28] Meanwhile, with the same reaction between the carboxyl groups on gelatin chains and amino groups on amino-modified silicon wafers, the polymer network is grafted onto the substrates.

The dry thickness of gelatin films corresponds to the thickness measured in air by ellipsometry. The thickness of gelatin films is controlled by the polymer concentration for spin-coating (C_p). **Figure 2a** and **Figure S1a** (**Supporting Information**) show that the Th_{dry} increases with increased C_p, corresponding to the viscosity of polymer solution. The thickness of ultrathin polymer films can be expressed by the scaling:[20]

$$Th_{dry} \sim \omega^{-\frac{1}{2}} M^{\frac{\alpha}{2}} C_p^{\frac{3}{2}} \quad (1)$$

where ω is the speed of spin, M is the molecular weight of polymer and α is the Mark-Houwink parameter (α is 0.8 for gelatins[33]). Since the ω and M are fixed for each type of gelatin in this work, the Th_{dry} of GB films as a function of $C_p^{3/2}$ is shown in the inset of **Figure 2a**, in which the experimental data are satisfactorily aligned on the same master curve in a concentration range from 1 to 8 wt%. On the other hand, as shown in **Figure 2a** and **Figure S1a** (**Supporting Information**), the Th_{wet} is much higher than Th_{dry} for both of the GB and GA films, because the surface-attached polymer network can swell underwater by absorbing water. The swelling

is completely reversible with the dry thickness of the hydrogel or the amount of grafted polymer being constant. The dry thickness of GA is slightly higher than GB, because the GA has a higher molecular weight than GB (**Table S1**, **Supporting Information**). The swelling ratio (*SR*) of films is defined as Th_{wet}/Th_{dry}, which is shown in **Figure 2b** and **Figure S1b** (**Supporting Information**). The swelling ratio of films increases with the increase in dry thickness below about 50 nm, then keeps in constant for thicker films at *SR* about 4.5 and 4.2 for GA and GB respectively. This is because the grafting density is much higher than crosslinking density of the hydrogel. When the film is very thin (in general lower than 50 nm), the grafting of high density limits the swelling of the gelatin network. For thicker films, the swelling of the hydrogel is determined by the crosslinking density while the grafting density of chains on the surface becomes negligible. The volume fraction of polymers in swollen state (ϕ_p) can also be calculated to compare with macroscopic hydrogels (**Figure 2c** and **Figure S1c**, **Supporting Information**). For films with thickness over 50 nm, the volume fraction is constant around 23%, which is in the normal range of gelatin hydrogels. For the study of physical chemistry of gelatin thin films in this work, dry thickness of films is always higher than 50 nm, to avoid the surface effect and keep the volume fraction comparable with macroscopic hydrogels. Moreover, as shown in **Figure 2d**, the swelling ratio could be tuned by the peptide reaction. With the increase in EDC/NHS concentration, the *SR* decreases from ~ 4.1 to ~3.2, in relation with the increase in crosslinking density.

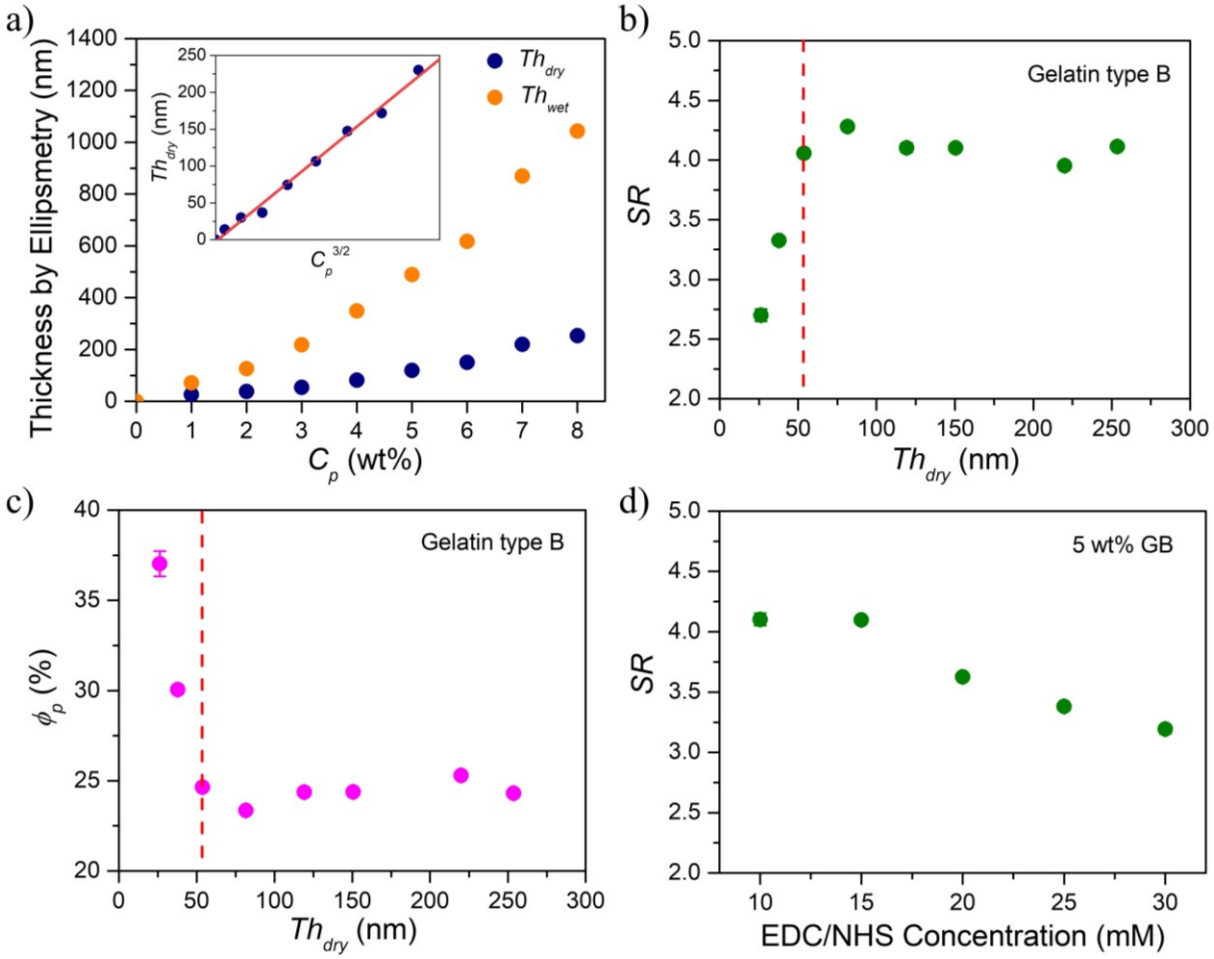

Figure 2. a) Dry (in air, Th_{dry}) and wet (in Milli-Q water, Th_{wet}) thickness, b) swelling ratio (*SR*) and c) volume fraction of polymers (ϕ_p) of gelatin B films. Inset of a) is the dry thickness of GB films as a function of $C_p^{3/2}$, in which the red line is a linear fit. d) Swelling ratio (*SR*) as a function of EDC/NHS concentration.

3.2 Synthesis of coatings on microfibers

The CLAG strategy is also used for coatings on silicone microfibers, with applications in biomedical fields such as surgical implants. In order to avoid trauma to biological tissues during implantation, one of the proposed solutions is to coat the surface of implants with biocompatible and biodegradable gelatin hydrogels.[34-35] The gelatin coatings also allow the incorporation and delivery of drugs such as dexamethasone anti-inflammatory agent.[27, 36]

The PDMS fiber covered with gelatin B is characterized by ATR-IR spectroscopy. As shown in **Figure 3**, the gelatin-coated PDMS fiber clearly had absorption bands of gelatin at ~3500-3200 cm^{-1}, ~1622 cm^{-1} and ~1520 cm^{-1}, which are characteristics of N-H stretching, C=O bending of primary amide and N-H bending of secondary amide, respectively, confirming the

presence of gelatin coating on the surface of the fiber. The infrared spectrum also shows the gelatin-absorption bands of PDMS, including the peak at ~2965 cm^{-1} and the sharp peak at ~1258 cm^{-1}, which are CH_3 stretching and Si-CH_3 symmetric stretching, respectively. As the gelatin layer has a thickness (measured by SEM as discussed in the next part) greater than the depth of penetration of the IR beam (which is at the maximum ~2.5 μm), the absorption band of PDMS should not appear in the ATR-IR spectrum. This could be explained by the local alteration of the gelatin coating due to high pressure exerted to contact the fiber with the diamond waveguide.

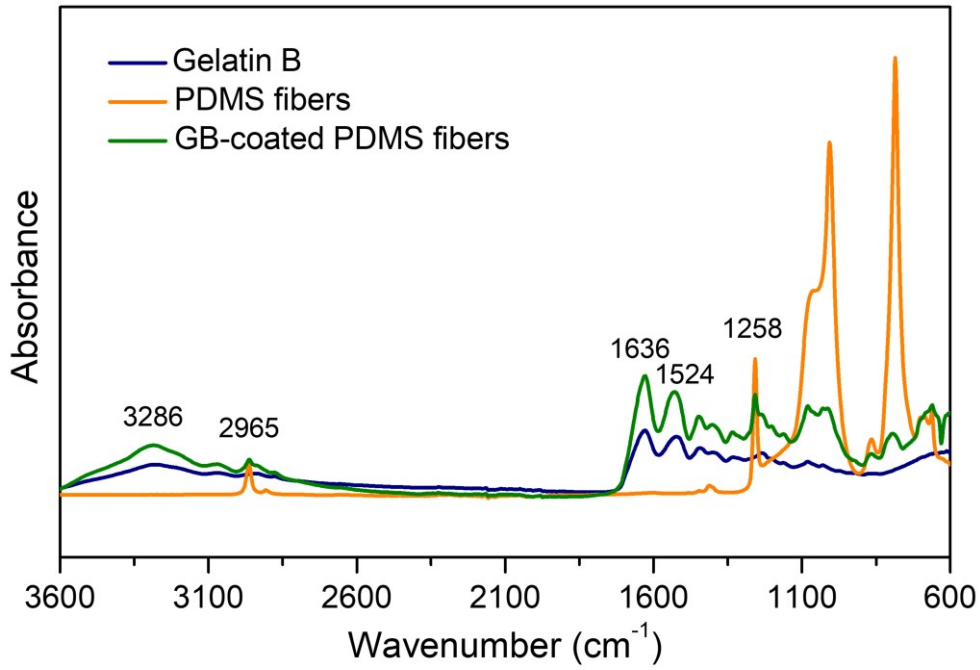

Figure 3. ATR-IR spectra of gelatin B (powder), bare PDMS fibers and GB-coated fibers. The absorbance is in arbitrary units as it depends on the fine contact with the diamond waveguide.

3.3 Gelatin hydrogel multi-layers

Since solubility and viscosity of gelatin solutions cannot increase infinitely, there is an intrinsic limitation of thickness of gelatin coatings. Inspired by layer-by-layer assemblies, a multi-layer strategy is developed in order to overcome the thickness limitation.[20] As shown in **Figure 4**, a new gelatin layer is successively deposited onto the top of the former layer (once each gelatin chemical hydrogel has been formed), resulting in the gelatin hydrogel coating with several layers. As the synthesis of the first layer on the top of amino-modified substrates shown in **Figure 1**, the multi-layer also allows intermolecular crosslinking among gelatin chains in each layer and anchoring points between adjacent layers, because the top of each layer is always

amino-rich. The thickness of each layer of a multi-layer GB film (each layer is coated by 7 wt% GB) is shown in **Figure 5**. It is demonstrated that both the dry and wet thickness increase linearly with the increase in the number of layers. The thickness of each layer which is determined by the slope of linear fits, gives 205.9 nm for the dry thickness (using 7 wt% gelatin solution for spin-coating) and 1049.7 nm for the swollen thickness. The same result is found for GA films (**Figure S2**, **Supporting Information**). It provides evidence of the simplicity of the multilayer process to fabricate surface-attached gelatin hydrogel films with a large range of thickness from a few nanometers to several micrometers.

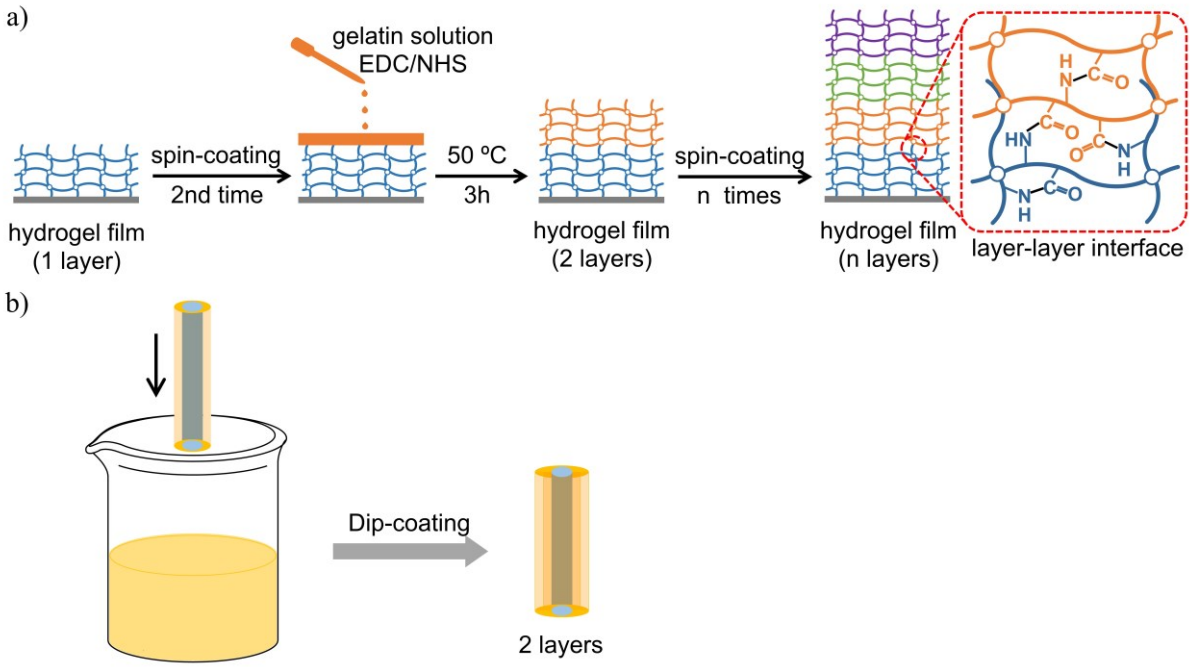

Figure 4. Schematics of building processes of gelatin multi-layers on: a) plane substrates and b) microfibers.

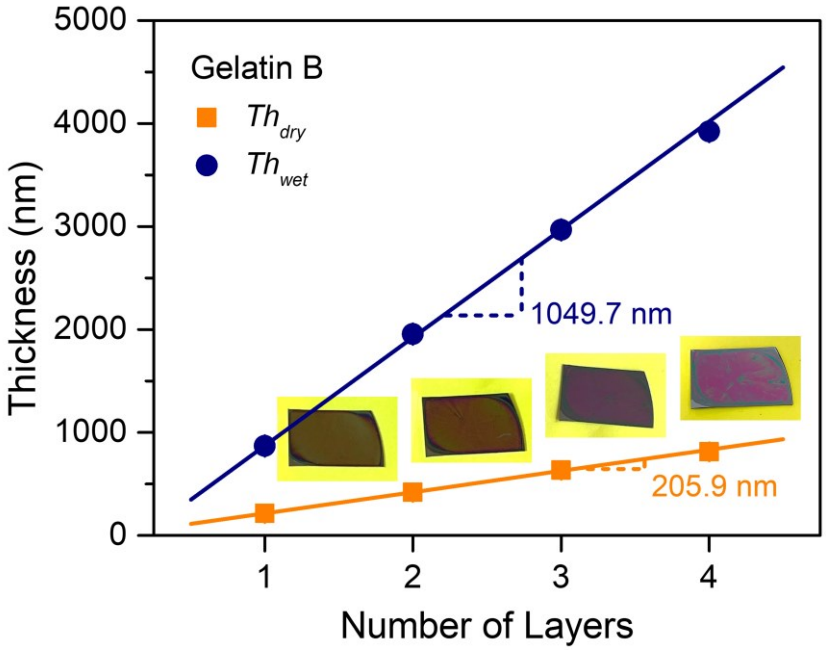

Figure 5. Dry thickness (measured in air, Th_{dry}) and wet thickness (underwater, Th_{wet}) of GB films with increased number of layers. 7 wt% gelatin is used for spin-coating of each layer.

Not only on plane substrates, the same strategy is also used on fibers by continuously dip-coating the fibers in GB solutions (**Figure 4b**). This multi-layer strategy allows the formation of stable and thick gelatin coatings. The gelatin coatings covering PDMS fibers are characterized by SEM, to determine the thickness of the coating. The SEM images of cross-section of GB-coated fibers are shown in **Figure 6a**. The contrast between the silicone core and the gelatin shell is clearly visible. This contrast is due to the difference of material toughness between the soft PDMS core (which can be easily sliced) and the brittle, glassy gelatin (which shows streaks due to fractures). The SEM images show that the gelatin coating homogeneously covers the PDMS fiber with a thickness of approximately 1.7 µm for 1 layer (**Figure 6a**). The multi-layer strategy is used to construct gelatin coatings on the silicone fibers with various thickness. Additional layers are stacked step by step onto the PDMS fibers, the gelatin solution being dip-coated once the precedent gelatin hydrogel coating is formed. As shown in **Figure 6a-d**. the average thickness is ~1.7 µm, 5-6 µm, ~7 µm and ~17 µm for 1 layer, 3 layers, 4 layers and 10 layers respectively. The linear increase of the thickness of the gelatin coating with the number of layers clearly demonstrates the ability to stack chemically crosslinked gelatin coatings.

The ESEM experiments under controlled humid atmosphere clearly demonstrates the swelling of the external gelatin layer. The swollen thickness of gelatin coatings covering the

PDMS fibers is measured under ambient humidity of 15% and wet condition of humidity of 100%. As shown in **Figure 6e-f**, the thickness increases from ~7 µm to ~12 µm with the increase in humidity to 100%, resulting in a swelling ratio of ~1.6. The swelling ratio of coatings on fibers is here lower than that of gelatin films on silicon wafers while the synthesis conditions are the same (concentration of silane for amino-modification, ratio between EDC/NHS and gelatin B). Nevertheless, this is not surprising as the swelling ratio of the gelatin shell on silicone fiber was measured by ESEM under 100% humidity, while the thickness of gelatin layer on silicon wafer was determined underwater.

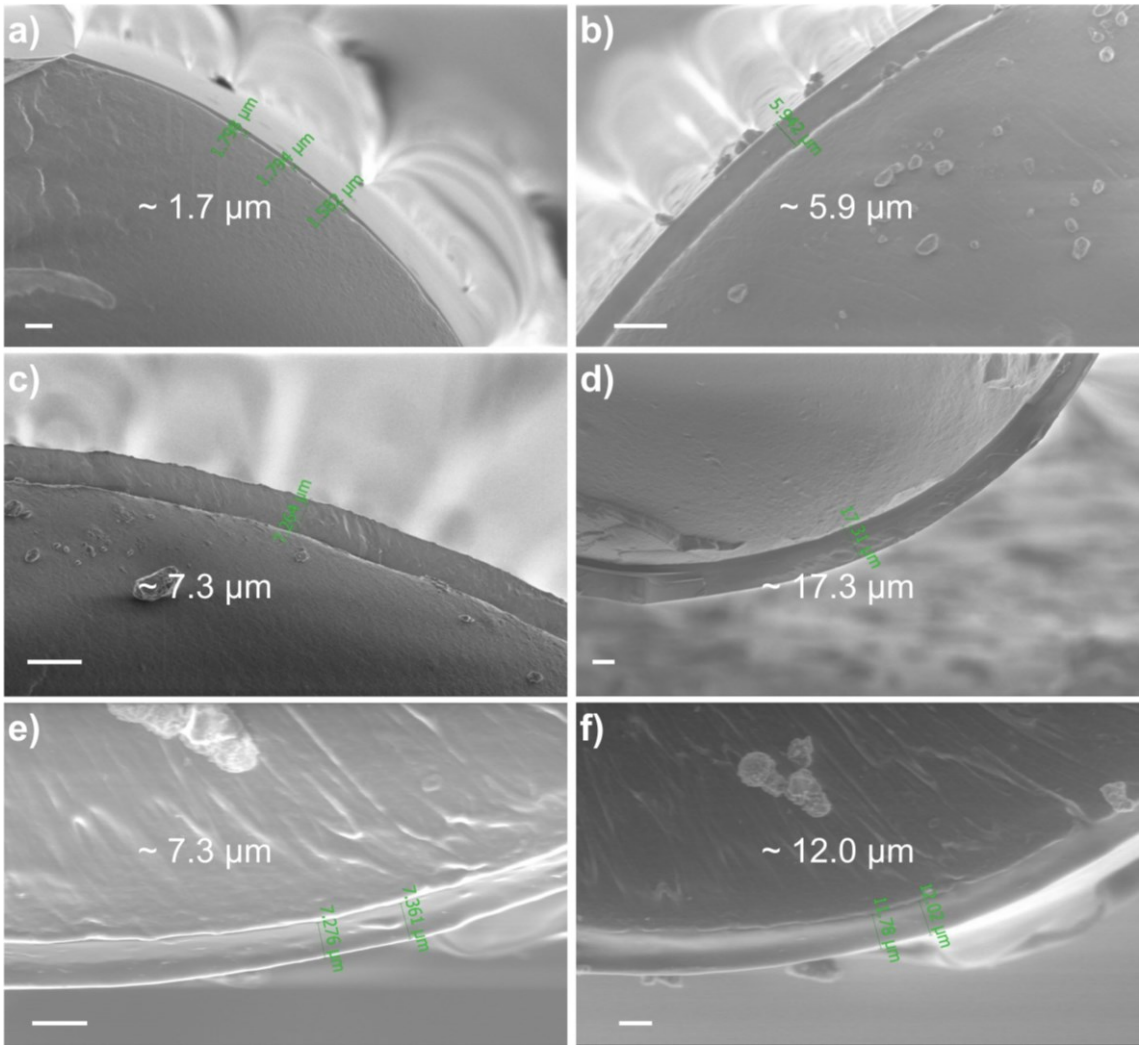

Figure 6. SEM and ESEM images of PDMS microfibers coated with gelatin hydrogels. The thickness deduced from SEM images is measured under vacuum for various layers. a) 1 layer, b) 3 layers, c) 4 layers and d) 10 layers. The thickness deduced from ESEM images is measured under controlled humidity e) 15% and f) 100%. The scale bars correspond to 10 µm.

3.4 Biodegradation of gelatin coatings

Biodegradation is also an important property of gelatins, as well as gelatin coatings.[37] In this work, it is measured by tracking the changes in appearance and the thickness of gelatin coatings. The gelatin coatings are immersed in PBS solutions at 37 °C for various time and dried to be characterized. As shown in **Figure 7a**, for the films on plane wafers, there is an obvious change in appearance for all the samples with various thickness over time. Partial and random removing of polymer layer is apparent after 8 days. Almost complete removing of gelatin coatings is obvious after 24 days resulting in bare silicon surface. We assume that this change originates from the biodegradation of polymer, as the latter was chemically grafted onto the surface and all the unreacted residues have been removed by the former washing steps. Moreover, the rate of degradation depends on the types of gelatin and the dry thickness. The degradation of GB is faster than GA as the GB hydrogel film of 240 nm becomes inhomogeneous from the 4th day, while the degradation of GA (335 nm) starts from the 12th day, indicating a faster degradation of GB than GA films. For both GA and GB films, the thinner films lose much more polymer layers than thicker films, indicating faster biodegradation of thinner gelatin thin films. In **Figure 7a**, the colors of films also change during the PBS immersion for all the samples, indicating the change in thickness. The daily variation of the dry thickness during immersion is also studied, by measuring the thickness of remained polymer part on silicon wafers. As seen in **Figure S3** (**Supporting Information**), the thickness of remaining polymer films decreases slightly with time, when being immersed in PBS solutions at 37 °C. The dry thickness loss at 2 positions on the surface of a fiber was followed by SEM, during the immersion in water of 37 °C. As shown in **Figure 7b**, the gelatin at different positions shows inhomogeneous loss along the coating due to biological degradation. Therefore, the biodegradation process of the surface-attached gelatin hydrogel coatings is not only the decrease in thickness of the films, but also accompanies by a partial removing of polymer layers.

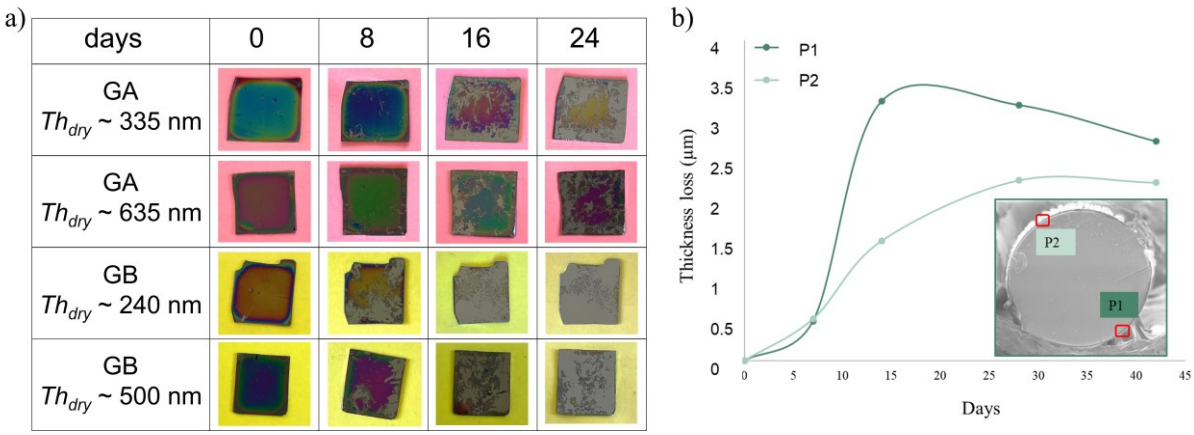

Figure 7. Evolution of gelatin coatings being immersed in aqueous solutions. a) Photography of the initial films on silicon wafers before and after 8, 16, 24 days of immersion in PBS solutions at 37 °C. b) Thickness loss of gelatin coatings at different positions of fibers.

3.5 Incorporation/release of DSP by gelatin coatings

Fibers and fibrous materials have essential applications in surgical implants, medical instruments and medical electronic devices.[38-39] The biopolymer coatings are fabricated on fibers to offer biocompatibility to the surfaces. In addition, in order to explore the biomedical applications, incorporation and release of drugs are shown in this work. The drug release system building on coatings has many important functions, for example, specific medicine released from the surface of surgical implants to the implanted area in tissue, could help patients reduce pains and trauma from the implantations. It is expected to have an immediate release of the active ingredient in an aqueous solution, the process of incorporation and release of drug is shown in **Figure 8a**. Dexamethasone sodium phosphate (DSP, **Figure 8b**), as the water-soluble version of dexamethasone due to the presence of a hydrophilic phosphate group in place of the primary alcohol group, is incorporated and released by the gelatin coatings. It is important to emphasize that the release kinetics could be influenced by the volume of the coatings (fibers) and the volume of the release solutions. In this work, the loading of DSP is in a solution with fixed volume of 200 µl and fixed fiber length of 35 mm. The quantity of released DSP is quantified by UV-vis by Lambert-Beer law, by measuring the intensity of absorption band at 242 nm (**Figure 8c**). We showed that the amount of DSP quickly released is suitable with that used in surgical implants such as in the inner ear. Actually, the expected amount of DSP released into the inner ear is around 1 mg per day with the volume of perilymph in this organ around 70 µl.[40]

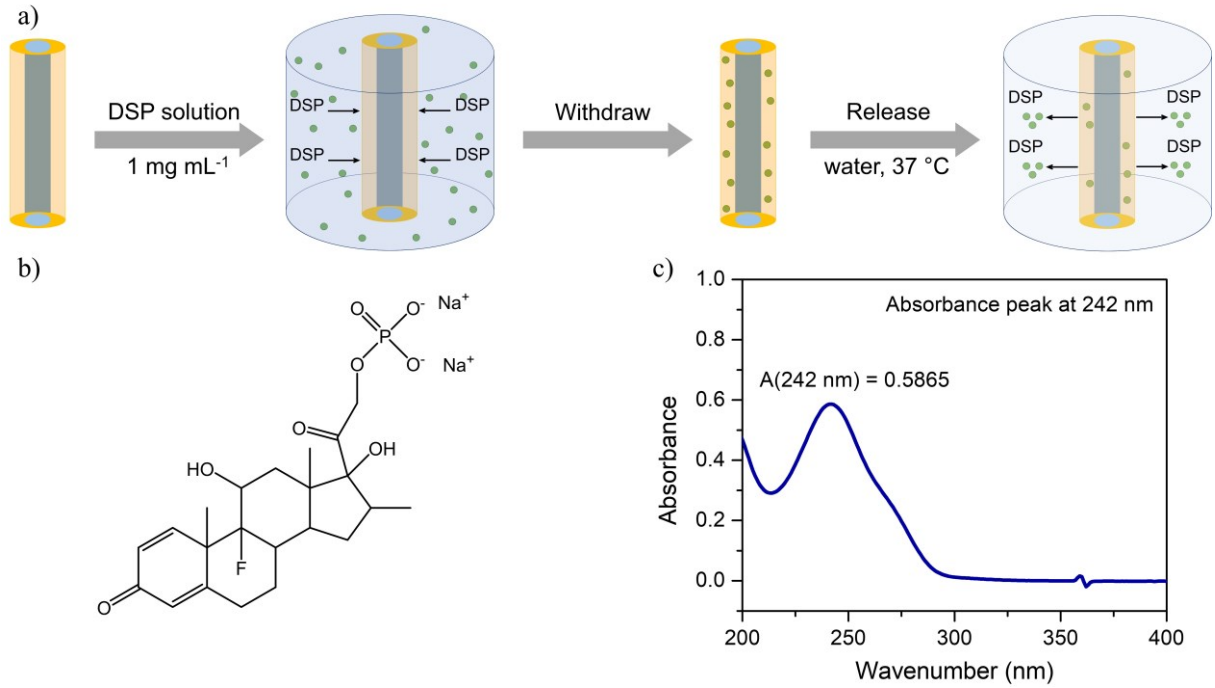

Figure 8. Incorporation and release of DSP by the gelatin coatings on PDMS microfibers. a) Illustration for the incorporation and release process. b) Chemical structure of DSP. c) UV-visible spectrum of DSP of 20 µg ml^{-1}.

4 Conclusion

A simple and versatile strategy of Cross-Linking and Grafting has been used to synthesize substrate-attached gelatin hydrogel films/coatings. With the chemical crosslinking and grafting of the gelatin, interfacially and thermally stable hydrogel coatings are built on various substrates such as plane silicon wafers and soft PDMS fibers. The physical chemistry properties of the coatings, including thickness, swelling and biodegradation, are finely investigated. We showed that surface-attachedgelatin hydrogel coatings are obtained over a wide range of thicknesses from nanometers to micrometers. The gelatin layer swells reversibly underwater while the amount of gelatin grafted on the substrate (or the dry thickness) is kept constant. The swelling ratio can be varied by adjusting the ratio of EDC/NHS coupling agent. The gelatin coatings are also shown as efficient platform for drug release such as dexamethasone. We believe that this strategy would have great potentials in biomedicine such as surgical implants.

References

1. Nechita, P.; Roman , M., Review on Polysaccharides Used in Coatings for Food Packaging Papers. *Coatings* **2020,** *10* (6), 566.

2. Priyadarshi, R.; Roy, S.; Ghosh, T.; Biswas, D.; Rhim, J.-W., Antimicrobial nanofillers reinforced biopolymer composite films for active food packaging applications - a review. *Sustainable Materials and Technologies* **2021**, e00353.

3. Li, X.; Ding, C.; Li, X.; Yang, H.; Liu, S.; Wang, X.; Zhang, L.; Sun, Q.; Liu, X.; Chen, J., Electronic biopolymers: From molecular engineering to functional devices. *Chemical Engineering Journal* **2020,** *397*, 125499.

4. Zhang, S.-J.; Gao, Z.-G.; Wang, W.-W.; Lu, Y.-Q.; Deng, Y.-P.; You, J.-H.; Li, J.-T.; Zhou, Y.; Huang, L.; Zhou, X.-D.; Sun, S.-G., A Natural Biopolymer Film as a Robust Protective Layer to Effectively Stabilize Lithium-Metal Anodes. *Small* **2018,** *14* (31), 1801054.

5. Chow, D.; Nunalee, M. L.; Lim, D. W.; Simnick, A. J.; Chilkoti, A., Peptide-based biopolymers in biomedicine and biotechnology. *Materials Science and Engineering: R: Reports* **2008,** *62* (4), 125-155.

6. Nathanael, A. J.; Oh, T. H., Biopolymer Coatings for Biomedical Applications. *Polymers* **2020,** *12* (12), 3061.

7. Decher, G.; Hong, J. D.; Schmitt, J., Buildup of ultrathin multilayer films by a self-assembly process: III. Consecutively alternating adsorption of anionic and cationic polyelectrolytes on charged surfaces. *Thin Solid Films* **1992,** *210-211*, 831-835.

8. Milner, S. T., Polymer Brushes. *Science* **1991,** *251* (4996), 905-914.

9. Muthukumar, M.; Ober, C. K.; Thomas, E. L., Competing Interactions and Levels of Ordering in Self-Organizing Polymeric Materials. *Science* **1997,** *277* (5330), 1225-1232.

10. Wang, L.; Wang, Z.; Zhang, X.; Shen, J.; Chi, L.; Fuchs, H., A new approach for the fabrication of an alternating multilayer film of poly(4-vinylpyridine) and poly(acrylic acid) based on hydrogen bonding. *Macromolecular Rapid Communications* **1997,** *18* (6), 509-514.

11. Stockton, W. B.; Rubner, M. F., Molecular-Level Processing of Conjugated Polymers. 4. Layer-by-Layer Manipulation of Polyaniline via Hydrogen-Bonding Interactions. *Macromolecules* **1997,** *30* (9), 2717-2725.

12. Decher, G., Fuzzy Nanoassemblies: Toward Layered Polymeric Multicomposites. *Science* **1997,** *277* (5330), 1232-1237.

13. Cheung, J. H.; Stockton, W. B.; Rubner, M. F., Molecular-Level Processing of Conjugated Polymers. 3. Layer-by-Layer Manipulation of Polyaniline via Electrostatic Interactions. *Macromolecules* **1997,** *30* (9), 2712-2716.

14. Kotov, N. A., Layer-by-layer self-assembly: The contribution of hydrophobic interactions. *Nanostructured Materials* **1999,** *12* (5), 789-796.

15. Zhao, J.; Pan, F.; Li, P.; Zhao, C.; Jiang, Z.; Zhang, P.; Cao, X., Fabrication of Ultrathin Membrane via Layer-by-Layer Self-assembly Driven by Hydrophobic Interaction Towards High Separation Performance. *ACS Applied Materials & Interfaces* **2013,** *5* (24), 13275-13283.

16. Tran, Y.; Auroy, P.; Lee, L. T., Determination of the Structure of Polyelectrolyte Brushes. *Macromolecules* **1999,** *32* (26), 8952-8964.

17. Sanjuan, S.; Perrin, P.; Pantoustier, N.; Tran, Y., Synthesis and Swelling Behavior of pH-Responsive Polybase Brushes. *Langmuir* **2007,** *23* (10), 5769-5778.

18. Sanjuan, S.; Tran, Y., Stimuli-Responsive Interfaces Using Random Polyampholyte Brushes. *Macromolecules* **2008,** *41* (22), 8721-8728.

19. Slim, C.; Tran, Y.; Chehimi, M. M.; Garraud, N.; Roger, J.-P.; Combellas, C.; Kanoufi, F., Microelectrochemical Patterning of Surfaces with Polymer Brushes. *Chemistry of Materials* **2008,** *20* (21), 6677-6685.

20. Chollet, B.; Li, M.; Martwong, E.; Bresson, B.; Fretigny, C.; Tabeling, P.; Tran, Y., Multiscale Surface-Attached Hydrogel Thin Films with Tailored Architecture. *ACS Applied Materials & Interfaces* **2016,** *8* (18), 11729-11738.

21. Sanjuan, S.; Tran, Y., Synthesis of random polyampholyte brushes by atom transfer radical polymerization. *Journal of Polymer Science Part A: Polymer Chemistry* **2008,** *46* (13), 4305-4319.

22. Chen, W.-L.; Cordero, R.; Tran, H.; Ober, C. K., 50th Anniversary Perspective: Polymer Brushes: Novel Surfaces for Future Materials. *Macromolecules* **2017,** *50* (11), 4089-4113.

23. Harrington, W. F.; Von Hippel, P. H., The Structure Of Collagen And Gelatin. In *Advances in Protein Chemistry*, Anfinsen, C. B.; Anson, M. L.; Bailey, K.; Edsall, J. T., Eds. Academic Press: 1962; Vol. 16, pp 1-138.

24. Zhao, X.; Lang, Q.; Yildirimer, L.; Lin, Z. Y.; Cui, W.; Annabi, N.; Ng, K. W.; Dokmeci, M. R.; Ghaemmaghami, A. M.; Khademhosseini, A., Photocrosslinkable Gelatin Hydrogel for Epidermal Tissue Engineering. *Advanced Healthcare Materials* **2016,** *5* (1), 108-118.

25. Huang, Y.; Onyeri, S.; Siewe, M.; Moshfeghian, A.; Madihally, S. V., In vitro characterization of chitosan–gelatin scaffolds for tissue engineering. *Biomaterials* **2005,** *26* (36), 7616-7627.

26. Mahony, O.; Tsigkou, O.; Ionescu, C.; Minelli, C.; Ling, L.; Hanly, R.; Smith, M. E.; Stevens, M. M.; Jones, J. R., Silica-Gelatin Hybrids with Tailorable Degradation and Mechanical Properties for Tissue Regeneration. *Advanced Functional Materials* **2010,** *20* (22), 3835-3845.

27. Piao, Y.; You, H.; Xu, T.; Bei, H.-P.; Piwko, I. Z.; Kwan, Y. Y.; Zhao, X., Biomedical applications of gelatin methacryloyl hydrogels. *Engineered Regeneration* **2021,** *2*, 47-56.

28. Kuijpers, A. J.; Engbers, G. H. M.; Feijen, J.; De Smedt, S. C.; Meyvis, T. K. L.; Demeester, J.; Krijgsveld, J.; Zaat, S. A. J.; Dankert, J., Characterization of the Network Structure of Carbodiimide Cross-Linked Gelatin Gels. *Macromolecules* **1999,** *32* (10), 3325-3333.

29. Toomey, R.; Freidank, D.; Rühe, J., Swelling Behavior of Thin, Surface-Attached Polymer Networks. *Macromolecules* **2004,** *37* (3), 882-887.

30. Prucker, O.; Brandstetter, T.; Rühe, J., Surface-attached hydrogel coatings via C,H-insertion crosslinking for biomedical and bioanalytical applications (Review). *Biointerphases* **2018,** *13* (1), 010801.

31. Chollet, B.; D'Eramo, L.; Martwong, E.; Li, M.; Macron, J.; Mai, T. Q.; Tabeling, P.; Tran, Y., Tailoring Patterns of Surface-Attached Multiresponsive Polymer Networks. *ACS Applied Materials & Interfaces* **2016,** *8* (37), 24870-24879.

32. Li, M.; Bresson, B.; Cousin, F.; Fretigny, C.; Tran, Y., Submicrometric Films of Surface-Attached Polymer Network with Temperature-Responsive Properties. *Langmuir* **2015,** *31* (42), 11516-11524.

33. *Polymer Data Handbook*. Oxford University Press: 1999.

34. Eshraghi, A. A.; Van De Water, T. R., Cochlear implantation trauma and noise-induced hearing loss: Apoptosis and therapeutic strategies. *The Anatomical Record Part A: Discoveries in Molecular, Cellular, and Evolutionary Biology* **2006,** *288A* (4), 473-481.

35. Seyyedi, M.; Nadol, J. B., Jr., Intracochlear inflammatory response to cochlear implant electrodes in humans. *Otol Neurotol* **2014,** *35* (9), 1545-1551.

36. Etxabide, A.; Long, J.; Guerrero, P.; de la Caba, K.; Seyfoddin, A., 3D printed lactose-crosslinked gelatin scaffolds as a drug delivery system for dexamethasone. *European Polymer Journal* **2019,** *114*, 90-97.

37. van den Bosch, E.; Gielens, C., Gelatin degradation at elevated temperature. *International Journal of Biological Macromolecules* **2003,** *32* (3), 129-138.

38. Gehrke, M.; Sircoglou, J.; Vincent, C.; Siepmann, J.; Siepmann, F., How to adjust dexamethasone mobility in silicone matrices: A quantitative treatment. *European Journal of Pharmaceutics and Biopharmaceutics* **2016,** *100*, 27-37.

39. Gehrke, M.; Verin, J.; Gnansia, D.; Tourrel, G.; Risoud, M.; Vincent, C.; Siepmann, F.; Siepmann, J., Hybrid Ear Cubes for local controlled dexamethasone delivery to the inner ear. *European Journal of Pharmaceutical Sciences* **2019,** *126*, 23-32.

40. Krenzlin, S.; Vincent, C.; Munzke, L.; Gnansia, D.; Siepmann, J.; Siepmann, F., Predictability of drug release from cochlear implants. *Journal of Controlled Release* **2012,** *159* (1), 60-68.

Supporting Information

Average molecular weight of GA and GB, dry and wet thickness, swelling ratio and volume fraction of polymers (ϕ_p) of GA films, multi-layer GA film, and dry thickness evolution of GA and GB films under physiological conditions.

Supporting Information

Substrate-attached Hydrogel Thin Coatings with Gelatins

Table S1. Average molecular weight and molecular weight distribution of gelatin A and B

	M_n (kg/mol)	M_w (kg/mol)	M_n/M_w
Gelatin A	140	160	1.2
Gelatin B	110	148	1.3

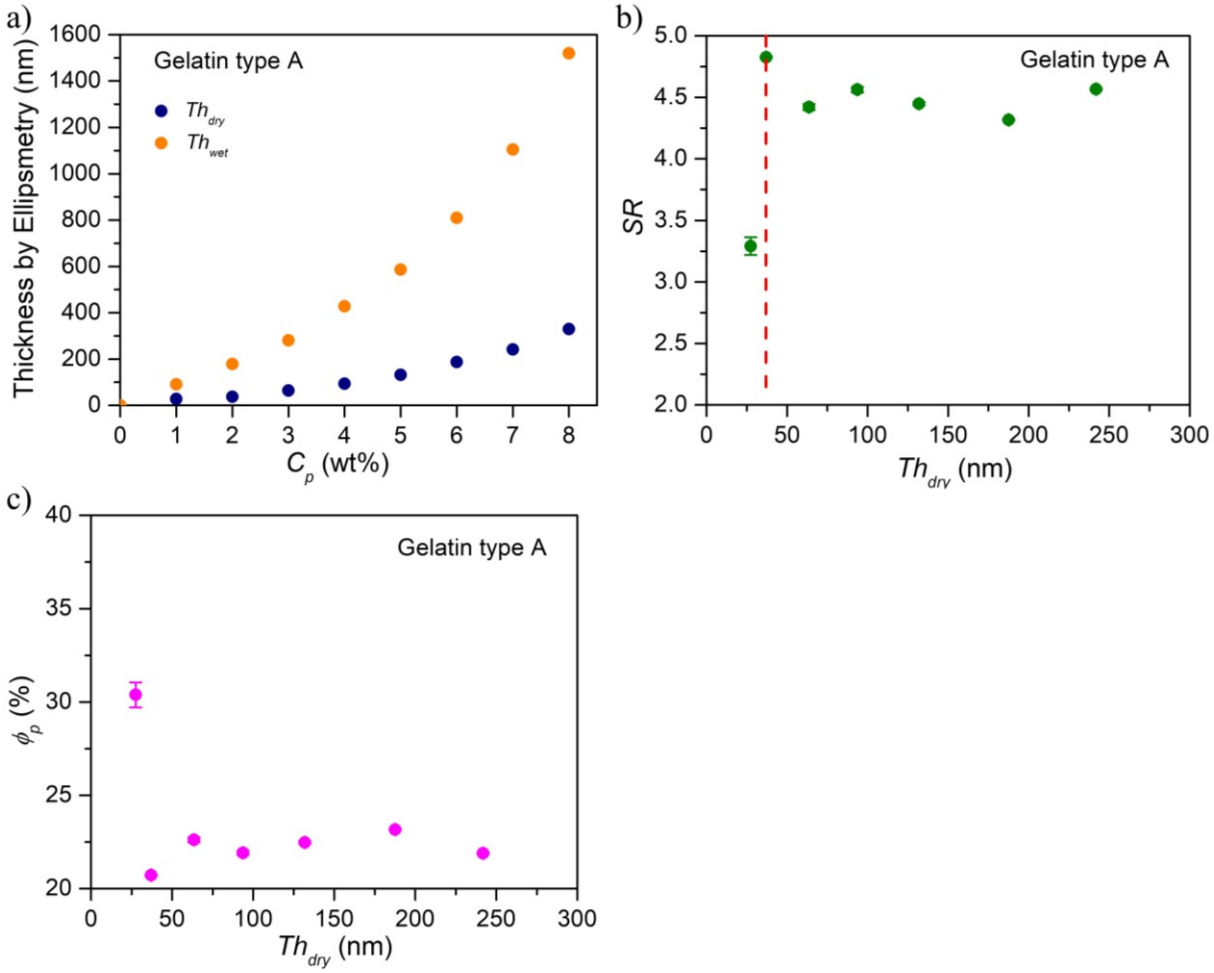

Figure S1. a) Dry (in air, Th_{dry}) and wet (in Milli-Q water, Th_{wet}) thickness, b) swelling ratio (SR) and c) volume fraction of polymers (ϕ_p) of gelatin A films.

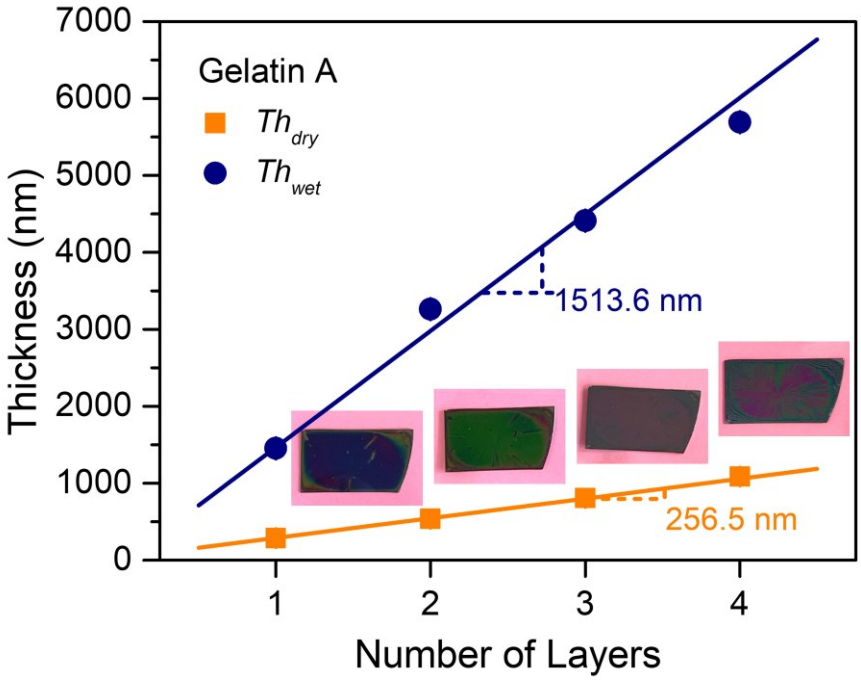

Figure S2. Multi-layer: dry thickness (measured in air, Th_{dry}) and wet thickness (underwater, Th_{wet}) of GA films with increased number of layers. 7 wt% GA is used for spin-coating of each layer.

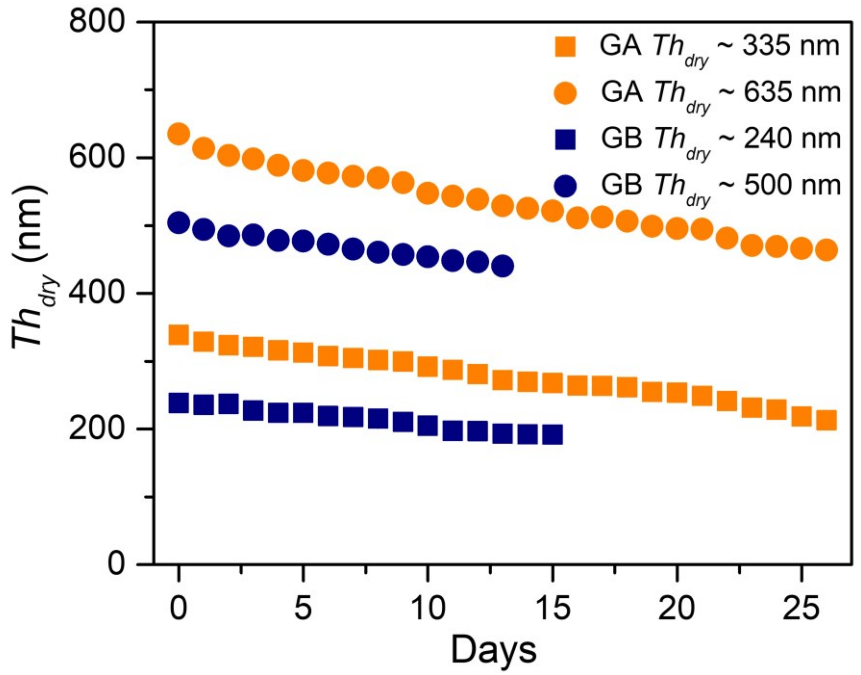

Figure S3. Dry thickness evolution of GA and GB thin films being immersed in PBS solutions at 37 °C.

Chapter 3

Molecular Mechanisms of Underwater Adhesion of Gelatins

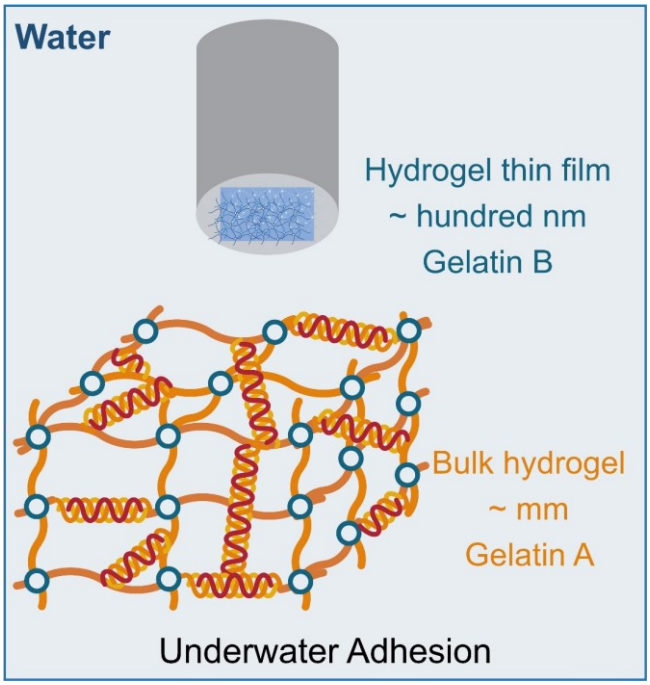

Abstract

Studying the relationship between molecular structure, viscoelasticity and adhesion properties of biosystems is important for building bioinspired underwater adhesives. In this work, gelatins have been used to fabricate a model system that allows the separation of surface and bulk contributions to adhesion. The underwater adhesion of macroscopic gelatin type A hydrogels against surface-attached microscopic gelatin type B thin films has been studied. The molecular structure and viscoelasticity of macroscopic hydrogels are controlled by an additional chemical network on physical gelatin network of triple-helices, to study their contributions on underwater adhesion. The results show that at low temperature, the work of adhesion increases with the level of physical crosslinks (increase of the polymer volume fraction and shear modulus), while it decreases with the increasing contribution of chemical crosslinks studied at high temperature. The chemical contribution on adhesion energy is predicted by Chaudhury's model with the key parameters such as the interface interaction surface density and the number of monomers between crosslinks. We also find that the additional chemical crosslinks reduce the physical crosslinking density without disturbing the underwater adhesion energy. This work provides the relationship between microscopic structure of gelatin hydrogels and macroscopic underwater adhesion performance, giving inspirations for designing bioadhesives.

Résumé

L'étude de la relation entre la structure moléculaire, la viscoélasticité et les propriétés d'adhérence des biosystèmes est importante pour le développement bioinspiré d'adhésifs en milieu aqueux. Dans ce travail, les gélatines ont été utilisées pour préparer un système modèle qui permet de séparer dans les propriétés d'adhérence les contributions relatives à la surface et au volume. Plus précisément, nous avons étudié l'adhérence en milieu aqueux d'hydrogels macroscopiques de gélatine de type A avec des films minces de gélatine de type B fixés à la surface d'un substrat. La structure moléculaire et la viscoélasticité des adhésifs hydrogels macroscopiques sont contrôlées par une double réticulation mettant en jeu la formation de points de jonction covalents (réticulation chimique) supplémentaires venant s'ajouter au réseau physique de gélatine lié à la formation des triples hélices à basse température. Les mesures réalisées en milieu aqueux à basse température montrent que si les propriétés d'adhésion augmentent avec le degré de réticulation physique (fraction volumique en polymère et module de cisaillement), elles diminuent lorsque l'on s'intéresse uniquement au degré de réticulation chimique (température élevée). Dans ce cas, la contribution du réseau chimique vis à vis de l'énergie d'adhésion peut être prédite à partir du modèle de Chaudhury avec les paramètres clés que sont la densité surfacique des interactions à l'interface et le nombre de monomères entre les points de réticulation. En présence des 2 modes de réticulation (température ambiante), nous constatons que si la réticulation chimique supplémentaire réduit sensiblement la densité de réticulation physique, elle affecte peu l'énergie d'adhésion en milieu aqueux. Ce travail permet ainsi de relier la structure microscopique des hydrogels de gélatine et leurs performances d'adhésion en milieu aqueux, tout en donnant quelques idées conceptuelles pour le développement de bioadhésifs.

Table of Contents

Chapter 3. Molecular Mechanisms of Underwater Adhesion of Gelatins

1 Introduction

Bioadhesion is relevant for the development of new biomaterials potneitally usefuyl for applications such as drug delivery,[1-4] tissue engineering,[5-6] surgical implants,[7-10] electronic skins,[11-13] *etc*. The main challenge comes from the water trapped between target surfaces and adhesives, which leads to poor interfacial contact and bond failure.[14-16] To overcome this general challenge, natural effective underwater adhesives have been already created by organisms, such as sea mussels, sandcastle worms, barnacles and sea anemones, which can secrete protein-based adhesives to bond different materials together in the presence of water in various environmental conditions.[17-21] Inspired by those biosystems, many strong and powerful artificial adhesives have been developed by focusing on the optimized binding at the interface and on the effective energy dissipation mechanisms in the bulk of the adhesives. For example, covalent bond between adhesive and substrate was incorporated to develop tough bonding of hydrogels onto diverse surfaces.[22] In order to avoid intermolecular interactions, some dome-like microscopic protuberances on the surface of underwater adhesives were fabricated, which worked as suction cups by mimicking octopus.[23] On the other hand, Li et al. developed tough adhesives for biological surfaces, with tough double network (DN) alginate hydrogels as the dissipative matrix.[24] The layer of tough hydrogel amplified energy dissipation through hysteresis, leading to a good adhesion performance. Kamperman and co-workers synthesized complex coacervate adhesives, consisting of oppositely charged polyelectrolytes grafted with thermoresponsive poly(*N*-isopropylacrylamide) (PNIPAM) chains.[25-28] Upon temperature change, the coacervates transited from a fluid state into a non-flowing hydrogel, holding by noncovalent ionic and hydrophobic interactions, which dissipated energy and increased the bulk cohesion. Those adhesives realize strong underwater adhesion through the enhancement of interfacial adhesion and bulk cohesion, which are known as the main contributions for adhesion performance.[22]

In order to better understand the mechanisms of underwater adhesion by separating the contributions of bulk and interface to adhesion, our group has recently developed an original methodology to study adhesion properties in aqueous environment, by measuring underwater the adhesion energy between thin films of polymers (brush or hydrogel) and macroscopic hydrogels.[29-31] The thin films are synthesized by a crosslinking and grafting (CLAG) strategy, in which a layer of polymer network (thickness ~ hundred nm) is grafted onto a silicon wafer.[32-34] The thin films on a solid substrate are supposed to act as a boundary condition and to have only the properties of a surface, in terms of chemistry and topography. The other material, a

macroscopic hydrogel works as a soft adhesive (thickness ~ mm) with a controlled degree of viscoelasticity. The model system separates the two important effects controlling adhesion: bulk properties and interfacial interactions into independent materials. The adhesion between synthetic polymers were studied. Sudre et al. investigated the underwater adhesion between poly(*N,N*-dimethylacrylamide) (PDMA) hydrogels and a surface of poly(acrylic acid) (PAAc) brushes.[29] The underwater adhesion was controlled by tuning interface interactions as hydrogen bonding between PDMA and PAA is pH sensitive. Macron et al. studied the influence of swelling equilibrium of hydrogels on the underwater adhesion by using the same PDMA/PAAc couple.[30] The equilibration led to changes in mechanical properties such as the elastic modulus. While significant experimental and theoretical advances in underwater adhesion have been made with synthetic materials, there is still a lack of knowledge on bioadhesion mechanisms, which could be tackled by using biopolymer systems.[35] However, this idea is limited by the difficulty in designing the structure and controlling the physical chemistry properties of biopolymer and biopolymer materials.

In this work, gelatin, as a representative candidate for mimicking biosystems, was used as biopolymer to mimic bioadhesives and biological surfaces. Gelatin is a biopolymer obtained from the hydrolysis of collagen, which is the main structural protein in the extracellular matrix of various connective tissues in animal bodies.[36] From different hydrolysis process of collagen, gelatin is divided into two main types: type A and type B, which are produced by acid and alkali precursors, respectively. The isoelectric point (pI) of gelatin A and B is ~ 9 and ~ 5, respectively.[37] Microscopic gelatin B films and macroscopic gelatin A hydrogels were combined into a model system to investigate the influence of surface and network properties on adhesion. The microscopic gelatin B films were prepared by the Cross-Linking and Grafting (CLAG) strategy using *N*-(3-dimethylaminopropyl)-*N′*-ethylcarbodiimide (EDC) and *N*-hydroxysuccinimide (NHS) coupling, to graft hydrogel thin films onto the substrates. The thickness, charge density and surface concentration of thin films were designed in order to have well-characterized surface properties. The macroscopic gelatin A hydrogels were dual-crosslinked by triple-helix formation between gelatin chains and amine coupling through EDC/NHS, to form physical and chemical networks. Both physical and chemical crosslinks in bulk hydrogels were controlled to have a tunable microscopic structure and a tunable bulk viscoelasticity of adhesives. The effects of physical and chemical networks on adhesion energy were also studied independently. Specifically, the contribution to the adhesion energy due to the presence of chemical crosslinks was predicted by Chaudhury's model.[38] In view of the

interfacial charge density, determined for the thin film or for the surface of bulk hydrogels, the adhesion energy could be qualitatively predicted by the average number of monomers between crosslinks and by the surface charge density of the hydrogels, respectively. Finally, the combined effect of physical and chemical crosslinks in hydrogels on adhesion properties was investigated.

2 Experimental Section

2.1 Materials

Gelatin type A (GA, bloom number ~ 300, from porcine skin), gelatin type B (GB, bloom number ~ 225, from bovine skin), *N*-(3-dimethylaminopropyl)-*N′*-ethylcarbodiimide hydrochloride (EDC), *N*-hydroxysuccinimide (NHS) and dry toluene (anhydrous, 99.8%) were purchased from Sigma-Aldrich. (3-Aminopropyl)trimethoxysilane was obtained from abcr. Gute Chemie. Silicon wafers were purchased from Neyco. All chemicals were used as received from the suppliers.

2.2 Synthesis of thin films

GB thin films were synthesized by simultaneously crosslinking and grafting gelatin chains onto the amino-modified silicon wafers with peptide covalent bond as shown in **Figure 1**. The amino self-assembled monolayer was prepared by immersing silicon wafers in a solution of 3-aminopropyl triethoxysilane in dry toluene (3% v/v) for 3 hours under N_2. After being dissolved in Milli-Q water at 50 °C, GB solution was mixed with freshly prepared EDC/NHS aqueous solution. After a stirring of 1 min, the mixture was deposited onto the amine-modified wafer by spin-coating at 5000 rpm during 30 s, always at ~ 50 °C to avoid physical gelation. The GB film was left under 50 °C for 3 h to crosslink gelatin chains and to graft the chemical network onto the wafer. Finally, after being washed under ultrasonic bath in hot water (50 °C) to remove unreacted polymer, the gelatin B hydrogel thin film grafted onto silicon wafer was obtained.

2.3 Thickness of thin films

The thickness of homogeneous hydrogel thin films on silicon wafers was measured with spectroscopic ellipsometer (UVISEL, Horiba). The angle of incidence was fixed at 60°, with a wavelength range from 400 nm to 800 nm. To determine the dry thickness (Th_{dry}) of gelatin

film, the refractive index (n_i) of the silicon substrate and of the gelatin was taken as 3.87 and 1.50, respectively. In order to measure the wet thickness (Th_{wet}), *in situ* underwater measurements were performed using a liquid cell, with thin glass walls fixed perpendicularly to the light path. The gelatin film was modeled as a single layer, with a constant refractive index between that of water (n_i = 1.33) and that of the polymer. Moreover, the swelling ratio of hydrogel films (SR) was calculated as Th_{wet}/Th_{dry}, assuming that the polymer amount remained the same before and after being immersed underwater, since the hydrogel film was covalently attached to the substrate and the free polymer chains were considered to be removed by washing in hot water. The volume fraction of gelatins in the swollen state was calculated as $\phi_p = 1/SR$.

2.4 Surface potential (ζ) of thin films

The surface potential (ζ) of the GB thin films was determined by streaming potential measurements using the SurPASS 3 (Anton Paar GmbH, Austria). Two pieces of silicon wafer (10 mm x 20 mm each) grafted with homogeneous GB films were attached to the rectangular cell with adhesive tape to let them face each other and form a streaming channel where the measuring fluid flowed through. During the experiment, the pressure inside the fluid channel (p) was continuously varied and the streaming potential at zero net current conditions (U) was measured for each value of p. The zeta potential ζ was then calculated using the expression developed by Smoluchowski[39]

$$\zeta = \frac{\mathrm{dU}}{\mathrm{dp}} \frac{\eta}{\varepsilon_r \varepsilon_0} \mathrm{k} \qquad (1)$$

where ε_0 is the vacuum permittivity constant (8.85×10^{-12} C^2 J^{-1} m^{-1}). ε_r, η and k are the dielectric constant, viscosity and the specific conductivity of the measuring fluid, respectively. ε_r, η and k were measured independently for each specific pH. The pH-dependence of the zeta potential (ζ) of GB thin films was determined in a KCl solution (1 mM) for a pH range from 2.5 to 10.5. Measurements started at pH 6, followed by stepwise addition of HCl or KOH (0.1 M) to sweep between more acidic and more basic pH ranges, respectively. One pair of films was used for the acidic environment and the other pair was used for the basic environment. Four measurements were conducted at each specific pH. The experiment of surface potential test was done by Cedano-Serrano.[40]

2.5 Synthesis of macroscopic hydrogels

The GA macroscopic hydrogels were chemically crosslinked by EDC/NHS coupling and physically crosslinked by triple helix formation between gelatin chains. After being dissolved in Milli-Q water at 50 °C overnight, GA solutions were mixed with a fresh solution of EDC/NHS (equal number of moles between EDC and NHS). Afterwards, the mixture was transferred into a glass mold and was left at 50 °C for 3 h for the carbodiimide reaction to proceed. Finally, the mold was kept at 4 °C overnight to form physical crosslinks. The dual-crosslinked hydrogels were stored in the fridge at 4 °C. The hydrogels were named as GAxRy, in which x represents the concentration of GA (wt%) (also defined as ϕ_0, the gelatin fraction in as-prepared state). EDC and NHS always have equal number of moles and the parameter y, proportional to the molar ratio between carbodiimide and free amino groups (ε-amino) on GA chains, was calculated as follows:

$$y = 10\frac{n_{EDC}}{n_{\varepsilon-amino}} \tag{2}$$

with 10 as a coefficient, n_{EDC} the mole number of EDC or NHS and $n_{\varepsilon\text{-}amino}$ the mole number of free amino groups determined by titration (**Figure S1 and S2**, **Supporting Information**). The GA concentration, x, used for the synthesis of macroscopic hydrogels was equal to 15, 20, 25 to 30 wt%, while the EDC/NH_2 ratio, y, was varied from 1 to 1.5, 2, 2.5 and 3.

2.6 Polymer fraction (ϕ_p) of gels in equilibrated state

In order to calculate the concentration of gelatin in equilibrated hydrogels, the equilibrium polymer fraction is calculated as:

$$\phi_p = \frac{m_{dry}}{m_{wet}} \tag{3}$$

where m_{dry} and m_{wet} refer to the weight of hydrogel in dry and wet (equilibrium) state, respectively.

2.7 Differential Scanning Calorimetry (DSC)

The thermal transitions of gelatin were determined by DSC measurements using a Q200 from TA instruments. GA hydrogels (~ 30 mg) were loaded into a Tzero® aluminum pan at room temperature. The samples, together with a reference filled with the same quantity of water, were

heated and equilibrated at 55 °C for 60 minutes. Then they were submitted to a cooling temperature ramp from 55 °C to 5 °C. Both heating and cooling rate was 1 °C min^{-1}.

2.8 Linear rheology measurement

Linear rheology was performed on a stress-controlled rheometer (HAAKE RheoStress 600, Thermo Scientific) using a cone-plate geometry to follow the crosslinking reactions with EDC/NHS and the formation/dissociation of triple helix in networks, with the gelatin solution at high temperature. GA was dissolved in water at 50 °C overnight, after adding the solution of EDC and NHS, the mixture was rapidly transferred to the rheometer plate thermostated at 50 °C. The gelation of GA occurred inside the geometry and the chemical crosslinking reaction was tracked with a time sweep for the first 60 min at 50 °C at a fixed frequency of 1 Hz and at a fixed maximum stress of 1 Pa. The time and temperature were selected in order to reach the maximum conversion of the chemical crosslinking, and defined as the synthetic procedure for GA hydrogel in this work. Furthermore, the formation of physical crosslinks was driven by cooling down the gelatin network from 50 °C to 5 °C and then waiting for 2 h to fully form the triple-helices. Finally, by heating up again to 50 °C, the dissociation of physical regions in hydrogel was monitored. The temperature rate during heating and cooling was constant at 1 °C min^{-1} as the same with DSC. Three replicas at least were conducted for each sample.

Linear rheology was also conducted on GA hydrogels at their equilibrium swelling using a plate-plate corrugated geometry. For GA gels with and without physical crosslinks, the equilibration was at 5 °C and 50 °C, respectively. Disk shape samples of 1 mm thickness and 20 mm diameter in the equilibrated state were used. Samples were placed between the geometries with a normal force of 0.5 N. An oscillatory time sweep of 300 s was performed at a fixed frequency of 1 Hz. The stress was fixed at 1000 Pa for 5 °C tests and 100 Pa for 50 °C. 60 data points were taken for each test. The average value of G' was taken as the result, with three replicas conducted for each gel.

2.9 Molecular weight between crosslinks

The molecular weight between crosslinks (M_x) of GA hydrogels was determined by the shear modulus in the as-prepared state. Ignoring the contribution of chain entanglements in this work, the phantom network model, assuming that the junctions in the network fluctuate over time, can be used to estimate the M_x:

$$G = \left(1 - \frac{2}{f}\right)\frac{cRT}{M_x} \quad (4)$$

where G is the shear modulus, f is the functionality of the junctions, c is the polymer concentration in the entire network with unit of kg m^{-3}, R is gas constant and T is the absolute temperature.[41]

For dual-crosslinked gelatin hydrogels, the network was considered as a bimodal network structure, where chemical and physical crosslinks were assumed to contribute additively to the shear modulus.[42-43] Therefore, at lower temperature when the triple-helices are stable in the gelatin network, the shear modulus (G_0) results from the additive contributions from the chemical (G_{ch}) and physical (G_{ph}) crosslinking:

$$G_0 = G_{ch} + G_{ph} = \left(1 - \frac{2}{f_{ch}}\right)\frac{cRT}{M_{ch}} + \left(1 - \frac{2}{f_{ph}}\right)\frac{cRT}{M_{ph}} \quad (5)$$

where f_{ch} and f_{ph} are the functionalities of chemical and physical crosslinks, respectively, with $f_{ch} = 4$ for chemical peptide bond and $f_{ph} = 6$ for triple-helices junctions. M_{ch} and M_{ph} are the average molecular weights between chemical and physical networks, respectively.[44]

At relatively higher temperature where the triple-helix structures between gelatin chains are dissociated, the shear modulus is estimated to be only contributed by the chemical network:

$$G_0 = G_{ch} = \left(1 - \frac{2}{f_{ch}}\right)\frac{cRT}{M_{ch}} \quad (6)$$

The molecular weight between chemical crosslinks (M_{ch}) was calculated with **Equation 6**, by taking the experimental elastic modulus G' at 50 °C as the shear modulus. Since the M_{ch} of a gel remains constant with the change in temperature at least in the range of 5-50 °C, M_{ph} was then calculated by using **Equation 5**, using the calculated M_{ch} and the experimental G' at 5 °C as the shear modulus (G_0).

2.10 Underwater Tack Test

The underwater tack test was conducted on a home-made setup designed by Sudre et al.[29] In this work, all hydrogels were tested in their equilibrated state in aqueous environment. Generally, the adhesion test consisted in forming a parallel contact and detachment between a GA macroscopic hydrogel (thickness ~ mm) and a GB hydrogel thin film (thickness ~ hundred

nm), while both were fully immersed underwater. The 5 mm × 5 mm silicon wafer grafted with GB hydrogel thin film was glued with a polyvinyl acetate adhesive (ref. L0196, 3M®, France) to a steel probe, which was fixed to a 10 N load cell and connected to a universal tensile machine (model 5333, Instron®, France). A sample of the GA hydrogel (thickness ~ 2 mm) was glued to a glass microscope slide with a cyanoacrylate adhesive (Loctite® 406, France). The contact between the macroscopic GA material and the GB hydrogel thin film was made underwater mostly at an approaching rate of 100 μm s^{-1}. A preload of 1 kPa was applied for a given contact time which was mostly fixed at 1 s. Finally, the probe was detached at a certain debonding rate (V_{deb}) while recording the probe displacement and force. From this experiment, the work of adhesion (W_a) could be calculated as follows:

$$W_a = T_0 \int_0^{\varepsilon_{max}} \sigma d\varepsilon \quad (7)$$

where ε was the nominal strain which was obtained by normalizing the displacement by the initial thickness of the bulk hydrogel (T_0). σ was the stress obtained by dividing the force by the contact area. Three replicates were conducted for each experiment.

3 Results and Discussion

3.1 Synthesis of gelatin B films

Surface-attached GB hydrogel thin films are synthesized on the top of silicon wafers using the CLAG strategy developed in our group.[32-34] The CLAG strategy consists in simultaneously Cross-Linking and Grafting gelatin with EDC/NHS coupling (**Figure 1**). The intermolecular reaction of activated carboxylic acid residues with the free ε-amino groups residues of lysine on gelatin chains results in the creation of peptide bonds as crosslinking points.[44] Meanwhile, with the same reaction between the carboxyl groups on gelatin chains and amino groups on amino-modified silicon wafers, the polymer network is grafted onto the substrate. Therefore, the resulting material is defined as gelatin hydrogel thin film.

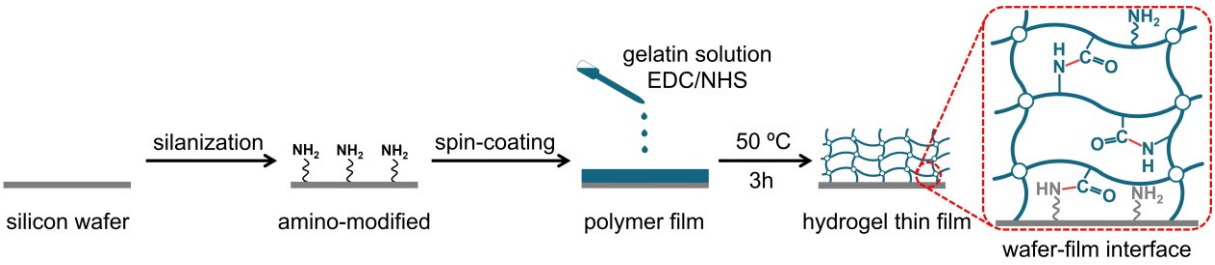

Figure 1. Synthesis process of surface-attached gelatin hydrogel thin films using the CLAG strategy. The CLAG strategy consists in Cross-Linking and Grafting gelatin chains onto the amino-modified silicon wafers with EDC/NHS coupling.

3.2 Thickness and swelling of surface-attached hydrogel films

The thickness of GB films is controlled by the concentration of polymer in the solution for spin-coating. As shown in **Figure 2a**, dry and wet thicknesses of films increase with the increase in polymer concentration for spin-coating. The Th_{wet} is much higher than Th_{dry}, because the polymer hydrogel can swell underwater by absorbing water. The swelling is completely reversible. Therefore, the equilibrium swelling ratio (SR) of films is defined as Th_{wet}/Th_{dry}, assuming that the amount of polymer is the same before and after being immersed in water, since gelatin is chemically grafted onto the substrate. The swelling ratio of films strongly increases with the dry thickness below ~ 50 nm and then keeps constant for thicker films at SR about 4.2 (**Figure 2b**). This originates from the gap between the grafting density and the crosslinking density as the grafting density is much higher than crosslinking density in surface-attached hydrogel films. When the film is very thin, the effect from the surface limits the swelling of the network, but for thicker films, the impact of the surface becomes negligible and the constant swelling ratio demonstrates that the degree of crosslinking does not depend on the gelatin concentration of the spin-coating solution (which determines the dry thickness of the layer). The volume fraction of polymer in GB films in the swollen state (ϕ_p) is calculated as follows:

$$\phi_p = \frac{1}{SR} \tag{8}$$

The volume fraction, inversely proportional to the swelling ratio, decreases with increasing dry thickness (Th_{dry} < 50 nm) and keeps constant when the film is thicker (**Figure 2c**). For films with thickness over 50 nm, the volume fraction is constant around 23%, which is in the normal range of gelatin macroscopic hydrogels. In this work, all the underwater adhesion experiments

were performed with the film made from 5 wt% gelatin B solution (Th_{dry} ~ 100 nm), to avoid the substrate effect of the film and to keep the polymer fraction comparable with macroscopic hydrogels.

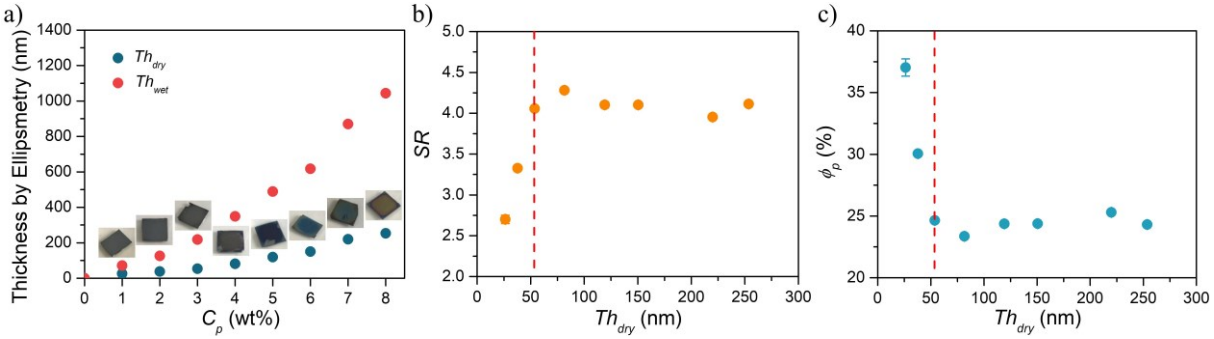

Figure 2. a) Dry (in air, Th_{dry}) and wet (in Milli-Q water, Th_{wet}) thickness, b) swelling ratio (SR) and c) volume fraction of polymers (ϕ_p) of gelatin B films.

3.3 Charge density at surface

GB hydrogel thin films obtained by spin-coating with solutions of 2.5 wt% (dry thickness ~ 30 nm) and 5.0 wt% (dry thickness ~ 150 nm) were prepared on silicon wafers for streaming potential measurements. As shown in **Figure 3**, the isoelectric point (pI = pH|ζ = 0) of both samples is found to be around pH 5, in good agreement with the potentiometric titration. It reflects the gelatin protein structure with a mixture of acidic and basic functional groups. The plateau ζ values ($\zeta_{plateau}$) are determined by the number of functional groups and by the swelling degree. The absolute plateau value of the zeta potential for films spin-coated from a 2.5 wt% GB solution is around -25 mV, slightly lower than for the sample coated by the 5 wt% GB solution of around -20 mV. This result suggests that the composition of the electrical double layer is influenced by the absorbed amount of water, since a film with lower $\zeta_{plateau}$ value has a higher swelling ratio (**Figure 2b**).

The charge density of GB thin film ($\Sigma_{i\text{-}film}$) is determined by

$$\Sigma_{i-film} = \sigma_a = \alpha_d N_a \tag{9}$$

where σ_a is the areal density of negative charges existing at the solid/liquid interface at a specific pH. α_d is the degree of dissociation of functional groups at certain pH. N_a is areal density of total groups capable of dissociating per unit area.

N_a is calculated by the Graham equation:[45-46]

$$N_a = \frac{1}{e_0}\sqrt{8\varepsilon_r\varepsilon_0 C^{\infty} RT}\sinh\left(\frac{F\zeta_{plateau}}{-2RT}\right) \quad (10)$$

where e_0 is the charge of an electron, which is 1.6×10^{-19} C. ε_r is the dielectric constant of the measuring fluid, which is approximately 80 for water here. ε_0 is the vacuum permittivity. C^{∞} is the ion concentration of the streaming solution (1 mol m^{-3}). F is the Faraday constant and T was 293.15 K for all the streaming potential test.

Finally, N_a is calculated to be 9.43×10^{15} m^{-2} and $\Sigma_{i\text{-}fillm}$ is 5.19×10^{15} m^{-2} at pH = 6.0 (α_d = 0.55).

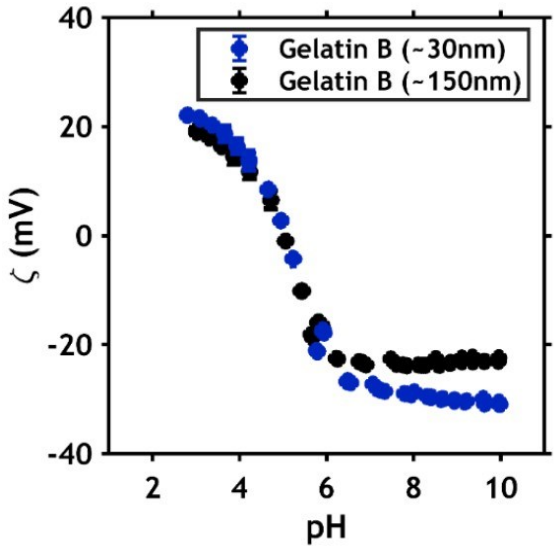

Figure 3. Zeta potential of the GB hydrogel thin film with different dry thickness at different pH values. The figure is from Cedano-Serrano.[40]

3.4 Synthesis of gelatin A hydrogels

In this work, the GA hydrogels are dual-crosslinked (physically and chemically), with additional chemical crosslinks in the physical network formed by triple-helices between gelatin chains. As shown in **Figure 4**, the gelatin is first chemically crosslinked through amine coupling between gelatin chains, by EDC and NHS. Then gelatin is allowed to form an additional physical network after cooling, by triple-helix formation between polypeptide chains. The formation process of dual networks during the synthesis is tracked by linear rheology (**Figure S3, Supporting Information**). After mixing the EDC/NHS with GA solution at 50 °C, the elastic modulus (*G'*) of the mixture is initially lower than the viscous modulus (*G''*). But after ~ 3 min, *G'* increases rapidly and becomes higher than *G''*, indicating the gelation of the GA

solution. At this temperature, the gelation is induced by the peptide bond formation between gelatin chains promoted by EDC/NHS. Then the *G'* of gel increases by cooling, with the formation of triple-helices within the gel. Finally, a dual-crosslinked gelatin type A hydrogel is obtained. The gelatin concentration for synthesizing macroscopic hydrogels is chosen to be around 20 wt%, as this concentration is close to the polymer fraction of thin films (**Figure 2c**). The similar swelling ratio of both hydrogel thin films and macroscopic hydrogels ensures that the main difference between them comes from the surface and bulk properties.

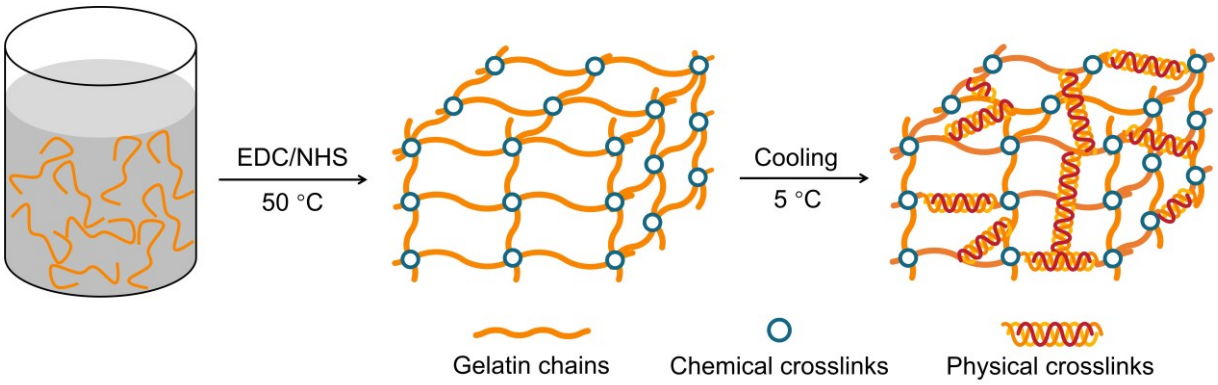

Figure 4. Synthesis process of dual-crosslinked GA hydrogels.

3.5 Control crosslinks in macroscopic GA hydrogels

Polymer concentration (x) and crosslinking reagent ratio (y), related to physical and chemical networks respectively, are used to control the physico-chemical properties of GA networks. In order to determine the amount of triple-helices and chemical crosslinks, DSC and rheology are used to follow the change of transition enthalpy and shear modulus during the temperature sweep, respectively.

The formation of triple-helices regions in gelatin gels is quantified by the cooling process in DSC. There is a heating process before cooling, which aims to remove the triple-helices form during the synthesis and to erase the structure history (**Figure S4, Supporting Information**). **Figure 5a** shows a thermogram of GA hydrogels with different ratios of chemical crosslinking reagents. By cooling, the gelatin hydrogel exhibits an endothermic peak centered around 21 °C, which corresponds to the formation of triple-helices between gelatin chains. As the heating flow ($W\ g^{-1}$) and enthalpy ($J\ g^{-1}$) are normalized in Watts per gram of gelatin and Joules per gram of gelatin respectively, the rather constant value of the enthalpy indicates that the number of physical bonds (triple-helices) is proportional to the chain concentration (**Figure 5b**). On the other hand, with an increasing ratio of EDC/NH_2, the enthalpy strongly decreases from ~ 22.7

(y = 0) to 17.6 (y = 1) and 10.2 J g^{-1} (y = 2), showing that existing chemical bonds hinder the formation of physical crosslinks between gelatin chains.

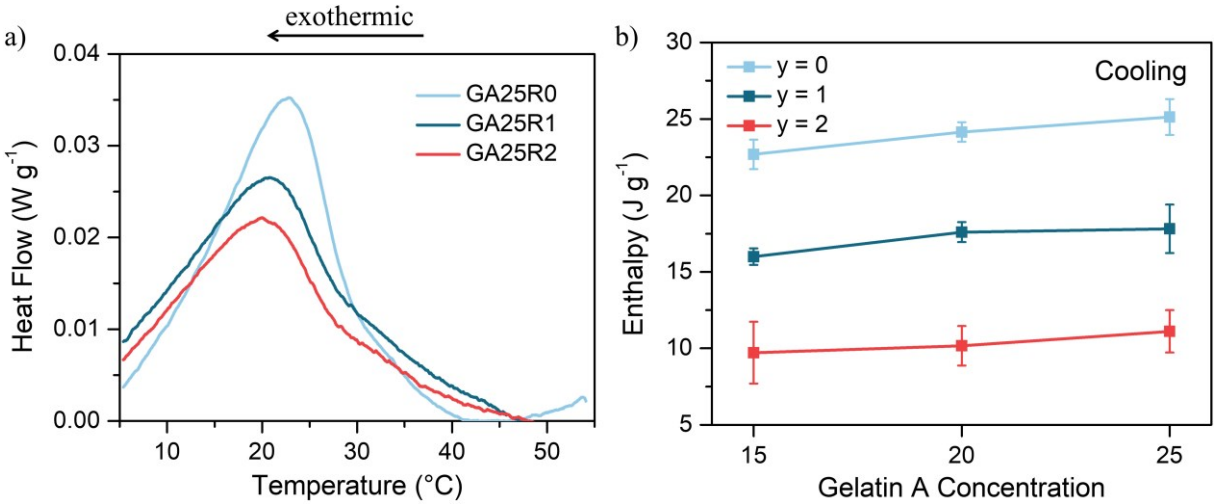

Figure 5. DSC on GAxRy gels following the cooling process after being kept at 55 °C for 60 min. a) thermogram. b) Enthalpy is calculated by the area under the thermogram, which is normalized by the weight of gelatin.

The change of *G'* for as-prepared GA hydrogels is shown in **Figure 6** for different polymer concentrations and EDC/NH_2 ratio, during a heating process from 5 to 50 °C. With the increase in temperature, the *G'* of hydrogels decreases, indicating the dissociation of triple-helices in the network. At high temperature (above ~ 35 °C), the gelatin chains are only chemically crosslinked, so the value of *G'* characterizes the chemical crosslinking density. *G'* increases with the ratio of EDC/NH_2 and with polymer concentration, indicating the increase in the density of chemical networks. On the other hand, at low temperature (below ~ 35 °C), the elastic modulus *G'* increases as expected with the polymer concentration but decreases with increasing EDC/NH_2 ratio. As previously described with DSC, the formation of chemical crosslinks between gelatin chains hinders the formation of triple-helices.

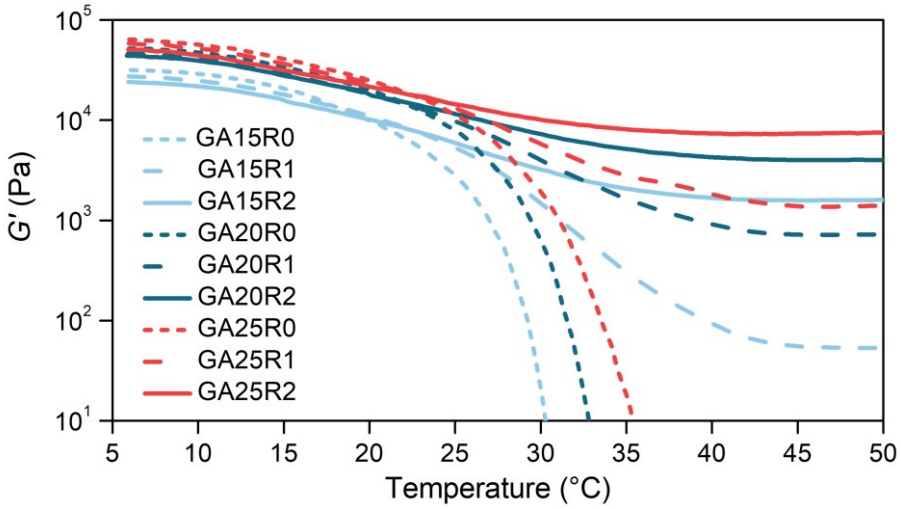

Figure 6. *G'* of as-prepared GA hydrogels with different polymer concentrations and EDC/NH_2 ratio, under a heating process from 5 to 50 °C.

3.6 Molecular weight between crosslinks

The average molecular weight between chemical and physical crosslinks, M_{ch} and M_{ph}, calculated from viscoelastic experiments using **Equation 5** and **6** are given in **Table S1** (**Supporting Information**). Their contributions to the shear modulus at 5 °C (G_{ch} and G_{ph}) is also calculated. From these results, we can see that at low temperature, the contribution from physical bonds (G_{ph}) is much higher than for chemical ones (G_{ch}) with at least 1 order of magnitude difference.

As shown in **Figure 7a**, M_{ch} is very large for y = 1, meaning that the peptide bond formation is not very effective in these conditions even if the increase of gelatin concentration from 15 to 25 wt% can improve the chemical crosslinking. M_{ch} is considerably lower for y = 2 but far from M_{ph} which dominates the network properties. As previously described, the quantity of triple-helices increases with the decrease in EDC/NH_2 ratio and the increase in gelatin concentrations respectively, indicating a well-controlled chemical and physical crosslinking density, by changing crosslinking reagent and polymer concentration. Moreover, as previously mentioned, M_{ph} weakly depends on gelatin concentration and decreases with the increase of EDC/NH_2 ratio, supporting the fact that the existence of the chemical network restricts the formation of a structure of triple-helices.

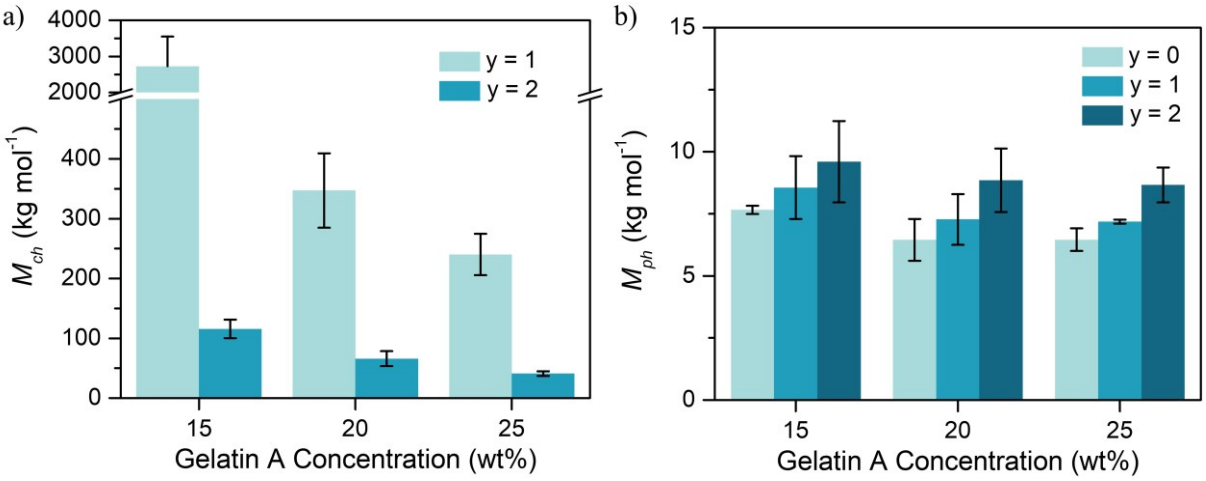

Figure 7. M_{ch} and M_{ph} of GA hydrogels with different polymer concentrations (as-prepared state) and EDC/NH_2 ratio (y value).

3.7 Underwater adhesion

Underwater adhesion of the biopolymer model system is now investigated to address the bioadhesion process. Indeed, gelatins consisting of amino acids can be viewed as a simple model system to mimick biological systems from the point of view of their molecular structure. Our model system consisting of thin films with well-defined surface properties and macroscopic hydrogels with controlled viscoelastic behaviors makes it possible to independently study of interface and network structure effects. At the interface, the interactions are controlled by using GB films of ~ 100 nm dry thickness. In front of that, the influence of the molecular structure of bulk hydrogels on macroscopic underwater adhesion is studied. As the GA hydrogel network is dual-crosslinked, both influences from M_{ch} and M_{ph} are investigated. The adhesion of dual-crosslinked hydrogels is also studied to understand the collective effect and potential synergy of both types of crosslinks. The underwater adhesion measurements are carried out in equilibrated conditions with the environment for both GB thin film and GA bulk hydrogels. The shear modulus (G_{eq}) and polymer fraction (ϕ_p) in the equilibrated state are shown in **Table 1** .

Table 1. GA hydrogels exist in this work, with their equilibrium polymer fraction (ϕ_p) and shear modulus in equilibrated state (G_{eq}) at 4 °C and 50 °C. At 4 °C, GA10R0, GA15R0, GA20R0, GA25R0 and GA30R0 are used for studying the contribution of physical network on adhesion. GA15R1, GA20R1 and GA25R1 are used for comparing adhesion of dual-crosslinked gel with different gelatin concentration. GA20R0.5, GA20R1, GA20R1.5 and GA20R2 are used for the

comparison of adhesion energy with the same hydrogel concentration but different chemical crosslinking reagent concentration. At 50 °C, GA20R2, GA25R2.5 and GA20R3 are equilibrated to study the contributions of chemical networks on work of adhesion.

Gel Name	ϕ_p (%) 4 °C	G_{eq} (kPa) 4 °C	ϕ_p (%) 50 °C	G_{eq} (kPa) 50 °C
GA10R0	7.03 ± 0.02	10.7 ± 0.7	/	/
GA15R0	10.33 ± 0.08	18.4 ± 1.4	/	/
GA20R0	12.95 ± 0.97	30.3 ± 3.2	/	/
GA25R0	15.24 ± 0.38	36.1 ± 0.8	/	/
GA30R0	17.58 ± 0.08	51.6 ± 5.9	/	/
GA15R1	10.11 ± 0.04	13.1 ± 1.9	/	/
GA20R1	11.43 ± 0.31	20.2 ± 1.6	/	/
GA25R1	12.59 ± 0.10	22.5 ± 1.3	/	/
GA20R0.5	9.64 ± 0.39	20.3 ± 3.5	/	/
GA20R1	10.66 ± 0.21	20.2 ± 1.9	/	/
GA20R1.5	10.37 ± 0.29	17.7 ± 2.8	1.65 ± 0.05	2.7 ± 0.4
GA20R2	10.48 ± 0.14	19.8 ± 2.2	3.24 ± 0.11	3.4 ± 0.4
GA25R2.5	/	15.9 ± 3.2	4.29± 0.31	7.2 ± 0.9
GA20R3	/	/	5.67 ± 0.21	8.7 ± 2.1

3.8 Interface interactions

Gelatin type A and B are known to have isoelectric points at pH ~ 8 and ~ 5, respectively. So between pH 5 and 8, the oppositely charged GA and GB materials should have electrostatic attractive interactions with each other. On the other hand, gelatin is also known to form triple-helices among polymer chains through hydrogen bonds. There is of course also a possibility to form hydrogen bonds during the contact between the two gelatin materials. The interfacial interactions are investigated by studying adhesion in extremely concentrated salt (NaCl) and urea solutions, which screen the non-covalent interactions, electrostatic and hydrogen bonding, respectively.[47] Underwater adhesion in 4 M NaCl and 30% urea solutions have been

investigated and will be compared with the same adhesion tests carried out in Milli-Q water. The contact time between surface and soft hydrogels is 60 s to potentially form quantitative interactions. As shown in **Figure 8,** in both NaCl and urea solutions, the GA and GB have a weaker adhesion than in Milli-Q water but adhesion remains measureable, indicating that both electrostatic interaction and hydrogen bonding serve as the interface interactions between gelatin. In addition, the effect of contact time is studied to compare with several previous works of our group performed on similar model systems. As shown in **Figure S5 (Supporting Information)**, the underwater adhesion between gelatins significantly increases from 16.8 to 37.7, 104.2 and 183.1 mJ m^{-2} with increasing contact time from 1 to 60, 600 and 1800 s. This result is consistent with the formation of interfacial hydrogen bonds between GB and GA as previous underwater experiments, performed on synthetic models, have shown that the formation of hydrogen bonds in water is rather slow[29-30] in contrast to electrostatic interactions which form rapidly at the interface.[31] These results, obtained from the gelatin-based model, demonstrate that cooperative interactions are important for designing underwater adhesives and bioadhesives.

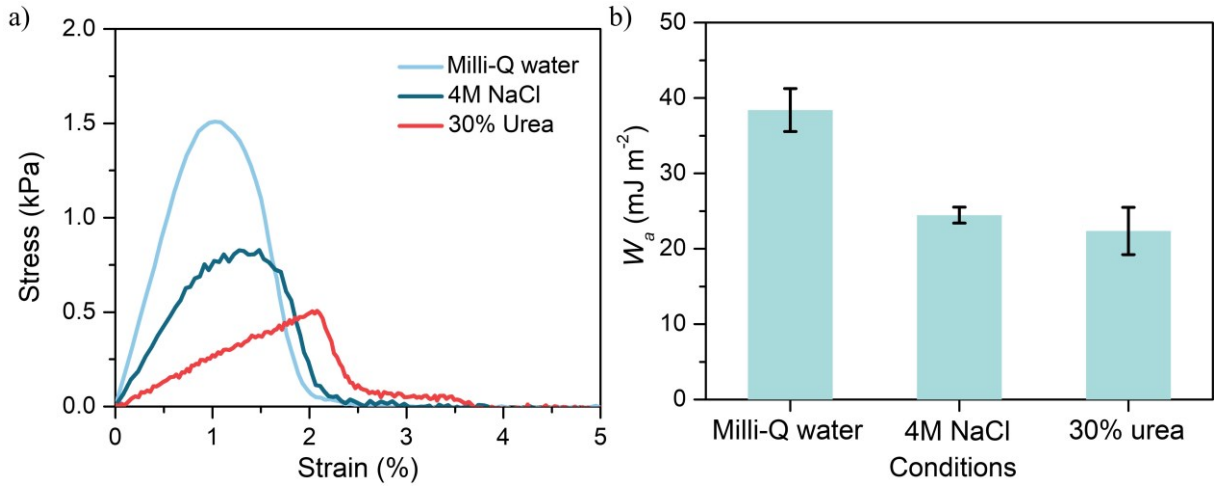

Figure 8. Underwater adhesion of GA20R2 gels in different solutions. a) Representative stress-strain curves of adhesion. b) Work of adhesion (W_a). The temperature is fixed at 4 °C and the gels are in their equilibrated state. The contact time is 60 s.

3.9 Effect of physical crosslinks on adhesion

The contributions of physical crosslinks are studied at low temperature (4 °C), by comparing work of adhesion of purely physical gels (without any chemical crosslinks). For example, GA10R0 is made from a 10 wt% solution of gelatin A without any EDC/NHS. **Figure 9a** shows representative stress-strain curves of the probe tack adhesion tests of physical gelatin gels made

at different concentrations. **Figure 9b** shows the average work of adhesion and shear modulus as a function of equilibrium polymer fraction in the gel. As shown in **Figure 9b**, with increasing gelatin equilibrium fraction from 7.0 wt% to 10.3, 13.0, 15.2 and 17.6 wt%, the work of adhesion increases from 12.7 mJ m^{-2} to 14.4, 17.8, 22.7 and 27.0 mJ m^{-2}. This is also related to the increase in shear modulus from 10.7 kPa to 18.4, 30.3, 36.1 and 51.6 kPa. This results show that for this GA vs GB adhesion a dense physical network with more "active bond" has more chances to interact and adhere with the other surface. The higher work of adhesion of more concentrated gelatin gels also corresponds to a higher strength, which is in turn related to the bulk cohesion.

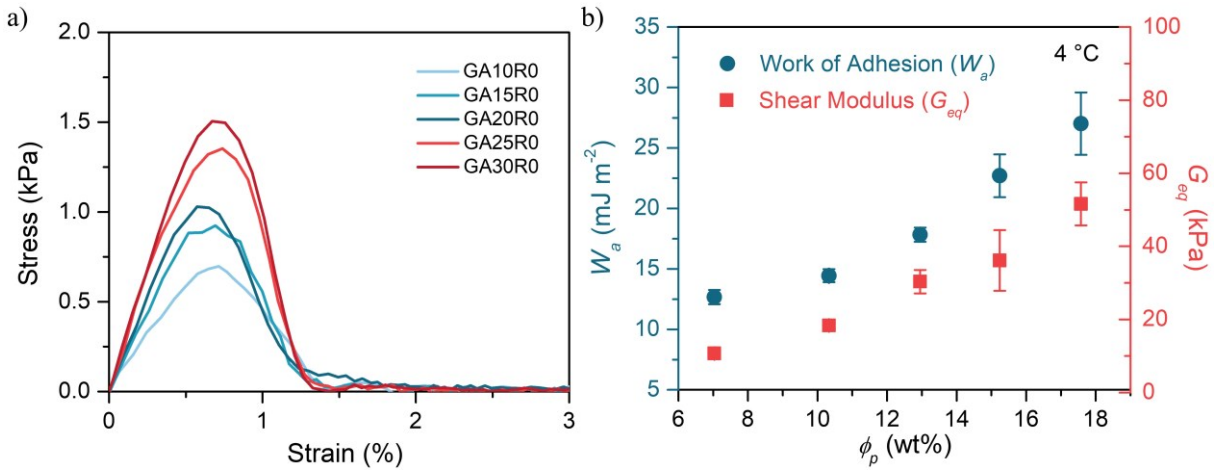

Figure 9. Underwater adhesion of physical gelatin gels (GAxR0) with different gelatin concentrations at 4 °C. a) Representative stress-strain curves of adhesion. b) Work of adhesion (W_a) and shear modulus (G_{eq}) versus polymer fraction (ϕ_p) in the equilibrium state.

3.10 Effect of the presence of chemical crosslinks on adhesion

On the other hand, the influence of chemical crosslinks is studied at 50 °C when triple-helices are dissociated, to avoid the existence and influence of the physical crosslinks between chains. **Figure 10a** shows representative stress-strain curves of hydrogels GA20R2, GA20R2.5 and GA20R3, made with increasing EDC/NH_2 ratio but with a constant gelatin concentration for gel preparation (20 wt%). As shown in **Figure 10b**, with increasing value of y (EDC/NH_2 ratio) from 2 to 2.5 and 3, the equilibrium polymer fraction, at 50 °C, increases from 3.2 wt% to 4.3 and 5.7 wt%, and the work of adhesion decreases from 9.9 mJ m^{-2} to 8.3 and 7.2 mJ m^{-2}, and shear modulus increases from 3.4 kPa to 7.2 and 8.6 kPa. That is to say, the work of adhesion decreases with increasing modulus, indicating an opposite effect from what is observed for the purely physical network.

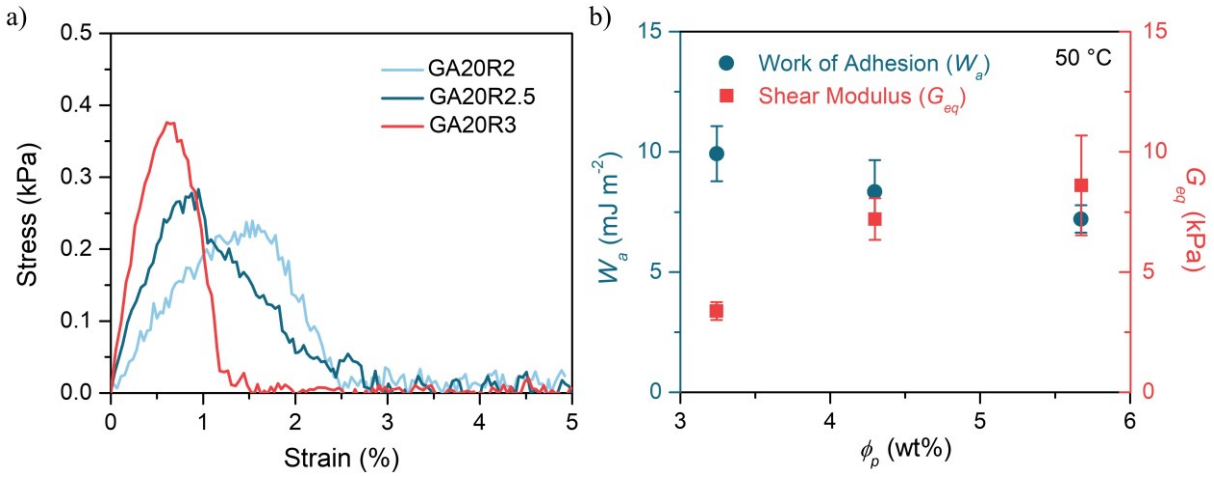

Figure 10. Underwater adhesion of chemical gelatin gels (GA20Ry) with different EDC/NH_2 ratio at 50 °C. a) Representative stress-strain curves of adhesion. b) Work of adhesion (W_a) and shear modulus (G_{eq}) versus polymer fraction (ϕ_p) in equilibrium state.

3.11 Chaudhury's model for adhesive properties of chemical networks

The adhesion weak bonds at the interface between deformable materials was theoretically described by Chaudhury, taking into account that the fracture energy of a soft interface is rate-dependent as the scission mechanism of individual bonds at the interface is itself rate-dependent. According to Chaudhury's model,[38] the work of adhesion (W_a) between a deformable elastic material and a functionalized surface could be described as follows:

$$W_a = \left(\frac{\Sigma_i}{2k_s}\right)\left[\left(\frac{k_B T}{\lambda}\right)\ln\left(\frac{k_s V \lambda \tau_-}{n k_B T}\right)\right]^2 \quad (11)$$

where Σ_i is the areal density of electrostatic interactions existing in the interfacial plane, i.e. the interfacial charge density. In our case, k_s can be taken as the linear spring constant of the GA gelatin chains which is inversely proportional to their length (molecular weight) of the chain. k_B is the Boltzmann's constant. T is the absolute temperature. V is the pulling velocity on the bond, which is proportional to the macroscopic pulling velocity (V_{deb}). λ is the activation length of the bond itself, which is assumed to be 0.1 nm on the order of a bond length, as a typical ionic bond length.[48] τ_- is the characteristic time of bond dissociation. n is the number of bonds in the polymer chain that can dissociate, which is 1. This model is applied to the case of gelatin gels at 50 °C, since a chemical hydrogel could be considered as soft and elastic. Note that a polymer chain has a markedly non-linear behavior because the spring constant is determined

by the entropic spring at small strains, but by the stiffness of the bonds on the chain near the maximum extension of the chain.

The interfacial charge density (Σ_i) can be estimated by comparing the surface charge density of gelatin B thin film ($\Sigma_{i\text{-film}}$) and the surface charge density of gelatin A hydrogels ($\Sigma_{i\text{-gel}}$). $\Sigma_{i\text{-film}}$ can be calculated from **Equation 9** as 5.19×10^{15} m^{-2}, assuming that the charge density is constant upon temperature change. The bulk charge density of GA hydrogels is defined as:

$$\Sigma_{gel} = c_+(1 - E_{cross})\phi_p N_{av} \tag{12}$$

where c_+ is the positive charge concentration of polymer, defined as the net excess concentration of positive groups in gelatin A (0.014 mol L^{-1}, **Figure S2, Supporting Information**). E_{cross} is the chemical crosslinking efficiency from EDC/NHS coupling, which is calculated by **Equation S6** and shown in **Figure S6** (**Supporting Information**). ϕ_p is the equilibrium polymer volume fraction and N_{av} is the Avogadro's constant. We assume that the hydrogel has an average distance between crosslinks (L, in the equilibrated state, shown in **Figure S7**, **Supporting Information**) that serve as a measure of the interface depth for adhesion with the film. The molecular weight between crosslinks could be estimated from the end-to-end distance between crosslinks (L_0, for as-prepared state), by considering the hydrogel networks from as-prepared state to equilibrium state undergoes uniform swelling by the same amount in all directions:[41]

$$L = L_0\left(\frac{\phi_0}{\phi_p}\right)^{\frac{1}{3}} = bN_c^{\frac{1}{2}}\left(\frac{\phi_0}{\phi_p}\right)^{\frac{1}{3}} \tag{13}$$

where ϕ_0 is the polymer fraction in as-prepared state (**Table 1**). b is the C-N bond length of a peptide bond (0.132 nm). N_c is the number of "monomers" between crosslinks. As gelatin is constituted of many different amino acids, so the representative "monomer" is assumed to be an amino acid and its average molecular weight ($M_{monomer}$) is estimated to be the weighted average molecular weight of amino acids of gelatin type A from pork skin which is 139.88 g mol^{-1} (**Table S2**, **Supporting Information**). N_c is defined by:

$$N_c = \frac{M_x}{M_{monomer}} \tag{14}$$

where M_x is the molecular weight between crosslinks, which is M_{ch} in the case of chemical networks, calculated from the phantom network model in **Figure 7**. Finally, the areal density of positive charges on the surface of macroscopic hydrogels ($\Sigma_{i\text{-gel}}$) is defined as

$$\Sigma_{i-gel} = \Sigma_{gel} \cdot L \tag{15}$$

The $\Sigma_{i\text{-gel}}$ of the three gels in **Figure 10** is shown in **Table 2**.

Table 2. Σ_{gel} and $\Sigma_{i\text{-gel}}$ of GA hydrogels in equilibrated state at 50 °C

Gel Name	Σ_{gel} (m^{-3})	$\Sigma_{i\text{-gel}}$ (m^{-2})
GA20R2	2.10×10^{23}	1.10×10^{15}
GA20R2.5	2.64×10^{23}	0.93×10^{15}
GA20R3	3.44×10^{23}	1.01×10^{15}

For the gels used for adhesion study, the $\Sigma_{i\text{-gel}}$ is approximately 5 times smaller than $\Sigma_{i\text{-film}}$ (5.19×10^{15} m^{-2}), indicating that the charge density in hydrogels controls the interfacial charge density as Σ_i. It also explains the weak adhesion measured in this work due to the low charge density, comparing with the synthetic gels with $\Sigma_i = 4 \times 10^{16}$ and W_a of ~ 200-1000 mJ m^{-2}.[31]

The k_s in this work can be estimated by rearranging the equation of the Chaudhury's model into the following form:

$$W_a^{\frac{1}{2}}\left(\frac{k_B T}{\lambda}\right)^{-1} = \left(\frac{\Sigma_i}{2k_s}\right)^{\frac{1}{2}} \ln V + \left[\left(\frac{\Sigma_i}{2k_s}\right)^{\frac{1}{2}} \ln\left(\frac{k_s \lambda \tau_-}{n k_B T}\right)\right] \tag{16}$$

Based on the experimental value of the adhesion energy as a function of the detachment rate V_{deb} (which is assumed to be proportional to the rate of interfacial crack growth), $W_a^{1/2}(k_BT/\lambda)^{-1}$ as a function of $\ln V_{deb}$ is plotted for the GA20R2.5 gel. The slope and intercept of this plot give an estimate of the spring constant k_s of the polymer chain and of the dissociation time τ_- of the electrostatic bond, respectively. Σ_i is taken from $\Sigma_{i\text{-gel}}$ of GA20R2.5. The values of k_s and τ_- are estimated to be 1.16×10^{-3} N m^{-1} and 2.01×10^{-3} s, respectively (**Figure 11**).

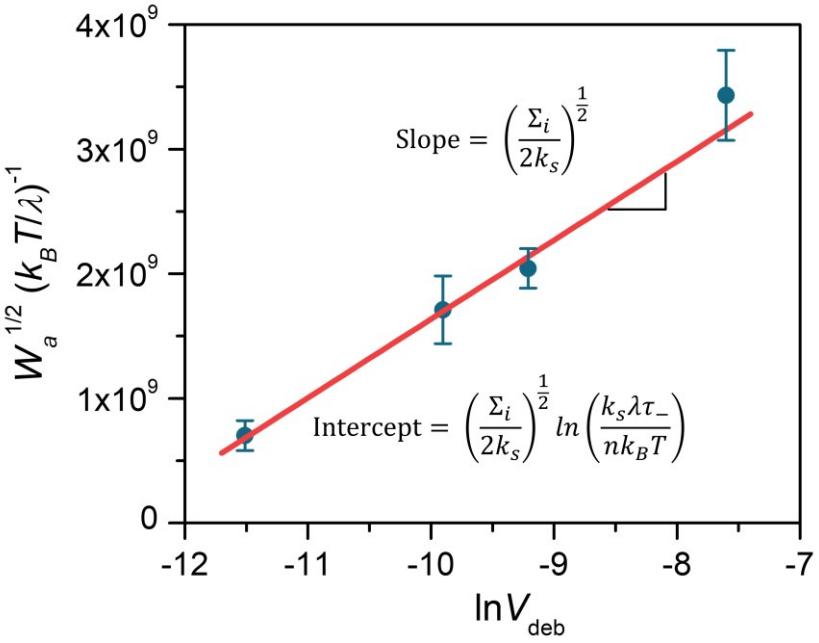

Figure 11. $W_a^{1/2}(k_BT/\lambda)^{-1}$ as function of $\ln V_{deb}$ of underwater adhesion between gel GA20R2.5 and gelatin B film. Cyan symbols are the experimental data and line is the linear fit.

As a comparison, the spring constant of a polymer chain in its enthalpic limit can be calculated by:

$$k_{s-enthalpic} = \frac{2N_cU_c/N_{av}}{\left(2N_c\cos\left(\frac{\theta}{2}\right)b\right)^2} \tag{17}$$

where U_c is the bond energy of the covalent bond which is 400 kJ mol^{-1}, N_{av} is the Avogadro's constant, b is the C-N bond length in a peptide bond (0.132 nm) and $\cos(\theta/2)$ equals to 0.81. N_c is the number of "monomers" between crosslinks. Using **Equation 17**, the $k_{s\text{-}enthalpic}$ of GA20R2.5 gel is calculated to be 1.17 × 10^{-1} N m^{-1}, which is 2 orders magnitude higher than the k_s obtained from fitting data of **Figure 11** (1.16 × 10^{-3} N m^{-1}). This result indicates that the electrostatic interactions at the interface (relatively weak bond attached to a polymer chain) break before the chain becomes fully extended.

Chaudhury's model assumes that at interfaces between macroscopic hydrogels, relatively weak bonds (electrostatic interactions, assuming the hydrogen bond does not contribute to adhesion at 50 °C) are attached to a polymer chain composed of strong bonds (covalent bonds) that is flexible but doesn't break. During debonding, only the deformation of the flexible chains

of the gels contributes to W_a. The work of adhesion of GA20R2, GA20R2.5 and GA20R3 are predicted by using $\Sigma_i = \Sigma_{i\text{-gel}}$, as shown in **Figure 12**.

3.12 Prediction of adhesion energy from the microscopic structure of hydrogels

However, since the analysis above is based on an assumption that there is a maximum depth of end-to-end distance between crosslinks (L) on the macroscopic hydrogel surface that is able to interact electrostatically with the film, it is also worthwhile to consider the situation of where ($\Sigma_i = \Sigma_{i\text{-film}}$). Considering $\Sigma_i = \Sigma_{i\text{-film}} = 5.19 \times 10^{15}$ m^{-2} for all the adhesion of GA20R2, GA20R2.5 and GA20R3. From **Figure 11**, the values of k_s and τ- are estimated to be 6.49 × 10^{-3} N m^{-1} and 2.01 × 10^{-3} s, respectively.

Chaudhury's model assumes that polymer chains are linear springs with a constant k_s, which is then used to predict the adhesion energy as a function of polymer chain length. There is a relationship between k_s and polymer chain length:

$$k_s = \frac{k_3}{N_c} \tag{18}$$

where k_3 is a coefficient that relates the spring constant of the polymer chain. N_c is calculated from **Equation 14**. According to the previous results in **Figure 7**, k_3 is calculated to be 1.61 N m^{-1}, for the hydrogel GA20R2.5 (M_{ch} = 35820.54 g mol^{-1}, k_s = 6.49 × 10^{-3} N m^{-1}).

In order to study the relationship between W_a and N_c, the Chaudhury's model can be written in the following form:

$$W_a = k_1 \cdot N_c \cdot \left[\ln\left(\frac{k_2}{N_c}\right)\right]^2 \tag{19}$$

where: $$k_1 = \left(\frac{\Sigma_i}{2k_3}\right)\left(\frac{k_B T}{\lambda}\right)^2, \qquad k_2 = \frac{k_3 V \lambda \tau_-}{n k_B T}$$

k_1 and k_2 are calculated to be 3.21 × 10^{-6} J m^{-2} and 7.27 × 10^3, respectively.

Finally, the work of adhesion (W_a) as function of number of monomers between crosslinks (N_c) predicted by Chaudhury's model is plotted and compared with the experimental data (**Figure 12**). In this result, the experimental N_c ranges from ~ 200 to ~ 500 because it was not feasible to synthesize hydrogels with extremely low crosslinking density that are still

mechanically stable. On the other hand, the fast EDC/NHS crosslinking reaction limits the formation of higher crosslinking density. As shown in **Figure 12**, the experimental W_a (cyan symbols) is between the prediction by $\Sigma_i = \Sigma_{i\text{-film}}$ (red curve) and $\Sigma_i = \Sigma_{i\text{-gel}}$ (cross symbols) from Chaudhury's model. This suggests that if the GA concentration is fixed, the energy of adhesion does indeed increase with increasing spring length (molecular weight between crosslinks of the GA). However, if we consider that the charge density is mainly limited by the bulk, the high experimental values suggest also that there may be more actual charges available for coupling at the interface than predicted by **Equation 13**. In other words, the length L may be larger than what is predicted by a simple swelling argument.

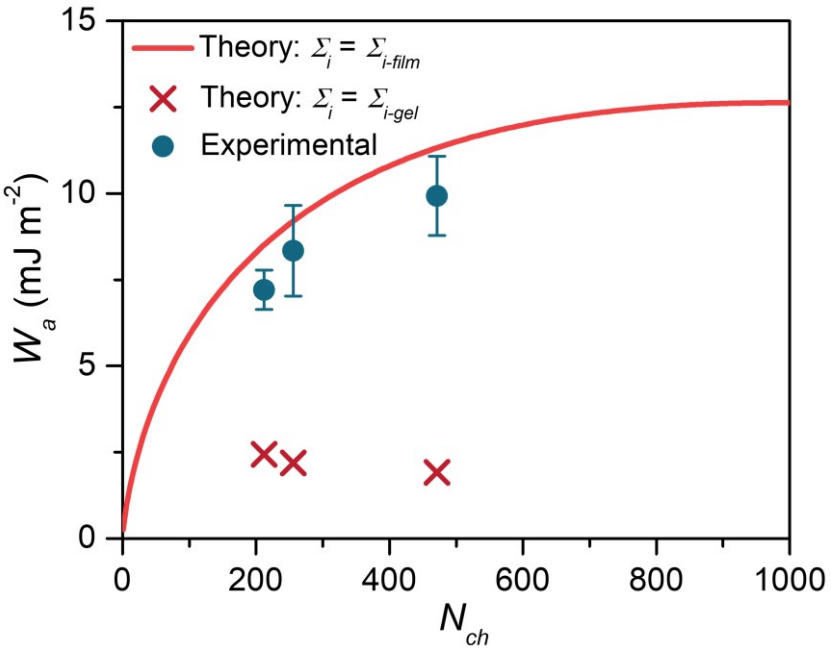

Figure 12. W_a of underwater adhesion between GA hydrogel and GB film as function of N_c. The red curve and red cross are the prediction from Chaudhury's model by considering $\Sigma_i = \Sigma_{i\text{-film}}$ and $\Sigma_i = \Sigma_{i\text{-gel}}$, respectively. Cyan symbols are the experimental data of GA20R2, GA20R2.5 and GA20R3.

3.13 Underwater adhesion of dual-crosslinked GA hydrogels

The underwater adhesion of GA gels was also performed at 4 °C to investigate the collective effect of physical and chemical crosslinks in the bulk gel and in the film on the adhesion. The dual-crosslinked gels have both physical and chemical crosslinks at 4 °C, at which the underwater probe tack test is performed. The physical network contribution is studied by comparing the work of adhesion of different gels with different GA concentration, with the

existence of a chemical network. As shown in **Figure 13a**, with a fixed *y* value at 1, the work of adhesion increases from 21.5 mJ m^{-2} to 22.75 and 33.2 mJ m^{-2}, with increasing GA bulk concentration from 10.1 to 10.7 and 12.6 wt%. This shows that unlike the case of 50 °C, at 4 °C the adhesion appears to be strongly related to the polymer concentration, which is similar to the condition of the adhesion of purely physically crosslinked gels shown in **Figure 9**.

Moreover, to study the contribution from chemical network in the dual-crosslinked GA hydrogels, the underwater adhesion of GA20Ry was investigated, at a fixed GA concentration and different EDC/NH_2 ratio. As shown in **Figure 13b**, with increasing *y* value from 0.5 to 1, 1.5 and 2, the work of adhesion remains around 20 mJ m^{-2}, showing no apparent difference as the degree of chemical crosslinking is increased. These results indicate that although the formation of chemical crosslinks decreases the density of triple-helix crosslinks, their impact remains negligible on the adhesion performance. However, it is important to note that the same result as for the purely physically crosslinked gelatin gels is found here, i.e. that the concentration of interactive sites (negative charges) present in the gel controls the work of adhesion. Although, according to **Equation 11**, increasing the modulus should increase k_s, i.e. decreasing the number of monomers between crosslinks involved in the detachment process, the main effect on the adhesion energy appears to be due to the increase in the areal density of interfacial bonds Σ_i, with increasing GA concentration (ϕ_p).

In addition, the very small variation in modulus of **Figure 13b** shows that adding dilute chemical crosslinks does not generate a huge decrease in physical crosslinking density, maintaining the gelatin network and the same adhesion performance.

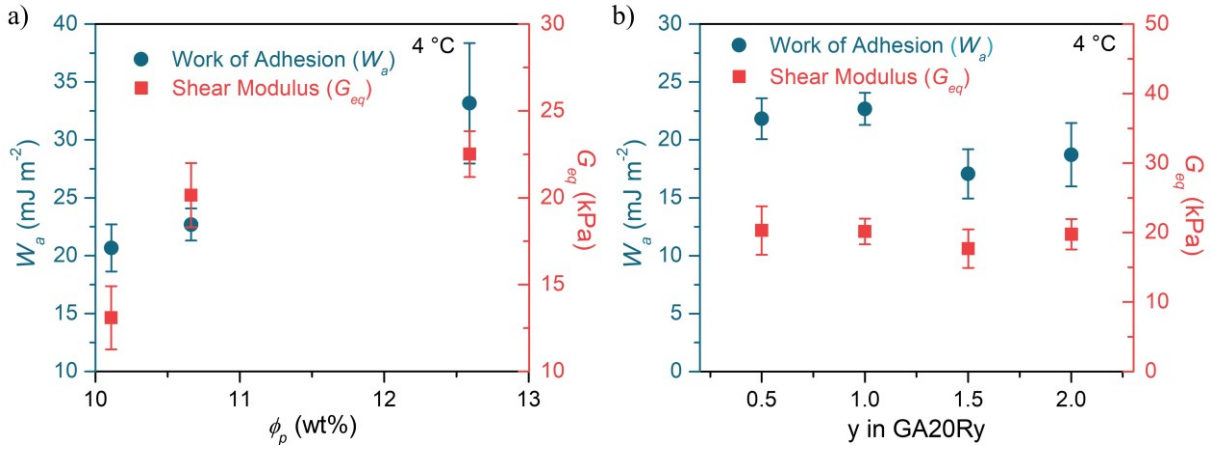

Figure 13. Physical and chemical crosslinking effect on work of adhesion at 4 °C. a) Work of adhesion (W_a) and shear modulus (G_{eq}) of GAxR1 gels as a function of equilibrium polymer fraction (ϕ_p). The hydrogels have varied x value from 15 to 20 and 25. b) Work of adhesion of

GA20Ry gels with varied y value from 0.5 to 1, 1.5 and 2. The gels as well as their work of adhesion (W_a), shear modulus (G_{eq}) and polymer fraction (ϕ_p) are all in equilibrium state.

4 Conclusion

In order to investigate bioadhesion process in a controlled way, a biopolymer has been used to build a model system consisting of hydrogel thin films (~ hundred nm thick) and macroscopic hydrogels (~ mm thick), which allows the separation of interfacial and bulk properties. Gelatin A and B are used as biopolymer and the model system allows the independent study of interface and network effects on underwater adhesion performance. Both gelatin materials are synthesized with a well-controlled chemical structure and reproducible and well controlled test parameters. The gelatin B hydrogel thin film is crosslinked and grafted onto a solid substrate. A sufficient dry thickness (~ 100 nm) is used in this work to avoid substrate effects and ensure that there is only an interface effect from the gelatin film. The gelatin A macroscopic hydrogels are dual-crosslinked with controlled physical (from triple-helices of gelatin chains) and chemical (from EDC/NHS coupling) crosslinks. In terms of molecular structure of the hydrogel networks, the molecular weight between both physical and chemical crosslinks, is calculated by using the phantom network model. Fully immersed underwater adhesion in 4 M NaCl and 30% urea solutions as well as the contact time dependence of the work of adhesion shows that hydrogen bonding and electrostatic interactions additively contribute to interface interactions between gelatins. The independent effect of physical and chemical crosslinks is studied by modifying the experimental temperature, showing an opposite influence of the shear modulus on adhesion: the work of adhesion increases with physical crosslinking density but decreases with chemical crosslinking density. The effect of the physical crosslinks appears to be mainly to increase the areal density of interactions while the effect of the chemical network can be well predicted by Chaudhury's model based on a change in the spring constant. Finally, the collective contributions of both physical and chemical networks in dual-crosslinked gels are studied, showing that the underwater adhesion performance mainly depends on the gelatin volume fraction in the gel, while the existence of chemical network only slightly influences the work of adhesion. This work provides a strategy to render macroscopic gelatin hydrogels more thermo-stable while maintaining the underwater adhesion, by an additional chemical network.

References

1. Liu, Y.; Guan, G.; Li, Y.; Tan, J.; Cheng, P.; Yang, M.; Li, B.; Wang, Q.; Zhong, W.; Mequanint, K.; Zhu, C.; Xing, M., Gelation of highly entangled hydrophobic macromolecular fluid for ultrastrong underwater in situ fast tissue adhesion. *Science Advances* **2022,** *8* (20), eabm9744.

2. Wijetunge, S. S.; Wen, J.; Yeh, C.-K.; Sun, Y., Wheat germ agglutinin liposomes with surface grafted cyclodextrins as bioadhesive dual-drug delivery nanocarriers to treat oral cells. *Colloids and Surfaces B: Biointerfaces* **2020,** *185*, 110572.

3. Chen, Y.; Cheng, W.; Teng, L.; Jin, M.; Lu, B.; Ren, L.; Wang, Y., Graphene Oxide Hybrid Supramolecular Hydrogels with Self-Healable, Bioadhesive and Stimuli-Responsive Properties and Drug Delivery Application. *Macromolecular Materials and Engineering* **2018,** *303* (8), 1700660.

4. Islam, M. S.; Reineke, J.; Kaushik, R.; Woyengo, T.; Baride, A.; Alqahtani, M. S.; Perumal, O., Bioadhesive Food Protein Nanoparticles as Pediatric Oral Drug Delivery System. *ACS Applied Materials & Interfaces* **2019,** *11* (20), 18062-18073.

5. Zhou, J.; Wu, Y.; Zhang, X.; Lai, J.; Li, Y.; Xing, J.; Teng, L.; Chen, J., Enzyme Catalyzed Hydrogel as Versatile Bioadhesive for Tissue Wound Hemostasis, Bonding, and Continuous Repair. *Biomacromolecules* **2021,** *22* (4), 1346-1356.

6. Wu, S. J.; Yuk, H.; Wu, J.; Nabzdyk, C. S.; Zhao, X., A Multifunctional Origami Patch for Minimally Invasive Tissue Sealing. *Advanced Materials* **2021,** *33* (11), 2007667.

7. Chen, X.; Yuk, H.; Wu, J.; Nabzdyk, C. S.; Zhao, X., Instant tough bioadhesive with triggerable benign detachment. *Proceedings of the National Academy of Sciences* **2020,** *117* (27), 15497-15503.

8. Deng, J.; Yuk, H.; Wu, J.; Varela, C. E.; Chen, X.; Roche, E. T.; Guo, C. F.; Zhao, X., Electrical bioadhesive interface for bioelectronics. *Nature Materials* **2021,** *20* (2), 229-236.

9. Sani, E. S.; Kheirkhah, A.; Rana, D.; Sun, Z.; Foulsham, W.; Sheikhi, A.; Khademhosseini, A.; Dana, R.; Annabi, N., Sutureless repair of corneal injuries using naturally derived bioadhesive hydrogels. *Science Advances* **2019,** *5* (3), eaav1281.

10. Wang, X.; Sun, X.; Gan, D.; Soubrier, M.; Chiang, H.-Y.; Yan, L.; Li, Y.; Li, J.; Yu, S.; Xia, Y.; Wang, K.; Qin, Q.; Jiang, X.; Han, L.; Pan, T.; Xie, C.; Lu, X., Bioadhesive and

conductive hydrogel-integrated brain-machine interfaces for conformal and immune-evasive contact with brain tissue. *Matter* **2022,** *5* (4), 1204-1223.

11. Wirthl, D.; Pichler, R.; Drack, M.; Kettlguber, G.; Moser, R.; Gerstmayr, R.; Hartmann, F.; Bradt, E.; Kaltseis, R.; Siket, C. M.; Schausberger, S. E.; Hild, S.; Bauer, S.; Kaltenbrunner, M., Instant tough bonding of hydrogels for soft machines and electronics. *Science Advances* **2017,** *3* (6), e1700053.

12. Kim, D. W.; Baik, S.; Min, H.; Chun, S.; Lee, H. J.; Kim, K. H.; Lee, J. Y.; Pang, C., Highly Permeable Skin Patch with Conductive Hierarchical Architectures Inspired by Amphibians and Octopi for Omnidirectionally Enhanced Wet Adhesion. *Advanced Functional Materials* **2019,** *29* (13), 1807614.

13. Min, H.; Baik, S.; Kim, J.; Lee, J.; Bok, B.-G.; Song, J. H.; Kim, M.-S.; Pang, C., Tough Carbon Nanotube-Implanted Bioinspired Three-Dimensional Electrical Adhesive for Isotropically Stretchable Water-Repellent Bioelectronics. *Advanced Functional Materials* **2022,** *32* (8), 2107285.

14. Hofman, A. H.; van Hees, I. A.; Yang, J.; Kamperman, M., Bioinspired Underwater Adhesives by Using the Supramolecular Toolbox. *Advanced Materials* **2018,** *30* (19), 1704640.

15. Fan, H.; Gong, J. P., Bioinspired Underwater Adhesives. *Advanced Materials* **2021,** *33* (44), 2102983.

16. Cui, C.; Liu, W., Recent advances in wet adhesives: Adhesion mechanism, design principle and applications. *Progress in Polymer Science* **2021,** *116*, 101388.

17. Stewart, R. J.; Weaver, J. C.; Morse, D. E.; Waite, J. H., The tube cement of Phragmatopoma californica: a solid foam. *Journal of Experimental Biology* **2004,** *207* (26), 4727-4734.

18. Waite, J. H., Mussel adhesion – essential footwork. *Journal of Experimental Biology* **2017,** *220* (4), 517-530.

19. Stevens, M. J.; Steren, R. E.; Hlady, V.; Stewart, R. J., Multiscale Structure of the Underwater Adhesive of Phragmatopoma Californica: a Nanostructured Latex with a Steep Microporosity Gradient. *Langmuir* **2007,** *23* (9), 5045-5049.

20. Priemel, T.; Palia, G.; Förste, F.; Jehle, F.; Sviben, S.; Mantouvalou, I.; Zaslansky, P.; Bertinetti, L.; Harrington, M. J., Microfluidic-like fabrication of metal ion–cured bioadhesives by mussels. *Science* **2021,** *374* (6564), 206-211.

21. Qureshi, D. A.; Goffredo, S.; Kim, Y.; Han, Y.; Guo, M.; Ryu, S.; Qin, Z., Why mussel byssal plaques are tiny yet strong in attachment. *Matter* **2022,** *5* (2), 710-724.

22. Yuk, H.; Zhang, T.; Lin, S.; Parada, G. A.; Zhao, X., Tough bonding of hydrogels to diverse non-porous surfaces. *Nature Materials* **2016,** *15* (2), 190-196.

23. Baik, S.; Kim, D. W.; Park, Y.; Lee, T.-J.; Ho Bhang, S.; Pang, C., A wet-tolerant adhesive patch inspired by protuberances in suction cups of octopi. *Nature* **2017,** *546* (7658), 396-400.

24. Li, J.; Celiz, A. D.; Yang, J.; Yang, Q.; Wamala, I.; Whyte, W.; Seo, B. R.; Vasilyev, N. V.; Vlassak, J. J.; Suo, Z.; Mooney, D. J., Tough adhesives for diverse wet surfaces. *Science* **2017,** *357* (6349), 378-381.

25. Dompé, M.; Cedano-Serrano, F. J.; Heckert, O.; van den Heuvel, N.; van der Gucht, J.; Tran, Y.; Hourdet, D.; Creton, C.; Kamperman, M., Thermoresponsive Complex Coacervate-Based Underwater Adhesive. *Advanced Materials* **2019,** *31* (21), 1808179.

26. Dompé, M.; Cedano-Serrano, F. J.; Vahdati, M.; Sidoli, U.; Heckert, O.; Synytska, A.; Hourdet, D.; Creton, C.; van der Gucht, J.; Kodger, T.; Kamperman, M., Tuning the Interactions in Multiresponsive Complex Coacervate-Based Underwater Adhesives. *International Journal of Molecular Sciences* **2020,** *21* (1), 100.

27. Dompé, M.; Cedano-Serrano, F. J.; Vahdati, M.; van Westerveld, L.; Hourdet, D.; Creton, C.; van der Gucht, J.; Kodger, T.; Kamperman, M., Underwater Adhesion of Multiresponsive Complex Coacervates. *Advanced Materials Interfaces* **2020,** *7* (4), 1901785.

28. van Hees, I. A.; Hofman, A. H.; Dompé, M.; van der Gucht, J.; Kamperman, M., Temperature-responsive polyelectrolyte complexes for bio-inspired underwater adhesives. *European Polymer Journal* **2020,** *141*, 110034.

29. Sudre, G.; Olanier, L.; Tran, Y.; Hourdet, D.; Creton, C., Reversible adhesion between a hydrogel and a polymer brush. *Soft Matter* **2012,** *8* (31), 8184-8193.

30. Macron, J.; Bresson, B.; Tran, Y.; Hourdet, D.; Creton, C., Equilibrium and Out-of-Equilibrium Adherence of Hydrogels against Polymer Brushes. *Macromolecules* **2018,** *51* (19), 7556-7566.

31. Cedano-Serrano, F. J.; Sidoli, U.; Synytska, A.; Tran, Y.; Hourdet, D.; Creton, C., From Molecular Electrostatic Interactions and Hydrogel Architecture to Macroscopic Underwater Adherence. *Macromolecules* **2019,** *52* (10), 3852-3862.

32. Chollet, B.; D'Eramo, L.; Martwong, E.; Li, M.; Macron, J.; Mai, T. Q.; Tabeling, P.; Tran, Y., Tailoring Patterns of Surface-Attached Multiresponsive Polymer Networks. *ACS Applied Materials & Interfaces* **2016,** *8* (37), 24870-24879.

33. Chollet, B.; Li, M.; Martwong, E.; Bresson, B.; Fretigny, C.; Tabeling, P.; Tran, Y., Multiscale Surface-Attached Hydrogel Thin Films with Tailored Architecture. *ACS Applied Materials & Interfaces* **2016,** *8* (18), 11729-11738.

34. Li, M.; Bresson, B.; Cousin, F.; Fretigny, C.; Tran, Y., Submicrometric Films of Surface-Attached Polymer Network with Temperature-Responsive Properties. *Langmuir* **2015,** *31* (42), 11516-11524.

35. Creton, C.; Ciccotti, M., Fracture and adhesion of soft materials: a review. *Reports on Progress in Physics* **2016,** *79* (4), 046601.

36. Harrington, W. F.; Von Hippel, P. H., The Structure Of Collagen And Gelatin. In *Advances in Protein Chemistry*, Anfinsen, C. B.; Anson, M. L.; Bailey, K.; Edsall, J. T., Eds. Academic Press: 1962; Vol. 16, pp 1-138.

37. Tabata, Y.; Ikada, Y., Protein release from gelatin matrices. *Advanced Drug Delivery Reviews* **1998,** *31* (3), 287-301.

38. Chaudhury, M. K., Rate-Dependent Fracture at Adhesive Interface. *The Journal of Physical Chemistry B* **1999,** *103* (31), 6562-6566.

39. Smoluchowski, M. V., *Handbuch der Elektrizität und des Magnetismus*. Barth, Leipzig, 1921; Vol. 2.

40. Cedano-Serrano, F. J. From molecular architecture and electrostatic interactions to underwater adherence of hydrogels. PhD Thesis, Sorbonne Université, 2019.

41. Rubinstein, M.; Colby, R. H., *Polymer Physics*. Oxford university press: New York, 2003; Vol. 23.

42. Narita, T.; Mayumi, K.; Ducouret, G.; Hébraud, P., Viscoelastic Properties of Poly(vinyl alcohol) Hydrogels Having Permanent and Transient Cross-Links Studied by Microrheology, Classical Rheometry, and Dynamic Light Scattering. *Macromolecules* **2013,** *46* (10), 4174-4183.

43. Zhao, J.; Mayumi, K.; Creton, C.; Narita, T., Rheological properties of tough hydrogels based on an associating polymer with permanent and transient crosslinks: Effects of crosslinking density. *Journal of Rheology* **2017,** *61* (6), 1371-1383.

44. Kuijpers, A. J.; Engbers, G. H. M.; Feijen, J.; De Smedt, S. C.; Meyvis, T. K. L.; Demeester, J.; Krijgsveld, J.; Zaat, S. A. J.; Dankert, J., Characterization of the Network Structure of Carbodiimide Cross-Linked Gelatin Gels. *Macromolecules* **1999,** *32* (10), 3325-3333.

45. Jacobasch, H.-J., Characterization of solid surfaces by electrokinetic measurements. *Progress in Organic Coatings* **1989,** *17* (2), 115-133.

46. Kinraide, T. B., Use of a Gouy-Chapman-Stern Model for Membrane-Surface Electrical Potential to Interpret Some Features of Mineral Rhizotoxicity. *Plant Physiology* **1994,** *106* (4), 1583-1592.

47. Dai, X.; Zhang, Y.; Gao, L.; Bai, T.; Wang, W.; Cui, Y.; Liu, W., A Mechanically Strong, Highly Stable, Thermoplastic, and Self-Healable Supramolecular Polymer Hydrogel. *Advanced Materials* **2015,** *27* (23), 3566-3571.

48. Israelachvili, J. N., *Intermolecular and Surface Forces*. Academic Press: 2011.

Supporting Information

Titration of GA and GB, formation of GA hydrogel dual crosslinks followed by linear rheology, heating process of GA gels followed by DSC, molecular weight between chemical and physical crosslinks, underwater adhesion under different contact time, calculation of chemical crosslinking efficiency, ene-to-end distance between crosslinks, calculation of molecular weight of "monomer" of gelatins, and the reversibility of underwater adhesion.

Supporting Information

Molecular Mechanisms of Underwater Adhesion of Gelatins

Potentiometric titration of free amino groups of gelatin A and B

In order to quantify the negative and positive charges in gelatin, the titration of gelatin solution was carried out to determine the concentration of carboxylic acid and amine groups on polymer chains (both type A and type B). The titration was performed at 40 °C with a gelatin solution of 8 wt%, by a titrant solution of NaOH (1M). The starting pH of the gelatin solution was 5.5 and then 2.5 mL HCl solution of 1 M was added to decrease the pH to 1.6. Afterwards, the titration started and the pH was measured after each adding of 0.1 mL NaOH, until reaching a stable pH around 12. The titration curves for GA and GB are shown in **Figure S1a** and the slopes of pH change ($m=\Delta pH/\Delta V_{NaOH}$) over the volume of added NaOH in **Figure S1b**. Three characteristic peaks can be distinguished for both gelatins. After the titration of excess HCl, at the first peak, the titration of carboxyl groups starts and ends at the second peak. Therefore, taking into account the moisture percentage in gelatin (~ 11 wt%), the carboxyl groups in gelatin A were calculated to be 0.77 mmol g^{-1} and gelatin B were 1.01 mmol g^{-1}. Additionally, the third peak corresponds to the titration of amino groups from the residues of histidine and lysine amino acids present in gelatin. The titration gives almost the same values for gelatins A and B with 0.39 and 0.37 mmol g^{-1}, respectively, in good agreement with values reported in the literature.[1] Moreover, as the positive charges must include the guanidine groups (pKa = 12.1) in the residues of the amino acid arginine which should be close to 0.5 mmol g^{-1} in both GA and GB,[2] this gives a total positive charges around 0.89 mmol g^{-1} for GA and 0.87 mmol g^{-1} for GB. The titration of GA and GB is a result taking from Cedano-Serrano.[3]

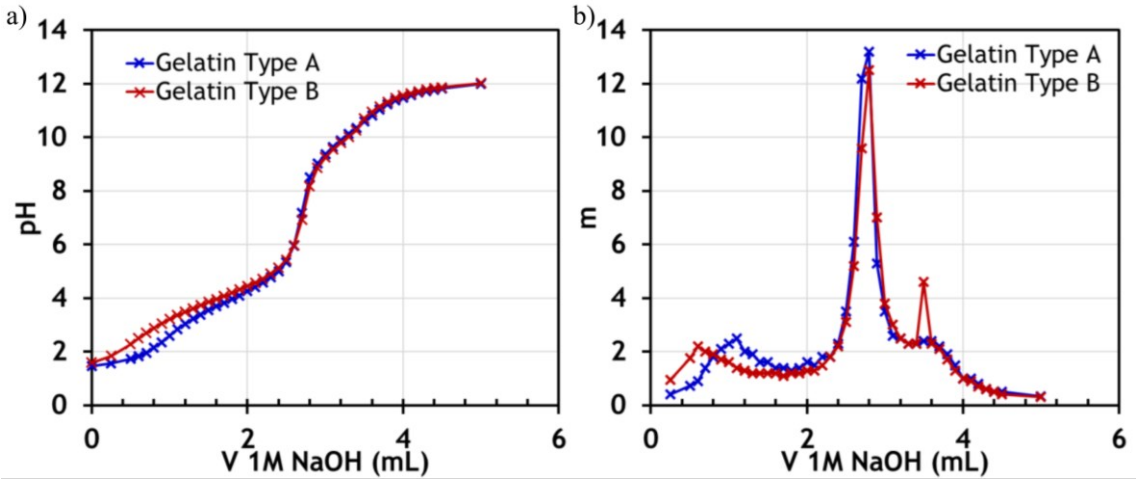

Figure S14. a) Titration curves of gelatin type A and gelatin type B. b) Change of pH as function of added solution of NaOH (1 M). The Figure is from Cedano-Serrano.[3]

Furthermore, **Figure S2** shows the total amount of carboxyl and amino groups as function of pH for GA and GB. This figure shows the isoelectric point for both gelatins when the curve of $[NH_x^+]$ (which was the same for both gelatins) crosses the curve of $[COO^-]$. Therefore, the pI for GA was calculated to be at pH ~9 and for GB was calculated to be at a pH of ~ 5.

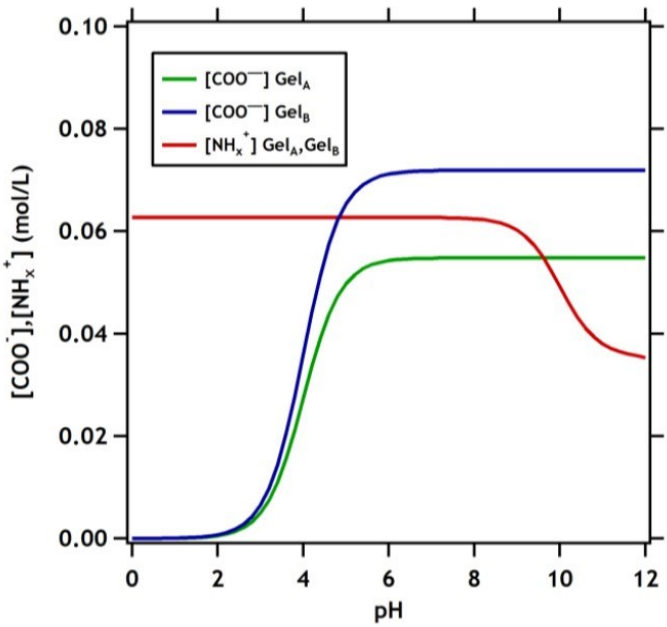

Figure S15. Concentration of total carboxyl and amino groups for gelatin type A and type B. The Figure is from Cedano-Serrano.[3]

Dual-crosslinked formation of GA hydrogel followed by linear rheology

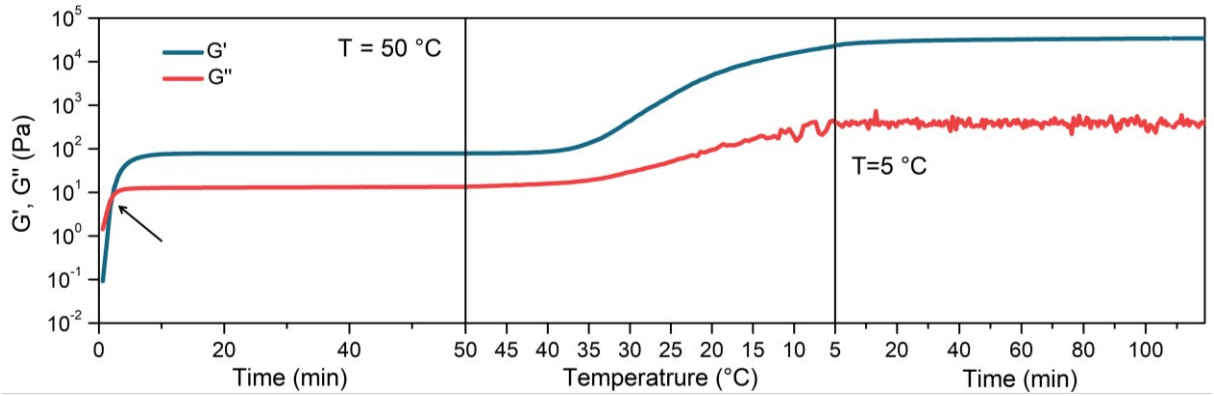

Figure S16. Change in G' and G'' of GA15R2 during synthesis and temperature sweep.

Formation history of triple-helices in GA hydrogels followed by DSC

When GA hydrogels are stored in a fridge at 4 °C after synthesis, triple-helices can continue to form. This generally leads to poor reproducibility of endotherms during the melting process and higher enthalpies compared to gelation on cooling (**Figure 5** and **Figure S4**), because the samples had different and uncontrolled experiences. In order to get a quantitative overview of the impact of crosslinking on physical gelation, all the samples were initially equilibrated in 55 °C to remove the story of their conditioning and the cooling process was well-controlled with temperature range (55 to 5 °C) and rate (1 °C min^{-1}), to set the conditions for the formation of triple-helices.

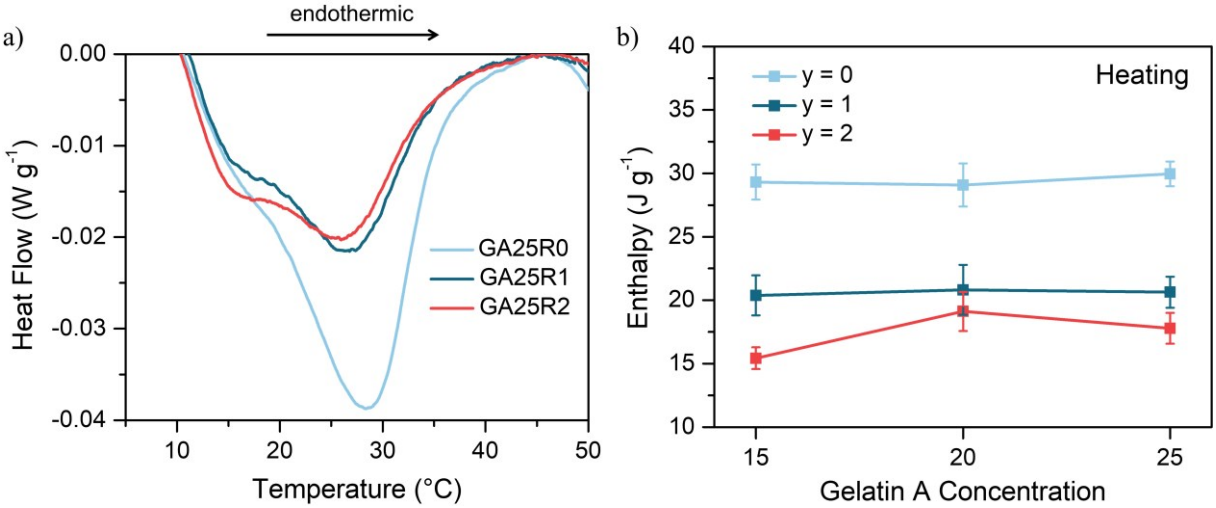

Figure S17. DSC on as-prepared GAxRy gels following heating process. a) Thermogram. b) Enthalpy calculated by the area under thermogram.

Molecular weight between chemical and physical crosslinks (M_{ch} and M_{ph})

M_{ch} and M_{ph} were calculated from viscoelastic experiments using **Equation 4** and **5**. From these results, their contributions to shear modulus at 5 °C (G_{ch} and G_{ph}) were also calculated (**Table S1**).

Table S1. Molecular weights between chemical and physical crosslinks of GA hydrogels and their contributions to shear modulus (as-prepared state) at 5 °C.

Gel Name	M_{ch} (kg mol^{-1})	G_{ch} (Pa)	M_{ph} (kg mol^{-1})	G_{ph} (Pa)
GA15R0	/	/	7.3	31800
GA15R1	2726	63	8.5	27200
GA15R2	141	1229	9.0	25900
GA20R0	/	/	6.1	50400
GA20R1	347	666	6.9	44700
GA20R2	66	3508	8.3	36900
GA20R2.5	36	3631	11.8	19700
GA20R3	30	4382	12.9	18000
GA25R0	/	/	6.1	63000
GA25R1	240	1204	6.8	57000
GA25R2	41	7058	8.2	47000

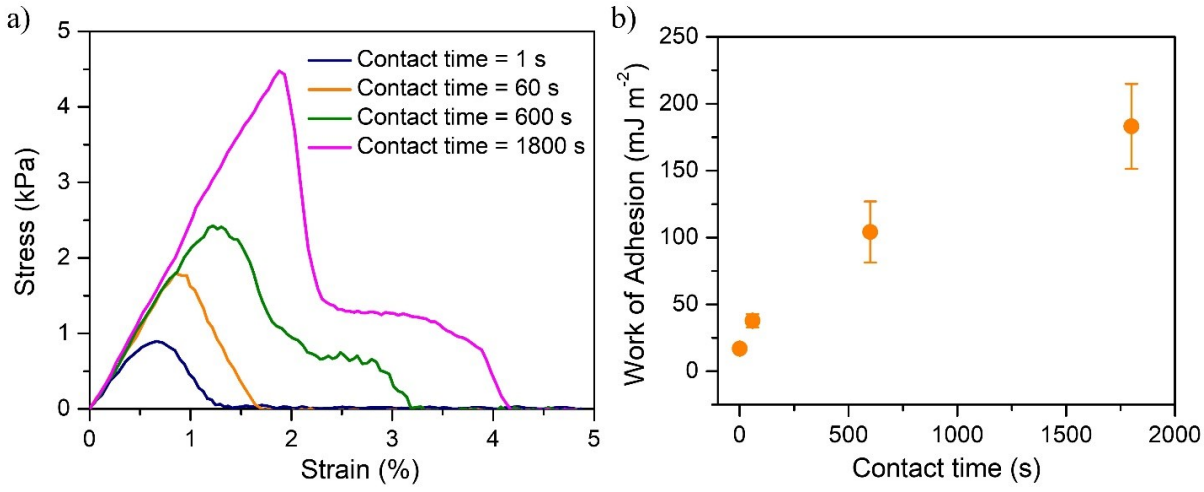

Figure S18. Underwater adhesion of GA20R2 gels under different contact time. a) Representative stress-strain curves of adhesion. b) Work of adhesion. The temperature was fixed at 4 °C and the gels were in equilibrated state.

Calculation of efficiency of chemical crosslinks (E_{cross})

The Gelatin A hydrogels is crosslinked by EDC and NHS (1:1 in molar), which serve together as crosslinking reagents to link amino and carboxyl groups. 1 unit of effective EDC/NHS generates 1 unit of crosslinking points, but not all the EDC and NHS crosslink the polymer chains. Therefore, the efficiency of crosslinking (E_{cross}) is introduced in this work, which is the ratio of EDC/NHS that participate in the crosslink over their total amount. E_{cross} is calculated as

$$E_{cross} = \frac{n_{cross}}{n_{100\%-cross}} \tag{S1}$$

where n_{cross} is the number of crosslinks in the network, $n_{100\%-cross}$ is the number of crosslinks when all the EDC/NHS participate in the crosslinking. Assuming that the EDC/NHS only crosslink gelatin intermolecularly, the n_{cross} could be calculated as

$$n_{cross} = \frac{N_{monomer}}{N_c} \tag{S2}$$

where N_c is the number of "monomers" between crosslinks, which is calculated in Equation 14. $N_{monomer}$ is the number of "monomers" on a polymer chain, which is calculated as

$$N_{monomer} = \frac{M}{M_{monomer}} \tag{S3}$$

where M is the molecular weight of polymer, $M_{monomer}$ is the molecular weight of monomer.

On the other hand, if all the EDC/NHS participate in crosslinking, the the $n_{100\%-cross}$ is estimated by

$$n_{100\%-cross} = \frac{n_{EDC}}{n_{chain}} \tag{S4}$$

where n_{EDC} is the number of EDC. n_{chain} is the number of polymer chains which is

$$n_{chain} = \frac{m}{M} \tag{S5}$$

where m the weight of polymer and M is the molecular weight of polymer (gelatin).

Finally, the efficiency of chemical crosslinking (E_{cross}) in the dual-crosslinked gelatin hydrogels is calculated by combining **Equation S1-S5**, as

$$E_{cross} = \frac{n_{cross}}{n_{100\%-cross}} = \frac{m}{M_{ch} \cdot n_{EDC}} \quad \text{(S6)}$$

The E_{cross} of GA hydrogels with varied gelatin concentration and EDC/NH_2 ratio (y) is shown in **Figure S6**, indicating that the crosslinking efficiency increases with the increase in gelatin concentration and EDC/NH_2 ratio.

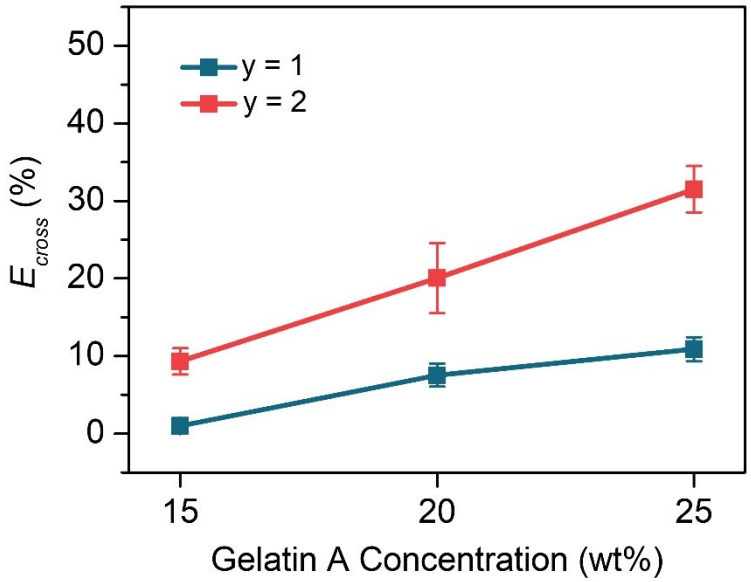

Figure S19. Chemical crosslinking efficiency (E_{cross}) of GA hydrogels. The gelatin concentration is in as-preparation state.

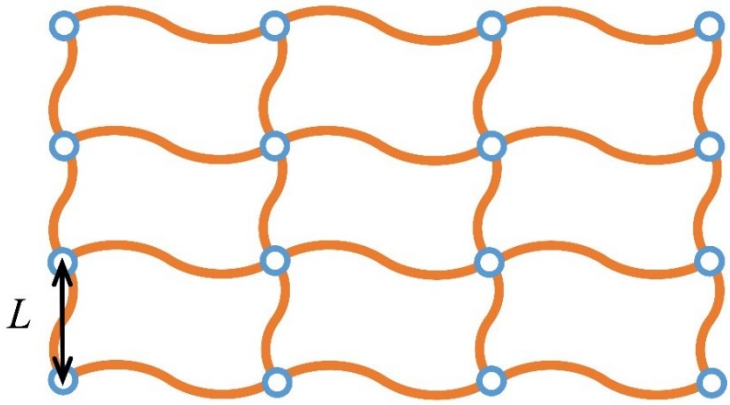

Figure S20. Illustration of end-to-end distance between chemical crosslinks

Calculation of molecular weight of "monomer" of gelatins

Comparing with typical synthetic polymers, "monomers" in gelatin chains are not identical, but different types of amino acids are connected by peptide bonds. So the "monomer" was assumed to be amino acid and the molecular weight was calculated to be an average value. The molecular weight (M_{amino}) and weight fraction (w_{amino}) of each amino acid in gelatin type A from pork skin and gelatin type B from calf skin are shown in **Table S2**. The average molecular weight of "monomer" in gelatin ($M_{monomer}$) was estimated to be the weighted average molecular weight of amino acids of gelatin, which is calculated as follows by the summation of contributions from each amino acid.

$$M_{monomer} = \sum (w_{amino} \cdot M_{amino}) \quad (S7)$$

Taking account of the range of w_{amino}, $M_{monomer}$ of GA and GB was calculated to be 132.29-147.48 g mol^{-1} and 133.59-144.64 g mol^{-1}, respectively. In this work, the average values of each were used as the $M_{monomer}$, which were 139.88 g mol^{-1} for GA and 139.11 g mol^{-1} for GB.

Table S2. Amino acids in Gelatins type A and type B. The molecular weight (M_{amino}) and weight fraction (w_{amino}) of each amino acid in GA (from pork skin) and GB (from calf skin).[4]

Amino acid	M_{amino} (g mol^{-1})	w_{amino} in GA (wt%)	w_{amino} in GB (wt%)
Alanine	89.1	8.6-10.7	9.3-11
Arginine	174.2	8.3-9.1	8.55-8.8
Aspartic acid	133.1	6.2-6.7	6.6-6.9
Cystine	240.3	0.1	0
Glutamic acid	147.1	11.3-11.7	11.1-11.4
Glycine	75.1	26.4-30.5	26.9-27.5
Histidine	155.0	0.9-1	0.74-0.8
Hydroxylysine	162.0	1	0.91-1.2
Hydroxyproline	131.1	13.5	14-14.5
Isoleucine	131.2	1.4	1.7-1.8
Leucine	131.2	3.1-3.3	3.1-3.4
Lysine	146.0	4.1-5.2	4.5-4.6
Methionine	149.2	0.8-0.9	0.8-0.9
Phenylalanine	165.2	2.1-2.6	2.2-2.5
Proline	115.1	16.2-18	14.8-16.4
Serine	105.1	2.9-4.1	3.2-4.2
Threonine	119.1	2.2	2.2
Tyrosine	181.2	0.4-0.9	0.2-1
Valine	117.2	2.5-2.8	2.6-3.4

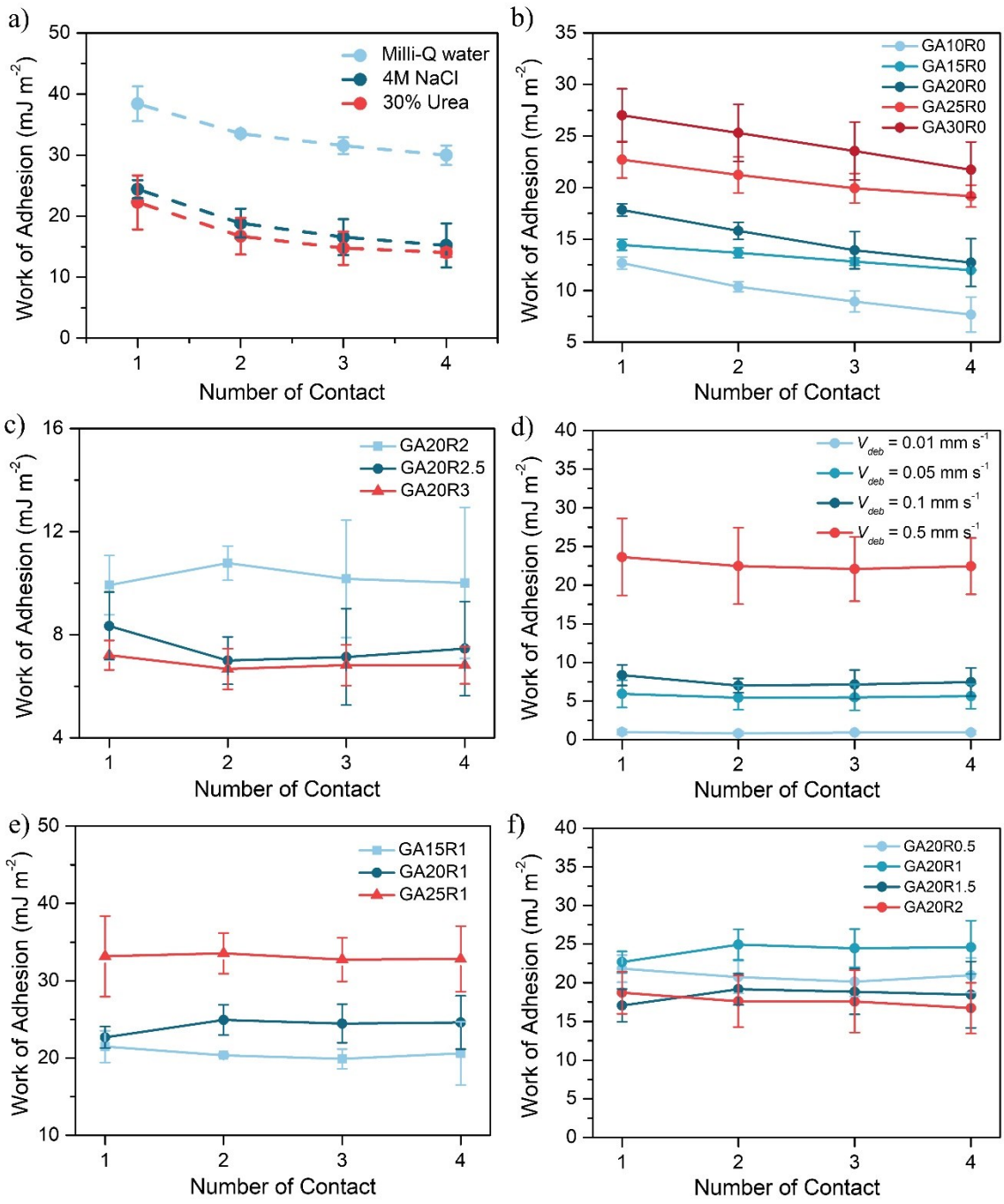

Figure S21. Reversibility of underwater adhesion. Change in work of adhesion with number of contact of: a) GA20R2 gels in Milli-Q water, 4 M NaCl and 30% urea solutions. b) physical gels GAxR0 (at 4 °C). c) Chemical gels GA20Ry (at 50 °C). d) Chemical gel GA20R2.5 (at 50 °C) with different debonding rates (V_{deb}). e) Dual-crosslinked gels GAxR1 (at 4 °C). f) Dual-crosslinked gels GA20Ry (at 4 °C).

References

1. Eastoe, J. E., The amino acid composition of mammalian collagen and gelatin. *Biochemical Journal* **1955,** *61* (4), 589-600.

2. Reinhard, S.; Herbert, G., From Collagen to Gelatine. In *Gelatine Handbook*, 2007; pp 45-117.

3. Cedano-Serrano, F. J. From molecular architecture and electrostatic interactions to underwater adherence of hydrogels. PhD Thesis, Sorbonne Université, 2019.

4. Gelatin Manufacturers Institute of America, *Gelatin Handbook*. 2012; Vol. 25.

Chapter 4

Reversible Underwater Adhesion between Tough Biopolymer Hydrogel and Surface Grafted with Hydrogel Microstructures

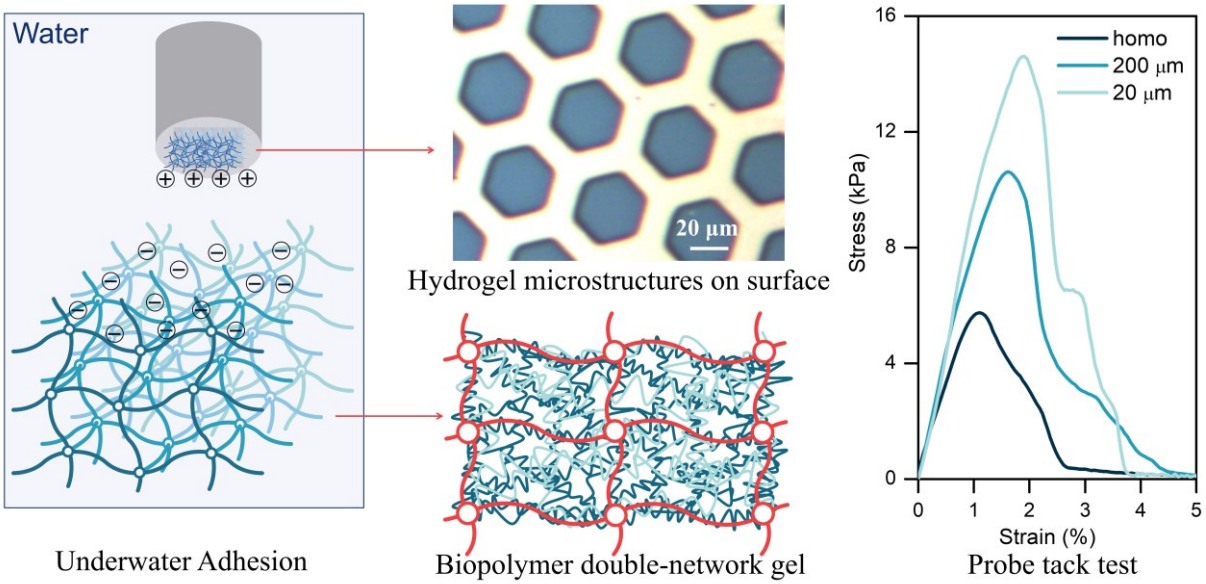

Abstract

We report reversible underwater adhesion between a biopolymer-based hydrogel double-network and a surface grafted with hydrogel microstructures. This study with two model systems designed from biosourced and biocompatible polymers allows to understand the mechanisms of underwater bioadhesion by separating the contributions of volume and surface to the adhesion, in particular by determining the effect of the surface topography on the adhesion properties. The molecular interactions are finely controlled by electrostatic complexations between the negatively charged adhesive and the positively charged surface. The adhesive is a tough double-network structure containing a physical network based on kappa-carrageenan and agarose biopolymers and a chemical network of poly(dimethylacrylamide). The surface is grafted with microscopic hexagonal poly(2-(dimethylamino)ethyl methacrylate) (PDMAEMA) hydrogel structures patterned by photolithography. The adhesive properties between the double-network and the surface are measured in water by a home-made experimental probe-tack device. The effects of topography (hexagonal structure size) and aqueous environment (pH and ionic strength) on the adhesion are investigated. The results show that the adhesion energy is much higher (more than 600 mJ m^{-2}) when the surface is grafted with small microstructures. It strongly decreases (ten times lower) when the electrostatic interactions between the adhesive and the surface are screened in physiological environment.

Résumé

Nous reportons l'adhésion réversible en milieux immergés aqueux entre un double-réseau d'hydrogels à base de biopolymères et une surface greffée de microstructures d'hydrogels. Cette étude avec deux systèmes modèles conçus à partir de polymères biosourcés et biocompatibles permet de comprendre les mécanismes de bioadhésion immergée en séparant les contributions du volume et de la surface à l'adhésion, notamment en déterminant l'effet de la topographie de la surface sur les propriétés d'adhésion. Les interactions moléculaires sont finement contrôlées par des complexations électrostatiques entre l'adhésif de charge négative et la surface de charge positive. L'adhésif est une structure double-réseau robuste constituée d'un réseau physique à base de biopolymères kappa-carraghénane et agarose et d'un réseau chimique de poly(diméthylacrylamide). La surface est greffée avec des structures hexagonales microscopiques d'hydrogel de poly(2-(diméthylamino)méthacrylate d'éthyle) (PDMAEMA) modelées par photolithographie. Les propriétés adhésives entre le double-réseau et la surface sont mesurées dans l'eau par un dispositif expérimental de probe-tack fait maison. Nous avons étudié les effets de la topographie (taille des motifs hexagonaux) et de l'environnement aqueux (pH et force ionique) sur l'adhésion. Les résultats montrent que l'énergie d'adhésion est beaucoup plus élevée (plus de 600 mJ m^{-2}) quand la surface est greffée avec des microstructures de petite taille. Elle diminue fortement (dix fois plus faible) quand les interactions électrostatiques entre l'adhésif et la surface sont écrantées en milieu physiologique.

Table of Contents

Chapter 4. Reversible Underwater Adhesion between Tough Biopolymer Hydrogel and Surface Grafted with Hydrogel Microstructures

1 Introduction

Adhesion in aqueous environment has significant applications in underwater sensors,[1-3] marine industry,[4-6] biomedical applications,[7-9] *etc*.[10] The main challenge comes from the interfacial water between surface and adhesive, leading to poor interfacial contact and bond failure.[11-13] Inspired by bioadhesion from marine creatures, one of the solutions to overcome this general challenge is to modify the microstructure of adhesive surfaces. For example, Pang and coworkers developed an underwater adhesive with some dome-like protuberances on the surface, to mimic the suction cups of octopus.[14] By an applied preload, the interfacial water was trapped in the upper chamber, which made the lower part serve as vacuum chamber by minimizing the volume of trapped air in it.[14-15] Since the stresses create at the interface did not rely on any molecular interactions, this adhesive showed a strong adhesion to various substrates and under different conditions, such as dry, moist, underwater and even oil environments. Furthermore, inspired by the structure of clingfish adhesion disc, Gong and coworkers designed a patterned hydrogel with hexagonal facets and grooves on the surface.[16] The grooves can rapidly drain water during the contact and delay crack propagation during the detachment. The underwater adhesion energy reached ~10 J m^{-2}, which is over 30 times of the flat gels without any patterns.

There are obviously significant contributions of surface microstructure on adhesion, but since the surface and cohesion effects are always coupled,[17] there is still a lack of study about the individual contribution of the surface microscopic structure and topography. The model system developed in our team can be used here to separately address the effects of surface adhesion and the bulk cohesion.[18] One material is a hydrogel thin film (~ hundred nm) attached on a solid substrate with controlled chemistry and topography, providing surface property. The other material is a macroscopic hydrogel with controlled viscoelastic properties. The model system has already been used to study the effect of bulk cohesion on reversible underwater adhesion using synthetic hydrogels.[19-20] In this work, a further study of surface is designed to understand surface topography effect on adhesion using biosourced and biocompatible hydrogels.

In this work, we have studied underwater adhesion of a tough biopolymer hydrogel with double-network (DN) structure on a surface grafted with hydrogel micropatterns (**Figure 1a**). The adhesive is a macroscopic double-network containing a first hydrogel with physical crosslinks made with *kappa*-carrageenan and agarose biopolymers physically crosslinked and

a second polyacrylamide (PAAm) network chemically crosslinked (the chemical structures are shown in **Figure 1b**). The DN hydrogels are synthesized by two steps of polymerizing the second network inside the first single network (SN) hydrogel (**Figure 1c**). The hydrogel micropatterns grafted on substrate are constructed by photolithography, based on CLAG (Cross-Linking and Grafting) strategy using UV-initiated thiol-ene click reaction (**Figure 1d**). Depending on the pH, electrostatic interactions can take place between positively-charged thin films and negatively-charged hydrogels, taking into account that the pKa of PDMAEMA and the sulphate groups of *kappa*-carrageenan are about 7.8[21] and 2.8, respectively. The patterns mimic the microscopic structure of substrates or biosurfaces such as the polygonal epithelial cells of tree frogs.[22-26] The biopolymer DN hydrogels mimic the high mechanical properties of biotissues. The effect of the surface patterns on adhesion energy is studied, providing inspirations for designing surface microstructures to improve underwater adhesion.

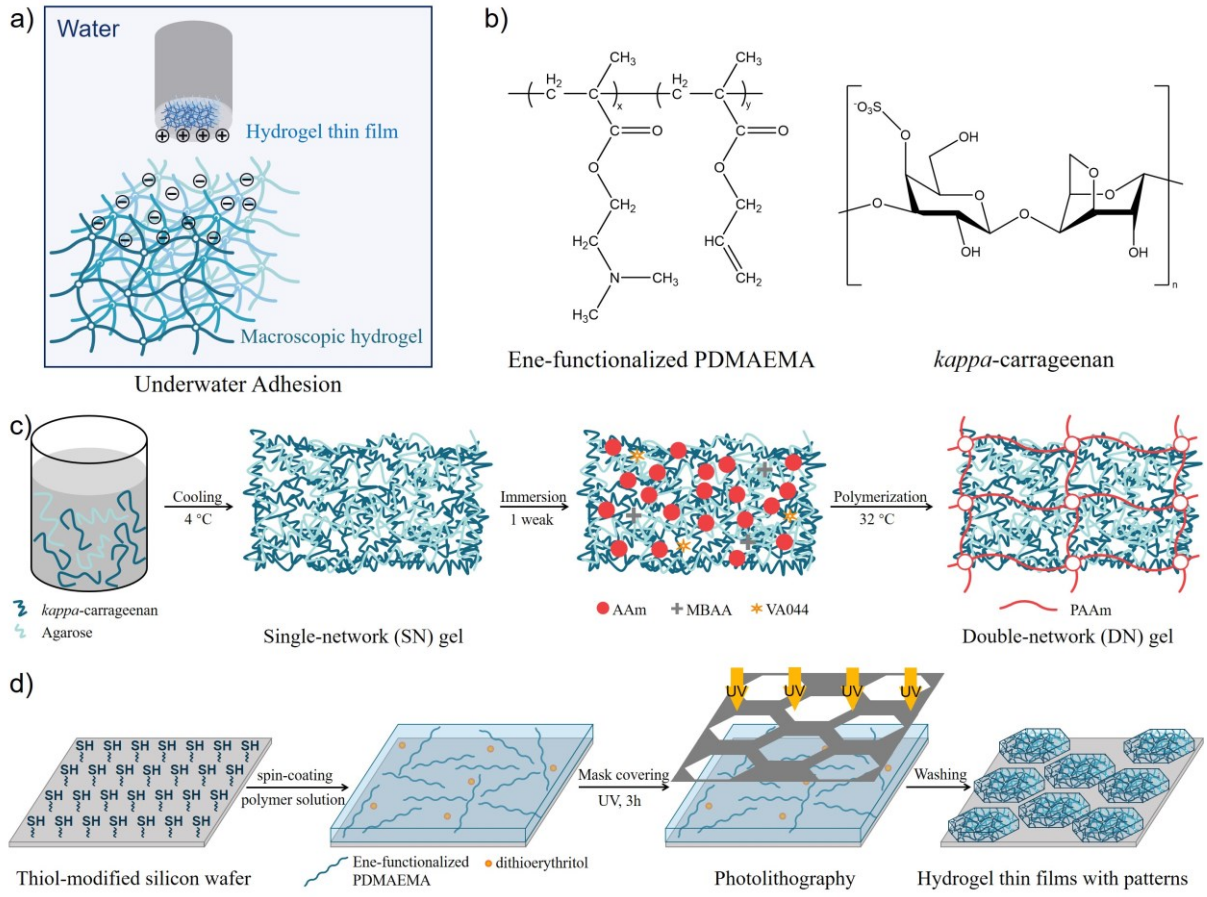

Figure 1. Illustration of the model system for underwater adhesion study. a) The model system contains a surface grafted with PDMAEMA hydrogel micro-patterns and a macroscopic

double-network hydrogel based on *kappa*-carrageenan and agarose. b) The chemical structure of ene-functionalized PDMAEMA (x = 96.7% and y = 3.3% shown in **Figure S1**, **Supporting Information**) and *kappa*-carrageenan. c) Synthesis of DN biopolymer hydrogels. The SN gel is made as a composite hydrogel by mixing *kappa*-carrageenan and agarose. Then the DN is obtained by polymerizing the second network inside SN hydrogel, with acrylamide (AAm) as monomer, *N,N'*-methylenebisacrylamide (MBAA) as crosslinker, and 2,2'-azobis[2-(2-imidazolin-2-yl)propane] dihydrochloride (VA044) as initiator. d) Fabrication of hydrogel patterns as thin film on solid substrate. Ene-functionalized PDMAEMA and dithioerythritol crosslinkers are spin-coated onto a thiol-modified silicon wafer, after which the hexagonal patterns are constructed by UV irradiation to activate thiol-ene click reaction.

2 Results and Discussion

2.1 Structure and physical chemistry of biocompatible hydrogel micropatterns

The surface-attached PDMAEMA hydrogel thin films are synthesized by Cross-Linking and Grafting (CLAG) method using thiol-ene click chemistry (**Figure 1b** and **Figure S1, Supporting Information**). This strategy has been discussed in our previous works.[27-29] The ene-functionalized PDMAEMA mixed with dithioerythritol crosslinkers is spin-coated onto a thiol-modified silicon wafer. Then the simultaneous crosslinking and grafting take place by heating or UV irradiation, through thiol-ene click reaction between both polymer-polymer and polymer-substrate, generating hydrogel thin films. The surface-attached hydrogel film can swell stably underwater thanks to the covalent grafting and crosslinking. This chemical and mechanical stability ensured by covalent bonds is essential for the study of reversible adhesion with double-network macroscopic hydrogels.

The dry thickness in air (Th_{dry}) and the wet thickness in water (Th_{wet}) of surface-attached PDMAEMA hydrogel films are measured by ellipsometry. The swelling ratio of films is calculated as $SR = Th_{wet}/Th_{dry}$. From the swelling ratio, the volume fraction of monomer can be deduced as $1/SR$ and can be compared to that of double-network macroscopic hydrogels.

The hydrogel patterns can be constructed by photolithography using UV irradiation to activate the thiol-ene reaction (**Figure 1d**). The structure of the patterns is determined by the pre-designed photomasks (**Figure S2**, **Supporting Information**). In this work, both patterned

and homogeneous hydrogel films are made by UV irradiation for 3 h (**Figure S3**, **Supporting Information**), with and without masks respectively. The dry thickness (Th_{dry}) for patterned and homogeneous films is fixed around 100 nm to avoid the surface effect. The volume fraction of monomer of the PDMAEMA hydrogel in water is similar to that of double-network macroscopic hydrogels (**Figure S4**, **Supporting Information**). The homogeneous film without patterns is named as "homo", while the films with hexagonal patterns are named as "hex 200 μm" for $l = d = 200$ μm and "hex 20 μm" for $l = d = 20$ μm (**Figure 2a**).

As seen from the photos in **Figure 2a-c**, the architecture of the hexagon patterns for both hex 200 μm and hex 20 μm is well-controlled with a distinct boundary. The thickness and swelling of patterns are studied by atomic force microscopy (AFM), by measuring the height difference between the hexagonal region and substrate (**Figure 2e and d**). As shown in **Table S1** (**Supporting Information**), the dry thickness (Th_{dry}), wet thickness (Th_{wet}) and swelling ratio (SR) of homo and hex 200 μm are compared. The dry thickness and swelling ratio of homogeneous and patterned films are very close to ~ 110 nm and ~ 5.0, proving that CLAG method is not disturbed by the use of masks.

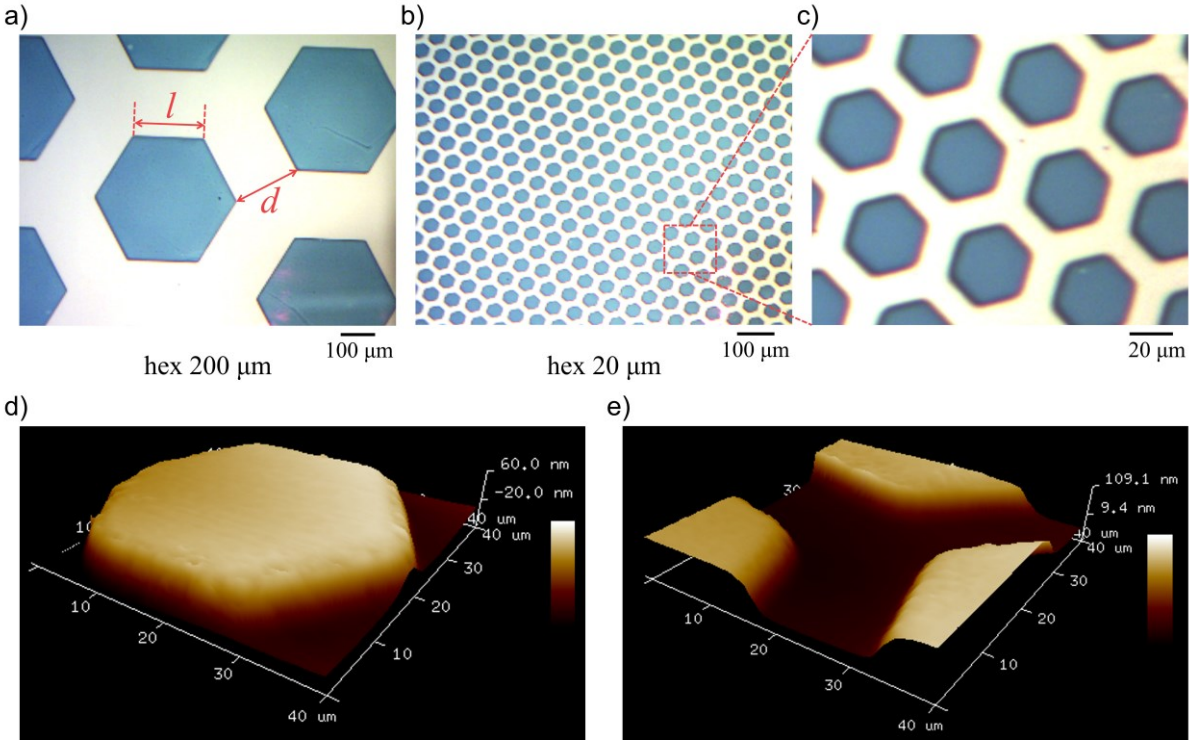

Figure 2. Hexagonal patterns on hydrogel thin films. Photos of a) hex 200 μm, b) hex 20 μm, and c) Zoom-in of hex 20 μm. The blue hexagons in photos are PDMAEMA hydrogel thin films and the white part is substrate without polymers. The hexagon has controlled side length (l) and

distance (*d*). AFM image on hex 20 μm hydrogel patterns of d) one hexagon and e) the gap between hexagons, which is the substrate. The thickness of film is determined by the height difference between the hexagon and substrate.

2.2 Design, synthesis and mechanical properties of biosourced DN hydrogels

The macroscopic hydrogel with double-network structure is synthesized using biopolymers in order to mimic tough biotissues and bioadhesives. As shown in **Figure 1d**, the DN gels are synthesized *via* two steps, by which the second network is polymerized inside the first network. In the DN gels, the first network with physical crosslinks is a mixture of *kappa*-carrageenan and agarose, while the second network is a chemical (but loosely) crosslinked PAAm. In the first network, *kappa*-carrageenan containing sulphate groups provides negative charges and agarose limits the swelling of SN gels for improving mechanical properties. The second network, PAAm is polymerized inside the SN to form a double-network structure, using VA044 as initiator (working at 32 °C) to polymerize below the melting temperature of the SN gels.

The mechanical properties of DN gels are studied by uniaxial tensile test. As shown in **Figure 3a**, there is a significant improvement of the mechanical properties of the hydrogels from SN to DN, by the adding of a second network, which is consistent with double-network hydrogels reported in other works.[30-33] The Young's modulus (*E*) increases from 138 kPa to 228, 296 and 349 kPa with the increase in concentration of *kappa*-carrageenan from 10 mg ml^{-1} to 20, 30 and 40 mg ml^{-1}, showing a high strength and good mechanical properties (**Figure 3b**). With the increase of the *kappa*-carrageenan concentration, the fracture stress ($\sigma_{fracture}$) increases and the fracture strain ($\varepsilon_{fracture}$) decreases (**Figure S5, Supporting Information**), indicating the formation of a denser crosslinking network. DN gels with 40 mg ml^{-1} *kappa*-carrageenan will be systematically used for reversible adhesion study thanks to their high strength; higher concentrations being limited by the solubility of *kappa*-carrageenan.

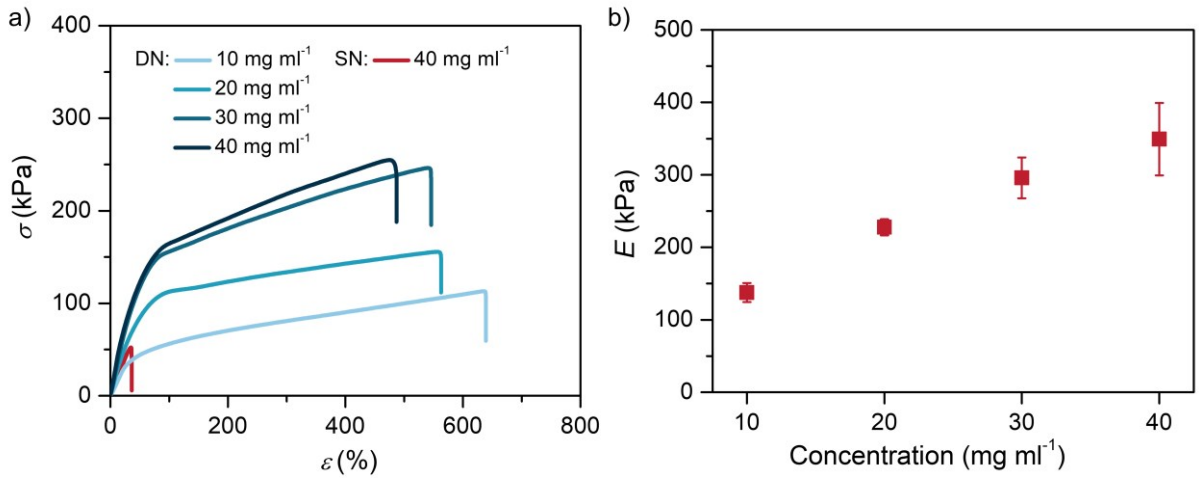

Figure 3. Tensile test of single-network and double-network hydrogels with different *kappa*-carrageenan concentrations. a) Representative stress-strain curves of SN (red) and DN (blue) gels. b) Young's modulus (E) of DN hydrogel as a function of *kappa*-carrageenan concentration. The agarose concentration is fixed at 10 mg ml^{-1} for all samples, the second network being synthesized using a fixed precursor of AAm with 2 M, MBAA and VA044 of 0.1 mol% of AAm. The concentration is the concentration of *kappa*-carrageenan.

2.3 Underwater adhesion between hydrogel patterns and DN hydrogels

Underwater adhesion between PDMAEMA microscopic hexagonal patterns and biopolymer double-network hydrogels is studied by probe tack test. Although the two materials are in microscopic and macroscopic scales, they have close equilibrium polymer volume fraction (ϕ_p): 20.5 vol% for the PDMAEMA patterns (**Figure S4c, Supporting Information**) and 13.3 vol% for the DN gels (**Figure S6**, Supporting Information). As the model system allows to separate the contribution of interface interactions and bulk cohesion to adhesion properties, the effect of surface topography on adhesion energy has been studied in this work, by varying the pattern size against the same DN gel. As shown in **Figure 4**, the adhesion of DN gel on surface grafted with micropatterns is much better than that with homogeneous films. The work of adhesion (W_a) of hex 200 μm and hex 20 μm reaches 437 and 659 mJ m^{-2}, respectively, while the W_a of homogeneous film without pattern is only 197 mJ m^{-2}. This result indicates that there is a significant improvement in adhesion after patterning the surface with periodical microscopic hexagons, although the actual surface area of patterned film is smaller than homogeneous one. Moreover, the adhesion increases with the decrease in pattern size. The first reason is that the patterning process not only generates periodical polymer hydrogels, but also forms interconnected channels with a width d (**Figure 2a**) and a height equal to the film thickness,

which could allow an efficient drainage of water during contact in aqueous environment.[16, 34] On the other hand, the well-arranged microscopic hydrogel arrays can limit the crack propagation during detachment of the interface, providing higher work of adhesion. The reversibility of adhesion is shown in **Figure S7a** (**Supporting Information**), indicating the work of adhesion drops after attachment-detachment. This is due to the strong adhesion that causes cohesion failure in the macroscopic gel, which remains on the top of the film and prevents reproducing a real interfacial contact as the first one.

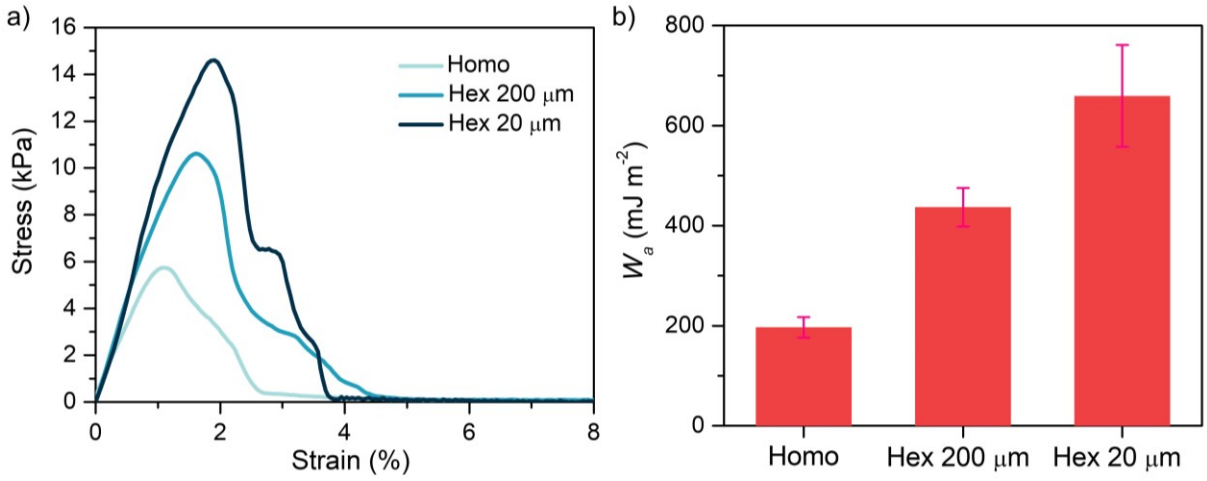

Figure 4. Underwater adhesion DN gels on surfaces grafted with PDMAEMA films and patterns in Milli-Q water. a) Representative stress-strain curves of adhesion. b) Work of adhesion (W_a) for different structures on surface. The contact stress is 5 kPa. Both the PDMAEMA and macroscopic DN hydrogels are in equilibrium state.

2.4 Underwater adhesion controlled by pH, ionic strength and temperature

The underwater adhesion can also be controlled by changing the pH, ionic strength and temperature by adjusting the charge density (**Figure 5**). As electrostatic interactions are the driving force of the model system used to study underwater adhesion, pH and ionic strength are the key parameters to control the adhesive properties. As shown in **Figure 5a**, these electrostatic interactions are active in the pH range between the pKa of PDMAEMA and *kappa*-carrageenan hydrogels, which are 7.8 and 2.8, respectively. Therefore, comparing with work of adhesion in Milli-Q water (387 mJ m^{-2}), there is a dramatic decrease of the work of adhesion in both acidic and basic conditions, pH 2 (53 mJ m^{-2}) and pH 9 (56 mJ m^{-2}), as the charge density decreases a lot. In PBS, the collective effect of pH and ionic strength leads to a work of adhesion of 66 mJ m^{-2}. Morevover, there is a higher decrease of adhesion in physiological conditions (PBS 37 °C)

into 24 mJ m^{-2} because of the additional thermo-responsiveness of *kappa*-carrageenan and agarose that changes the viscoelasticity of DN gels.

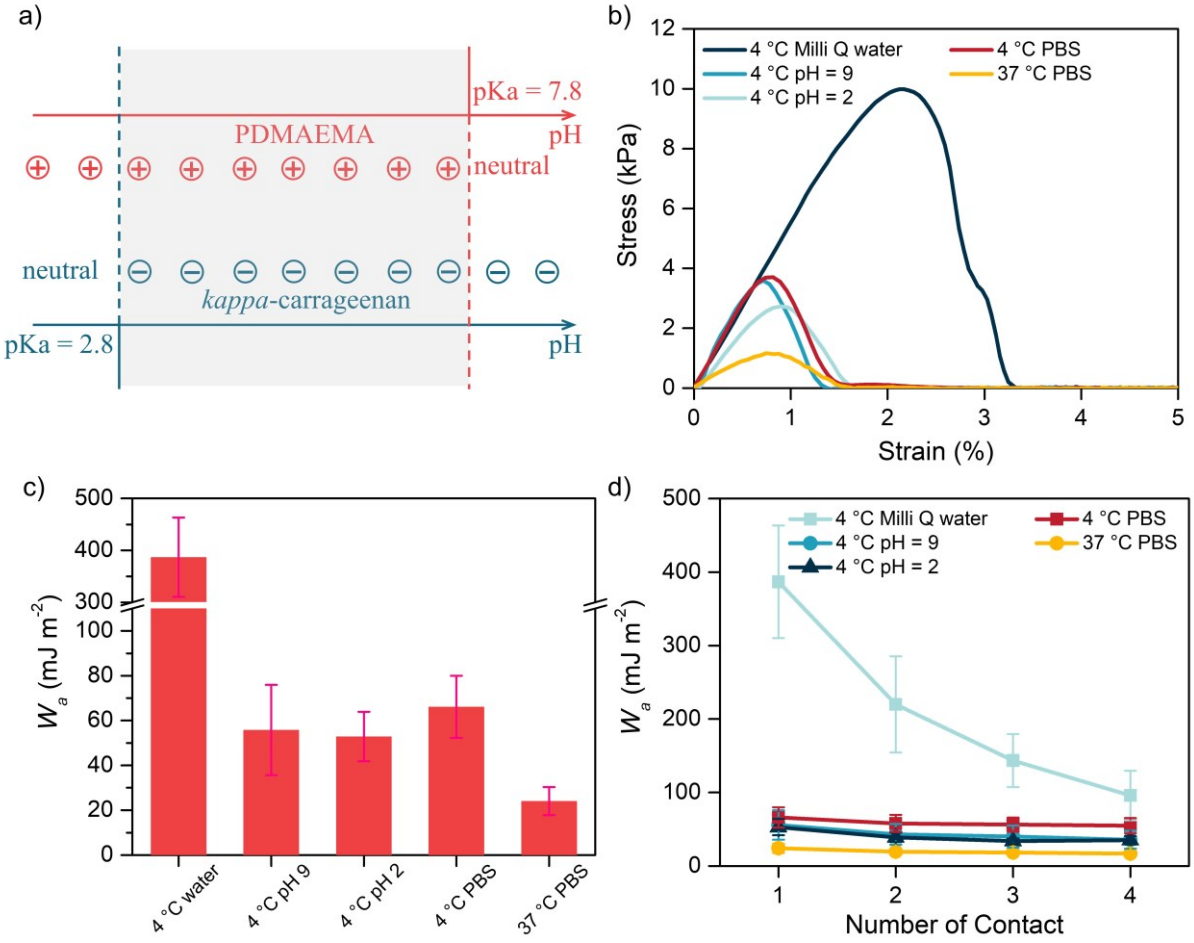

Figure 5. Underwater adhesion of hex 20 µm PDMAEMA patterns and DN gels in various pH, ionic strength and temperature. a) Schematics of charge density of PDMAEMA and carrageenan hydrogels as a function of pH. b) Stress-strain curves of adhesion tests for different aqueous conditions. c) Work of adhesion (W_a) deduced from stress-strain curves for different aqueous conditions. d) Work of adhesion as a function of number of contact for different aqueous conditions. The contact stress is 3 kPa. All PDMAEMA and DN hydrogels are at equilibrium state.

3 Conclusion

Reversible underwater adhesion between a biopolymer-based hydrogel double-network and a surface grafted with hydrogel microstructures was investigated. This study with two model systems designed from biosourced and biocompatible polymers allows to separate the

contributions of interfacial interaction and bulk cohesion to the adherence properties. The effect of the surface topography was focused and the electrostatic complexation between the adhesive and the surface was on the adhesion properties. A patterned surface with periodical arrays of surface-attached hydrogels with well-controlled structure and physical chemistry was fabricated. The underwater adhesion against a tough biopolymer hydrogel was measured, showing that the size of the pattern has a significant effect on work of adhesion. The adhesion energy on 20 μm-size hexagonal microstructures is twice higher than that on hexagonal microstructures of 200 μm-size microstructures and three times higher than that on homogeneous film (without patterns). This could be due to the formation of water drainage tunnels during underwater contact and the prevention of crack propagation within each hexagon pattern during debonding of interface. Furthermore, the adhesion could be controlled by pH, ionic strength and temperature. This work provides significant inspirations for designing strong underwater adhesion considering the topography of the adhesives surface.

4 Experimental Section

4.1 Materials

2-(Dimethylamino)ethyl methacrylate (DMAEMA), allyl methacrylate (AMA), 2,2'-azobis(2-methylpropionitrile) (AIBN), *N,N*-dimethylformamide (DMF), 3-mercaptopropyltrimethoxysilane (95%), toluene (≥99.5%), dithioerythritol, agarose, acrylamide (AAm), *N,N'*-methylenebisacrylamide (MBAA), 2,2'-azobis[2-(2-imidazolin-2-yl)propane] dihydrochloride (VA044) and phosphate buffer saline (PBS) tablets were purchased from Sigma-Aldrich. *Kappa*-carrageenan was a gift from Cargill. Silicon wafers were purchased from Neyco. Milli-Q water (Millipore) was used for all experiments. The DMAEMA and AMA monomers were purified prior to use by passing through the basic alumina column to remove inhibitors. Other chemicals were used without any further purifications.

4.2 Synthesis of ene-functionalized PDMAEMA

The ene-functionalized PDMAEMA was synthesized by free radical polymerization of DMAEMA and AMA in organic solvent using AIBN as thermal radical initiator. 10 g of DMAEMA, 0.422 g of AMA and 0.033 g of AIBN were mixed in 50 g of DMF. After being

deoxygenated by nitrogen bubbling of 1 h, the solution was put in pre-heated oil bath at 70°C. The reaction was carried out at 70°C under nitrogen for 24 h. The final solution was purified by dialysis using Milli-Q water, to remove impurities and displace DMF by water. After a dialysis of at least 7 days, the ene-functionalized PDMAEMA was obtained by freeze drying.

4.3 Thiol-modification of silicon wafers

Thiol-modification of silicon wafers was performed by silanization using 3-mercaptopropyltrimethoxysilane. The silicon wafers were cleaned by O_2/O_3 inside UV ozone (PSD Pro Series·Digital UV Ozone System Novascan) before being immersed in a solution of anhydrous toluene with 5 vol% of 3-mercaptopropyltrimethoxysilane under nitrogen for 3 h. They were then rinsed in toluene in ultrasonic bath before being dried under nitrogen flow.

4.4 Synthesis of PDMAEMA hydrogel thin films and micropatterns

The synthesis of hydrogel thin films followed the CLAG strategy which has been developed in our group.[27-29] A DMF solution containing ene-functionalized PDMAEMA and excess of dithioerythritol crosslinkers (50 wt% of ene-functionalized PDMAEMA) was spin-coated onto thiol-modified silicon wafers, with spin speed of 5000 rpm during 60 s. The thiol-ene reaction was then initiated by UV irradiation (16 W, wavelength of 254 nm) to obtain surface-grafted patterned hydrogels using quartz photomasks or homogeneous films without mask (**Figure 1c**). The irradiation time for both homogeneous and patterned films for adhesion studies was kept at 3 h. Finally, after being washed by water under ultrasonic bath to remove unreacted components, surface-attached hydrogel thin films and micropatterns were obtained.

4.5 Thickness of PDMAEMA hydrogels

Ellipsometry. The thickness of homogeneous hydrogel thin films on silicon wafers was measured using spectroscopic ellipsometer (UVISEL, Horiba). The angle of incidence was fixed at 60°, with a wavelength range from 400 nm to 800 nm. To determine the dry thickness (Th_{dry}) of gelatin film, the refractive index (n_i) of silicon substrate and gelatin was fixed to 3.87 and 1.50, respectively. In order to measure the wet thickness (Th_{wet}), *in situ* underwater

measurements were performed using a liquid cell, with thin glass walls fixed perpendicularly to the light path. The gelatin film was modeled as a single layer, with a constant refractive index between that of water (n_i = 1.33) and of the polymer. Moreover, the swelling ratio of hydrogel films (*SR*) was calculated as Th_{wet}/Th_{dry}, assuming that the polymer amount kept the same before and after being immersed underwater, since the hydrogel film was covalently attached to the substrate and the free polymer chains were considered to be removed by washing in hot water. The volume fraction of gelatins in swollen state was calculated by $\phi_p = 1/SR$. The temperature, pH and ionic strength within the liquid cell were controlled to allow the measurements in different conditions.

AFM. The thickness of hydrogel patterns was measured by atomic force microscopy (AFM), which was performed on an ICON microscope equipped with a Nanoscope V controller (Bruker), ContAl-G tip (Budget Sensors) and in contact mode in both air and water conditions. The working conditions were the following: force constant of 0.2 N m^{-1}, a scan rate of 1 Hz, 256 points/line and a typical scan size ranging from 20 to 40 μm. The contact mode was used with a setpoint deflection of 60 nm and a typical force of 10 nN. The thickness of the film was determined by the height difference between the polymer surface and the surface substrate.

4.6 Synthesis of double-network hydrogels

The double network (DN) hydrogel was synthesized by polymerizing the second network inside the first network *via* two steps (**Figure 1d**). The first network (single network, SN) was formed by cooling an aqueous solution of *kappa*-carrageenan and agarose mixture, which was dissolved in water at 70 °C overnight and then transferred in to a glass mold of 1.5 mm thickness. The concentration of *kappa*-carrageenan varied from 10 to 40 mg ml^{-1}, while the agarose was always fixed at 10 mg ml^{-1} in this work. After being cooled at 4 °C for 24 h, the SN gel was immersed inside the precursor solution of the second network, which contains monomer (AAm of 2 M), crosslinker (MBAA of 0.1 mol% of AAm) and initiator (VA044 of 0.1 mol% of AAm), for at least one week. Then the second network was polymerized and loosely crosslinked by putting the gel at 32 °C for 10 hours, before which the surface of gel was dried to remove excess second network precursor. A DN hydrogel was thus obtained.

4.7 Tensile test of hydrogels

Uniaxial tensile test was performed on SN and DN hydrogel using an Instron device (model 5333, Instron®, France) fitted with a 100 N load cell in equilibrated state. The hydrogels were cut into dumbbell-shaped bars of 20 mm length and 2 mm width (thickness around 1.5 mm depending on the swelling ratio), with 10 mm of gauge length. The tensile rate was fixed at 1.0 mm s^{-1}. The engineering tensile stress (σ) and engineering tensile strain (ε) were recorded for the calculation of the ultimate tensile strength and elongation at break. The Young's modulus (E) was calculated as the slope of the stress-strain curve within the strain (ε) range from 5% to 10%. The toughness was calculated by integrating the area under the stress–strain curve. Three replicas were performed for each sample.

4.8 Underwater tack-test of DN hydrogels on surface grafted with hydrogel patterns

The underwater tack test was conducted on a home-made setup designed by Sudre et al. [18] In this work, all hydrogels were tested under equilibrated state in aqueous environments. Generally, the adhesion tests consisted in forming a parallel contact and detachment between a DN hydrogel (thickness ~ mm) and PDMAEMA hydrogel thin film (thickness ~ hundred nm), while both were fully immersed underwater. The 5 mm × 5 mm silicon wafer grafted with PDMAEMA hydrogel was glued with a cyanoacrylate adhesive (Loctite® 406, France) to a steel probe, which was fixed to a 10 N load cell and connected to a universal tensile machine (model 5333, Instron®, France). The sample of DN hydrogel (20 mm × 20 mm × 1 mm) was glued to a glass microscope slide with also the cyanoacrylate adhesive. The contact between the DN hydrogel and the PDMAEMA thin film was made underwater at an approaching rate of 100 μm s^{-1}. A preload of 5 or 3 kPa was applied for a given contact time which was fixed at 60 s. Finally, the probe was detached at a fixed debonding rate (V_{deb}) of 100 μm s^{-1} while recording the probe displacement and force. Another attachment-detachment with the same parameters was performed after waiting for 120 s underwater, with totally four cycles. From this experiment, the work of adhesion (W_a) could be calculated as follows:

$$W_a = T_0 \int_0^{\varepsilon_{max}} \sigma d\varepsilon \quad (1)$$

where ε was the nominal strain which was obtained by normalizing the displacement by the initial thickness of the bulk hydrogel (T_0). σ was the stress obtained by dividing the force by the contact area. Three replicates were conducted for each experiment.

References

1. Zhang, C.; Zhou, Y.; Han, H.; Zheng, H.; Xu, W.; Wang, Z., Dopamine-Triggered Hydrogels with High Transparency, Self-Adhesion, and Thermoresponse as Skinlike Sensors. *ACS Nano* **2021,** *15* (1), 1785-1794.

2. Drotlef, D.-M.; Amjadi, M.; Yunusa, M.; Sitti, M., Bioinspired Composite Microfibers for Skin Adhesion and Signal Amplification of Wearable Sensors. *Advanced Materials* **2017,** *29* (28), 1701353.

3. Wei, J.; Zheng, Y.; Chen, T., A fully hydrophobic ionogel enables highly efficient wearable underwater sensors and communicators. *Materials Horizons* **2021,** *8* (10), 2761-2770.

4. Corigliano, P.; Crupi, V.; Bertagna, S.; Marinò, A., Bio-Based Adhesives for Wooden Boatbuilding. *Journal of Marine Science and Engineering* **2021,** *9* (1), 28.

5. Li, X.; Deng, Y.; Lai, J.; Zhao, G.; Dong, S., Tough, Long-Term, Water-Resistant, and Underwater Adhesion of Low-Molecular-Weight Supramolecular Adhesives. *Journal of the American Chemical Society* **2020,** *142* (11), 5371-5379.

6. Yang, N.; Yuan, R.; You, D.; Zhang, Q.; Wang, J.; Xuan, H.; Ge, L., Gallol-based constant underwater coating adhesives for severe aqueous conditions. *Colloids and Surfaces A: Physicochemical and Engineering Aspects* **2022,** *634*, 127948.

7. Nam, S.; Mooney, D., Polymeric Tissue Adhesives. *Chemical Reviews* **2021,** *121* (18), 11336-11384.

8. Chen, X.; Yuk, H.; Wu, J.; Nabzdyk, C. S.; Zhao, X., Instant tough bioadhesive with triggerable benign detachment. *Proceedings of the National Academy of Sciences* **2020,** *117* (27), 15497-15503.

9. Wu, S. J.; Yuk, H.; Wu, J.; Nabzdyk, C. S.; Zhao, X., A Multifunctional Origami Patch for Minimally Invasive Tissue Sealing. *Advanced Materials* **2021,** *33* (11), 2007667.

10. Tian, Y.; Huang, X.; Cheng, Y.; Niu, Y.; Ma, J.; Zhao, Y.; Kou, X.; Ke, Q., Applications of adhesives in textiles: A review. *European Polymer Journal* **2022,** *167*, 111089.

11. Hofman, A. H.; van Hees, I. A.; Yang, J.; Kamperman, M., Bioinspired Underwater Adhesives by Using the Supramolecular Toolbox. *Advanced Materials* **2018,** *30* (19), 1704640.

12. Fan, H.; Gong, J. P., Bioinspired Underwater Adhesives. *Advanced Materials* **2021,** *33* (44), 2102983.

13. Cui, C.; Liu, W., Recent advances in wet adhesives: Adhesion mechanism, design principle and applications. *Progress in Polymer Science* **2021,** *116*, 101388.

14. Baik, S.; Kim, D. W.; Park, Y.; Lee, T.-J.; Ho Bhang, S.; Pang, C., A wet-tolerant adhesive patch inspired by protuberances in suction cups of octopi. *Nature* **2017,** *546* (7658), 396-400.

15. Wilker, J. J., How to suck like an octopus. *Nature* **2017,** *546* (7658), 358-359.

16. Rao, P.; Sun, T. L.; Chen, L.; Takahashi, R.; Shinohara, G.; Guo, H.; King, D. R.; Kurokawa, T.; Gong, J. P., Tough Hydrogels with Fast, Strong, and Reversible Underwater Adhesion Based on a Multiscale Design. *Advanced Materials* **2018,** *30* (32), 1801884.

17. Creton, C.; Ciccotti, M., Fracture and adhesion of soft materials: a review. *Reports on Progress in Physics* **2016,** *79* (4), 046601.

18. Sudre, G.; Olanier, L.; Tran, Y.; Hourdet, D.; Creton, C., Reversible adhesion between a hydrogel and a polymer brush. *Soft Matter* **2012,** *8* (31), 8184-8193.

19. Macron, J.; Bresson, B.; Tran, Y.; Hourdet, D.; Creton, C., Equilibrium and Out-of-Equilibrium Adherence of Hydrogels against Polymer Brushes. *Macromolecules* **2018,** *51* (19), 7556-7566.

20. Cedano-Serrano, F. J.; Sidoli, U.; Synytska, A.; Tran, Y.; Hourdet, D.; Creton, C., From Molecular Electrostatic Interactions and Hydrogel Architecture to Macroscopic Underwater Adherence. *Macromolecules* **2019,** *52* (10), 3852-3862.

21. Plamper, F. A.; Ruppel, M.; Schmalz, A.; Borisov, O.; Ballauff, M.; Müller, A. H. E., Tuning the Thermoresponsive Properties of Weak Polyelectrolytes: Aqueous Solutions of Star-Shaped and Linear Poly(N,N-dimethylaminoethyl Methacrylate). *Macromolecules* **2007,** *40* (23), 8361-8366.

22. Drotlef, D. M.; Appel, E.; Peisker, H.; Dening, K.; del Campo, A.; Gorb, S. N.; Barnes, W. J. P., Morphological studies of the toe pads of the rock frog, Staurois parvus (family: Ranidae) and their relevance to the development of new biomimetically inspired reversible adhesives. *Interface Focus* **2015,** *5* (1), 20140036.

23. Langowski, J. K. A.; Dodou, D.; Kamperman, M.; van Leeuwen, J. L., Tree frog attachment: mechanisms, challenges, and perspectives. *Frontiers in Zoology* **2018,** *15* (1), 32.

24. Scholz, I.; Barnes, W. J. P.; Smith, J. M.; Baumgartner, W., Ultrastructure and physical properties of an adhesive surface, the toe pad epithelium of the tree frog, Litoria caerulea White. *Journal of Experimental Biology* **2009,** *212* (2), 155-162.

25. Iturri, J.; Xue, L.; Kappl, M.; García-Fernández, L.; Barnes, W. J. P.; Butt, H.-J.; del Campo, A., Torrent Frog-Inspired Adhesives: Attachment to Flooded Surfaces. *Advanced Functional Materials* **2015,** *25* (10), 1499-1505.

26. Wang, X.; Tan, D.; Zhang, X.; Lei, Y.; Xue, L., Effective Elastic Modulus of Structured Adhesives: From Biology to Biomimetics. *Biomimetics* **2017,** *2* (3), 10.

27. Chollet, B.; Li, M.; Martwong, E.; Bresson, B.; Fretigny, C.; Tabeling, P.; Tran, Y., Multiscale Surface-Attached Hydrogel Thin Films with Tailored Architecture. *ACS Applied Materials & Interfaces* **2016,** *8* (18), 11729-11738.

28. Chollet, B.; D'Eramo, L.; Martwong, E.; Li, M.; Macron, J.; Mai, T. Q.; Tabeling, P.; Tran, Y., Tailoring Patterns of Surface-Attached Multiresponsive Polymer Networks. *ACS Applied Materials & Interfaces* **2016,** *8* (37), 24870-24879.

29. Li, M.; Bresson, B.; Cousin, F.; Fretigny, C.; Tran, Y., Submicrometric Films of Surface-Attached Polymer Network with Temperature-Responsive Properties. *Langmuir* **2015,** *31* (42), 11516-11524.

30. Gong, J. P.; Katsuyama, Y.; Kurokawa, T.; Osada, Y., Double-Network Hydrogels with Extremely High Mechanical Strength. *Advanced Materials* **2003,** *15* (14), 1155-1158.

31. Gong, J. P., Materials both Tough and Soft. *Science* **2014,** *344* (6180), 161-162.

32. Sun, J.-Y.; Zhao, X.; Illeperuma, W. R. K.; Chaudhuri, O.; Oh, K. H.; Mooney, D. J.; Vlassak, J. J.; Suo, Z., Highly stretchable and tough hydrogels. *Nature* **2012,** *489* (7414), 133-136.

33. Du, G.; Gao, G.; Hou, R.; Cheng, Y.; Chen, T.; Fu, J.; Fei, B., Tough and Fatigue Resistant Biomimetic Hydrogels of Interlaced Self-Assembled Conjugated Polymer Belts with a Polyelectrolyte Network. *Chemistry of Materials* **2014,** *26* (11), 3522-3529.

34. Chen, Y.; Meng, J.; Gu, Z.; Wan, X.; Jiang, L.; Wang, S., Bioinspired Multiscale Wet Adhesive Surfaces: Structures and Controlled Adhesion. *Advanced Functional Materials* **2020,** *30* (5), 1905287.

Supporting Information

The ^{1}H NMR spectrum of ene-functionalized PDMAEMA, the processing of photo masks, effect of UV irradiation time on PDMAEMA film, thickness, swelling and volume fraction of PDMAEMA film, tensile fracture stress ($\sigma_{fracture}$) and fracture strain ($\varepsilon_{fracture}$) of DN hydrogels, polymer fraction (ϕ_p) of DN hydrogels, and work of adhesion between films and DN hydrogels as a function of the number of contact.

Supporting Information

Reversible Underwater Adhesion between Tough Biopolymer Hydrogel and Surface Grafted with Hydrogel Microstructures

Chemical structure of ene-functionalized PDMAEMA

The ^{1}H NMR spectrum of ene-functionalized PDMAEMA is shown in **Figure S1**, which can be interpreted as follows:

^{1}H NMR (400 MHz, 25 °C, D_2O, δ = 4.46). δ = 0.60 (2*3H, -CH_2-C**H_3**-, c), δ = 2.00 (6H, C**H_3**-N-C**H_3**, d and h), δ = 2.41 (2H, O-CH_2-C**H_2**-, f), δ = 3.84 (2H, O-C**H_2**-CH_2-, e), δ = 4.46 (2H, O-C**H_2**-CH=CH_2, g), δ = 5.15 (2H, O-CH_2-CH=C**H_2**, b), δ = 5.72 (H, O-CH_2-C**H**=CH_2, a).

As shown in **Figure S1**, the peak at 5.6-5.8 ppm and 5.1-5.4 ppm correspond to the protons on the ene group marked as “a” and “b” respectively, while the peak at 3.3-4.2 ppm corresponds to secondary carbon marked as “e”. The ratio of ene groups is determined by comparing the integral of the peak, with x = 96.7% and y = 3.3%.

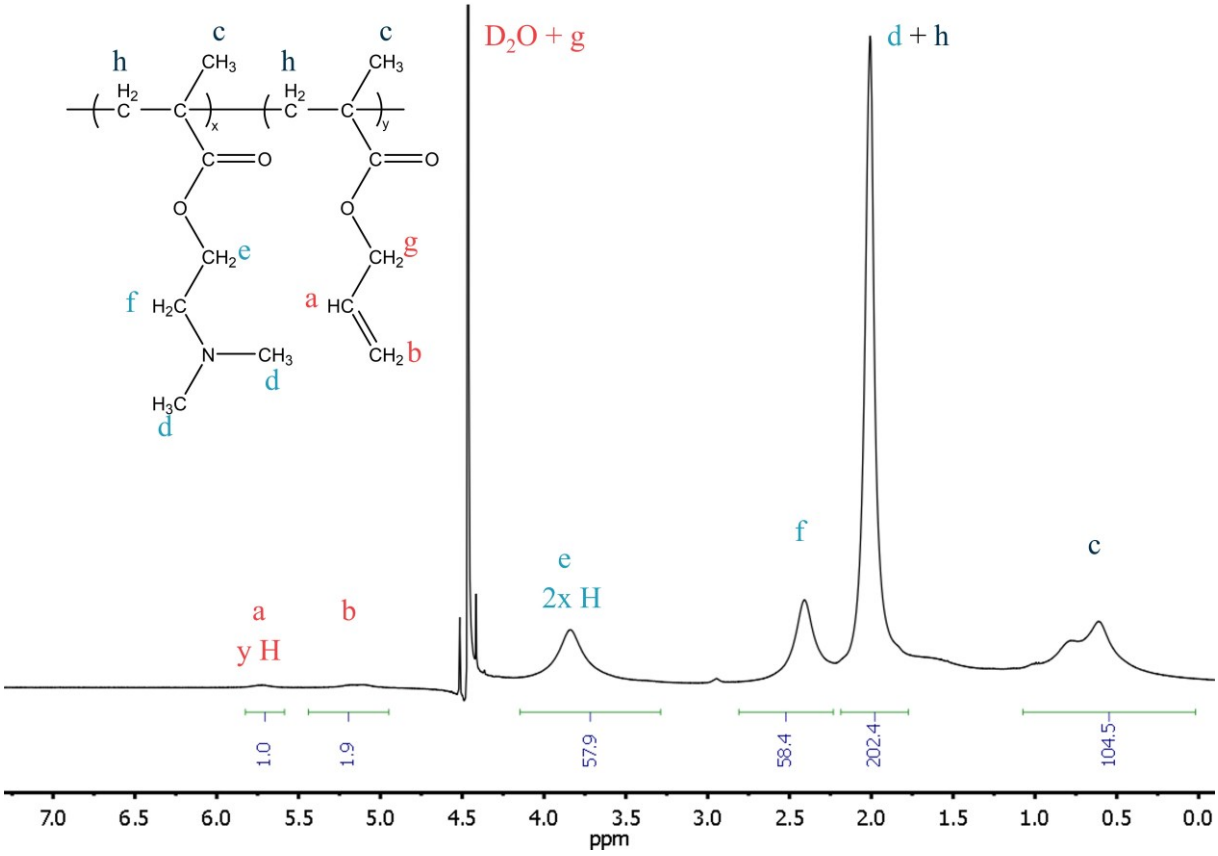

Figure S1. ^{1}H NMR spectrum of ene-functionalized PDMAEMA in D_2O.

Processing of making masks

The processing of photo masks is shown in **Figure S2**. The quartz masks were purchased as being coated with a chromium layer of thickness around 90 nm, above which there was a photoresist resin of 360 nm. The pattern for the defects was designed and drawn using Clewin Software. Then the laser was exposed only to the pre-designed area by using Heidelberg microPG. After the patterning, the mask was washed using an AZ 351 B developer, in which only the exposed resin was removed. The bare chromium layer, that appears once the resin has been removed, was then etched in an acid bath. Finally, after removing the remaining photoresist by acetone, the photomask of quartz covered by patterned chromium layer was obtained. Only the region without Cr coating can then allow the UV irradiation to pass.

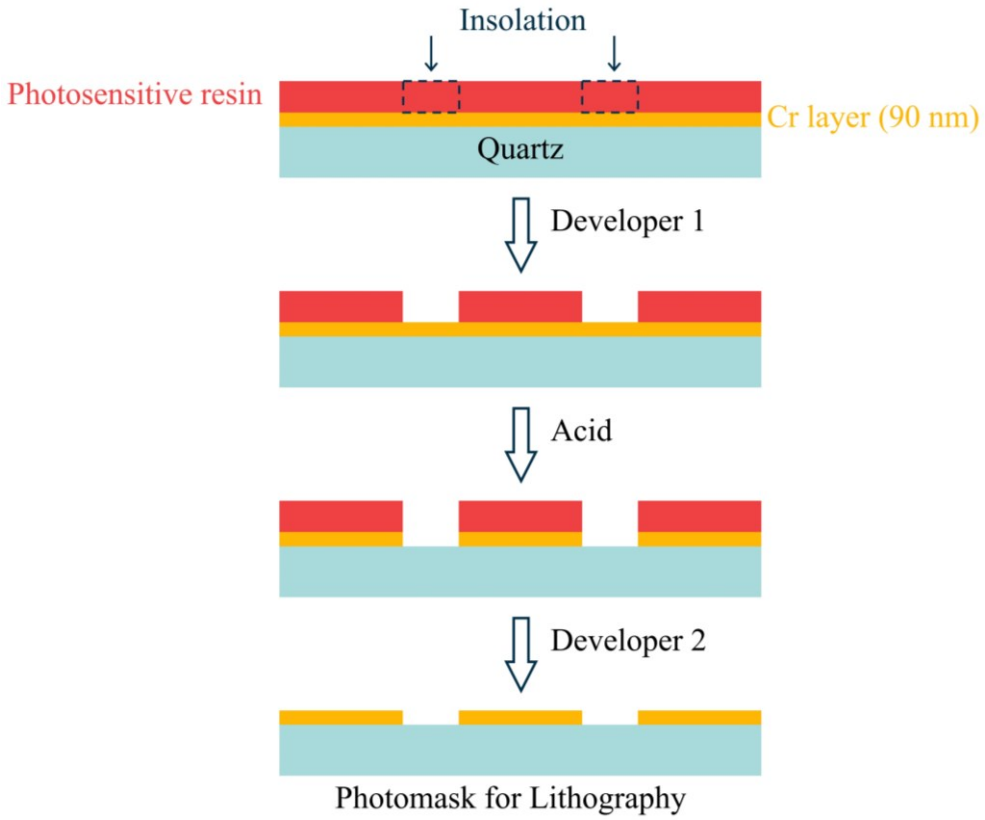

Figure S2. Processing of photomasks. Red and orange layer represent photosensitive resin and chromium layer. Cyan refers to quartz. UV with a wavelength of 254 nm can pass through the quartz but not through the Cr layer on the top of it.

Effect of UV irradiation time on PDMAEMA film

Surface-attached hydrogel films were synthesized by CLAG strategy under UV irradiation. In order to find a proper condition, homogeneous films (without patterns) irradiated for different time are compared. As shown in **Figure S3**, the color of silicon wafers after 2 h of irradiation is close to a bare wafer, indicating there is no or only a very thin polymer layer grafted during the first 2 hours. After 3 hours, a layer with blue color appears on the wafer, showing an effective grafting. The blue color due to Newton's interferences corresponds to the thickness of about 100 nm. However, with the increase in irradiation time, the films show loss of homogeneity accompanied by slight color change. The reason is probably due to the degradation of polymer under UV. The result indicates that when the irradiation time is too short, the grafted film will not be thick enough, but long irradiation time causes inhomogeneity. Finally, a 3-hours irradiation was set for the whole work.

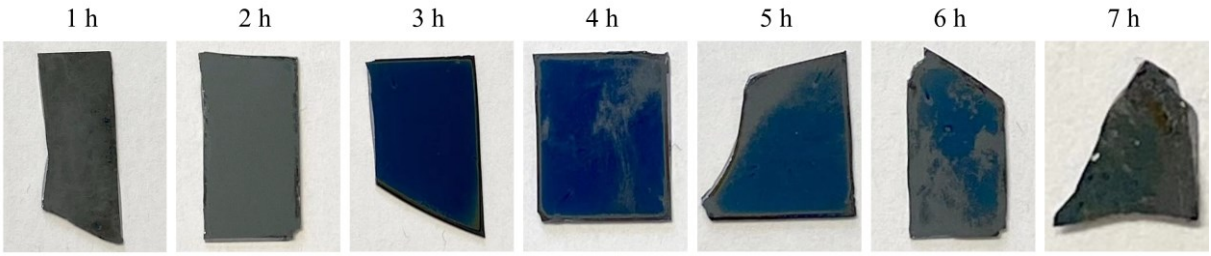

Figure S3. Photos of the PDMAEMA film after different UV irradiation time. All the samples are spin-coated by 70 mg ml^{-1} ene-functionalized PDMAEMA solution. After irradiation for a certain time, the films are washed during 2 min with water under ultrasonic bath.

Thickness, swelling and volume fraction of PDMAEMA film

Surface-attached PDMAEMA hydrogel films are synthesized on the top of silicon wafers by simultaneously crosslinking and grafting gelatins *via* thiol-ene click reaction. The intermolecular reaction of ene groups on polymer chains with the thiol groups of dithioerythritol (crosslinker) results in the creation of crosslinking points. Meanwhile, with the same reaction between the ene groups on polymer chains and thiol groups on thiol-modified substrate, the polymer network is grafted onto the substrate. Homogeneous PDMAEMA films are used to study the physico-chemical properties of the film.

The dry thickness (Th_{dry}) of PDMAEMA films corresponds to the thickness measured in air by ellipsometry. The thickness of films is controlled by the polymer concentration for spin-coating (C_p). **Figure S4a** shows that the Th_{dry} increases with increased C_p, corresponding to the viscosity of polymer solution. On the other hand, as shown in **Figure S4a**, the wet thickness (Th_{wet}) is much higher than Th_{dry}, because the surface-attached polymer network can swell underwater by absorbing water. The swelling is completely reversible with the dry thickness of the hydrogel or the amount of grafted polymer being constant. The swelling ratio (SR) of films is defined as $Th_{wet}/\ Th_{dry}$, which is shown in **Figure S4b**. The swelling ratio of films increases with the increase in dry thickness below about 50 nm, then keeps in constant for thicker films at SR about 4.8. This is because the grafting density is much higher than crosslinking density of the hydrogel. When the film is very thin (in general lower than 50 nm), the grafting of high density limits the swelling of the gelatin network. For thicker films, the swelling of the hydrogel is determined by the crosslinking density while the effect of the grafting density of chains on the surface becomes negligible. The volume fraction of polymers in swollen state (ϕ_p) can also be deduced ($\phi_p = 1/SR$) to compare with macroscopic hydrogels (**Figure S4c**). For films with

thickness over 50 nm, the volume fraction is constant around 21%, which is in the normal range of gelatin hydrogels. For the study of adhesion in this work, the film chosen always have a dry thickness higher than 50 nm, to avoid the surface effect and keep the volume fraction comparable with macroscopic hydrogels. The polymer fraction (ϕ_p) of hydrogels at swelling equilibrium under different conditions has been measured, since the PDMAEMA is charged polymer with a pKa of 7.8 (**Figure S4d**).[1]

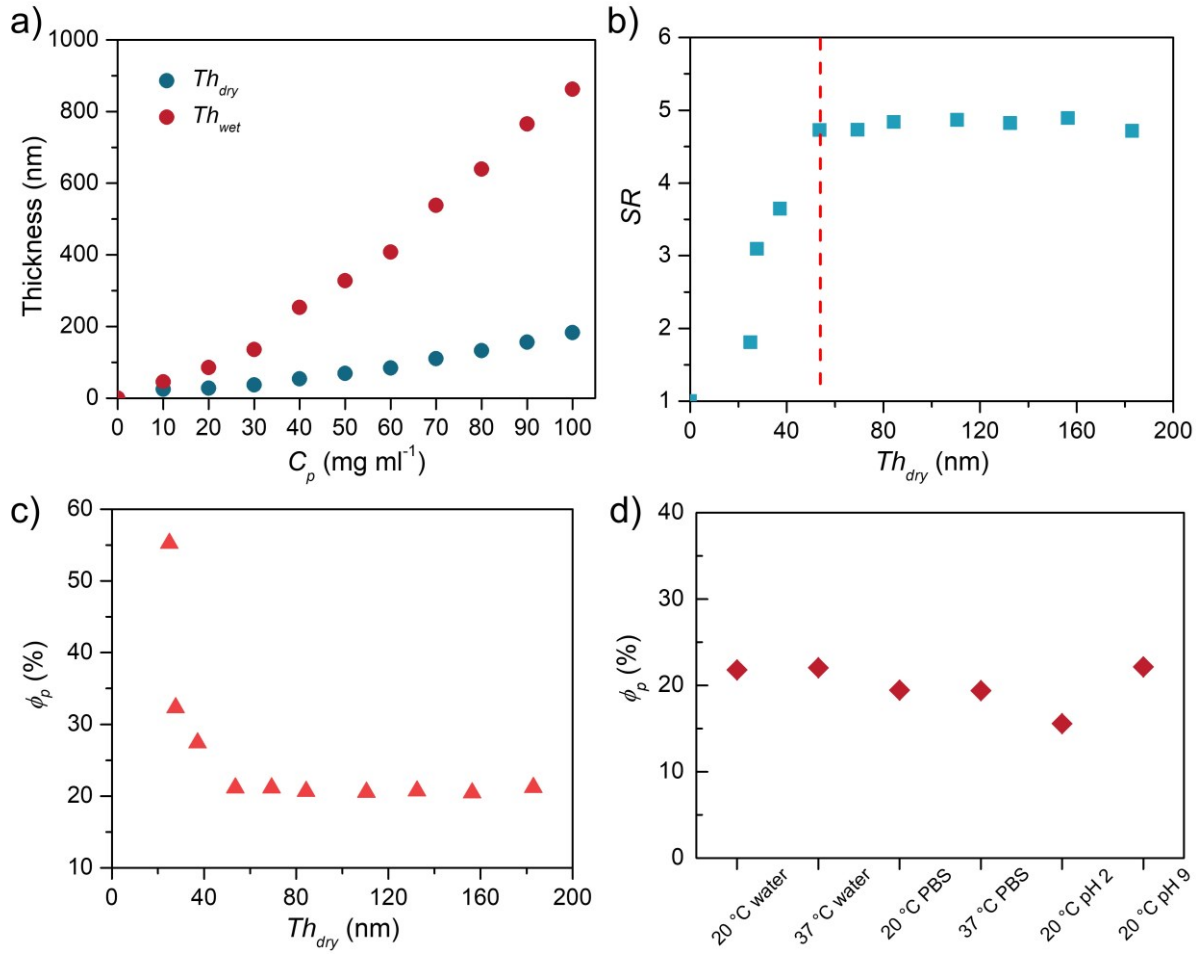

Figure S4. a) Dry (in air, Th_{dry}) and wet (in Milli-Q water, Th_{wet}) thickness, b) swelling ratio (SR) and c) volume fraction of polymers (ϕ_p) of PDMAEMA films. d) polymer fraction (ϕ_p) of PDMAEMA films at swelling equilibrium in different conditions, including temperature, pH and ionic strength.

Table 1. Dry (Th_{dry}), wet thickness (Th_{wet}) and swelling ratio (SR) of homogeneous and patterned films.

Film name	Thickness measurement	Th_{dry} (nm)	Th_{wet} (nm)	SR
homo	Ellipsometry	110.5 ± 0.1	538.2 ± 0.5	4.9
hex 200 μm	AFM	114.4 ± 2.6	578.5 ± 10.5	5.1

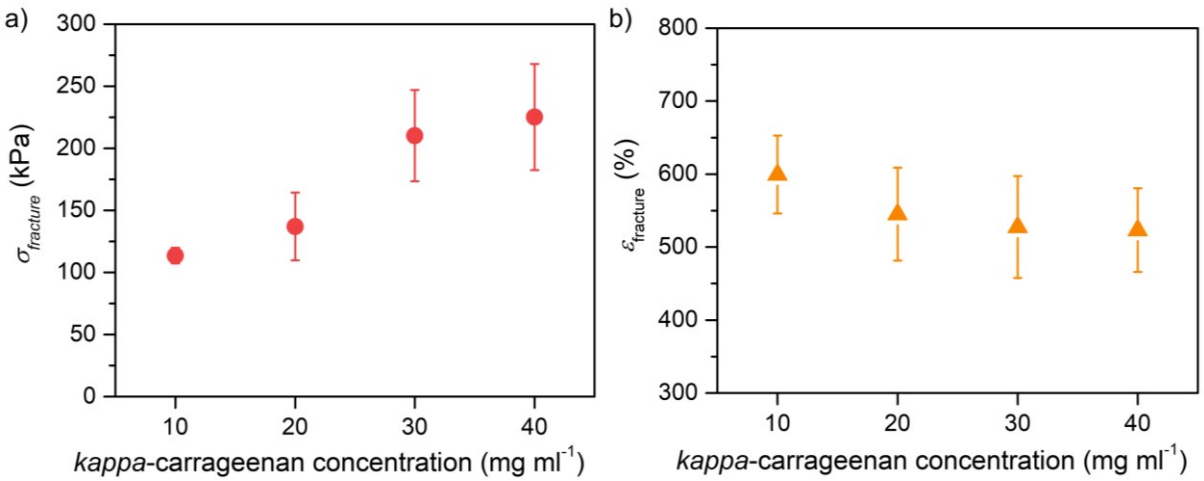

Figure S5. a) Fracture stress ($\sigma_{fracture}$) and b) fracture strain ($\varepsilon_{fracture}$) of tensile test on DN hydrogels as a function of *kappa*-carrageenan concentration.

Polymer fraction (ϕ_p) of DN hydrogels

In order to study the swelling behavior of DN gels and compare with the PDMAEMA thin films, the polymer fraction (ϕ_p) of macroscopic hydrogel are calculated as:

$$\phi_p = \frac{m_{dry}}{m_{wet}} \tag{S1}$$

where m_{dry} and m_{wet} refer to the weight of hydrogel in dry and wet (equilibrium) state, respectively. As shown in **Figure S6**, the polymer fraction of DN gels increases with the increase in the concentration of *kappa*-carrageenan, which is consistent with the tensile test result showing an increased crosslinking density.

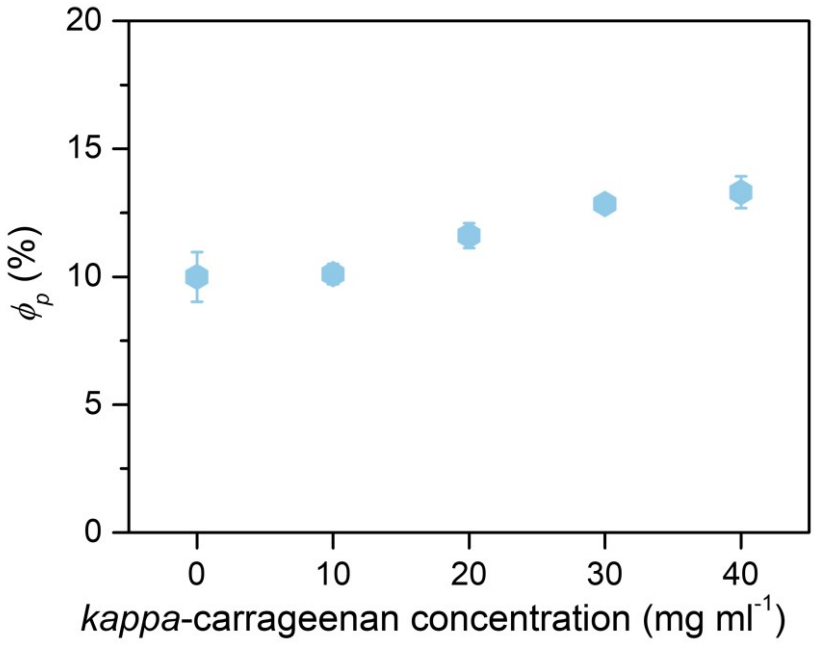

Figure S6. Polymer fraction (ϕ_p) of the DN hydrogel in equilibrated state as a function of the carrageenan concentration.

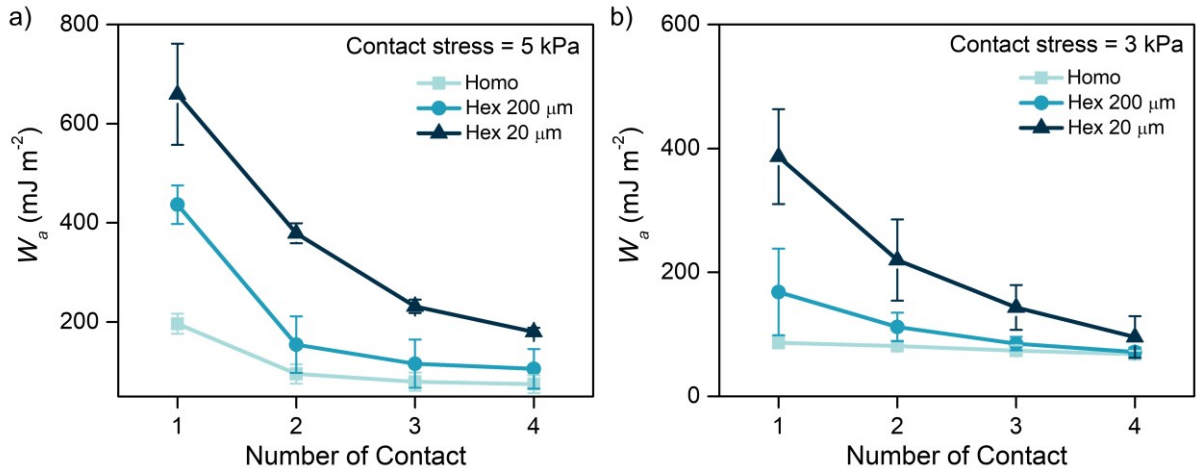

Figure S7. Work of adhesion between films and DN hydrogels, as a function of the number of contact. The contact stress is a) 5 kPa and b) 3 kPa.

References

1. Plamper, F. A.; Ruppel, M.; Schmalz, A.; Borisov, O.; Ballauff, M.; Müller, A. H. E., Tuning the Thermoresponsive Properties of Weak Polyelectrolytes: Aqueous Solutions of Star-Shaped and Linear Poly(N,N-dimethylaminoethyl Methacrylate). Macromolecules 2007, 40 (23), 8361-8366.

General Conclusion and Perspectives

1 General Conclusion

1.1 Overview of underwater adhesives

Recently, inspired by bioadhesion systems, there has been a significant progress in building artificial underwater adhesives, generally by strengthening interfacial adhesion and bulk cohesion. Those two effects are known as the main contributions for adhesion, which are always coupled unavoidably. Construction of underwater adhesives focuses at least one of the two effects, which is an important way to classify different types of adhesives. In **Chapter 1**, an overview of underwater adhesives from the perspective of interface and bulk has been summarized. At interface, the main challenge is from the hydration layer of water that prevents the interfacial binding and contact. Representative approaches include optimizing interface molecular interactions, interfacial physical suction, and dehydration of interface. On the other hand, the bulk cohesion could be enhanced by introducing non-covalent interactions and sacrificial mechanisms to form strong bulk adhesives. Moreover, different underwater adhesion measurements have been introduced and compared.

1.2 Gelatin coatings on various substrates

A simple and versatile strategy of Cross-Linking and Grafting (CLAG) has been used to synthesize substrate-attached gelatin hydrogel films/coatings. With the chemical crosslinking and grafting of the gelatin, interfacially and thermally stable hydrogel coatings were built on various substrates such as plane silicon wafers and soft PDMS fibers. The physical chemistry properties of the coatings, including thickness, swelling and biodegradation, were finely investigated. We showed that surface-attached gelatin hydrogel coatings can be obtained over a wide range of thicknesses from nanometers to micrometers. The gelatin layer swells reversibly underwater while the amount of gelatin grafted on the substrate (or the dry thickness) keeps constant. The swelling ratio can be varied by adjusting the ratio of EDC/NHS coupling agent. The gelatin coatings have also proven to be an effective platform for drug release such as dexamethasone.

1.3 Underwater adhesion between gelatin hydrogel and surface

In order to investigate bioadhesion process, a biopolymer has been used to build a model system consisting of hydrogel thin films (~ hundred nm) and macroscopic hydrogels (~ mm), which allows the separation of interfacial and bulk properties. Gelatin A and B were used as biopolymer and the model system allows the independent study of interface and network effects on underwater adhesion performance. Both gelatin materials were synthesized with well-controlled chemistry and physical parameters. The gelatin B hydrogel thin film is crosslinked and grafted onto a solid substrate. A proper dry thickness (~ 100 nm) was kept in this work to avoid substrate effect and ensure that there is only interface effect from gelatin film. The gelatin A macroscopic hydrogels were dual-crosslinked with controlled physical (from triple-helices of gelatin chains) and chemical (from EDC/NHS coupling) crosslinks. The molecular weights between both physical and chemical crosslinks, were calculated on the basis of the phantom network model. The study of underwater adhesion carried out under various environmental conditions and for different contact times showed that hydrogen bonds and electrostatic interactions additively both contribute to the interfacial interactions between gelatins A and B. The independent effect of physical and chemical crosslinks was studied by modifying the experimental temperature, showing an opposite influence on adhesion: the work of adhesion increased with physical crosslinking density but decreased with chemical crosslinking density. The impact of the physical crosslinks (low temperature) is related to the increased modulus and equilibrium polymer fraction, which is consistent with the model system of PDMA/PAAc reported by Macron et al. (*Macromolecules* 2018 51, 7556-7566). On the other hand, considering only covalent crosslinks (high temperature), the work of adhesion decreases with the increase of the modulus and the equilibrium polymer fraction, such as the poly(methacryloyloxyethyl)trimethylammonium chloride/PAAc model system reported by Cedano-Serrano et al. (*Macromolecules* 2019 52, 3852-3862). This result related to the chemical network can be predicted by the Chaudhury's model, considering the interfacial charge density determined by the thin film or the surface of bulk hydrogels. Finally, the collective contributions of both physical and chemical networks in dual-crosslinked gels were studied, showing that the underwater adhesion performance mainly depends on the gelatin density, while the existence of the chemical network slightly influence the work of adhesion.

Furthermore, we have found that the gelatins show weak adhesion comparing with synthetic systems. The model system based on electrostatic interactions reported by Cedano-Serrano et

al. (*Macromolecules* 2019 52, 3852-3862) leads to a work of adhesion of around 1000 mJ m^{-2}, while the gelatins show adhesion of less than 40 mJ m^{-2}. This is reasonable because of the weaker interface adhesion and bulk cohesion. The areal charge density of gelatins ranges from ~ 1×10^{15} to 5×10^{15} m^{-2}, while it is 4×10^{16} m^{-2} for the synthetic PAAc film, which is more than 1 order of magnitude higher than that of gelatins.

1.4 Underwater adhesion by controlling surface topography and microstructure

The model system that divides surface and bulk of adhesives has been used for studying the individual effect of surface microstructure and topography. A patterned surface with sophisticated periodical arrays of surface-attached hydrogel thin films was fabricated with well-controlled structure and physical chemistry. The underwater adhesion of the film against a strong biopolymer hydrogel was then studied, showing that the size of the pattern has a significant effect on work of adhesion. The study of adhesion performance, carried out with homogeneous film (without patterns) and microstructured films with hexagonal patterns of 200 μm and 20 μm, showed that the adhesion energy increases with the decrease in pattern size. This could be due to the formation of water drainage tunnels during underwater contact and the prevention of crack propagation within each hexagon pattern during debonding of interface. The pattern with smaller size provides higher adhesion energy. Furthermore, the adhesion could be controlled by pH, ionic strength and temperature.

2 Perspectives

In **Chapter 2**, biopolymer coatings have been synthesized with well-controlled chemistry, structure and physical properties. Comparing with typical coatings that have been published, the interfacial stability was improved by chemically grafting the polymer network onto the substrates. The coatings can have great potentials in biomedical applications especially surgical implants. The application could be explored with further studies of drug release kinetics. Although the versatility of the coating process has been demonstrated with different types of gelatin, different coating thicknesses and different varieties of substrate, it seems important to explore other biopolymer or biocompatible systems in order to expand their functionality and their range of applications.

In **Chapter 3**, molecular mechanisms of underwater adhesion of gelatins has been studied. Although the introduction of chemical bonds slightly reduces the crosslinking density of the physical network, by hindering the formation of triple helices, the chemical crosslinking of gelatin hydrogels allows to improve their stability while preserving their adhesion properties. Like thin films of gelatin, it would be interesting to explore other model hydrogels, of natural or synthetic origin, in order to broaden the understanding of bioadhesion mechanisms. One can think of anionic or cationic macromolecules, or of a complex of the two capable of undergoing modifications of their adhesive properties as a function of pH, ionic strength, temperature… Similarly, achieving strong underwater adhesion with a biopolymer system may also provide inspirations for the development of bioadhesives.

In **Chapter 4**, a strategy of modifying the surface topography has been studied to improve underwater adhesion. It would therefore be interesting to continue this work with a systematic study of the control of the substrate topography by modifying either the size of the pattern (from ~ nm to ~ μm and ~ mm) or its shape (circle, triangle, square, *etc*) to better understand their impact on adherence performance and optimize the surface topology. Similarly, the improvement of adhesion properties with patterned surfaces, a phenomenon that has been justified by a mechanism of interfacial water drainage and by a limitation of the crack propagation process, requires more experimental evidence to be clearly interpreted.

The study in this thesis shows some mechanisms and approaches for underwater adhesives. Taking account of literatures reviewed in **Chapter 1**, the thesis also provides some general strategies for building strong underwater adhesives:

a) **Water drainage mechanisms**. The negative effect of interfacial water should be removed or weakened, to ensure a good interfacial contact in water.

b) **Strong and multiple interfacial molecular interactions**. Strong interfacial interactions are a fundamental requirement for adhesion, but single molecular interactions are usually effective only in specific conditions. In order to maintain stable adhesion properties under a broad spectrum of environmental conditions, multiple molecular interactions should be combined together into the adhesive.

c) **Strong but soft bulk**. For pressure sensitive adhesives (PSA), based on firm interface binding, a strong and soft adhesive has better strechability, leading to higher adhesion energy.

RÉSUMÉ

Alors que l'adhésion entre matériaux synthétiques a été plutôt bien étudiée expérimentalement et théoriquement, les mécanismes de bioadhésion sont encore très peu compris. Une manière de les aborder serait d'utiliser des systèmes biopolymères qui pourraient imiter biosurfaces, biotissus et bioadhésifs. Cependant, cette idée est confrontée à la difficulté de concevoir une structure modèle et de contrôler les propriétés physico-chimiques des matériaux fabriqués à partir de biopolymères. Les mécanismes de bioadhésion peuvent être mieux compris en étudiant l'adhésion en milieu immergé entre adhésifs hydrogels et substrats solides modifiés par des films minces d'hydrogel. Cela permet de séparer la contribution interfaciale avec des interactions spécifiques moléculaires et de la contribution du volume avec les propriétés viscoélastiques à l'adhésion. Dans un premier temps, nous avons conçu un système modèle avec de la gélatine et noua avons étudié l'adhésion en milieu immergé favorisée par des interactions électrostatiques. D'une part, des films stables de gélatine attachés en surface d'épaisseur et de gonflement finement ajustables ont été réalisés en utilisant la stratégie Cross-Linking and Grafting (CLAG). D'autre part, des adhésifs hydrogels de gélatine à double réticulation ont été synthétisés en ajoutant des réticulations chimiques aux réseaux de gélatine physiques. La structure microscopique des réticulations physique et chimique a été bien contrôlée, avec la détermination de la longueur de chaîne entre les réticulations à partir du module de cisaillement et du modèle de réseau fantôme. L'adhésion en milieu immergé mesurée par des tests de probe-tack a montré que les hydrogels de gélatine à double réticulation ont les mêmes propriétés adhésives quelle que soit la température, même si leur résistance diminue avec le chauffage. Nous avons également été en mesure de séparer les effets des réseaux physiques et chimiques sur l'adhésion. Dans un deuxième temps, nous avons étudié l'adhésion en milieu immergé entre des réseaux doubles contenant du carraghénane et des substrats solides modifiés par des micro-motifs d'hydrogels. Il a été démontré que plus les micro-motifs sont petits, plus l'énergie d'adhésion est élevée. Ce travail a fourni un aperçu des paramètres physico-chimiques et physiques qui contrôlent l'adhésion en milieu immergé des systèmes biopolymères tels que les propriétés viscoélastiques en volume, la charge et la topographie de la surface. Il aidera à mieux comprendre la bioadhésion et à concevoir des adhésifs efficaces en milieux aqueux.

MOTS CLÉS

biopolymère, gélatine, hydrogel, adhésion, milieu aqueux, films minces

ABSTRACT

While the adhesion between synthetic materials has been rather well-studied experimentally and theoretically, there is still a lack of knowledge on bioadhesion, which could be tackled with biopolymer systems which could mimic biosurfaces, biotissues and bioadhesives. However, this idea is limited by the difficulty in designing a model structure and controlling the physical chemistry properties of biopolymer-made materials. Bioadhesion mechanisms can be tackled by studying the underwater adhesion between hydrogel adhesives and solid substrates modified by hydrogel thin films. This allows to separate interfacial contribution with molecular specific interactions and bulk contribution with viscoelastic properties to adhesion. First, a model system based on gelatins has been designed and underwater adhesion promoted by electrostatic interactions was investigated. On one side, stable surface-attached gelatin films with finely adjustable thickness and swelling were achieved using Cross-Linking and Grafting (CLAG) strategy. On the other side, dual-crosslinked gelatin hydrogel adhesives were synthesized by adding chemical crosslinks to physical gelatin networks. The microscopic structure of both physical and chemical crosslinks was well-controlled, with the determination of the chain length between crosslinks from shear modulus and phantom network model. Underwater adhesion measured by probe tack tests showed that dual-crosslinked gelatin hydrogels have the same adhesive properties at all temperatures even if their strength decreases with heating. We were also able to separate the effects of physical and chemical networks on adhesion. Second, the underwater adhesion between double-networks containing carrageenan and solid substrates modified by micro-patterned hydrogels was investigated. It was shown that the smaller the micro-patterns the higher the adhesion energy. This work has provided an insight of the physico-chemical and physical parameters that control underwater adhesion of biopolymers systems such as the bulk viscoelastic properties, the charge and the topography of the surface. It would help for better understanding bioadhesion and designing underwater adhesives.

KEYWORDS

biopolymer, gelatin, hydrogel, adhesion, underwater, thin films